Stresses in a single step joint

de Rijk, R.J.C.W.

Award date:
2016

Technische Universiteit
Eindhoven
University of Technology

Where innovation starts

Master thesis Structural Design

Stresses in a Single Step Joint

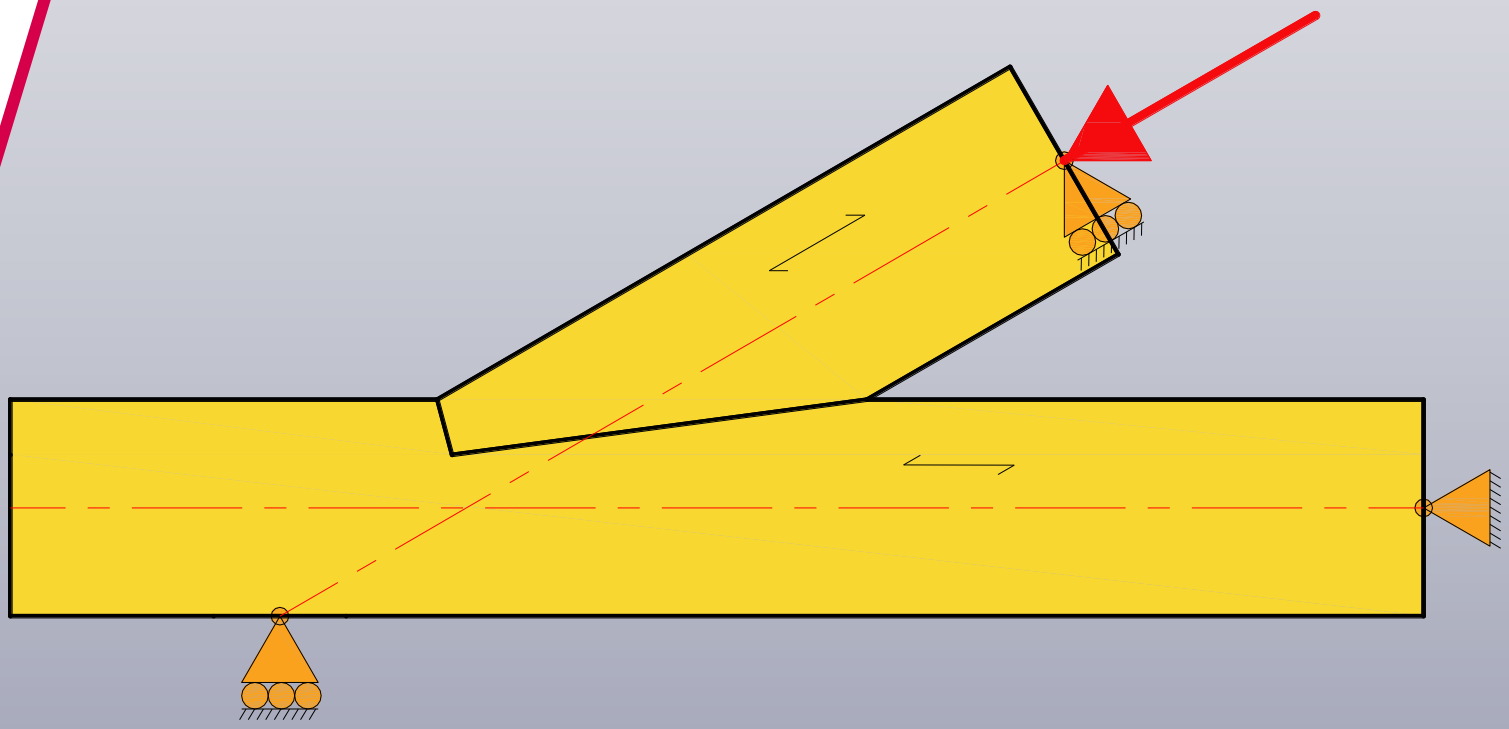

R.J.C.W. (RICHARD) DE RIJK

0823656 | April 20, 2016 | TU/e Structural Design

Prof. dr. ir. A.J.M. (André) Jorissen, dr. ir. A.J.M. (Ad) Leijten, Prof. ir. H.H. (Bert) Snijder, L. (Lambert) van den Bosch

Master thesis Structural Design

Stresses in a Single Step Joint

R.J.C.W. (RICHARD) DE RIJK

0823656 | April 20, 2016 | TU/e Structural Design

Prof. dr. ir. A.J.M. (André) Jorissen, dr. ir. A.J.M. (Ad) Leijten, Prof. ir. H.H. (Bert) Snijder, L. (Lambert) van den Bosch

Eindhoven University of Technology

Department of the Built Environment
Unit Structural Design

Address:

Vertigo floor 9
Groene Loper 6
5600 MB, Eindhoven

Post address:

P.O. Box 513
5600 MB, Eindhoven
the Netherlands

T: +31 (0)40 247 3992
F: +31 (0)40 247 4747
E: secretariaat.sd@tue.nl

Laboratory:

Pieter van Musschenbroek Laboratory
T: +31 (0)40 247 4177

Supervisors:

prof. dr. ir. A.J.M. (André) Jorissen a.j.m.jorissen@tue.nl
dr. ir. A.J.M. (Ad) Leijten a.j.m.leijten@tue.nl
prof. ir. H.H. (Bert) Snijder h.h.snijder@tue.nl
L. (Lambert) van den Bosch lvdb@hekospanten.nl

R.J.C.W. (Richard) de Rijk

E: r.j.c.w.d.rijk@student.tue.nl / rjcwrijk@live.nl
S126728
0823656

Summary

In this master thesis, the findings of a research into the stresses in a Single Step Joint are presented. A Single Step Joint is a traditional timber carpentry connection which often occurs in old monumental buildings and is recently regaining popularity in building construction. The connection occurs at locations where a timber diagonal loaded in compression intersects a horizontal or vertical timber element. For this reason, the connection often occurs in triangular timber trusses in roof structures.

No international design rules for designing a Single Step Joint are enclosed in the Eurocode. Instead of this, several countries use their own pre-Eurocode standards in the national annexes of the Eurocode. This leads to significant differences in the approach of the codes to the same design. The national codes of the Netherlands, Germany and Switzerland are the subject of a previously made literature study at which these codes are investigated and an attempt was made to find backgrounds for these design rules. The three mentioned codes are briefly discussed in this report. Several research questions, based on these codes, have been defined in order to find the real stress distribution in the connection. By investigating geometric differences in the connection, also the influence of these differences on the stress distribution is considered. With the help of the different research questions, the main question of the research is answered; “What geometric boundaries (angle γ, depth t_{notch}, length s_{notch}) can be applied to the connection according to the results of this research?”

To answer all research questions (see page 8), two different studies have been done. Firstly, a numerical study using finite element software ‘Simulia Abaqus CAE’. Secondly, an experimental study in the ‘Pieter van Musschenbroek Laboratory’ at the ‘Eindhoven University of Technology’. The reports of these numerical and experimental study are enclosed in this report in part II and III respectively.

The report of the numerical study starts with the explanation of the building of the numerical model. For this, timber material parameters to simulate the correct model behavior are investigated, and which parameters must be used to represent failure strengths of the model. Also, the choices of simulation methods are considered. This results in a numerical model, of which the behavior is verified by comparing the numerical results to the experimentally obtained ‘Electronic Speckle Pattern Interferometry’ (ESPI) behavior. After this, several numerical models are build, containing geometric differences in values which are mentioned in the national codes. These are: differences in shearplane length in front of the notched area, and different orientations of the angle of the front contact surface in the notch (frontnotch). During these simulations, the stress distribution in relevant planes are investigated during load inreasement. The results of these simulations are presented in 3D area plots of the stress distribution. In order to compare the differences in the geometry to each other, stress distributions at key load conditions are compared.

In the experimental study, firstly the design of the test setup and the used measurement methods are considered. A hypothesis of the failure loads and failure mechanisms is done, using the design rules of the three national standards. A total of 15 experiments have been done, in which the same

geometric differences as mentioned in the numerical study have been tested. The results of the tests are considered and compared to the hypothesis of the national design rules.

Finally, the results of the numerical-, and experimental study are compared to each other, and the research questions are answered. With this, the current national design rules of the Netherlands, Germany and Switzerland for Single Step joints are regarded.

Samenvatting

In dit afstudeerverslag worden de bevindingen van het afstudeeronderzoek naar spanningen in een Tandverbinding beschreven. Een tandverbinding is een traditionele houten timmermansverbinding die vaak voorkomt in oude monumentale panden en tegenwoordig ook weer in populariteit toeneemt bij nieuwbouw. De verbinding wordt gemaakt tussen een op druk belaste diagonaal houten element en een horizontaal of verticaal houten element. Om deze reden komt de verbinding vaak voor in driehoekige houten spanten.

Voor het ontwerpen van een Tandverbinding zijn geen (internationale) ontwerpregels opgenomen in de Eurocode. In plaats hiervan wordt door verschillende landen de normtekst uit de nationale norm uit het pre-Eurocode tijdperk opgenomen in de nationale bijlage van de Eurocode. Dit leidt tot grote verschillen in benadering van de verbinding tussen Europese landen onderling. In een aan dit afstudeeronderzoek voorafgegane literatuurstudie zijn deze nationale normteksten onderzocht en is getracht de achtergrond van deze normen te achterhalen. In dit rapport zullen de nationale normen van Nederland, Duitsland en Zwitserland kort worden toegelicht. Op basis van de teksten en methodes in deze normen zijn enkele onderzoeksvragen opgesteld waaraan wordt getracht om de werkelijke spanningsverdeling in de verbinding te achterhalen. Met een variantenstudie in de geometrie van de verbinding wordt gekeken naar eventuele verschillen die ontstaan in de spanningstoestand. Aan de hand van de verschillende onderzoeksvragen wordt een antwoord gegeven op de hoofdvraag van dit onderzoek; “Welke geometrische randvoorwaarden, (hoek γ, diepte t_{notch}, en lengte s_{notch}), kunnen worden toegepast in de verbinding volgens de bevindingen in dit onderzoek?”

Om alle onderzoeksvragen te beantwoorden zijn er op twee manieren studies gedaan naar de Tandverbinding. Ten eerste is de verbinding numeriek gesimuleerd in het eindig elementen software pakket ‘Simulia Abaqus CAE’. Daarnaast zijn er experimentele testen gedaan in het ‘Pieter van Musschenbroek Laboratorium’ van de ‘Technische Universiteit Eindhoven’. De verslagen van dit numeriek en experimenteel onderzoek zijn opgenomen in dit afstudeerverslag in respectievelijk Deel II en III.

Het verslag van het numeriek onderzoek is ten eerste gewijd aan de opbouw van het numerieke model. Hiervoor is gekeken naar de juiste parameters welke het materiaalgedrag van hout simuleren, en welke grenswaardes voor de sterkte van het materiaal moeten worden gebruikt. Ook de gekozen numerieke methodes worden beschouwd. Het uiteindelijke numerieke model wordt geverifieerd door een vergelijking te maken met de experimentele resultaten van een ‘Electronic Speckle Pattern Interferometry’ (ESPI) meting. Vervolgens wordt er met behulp van meerdere modellen een variantenstudie gedaan naar verschillende geometrische parameters die in de nationale normen worden genoemd, zijnde; verschillende afschuiflengtes in het houten balk element voorbij de verbinding, en verschillende schuinten van de inkeping die voorkomt in de verbinding. In deze modellen wordt de spanningsverdeling in de relevante vlakken, gedurende het belasten, onderzocht. Deze resultaten worden overzichtelijk gemaakt met behulp van 3D oppervlakte grafieken. Om de verschillen tussen de spanningsverdeling in de modellen onderling duidelijk te maken worden voor belangrijke belastingen de spanningsverdelingen vergeleken.

In het verslag van het experimentele onderzoek worden ten eerste de proefopstelling en de gebruikte meetmethodes beschouwd. Een hypothese voor de bezwijklast en bezwijkmethode wordt gedaan met behulp van de drie onderzochte nationale ontwerpregels. In totaal zijn er 15 proeven gedaan waarin wederom is gevarieerd in dezelfde geometrische afmeting als onderzocht in de numerieke studie. De resultaten van de experimenten worden beschouwd en worden aan de hand van de hypothese geanalyseerd en vergeleken met de nationale normen.

Uiteindelijk worden in dit verslag de resultaten van het numerieke-, en experimentele onderzoek vergeleken en worden de onderzoeksvragen beantwoord. Aan de hand hiervan worden de huidige nationale normen van Nederland, Duitsland en Zwitserland over het ontwerpen van een Tandverbinding beschouwd.

Acknowledgements

This report is the result of my master study in Structural Design at the department of the Built Environment at the Eindhoven University of Technology. During my student life I have done research projects mostly concerning steel and concrete as building material. Since I have not been in-depth with one of the most common building materials available today more than following the courses during my study, I decided to do my master thesis at the timber section of the department.

Prof. Jorissen gave me the opportunity to do research on a timber carpentry connection that is very common in historical timber structures. Since the connection does not have uniform design rules, a European COST (European Cooperation in Science and Technology) FP1101 workgroup was established to gather information on these carpentry connections.

I would like to thank the members of my graduation committee.
Firstly, I would like to thank Prof. André Jorissen, my first supervisor. He shared with me his great knowledge of timber structural design and gave me the opportunity to connect with members of the COST FP1101 working group during a meeting in Eindhoven, and in Guimaraẽs, Portugal.
Secondly, I would like to thank Dr. Ad Leijten for his knowledge and support during my experimental campaign and for handing me literature on carpentry connections and material related topics.
Finally, I would like to thank Mr. Lambert van den Bosch, who has helped me with the manufacturing of the test specimens for the experimental study.

I also would like to thank all employees of the 'Pieter van Musschenbroek Laboratory' for providing support, practical knowledge and occasional laughs during my experimental campaign. Special thanks goes out to Ir. Hans Lamers, head of the laboratory, for helping me with the planning and logistics. And also special thanks goes out Ing. Eric Wijen with whom I worked together intensively during the experimental campaign and for sharing me his knowledge about ESPI measuring and photography.

Finally I would like to thank my fellow students of the Vertigo building's fifth floor. During our thesis work, we supported each other, although we were all working on different topics.

Richard de Rijk

Eindhoven, April 20th 2016

Table of contents

1. Introduction

1.1 Carpentry connections

Timber is one of the oldest materials in building construction. Timber was used long before steel connectors, reinforced concrete and electricity for power tools were invented. This meant that connections between timber elements had to be made, using the craftsmanship of carpenters. In many cases this resulted in wood-to-wood connections using compression and shear to transfer connection forces. Many of these solutions are shown in **Fout! Verwijzingsbron niet gevonden.**:

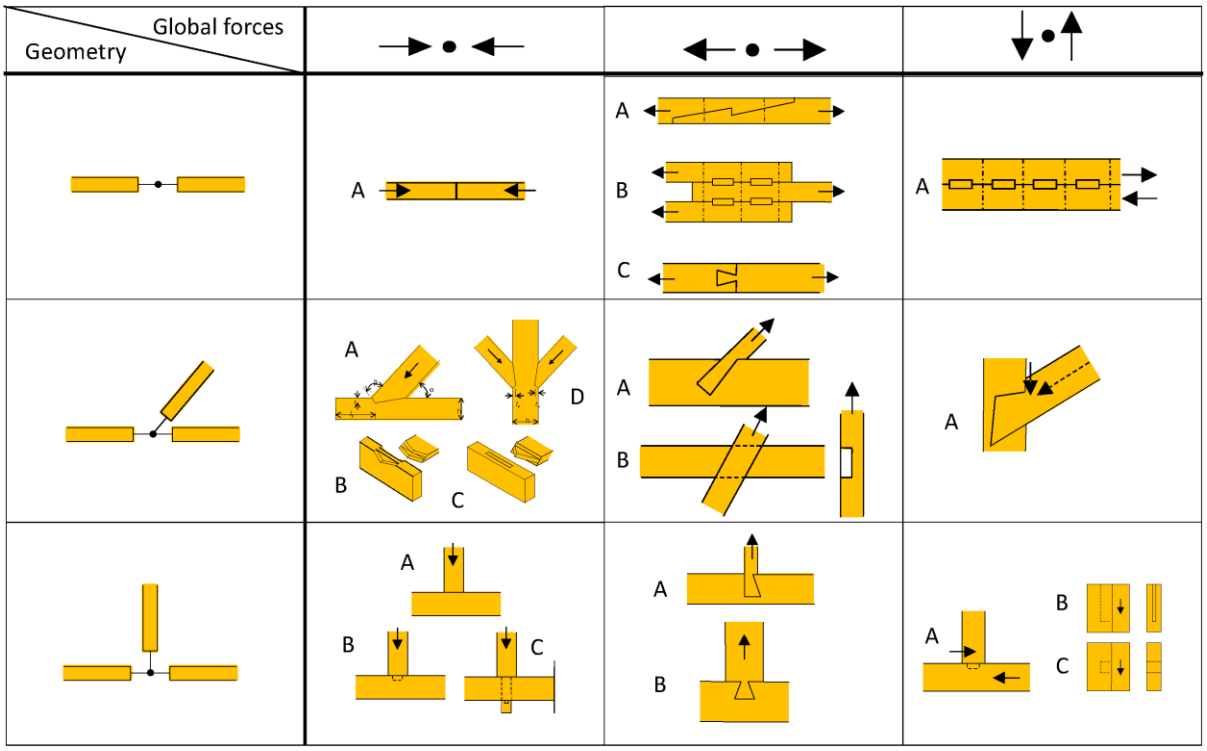

Figure 1: Most common carpentry joints in plane structures for different geometries and connection forces [1]

Today, many buildings which contain these connections still exist. The connections can be found mainly in monumental buildings, as they have been preserved in their original state over time. The majority of new buildings containing timber, use mechanical (steel) fasteners and plates to connect timber elements. As this type of connecting is very popular, many design rules have been made to design and engineer these connections. The historic carpentry connections, although they still exist in many historic buildings, do not have well thought-through uniform design rules as their modern equivalents do. Design rules that are available for carpentry connections tend to have no-, or very little scientific background. Most design rules are based on experience and experimental tests. Also, many national normalization institutes have different views on how to design these connection, and therefore design rules show many different approaches in designing the same connection. All this, led to the exclusion of design rules on carpentry connections in the new European design rules for designing timber structures; Eurocode 5. [2]

This research is done to compare different national design rules, and finding their background for a specific carpentry connection; the Single Step Joint. Besides this literature study, a numerical and experimental study is conducted on the connection to test the design methods used in the national codes.

More research is done on carpentry connections as part of a European group within ‘COST’ (European Cooperation in Science and Technology). This COST group FP1101 is called ‘Assessment, reinforcement and monitoring of timber structures’.

1.2 Single Step Joints

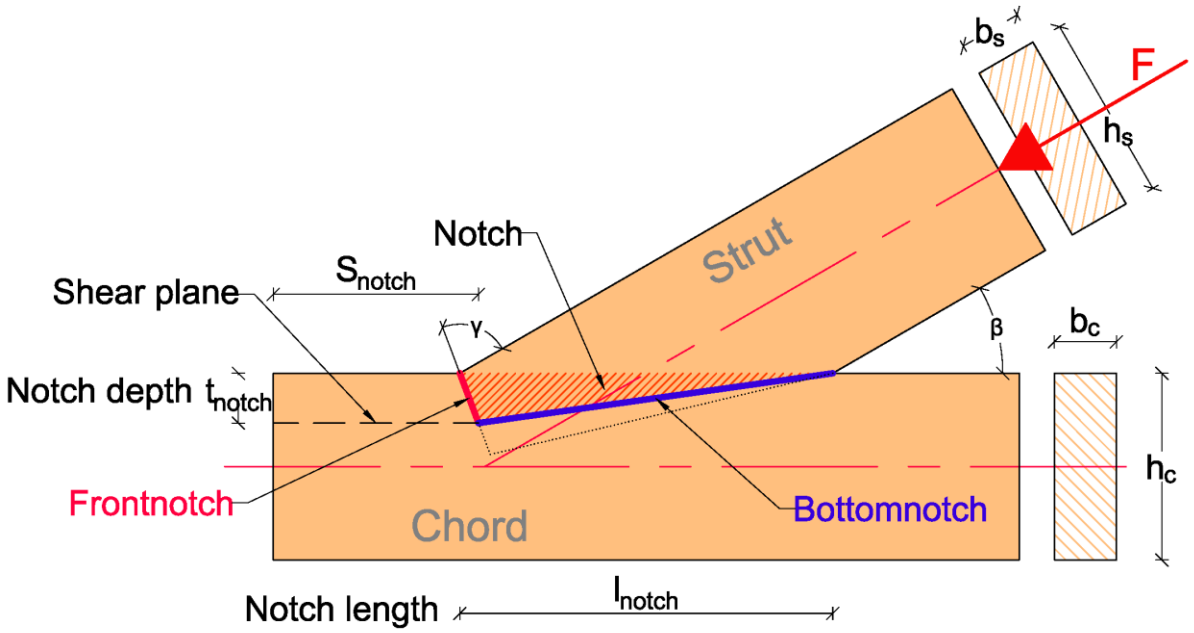

Figure 2: An illustration of a Single Step Joint with the used denominations in this report

A Single Step Joint is a connection between two timber elements and is loaded in compression. These two elements intersect under an angle β lower than 90°, with the majority practically intersecting in a range of 30° to 45°. In this situation, a Single Step Joint is very common, but is not the only option to connect the two elements. Several solutions are presented in Figure 3. All solutions include a chord (beam) member which is notched. The strut (diagonal) element is shaped to fit this notch. A compressive load in the diagonal element is transferred via the contact surfaces into the beam member. The Single Step Joint is mostly seen in triangular timber roof trusses, and in particular in the connection between a horizontal tensional beam and the diagonal roof-supporting beam. To prevent the connection from disconnecting out-of-plane, in practice, usually a deepened notch is applied in the heart of the beam to act as mortise, and a tenon is cut in the diagonal element, ensuring the diagonal element is enclosed by the beam out-of-plane.

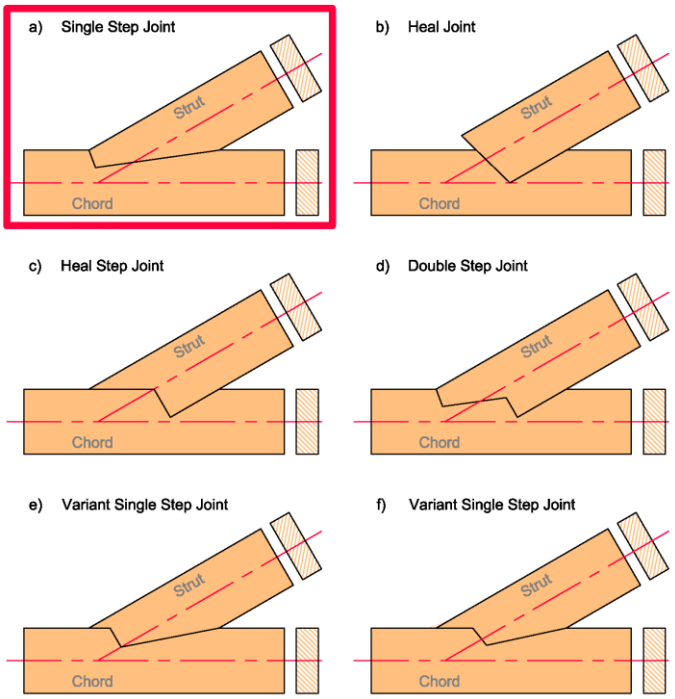

Figure 3: Different geometries for a connection between a horizontal and diagonal element.

1.3 COST action FP1101 Training School

Figure 4: University of Minho in Guimaraẽs

From 11 to 14 may 2015, a 'Training School' was held at the University of Minho in Guimaraẽs, Portugal. This training school was organized for the COST FP1101 action-topics assessment and reinforcement of historic timber structures. During this Training School, a truss which was saved from demolition was used to do full-scale destructive tests in original state, and later, reinforced. Special attention was given to carpentry connections using also scaled tests on Single Step and Dovetail joints. Next to the lab tests, lectures on assessing, monitoring and reinforcing of historical timber structures where performed by COST FP1101 members.

1.3.1 Program

Table 1: Monday 11 may Lectures

Welcome and Presentation of the TS	Jorge Branco, University of Minho
Heritage Timber Structures: The role of Knowledge, challenges and applications	Paula B. Lourenço, University of Minho
Principles of dendrochronology to understand timber elements	Lúcia de Soto, University of Coimbra
Visual Inspection and grading	Hélder Sousa, University of Minho
Non-destructive methods	Hélder Sousa, University of Minho
Probabilistic safety assessment of timber elements combining onsite and laboratory data	Hélder Sousa, University of Minho
Structural analysis as an assessment tool	Eleftheria Tsakanika, N.T. University of Athens
Assessment of the truss	Fotis Kondis, N.T. University of Athens

Monday 11 may Laboratory

- Non-destructive test methods;
- Visual inspection;
- Test preparation;
- Tests on dovetail joints with dowel (Tension).

Figure 5: Non-destructive tests, test preparation in the lab

The first day of the Training School was dedicated to general topics and assessment methods of cultural heritage timber structures. After a welcome presentation by the host; Jorge Branco, the lectures started. After lunch the program continued with a first visit to the lab and the assembled truss. Several methods of non-destructive tests (UPV, Pilodyn, Resistograph) were demonstrated and an explanation of the preparations for the full-scale tests were given.
After the Monday-program was finished, a group dinner at Histórico by Papaboa ended the first day.

Table 2: Tuesday 12 may Lectures

Structural analysis of timber trusses. Evaluation and load-carrying tests	Jorge Branco, University of Minho
Analysis of Carpentry joints	Jorge Branco, University of Minho
Experimental evaluation of carpentry joints at UM	Jorge Branco, University of Minho
Tests on dovetail joints with dowel - Tension	Karel Sobra, Czech Technical University in Prague

Tuesday 12 may Laboratory

- Tests on dovetail joints without dowel – Tension;
- Tests on dovetail joints – Compression;
- Tests on Single Step joints – Compression;
- Load-carrying test on the full-scale truss.

The theme of the lectures of the second day was 'Structural Analysis'. While the truss was prepared for testing in the afternoon, all aspects of making a structural design for trusses and joints were lectured along with previously conducted experiments on carpentry connections. In the afternoon it was time to do the full-scale test on the truss and several scaled tests on carpentry connections.

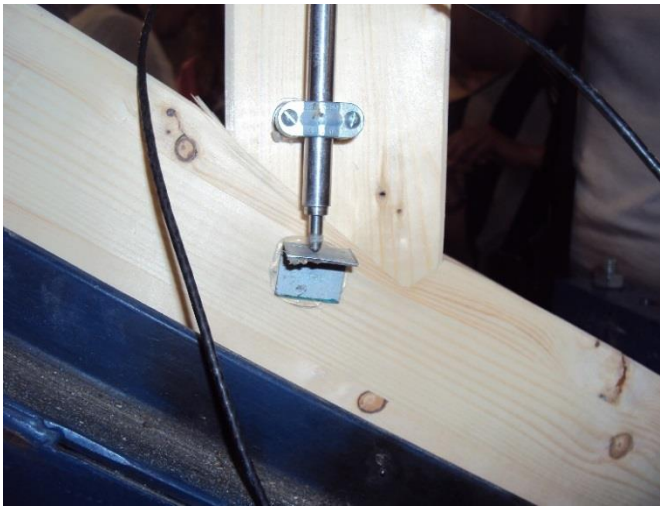

Figure 6: Small scale compression test on a Single Step Joint

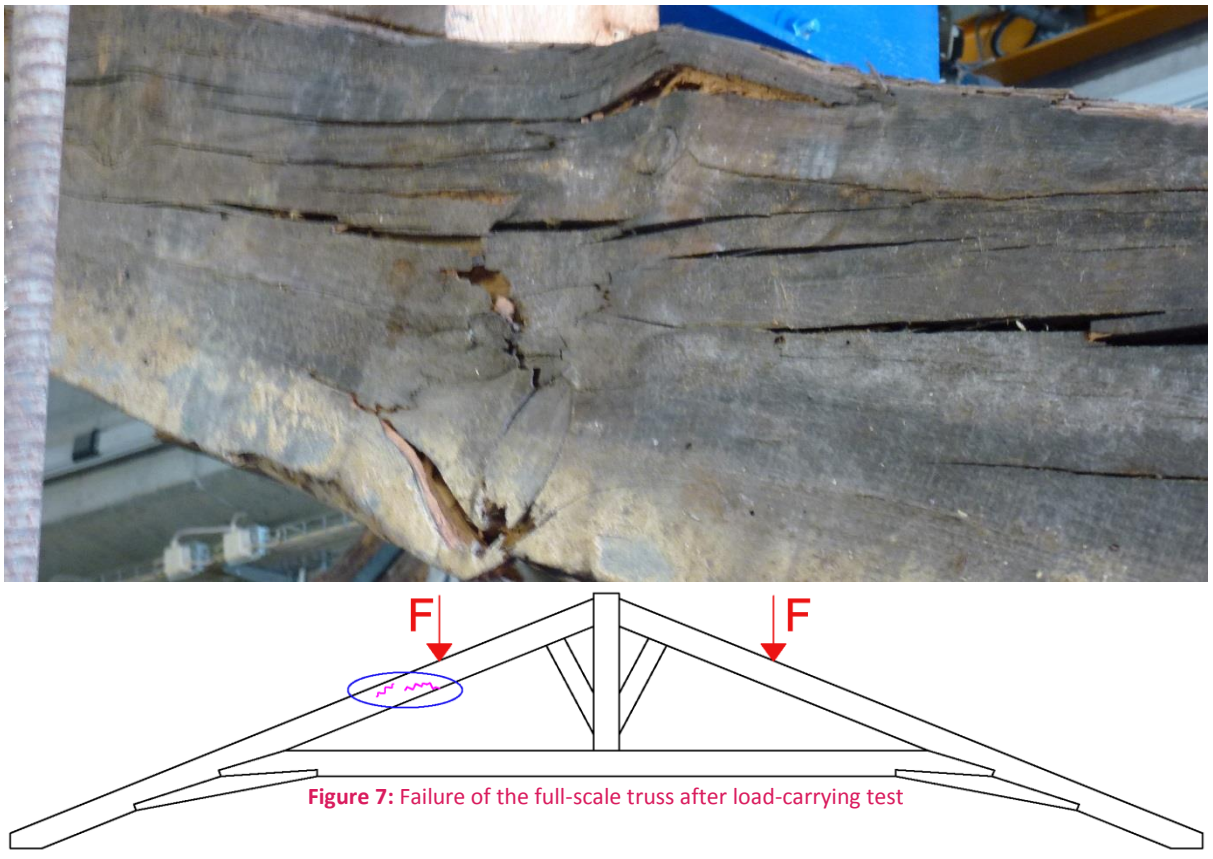

Figure 7: Failure of the full-scale truss after load-carrying test

Table 3: Wednesday 13 may Lectures

Truss assessment vs load-carrying test	Jorge Branco, University of Minho
Reinforcement of the timber truss	Jorge Branco, University of Minho
Reinforcement of carpentry joints	Jorge Branco, University of Minho
Reinforcement methods of historic and existing timber structures: Case studies from Greece	Eleftheria Tsakanika, N.T. University of Athens

Wednesday 13 may Laboratory

- Application of NSM (Near-surface mounted), EBR (externally bonded reinforcement) and MF-EBR (Mechanically fastened externally bonded reinforcement) strengthening techniques, on timber elements.
- Workshop: Reinforcement proposal for the truss and joints tested.

Figure 8: Strengthening techniques, EBR

The third day of the Training School started with the assessment of the test results of the truss that was tested on Tuesday. After the test results were treated, several reinforcement methods for timber were explained and reviewed for their application. Several methods did get a deeper explanation as they were treated in case studies. In the afternoon the lecture schedule was finished and the Training School continued in the lab by a workshop on several applications for the reinforcement methods; NSM, EBR and MF-EBR. After the truss was brought back as much as possible to the original shape (closing cracks and by diagonal internal screws), the chosen reinforcement was applied. The left side was reinforced by steel plates at the bottom and lots of screws to mount the plates. The other side was reinforced using timber elements at both sides which doubled the area of the rafter.

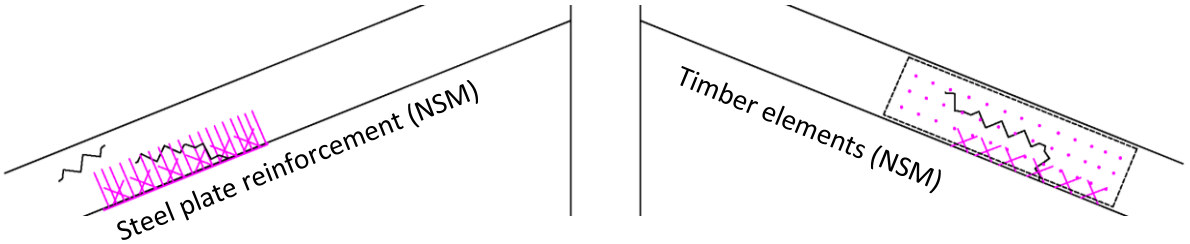

Figure 9: Two different strengthening techniques are applied on the failed truss before re-testing

Figure 10: Left side: Mounted steel plates at the bottom. Right side: Timber elements at both sides.

Thursday 14 may Laboratory

- Scaled tests of the reinforced joints;
- Test of the reinforced truss.

The fourth and final day of the training school had no lectures planned. Only tests in the laboratory were scheduled. While the final preparations for the reinforced truss where made, some scaled tests were performed on the reinforced version of the specimen (Single Step joint and Dovetail joint) that where tested earlier.
After these tests finished the full scale test on the reinforced truss started. The truss never reached its original strength due to the severe damage on the left rafter (that was reinforced by steel plates at the bottom) that was done in the earlier test on the second day.

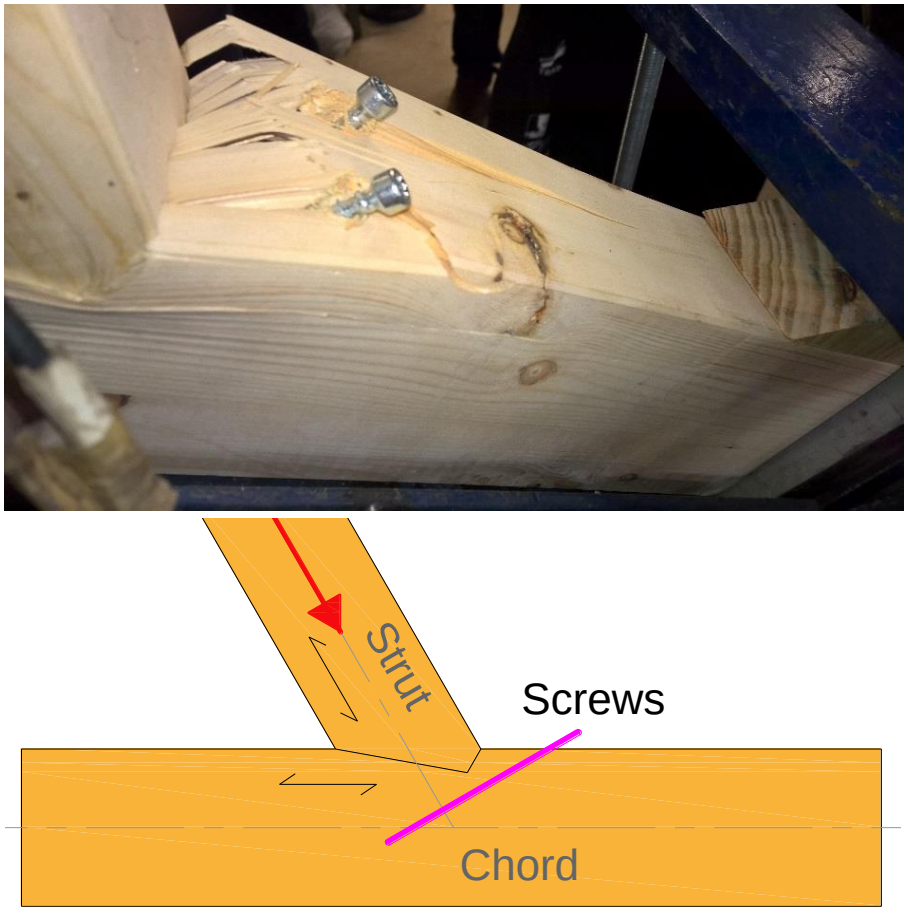

Figure 11: Tested strengthening technic on a Single Step Joint

1.4 Research problem and objectives

Problem

The Single Step Joint, and carpentry connections in general, are very common in historic buildings with a timber structure. This joint is mostly applied in the roof-supporting structure. Next to their presence in historical buildings, also, the connection is regaining popularity in construction of new buildings. This is due to their architectural look and due to increasing simplicity in cutting the complex geometry using computer controlled cutting techniques.

As mentioned in the introduction there are no design rules for carpentry connections included in the international design rules for timber structures in Eurocode 5. Instead, several countries have enclosed their old design rules for carpentry connections in the National Annex (NA). This raises a problem for structural engineers in designing new buildings with carpentry connections, and for renovations or the redesignation of historical buildings.

Objectives

The objectives of this research are to:

- Describe and explain the different national design rules enclosed in national annexes to EC5, and (if available), find their backgrounds;
- Testing the "real" stress distribution in connection using numerical simulations and experiments;
- Assessing design rules with the results of the numerical simulations and the experimental results.

All these objectives are in order to contribute to uniform (European) design rules for Single Step joints.

1.5 Research questions

The objectives are investigated by doing research to the following research questions:

Main research question:

"What geometric boundaries (angle γ, depth t_{notch}, length s_{notch}) can be applied to the connection according to the results of this research?"

Sub question A:
"What is the difference in stress-distribution for the shear stresses in the shear plane as it varies in length?"

Sub question B:
"What is the stress-distribution over the length of the front-, and bottomnotch?"

Sub question C:
"What is the influence of frontnotch angle γ on the stress-distribution in the frontnotch and the shearplane?"

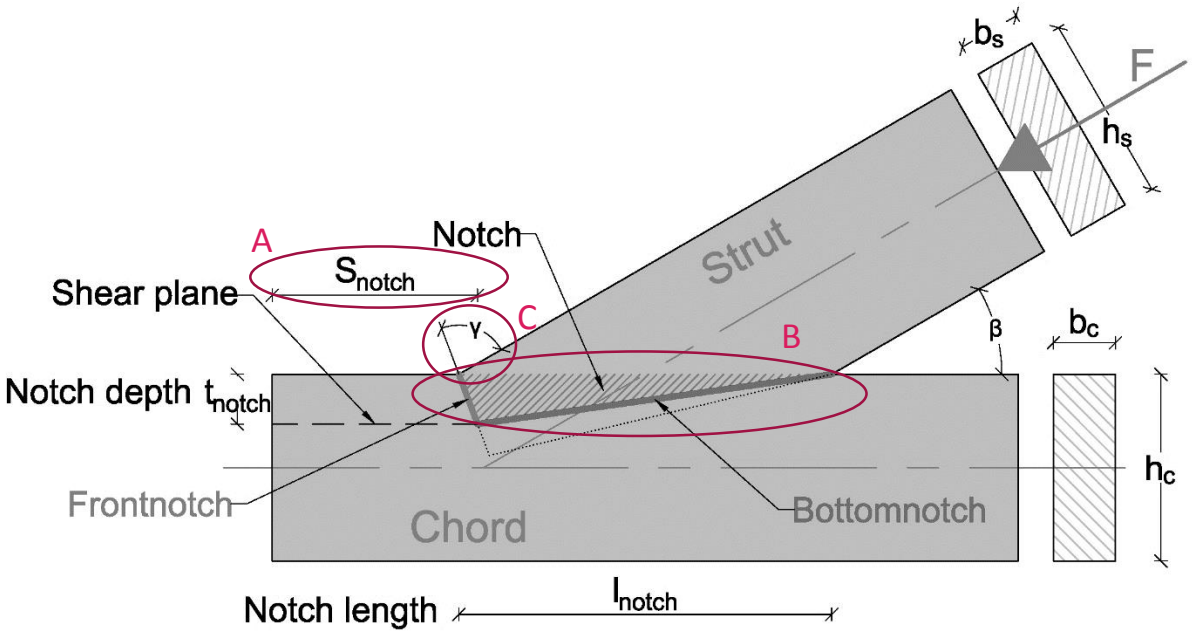

Figure 12: Research areas of the sub questions

2. Literature

The results from the literature study concerning three national design rules (Netherlands, Germany and Switzerland) are summarized in this chapter.

2.1 Dutch National Annex to Eurocode 5

The Dutch National Annex (NA) to Eurocode 5 [3] does, like the German NA to Eurocode 5 [4] and the Swiss SIA 256 Holzbau [5], make a distinction between a set of geometric boundary conditions which the design must fulfill, and the stress levels in the connection that must be checked. The geometric boundary conditions concern the notch depth, and the angle of the frontnotch:

Notch depth

$$t_{notch} \leq \frac{1}{5} * h \qquad for\ \beta > 50° \qquad \text{(II-1)}$$

$$t_{notch} \leq \frac{1}{4} * h \qquad for\ \beta \leq 50° \qquad \text{(II-2)}$$

Where h is the height of the chord (mm), and α is the angle between the center lines of the strut and chord (°).

Frontnotch angle

$$90° - \frac{1}{2} * \beta \leq \gamma \leq 90° \qquad \text{(II-3)}$$

Where β is the angle between the center lines of the strut and chord (°), and γ is the angle of the frontal area of the frontnotch and the center line of the components (°).

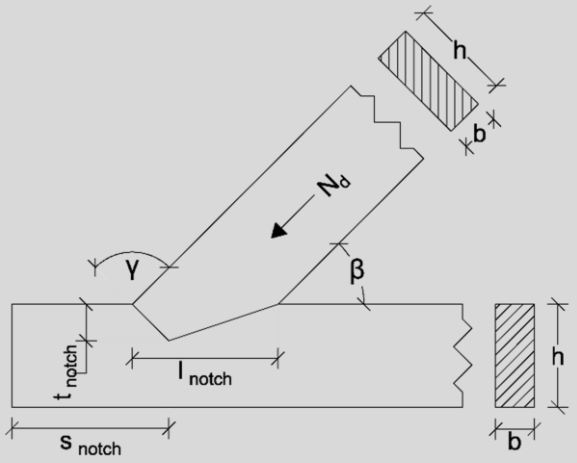

Figure 13: Example of a Single Step Joint

Quote 1: Geometric boundary conditions in the Dutch National Annex to Eurocode 5

After these geometric boundaries are fulfilled, the stress levels in the connection must be checked. These are: the shear stresses in the shearplane, the normal stresses in the contact surfaces, and the stresses under an angle to the fiber in the frontnotch:

From the international part of EC 5 in section 6.2.2 'Compression under an angle to fiber direction':

$$\sigma_{C,\alpha,d} \leq \frac{f_{c,0,d}}{\frac{f_{c,0,d}}{K_{c,90} * f_{c,90,d}} * \sin\alpha^2 + \cos\alpha^2} \quad \text{(II-4)}$$

Where:

α is the angle between the direction of the stress and the fiber direction;

$f_{c,0,d}$ is the material compressive strength, parallel to fiber direction;

$f_{c,90,d}$ is the material compressive strength, perpendicular to fiber direction;

$K_{c,90}$ is a geometric factor;

$\sigma_{C,\alpha,d}$ is the acting stress under an angle to the fiber direction.

And from the Dutch NA to EC5:

Compressive and shear stresses

$\sigma_{c;0;d} \leq f_{c;0;d}$ $where$ $\sigma_{c;0;d} = \frac{N_d * \cos\beta}{t_{notch} * b}$ (II-5)

$\sigma_{c;90;d} \leq f_{c;90;d}$ $where$ $\sigma_{c;90;d} = \frac{N_d * \sin\beta}{l_{notch} * b}$ (II-6)

$\sigma_{v;d} \leq f_{v;d}$ $where$ $\sigma_{v;d} = \frac{N_d * \cos\beta}{0.8 * s_{notch} * b}$ (II-7)

Where

N_d is the design value of the normal compressive force to be transmitted (N);

b is the width of the contact elements (mm);

s_{notch} is the shear-loaded end distance (shear plane) (mm);

t_{notch} is the front notch depth (mm);

l_{notch} is the length of the notch (mm);

β is the angle between axial compressive force N_d and the center line of the adjoining member (°)

Quote 2: design stress resistance check in the Dutch National Annex to Eurocode 5

2.2 German National Annex to Eurocode 5

The German NA to EC5 [4] also states geometric boundaries. Where the Dutch NA gives a range for the frontnotch angle γ, the German NA defines a fixed value for γ of 90°-β/2. For notch depth:

Notch depth

$$t_v \leq \begin{cases} \frac{h}{4} & for \quad \beta \leq 50° \\ \frac{h}{6} & for \quad \beta > 60° \end{cases} \qquad \text{(II-8)}$$

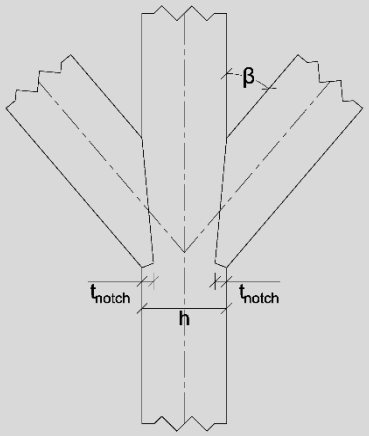

Where h is the height of the notched chord (mm), and β is the angle of the connection (°)

Values between 50° and 60° may be interpolated.

The notch depth t_{notch} of a two-sided Single Step Joint may not be larger than $h/6$ also for $\beta \leq 50°$.

Quote 3: Geometric boundary conditions in the German national annex to Eurocode 5

To check the stress levels, the German NA to EC5 only states a check for the stresses under an angle to the fiber, as shown in Quote 4. The shear stresses must be checked by dividing the shear force over the available area:

$$N_{H,d} = N_d * \cos\beta \qquad \text{(II-9)}$$

$$\tau_{v,d} = \frac{N_{H,d}}{s_{notch} * b_{ef}} \qquad \text{(II-10)}$$

$$\frac{\tau_{v,d}}{f_{v,d}} \leq 1.0 \qquad \text{(II-11)}$$

Where:

N_d is the force acting in the diagonal;

$N_{H,d}$ is the acting force's horizontal component;

s_{notch} is the shearplane length;

b_{ef} is the effective beam with as defined in EC5 section 6.1.7;

$\tau_{v,d}$ is the acting shear stress;

$f_{v,d}$ is the material shear strength.

Deviating from section 6.2.2 the compressive stresses in the connection can be found in the following manner:

$$\frac{\sigma_{c,\alpha,d}}{f_{c,\alpha,d}} \leq 1 \qquad \text{(II-12)}$$

Where

$$\sigma_{c,\alpha,d} = \frac{F_{c,\alpha,d}}{A} \qquad \text{(II-13)}$$

$$f_{c,\alpha,d} = \frac{f_{c,0,d}}{\sqrt{\left(\frac{f_{c,0,d}}{2*f_{c,90,d}}*sin^2\alpha\right)^2+\left(\frac{f_{c,0,d}}{2*f_{v,d}}\sin\alpha*\cos\alpha\right)^2+cos^4\alpha}} \qquad \text{(II-14)}$$

and

A is the front notch surface area;

α is the angle between the direction of the force and the direction of the grain.

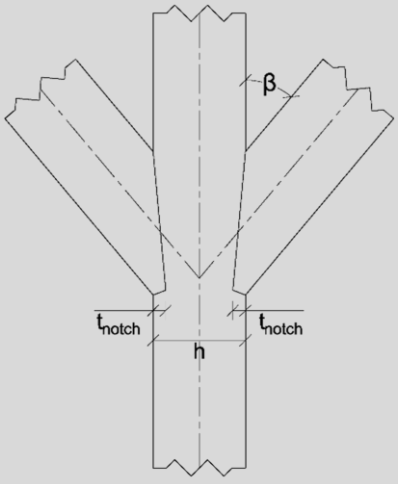

The shear stresses in the connection can be assumed uniformly distributed along the length of the shear-plane. If this is assumed, a shearplane length S_{notch} may not be longer then $8 * t_{notch}$ For the calculation of the shear stress in this section an effective width according to 6.1.7 of Eurocode 5 must be taken into account.

Quote 4: Design stress resistance check in the German national annex to Eurocode 5

2.3 Swiss SIA 256 Holzbau

The Swiss codes defines geometric boundary conditions which are identical to the German standard:

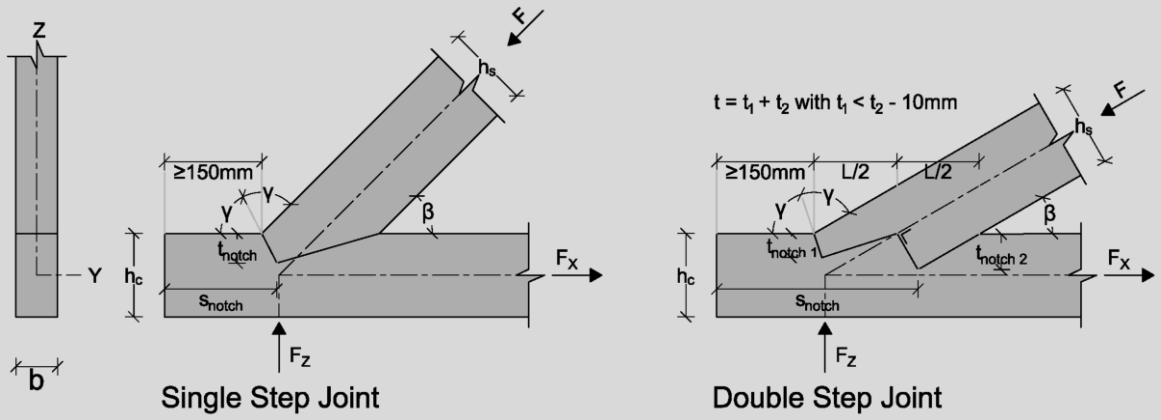

Figure 14: Example of a Single Step Joint and a Double Step Joint

The boundaries for t_{notch} are set in Table 4

Table 4: Notch depth t_{notch} in carpentry connections

Single Step Joint	Double Step Joint
$t_{notch} \leq \frac{h_c}{4} \quad for \quad \beta \leq 50°$ $t_{notch} \leq \frac{h_c}{6} \quad for \quad \beta \geq 60°$ Angles between 50° and 60° can be interpolated linearly	$t_{notch\ 1} \leq \frac{h_c}{6}$ $t_{notch\ 2} \leq \frac{h_c}{4}$ $t_{notch\ 1} < t_{notch\ 2} - 10mm$

Quote 5: Geometric boundary conditions in the Swiss SIA 256 Holzbau

After these conditions are met, the standard gives checks for:

- The shear stresses in the shearplane (s_{notch});
- The compressive stresses in the frontnotch (t_{notch});
- The stresses under an angle in the beam element.

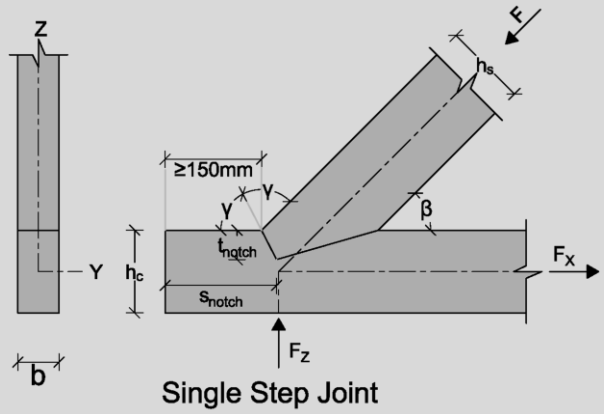

For the transference of compressive force F_{Ed} the following equations may be used:

Shear-plane length: $s_{notch} \geq \frac{F_{Ed} * \cos\beta}{b * k_{red} * f_{v,d}}$ (II-15)

- k_{red}=0,6 *for sawn timber*
- k_{red}=0,8 *for glulam timber*

Notch depth: $t_{notch} \geq \frac{F_{Ed} * \cos\beta}{b * f_{c,\alpha,d}}$ (II-16)

- $\alpha = \frac{1}{2}\beta$ *for Single Step Joints*
- $\alpha = \frac{3}{4}\beta$ *for Double Step Joints*

Strut height: $h_s \geq \frac{F_{Ed}}{b * f_{c,\alpha,d}}$ (II-17)

- $\alpha = \beta$

Where

b is the width of the strut;

β is the angle between force F_{Ed} and the fiber direction.

$f_{c,\alpha,d}$ is calculated as follows:

$$f_{c,\alpha,d} = \frac{0{,}8 * f_{c,0,d} * f_{c,90,d}}{0{,}8 * f_{c,0,d} * sin^2\alpha + f_{c,90,d} * cos^2\alpha} \quad \text{(II-18)}$$

α is the angle between the acting stress and the direction of the fiber

Quote 6: Design stress resistance check in the Swiss SIA 256 Holzbau

3. Conclusions

In this research the stress distributions in a Single Step joint are investigated. This is done by a numerical and experimental study. Results from these studies are compared with assumptions made in national standards. Conclusions are made using the set research questions.

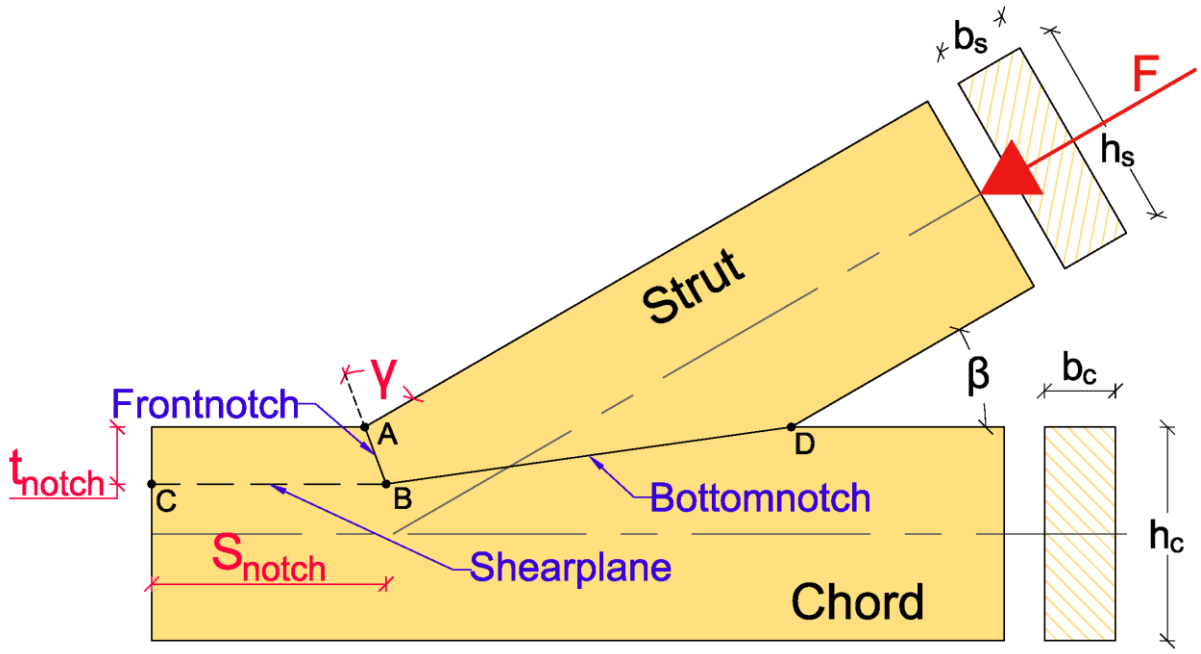

Figure 15: Terms and plane definitions used in the conclusion

3.1 Sub question A

"What is the difference in stress-distribution for the shear stresses in the shearplane as it varies in length?"

To answer this question, three different shearplane lengths s_{notch} are investigated. A reference length of 500mm is taken, as this is the upper limit over which the shear stresses may be distributed according to the German code ($max. = 8 \cdot t_{notch}$). A length of 750mm is taken to investigate the differences in stress distribution if the shearplane length is larger than 500mm, a shorter length of 300mm is taken to see the influence of a shorter shearplane length. The results from the numerical simulations are shown in Figure 16. These simulations showed very similar behavior between lengths of 500mm and 750mm. From this, it can be concluded that a shearplane length larger than $8 \cdot t_{notch}$ does not have any influence on the shear strength of the connection. Where the two larger shearplane lengths give an "exponential" stress distribution, the 300mm shearplane length has an almost linear stress distribution. This short length clearly has an influence on the stress distribution. This is confirmed by the lower ultimate load of 64.8kN in the 300mm simulation compared to 81.4kN in the other two simulations.

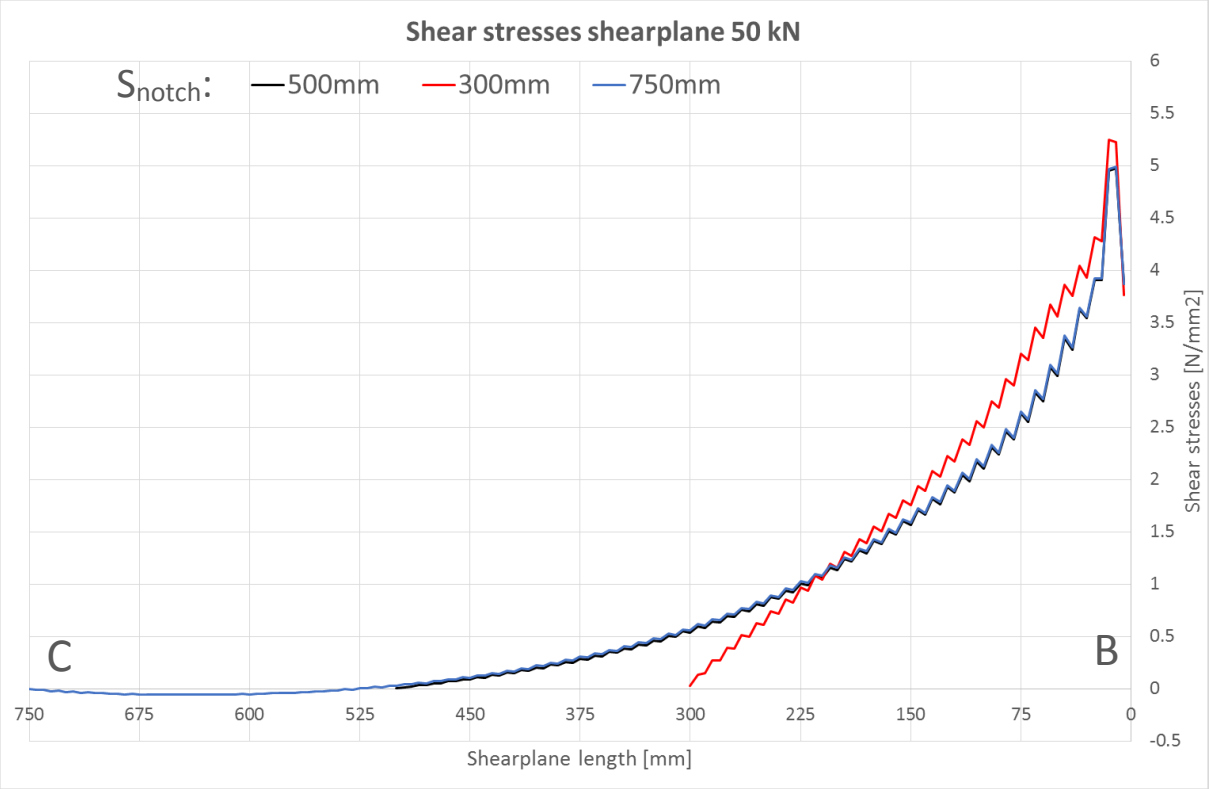

Figure 16: Shear stress distributions in the shearplane (CB) for different shearplane lengths.

The ultimate loads measured in the experimental tests are higher than that of the numerical simulations. This can be related to conservative numerical strength values, different failure mechanisms, or the influence of inhomogeneous test specimens. The ratio between failure loads however, shows the same pattern as in the numerical simulations. Specimens with a 300mm shearplane length failed at an average load of 82.3kN. It is important to notice that all specimens failed in shear. The specimens with 500mm and 750mm shearplane length failed at a larger ultimate load of respectively 93.3kN and 90.4kN. Only one specimen in each series failed in shear.

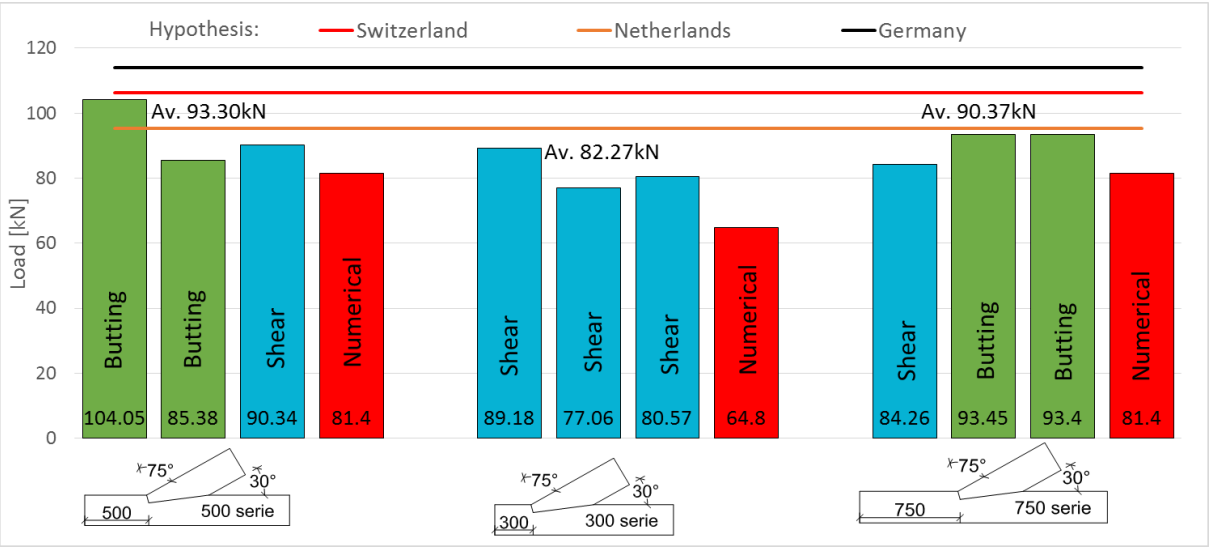

Figure 17: Results of different shearplane lengths of the experimental tests and numerical simulations

The hypothesis (based on the national standards) of the experimental tests showed a large overestimation of the shear strength. The hypothesis showed shear capacities for all geometries above 100kN, and a maximum up to 303kN. Together with the results of the stress distribution in the numerical simulation, this overestimation can be explained by the assumption of an equally distributed stress distribution that is assumed. In reality this stress distribution is not at all equally distributed. A triangular linear stress distribution would be much more representative.

3.2 Sub question B

"What is the stress-distribution over the length of the front-, and bottomnotch?"

This sub question can be answered using the results of the numerical simulations. The numerical study showed very identical stress distributions in both contact areas of the notch independent of the differences in geometry. The stresses in the bottomnotch are only investigated in the REFGEOM simulation, as the stresses in the bottomnotch are very low. Even peak stresses are well below the characteristic strength. These stresses are likely to increase if the connection angle β is increased. This was not investigated in this research. The stress distribution of the bottomnotch showed relatively high stresses near the back of the notch compared to the rest of the bottomnotch length. This can be related to bending of the beam member which is caused by the displacement of the diagonal element. The stress distribution in the bottomnotch during loading is shown in Figure 18.

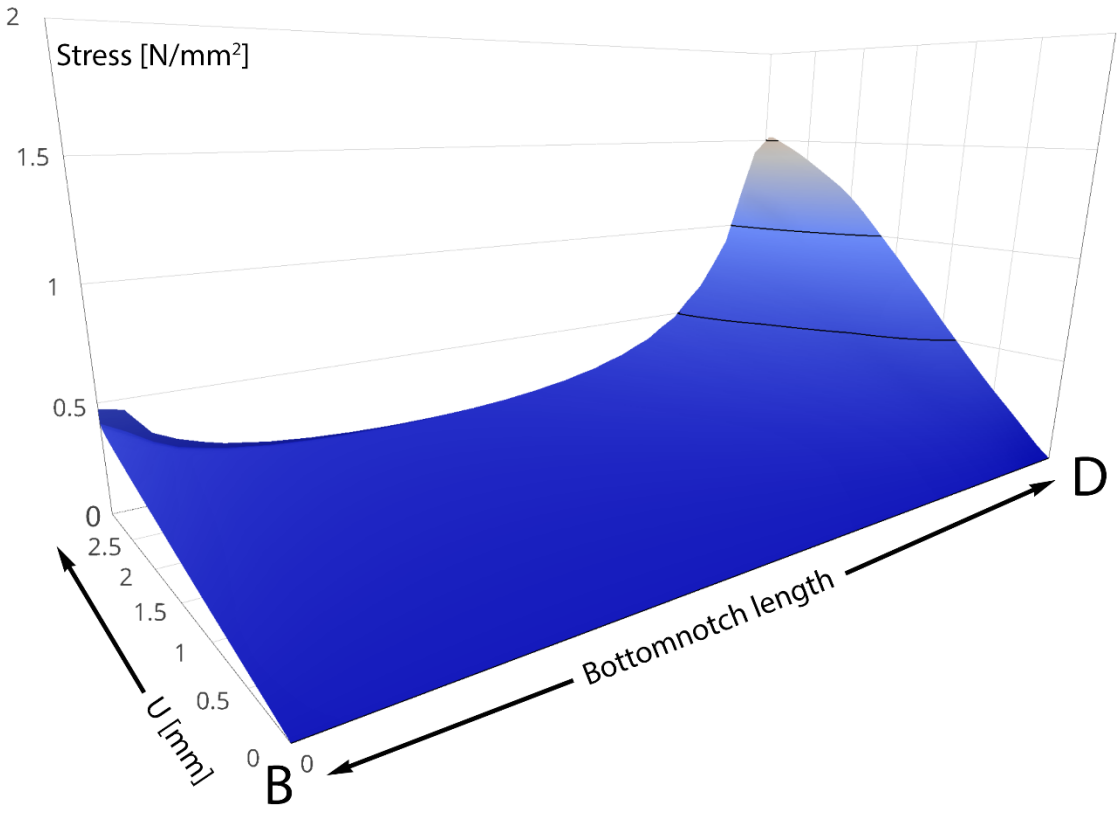

Figure 18: Stress distribution of the principal stresses orientated perpendicular to the bottomnotch (BD) surface

The stresses in the frontnotch showed almost identical distributions. This is shown in Figure 19. Peak stresses occur at both sides of the frontnotch, with the total distribution acting parabolically shaped. As the load increases towards the ultimate load, the peak stresses disappear and the load can be considered equally distributed (Figure 20). This equally distributed load in the frontnotch is also assumed in the considered national standards. The results of the numerical simulations does not give results to assume this is not representative.

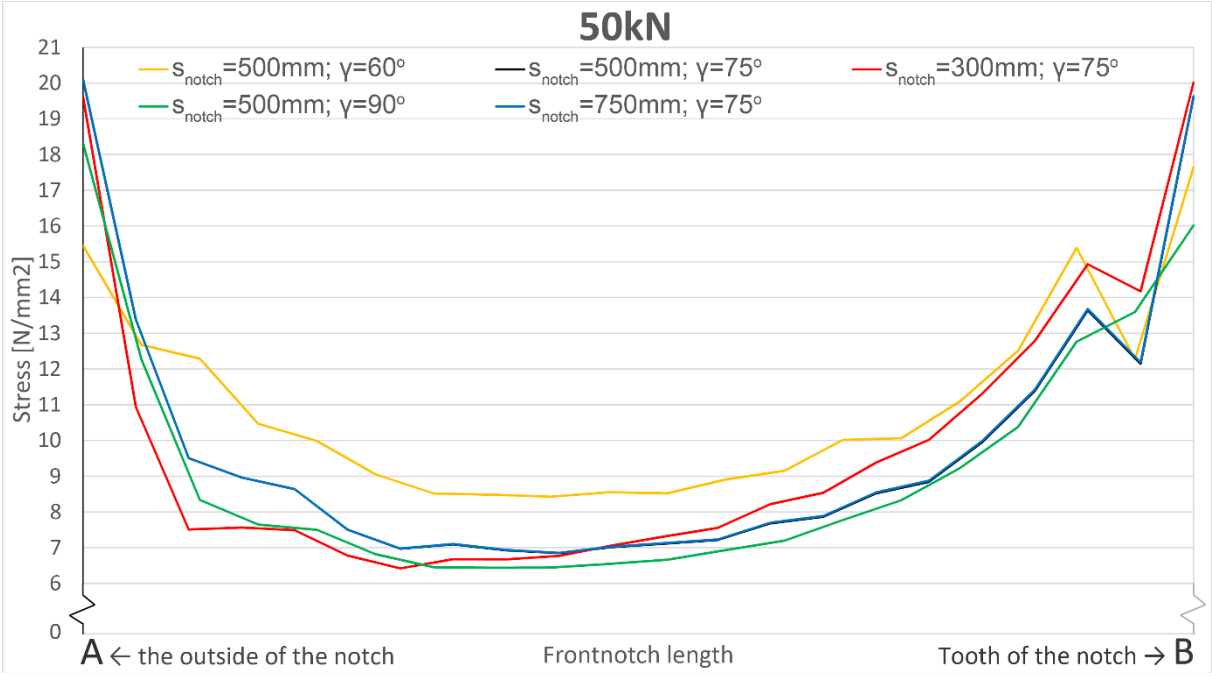

Figure 19: Stress distribution of the principal stresses in the frontnotch (AB) at a load of 50kN

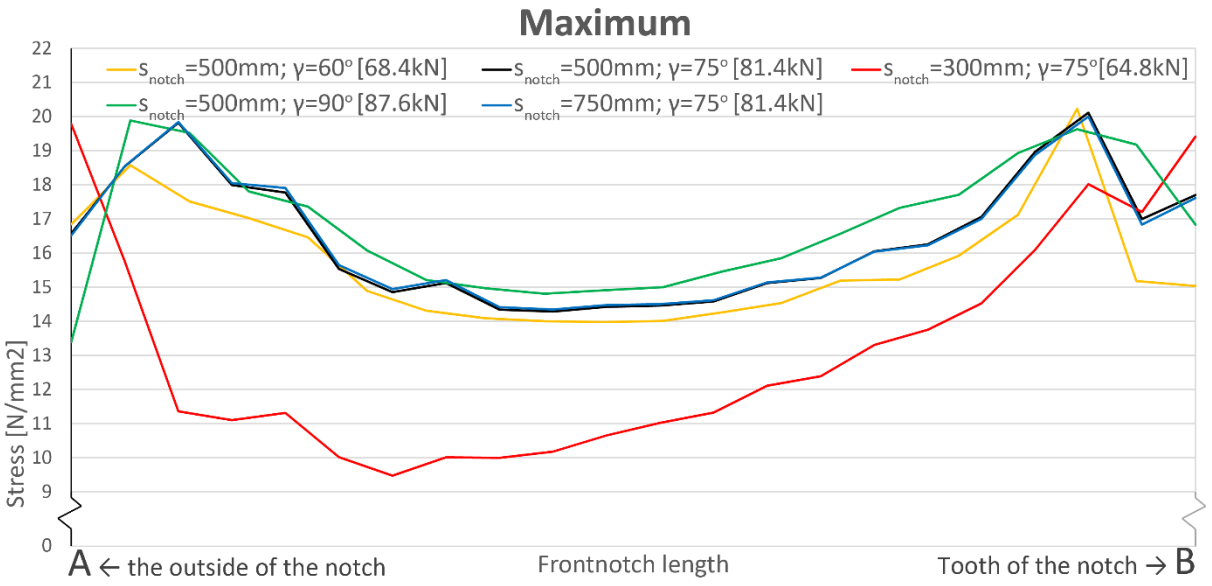

Figure 20: Stress distribution of the principal stresses in the frontnotch (AB) at the maximum load

3.3 Sub question C

"What is the influence of frontnotch angle γ on the stress-distribution in the frontnotch and the shearplane?"

To investigate the influence of the angle of the frontnotch on the stress distributions, three different angles are investigated. The reference angle of γ, in the case of the geometry in this research is 75°. This angle is the intermediate value of two extremes. These extremes are shown in Figure 21:

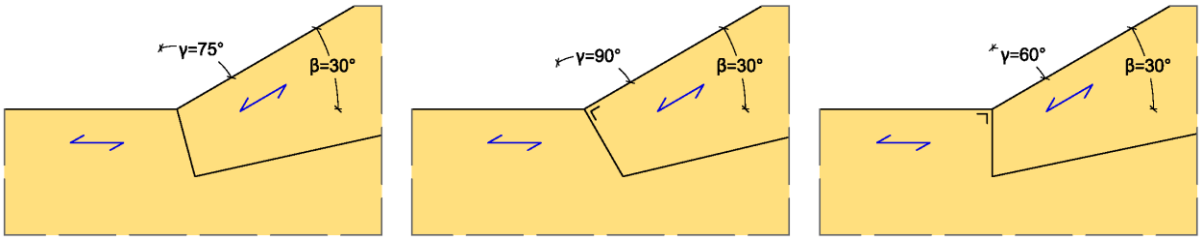

Figure 21: Angles of the frontnotch used in this research

As the connection angle β is 30°, also the difference in fiber direction between both elements is 30°. The results of the numerical simulations show that the principal stresses in the frontnotch act at the intermediate angle of 15° to the fiber direction in all simulations, independent of the angle γ of the frontnotch. For the reference geometry with a frontnotch angle γ of 75° this principal stress angle is to be expected as this means that the stresses act perpendicular to the frontnotch surface. This is not the case for frontnotch angles γ of 60° and 90°. As the stresses still are orientated 15° to the fiber direction of both elements, these stresses do not act perpendicular to the frontnotch surfaces. This can only be explained by the presence of friction in the contact surfaces of the timber elements in the frontnotch. Even using a for timber low friction coefficient, the stresses are still able to orientate towards the intermediate angle, as shown in Figure 22.

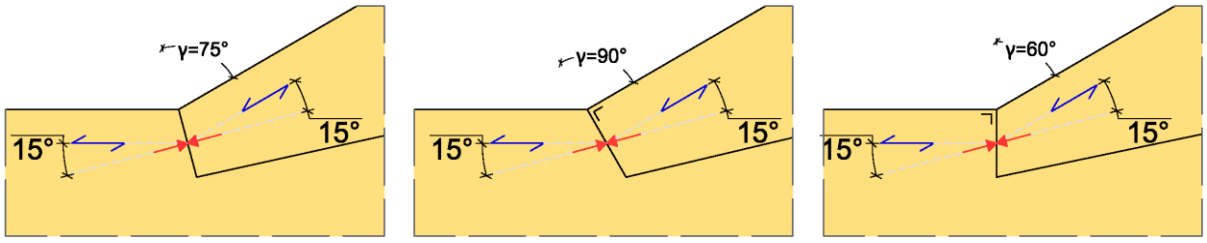

Figure 22: Orientation of the principal compressive stresses to the fiber direction in the frontnotch for different angles of γ

Although the angle of the frontnotch seems to have no influence on the angle of the principal compressive stresses in the frontnotch, angle γ does seem to have an influence on the shear stresses in the shearplane under high loads. This shear stress distribution is shown in Figure 23. For frontnotch angle γ = 90°, the ultimate load of the model is highest; 87.6kN. The stress distribution also shows the highest capacity. The simulation with frontnotch angle γ = 60° shows the lowest ultimate load of the trio of 75.4kN. The stress distribution confirms this, as it shows the lowest capacity.

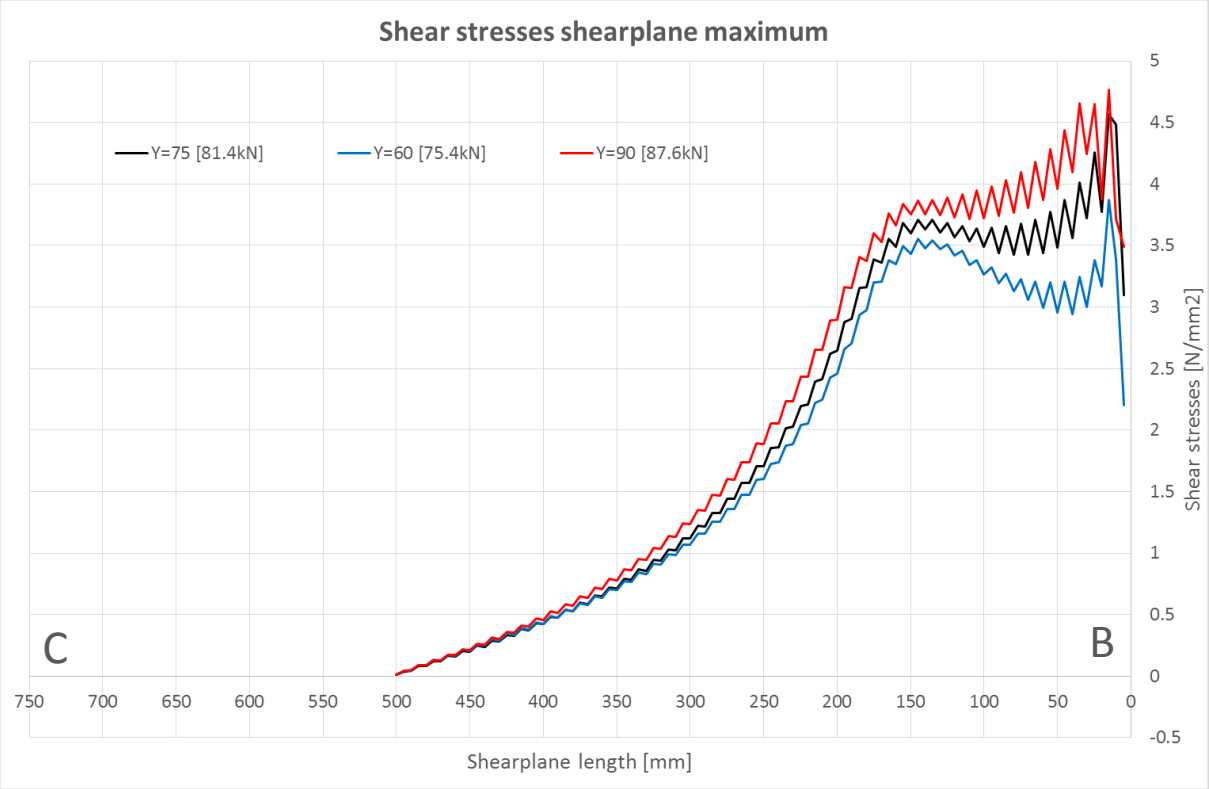

Figure 23: Shear stress distribution in the shearplane (CB) at maximum loads for different frontnotch angles γ

The behavior of the simulations is confirmed by the results of the experiments. Here, the specimens with the frontnotch angle γ of 90° (90D series) showed significantly higher failure loads. Although the hypothesis predicts butting failure much earlier than shear failure, two specimens failed in shear. The specimens with frontnotch angle γ of 60° (90B series) show lower failure loads, also two times due to shear failure.

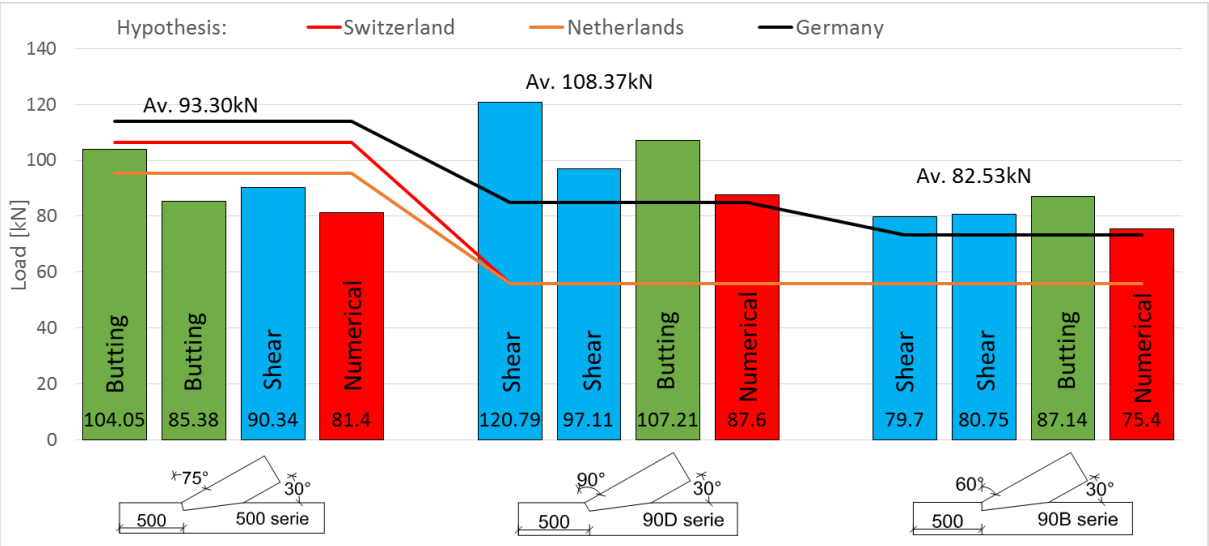

Figure 24: Failure loads of the experimental test specimens with different frontnotch angles γ

3.4 Main research question

"What geometric boundaries (angle γ, depth t_{notch}, length s_{notch}) can be applied to the connection according to the results of this research?"

Frontnotch angle γ

The results of this research show that the influence of the frontnotch angle on the principal stresses in the frontnotch is very little. Looking at the shear stress resistance, the angle of the frontnotch γ preferable would be between 75° and 90°. This is in accordance with the design rules for the frontnotch angle in the Dutch NA to EC5. (II-3) The 75° angle leads to an intermediate angle of the frontnotch, giving it the same orientation for the diagonal element and beam element. The angle γ lower than 75° that was tested showed less load carrying capacity. The tested angle of 90° showed slightly higher capacity, but this requires sufficient friction to occur in the frontnotch plane. Angles larger than 90° give a high risk of the diagonal element 'popping out' of the notched beam, resulting in failure of the connection.

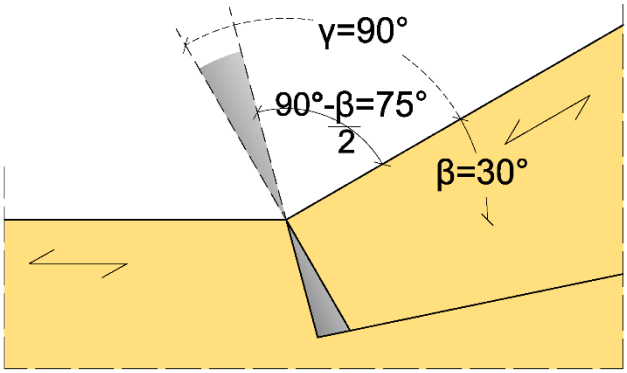

Figure 25: Boundary conditions for Frontnotch angle γ

β = 30° was the only investigated connection angle in this research. With this angle, the orientation of the principal stresses remained unchanged, regardless the frontnotch angle γ, due to sufficient friction in the frontnotch contact surface. It is recommended to do further research on the orientation of principal stresses when the angle β is increased over 30°.

Notch depth t_{notch}

The used notch depth of 62.5mm (h_c / 4) is according to the maximum notch depth as defined in the codes (II-2), (II-8), (Table 4). This was the only depth that was used in this research.

It is assumed that the notch depth does have influence on the butting failure behavior of the connection. The depth dictates the available surface area over which the compressive forces can distribute. As seen in the numerical simulations and experimental tests, the connection can fail in shear. This is a brittle behavior, and is therefore not wanted. To prevent brittle shear failure, the butting capacity of the connection can be reduced by reducing notch depth, ensuring butting failure before critical shear stresses are reached.

It is advised to not increase the notch depth larger than the tested h_c / 4. Instead, reducing the notch depth could prevent brittle shear failure. The ratio between probabilities of brittle shear failure versus butting failure, also is influenced by the connection angle β. This variable β could therefore also be included for determining the notch depth t_{notch}.

It is recommended to do further research on the topic of the notch depth.

Shearplane length s_{notch}

The results of the numerical simulation show that the shear stress distribution does not change for shearplane lengths larger than 500mm ($8 \cdot t_{notch}$). This upper limit, as defined in the German NA to EC5, should therefore be kept. Lengths smaller than this limit lead to unnatural (forced) shear stress distributions. Therefore, design rules should advise to design a shearplane length of $8 \cdot t_{notch}$, and if this is not possible, reduction factors on shear strength, due to the forced stress distribution, could be applied.

The numerical simulations showed a shear stress plateau was able to form in the first 150mm of the shearplane. The Swiss 'SIA 256 Holzbau' code requires a minimum shearplane length of also 150mm. With the numerical study showing that this length is able to take a large value of shear stresses (independent of the full shearplane length) it is advised to give the shearplane a minimum length of 150mm, as stated in the Swiss code.

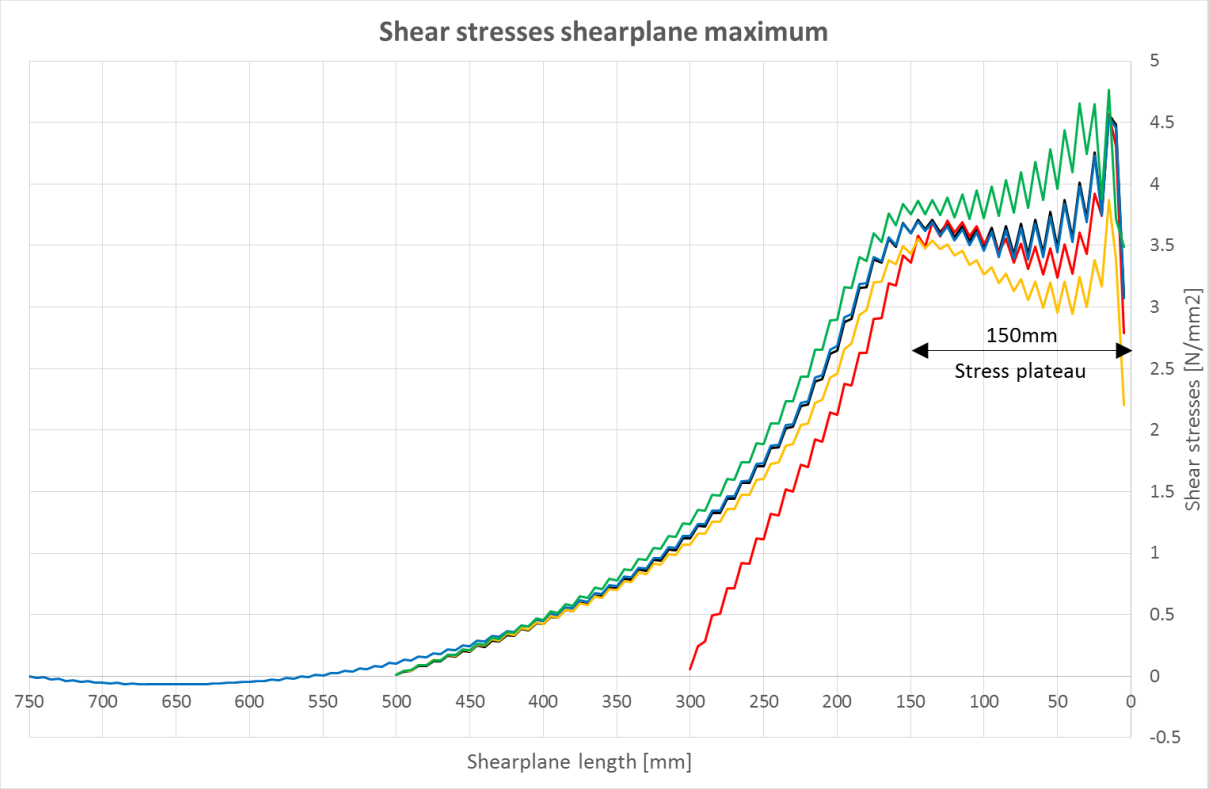

Figure 26: Shear stress plateau able to form in the first 150mm of the shearplane

The assumption in the three investigated codes, that the shear stresses are uniformly distributed over the shearplane length, is incorrect. This assumption can lead to a very large overestimation of the resistance against shear failure, even using characteristic shear strengths. Instead, codes allow a much less brittle 'butting' failure to appear governing. The majority of the experiments, and all numerical simulations, showed brittle shear failure before the ultimate compressive strength (under an angle α) in the frontnotch (butting) was reached.

4. Further research

Results from the numerical simulations and the experiments helped answering the research questions in this research, but it has also raised new questions. Recommendations for further research are given in order to investigate several topics:

Notch depth t_{notch}
The notch depth was kept constant in this research. Upper-, or lower limits for the notch depts. Are not investigated. More research must be done in order to find these limits. Also, it is recommended to do a study on the influence of a (reduced) notch depth on the ratio of probability on brittle shear failure, versus butting failure (stresses under an angle α) in the frontnotch.

Connection angle β
The value of frontnotch angle γ is dependent on the connection angle β. This influence the orientation of the principal stresses to the grain direction (α). This research showed that for an angle β of 30°, the principal stresses are not influenced by frontnotch angle γ, due to the presence of friction in the frontnotch contact surface. It is recommended to investigate the influence of friction on the orientation of the principal stresses in the frontnotch for angles β > 30° (as they are most common in Single Step joints).

Shear resistance
Much is still unclear about the shear strength of timber in general. Although codes assume the shear strength of a timber beam is related to its strength class, several researches [6]–[8] state that this is not the case. As the shear strength of timber is of great influence on the strength of a Single Step joint, more research on this topic is recommended.

Bibliography

[1] J. Siem and A. Jorissen, “COST Action FP1101 Assessment , Reinforcement and Monitoring of Timber Structures,” Eindhoven, 2014.

[2] NEN, “NEN-EN 1995-1-1.” 2005.

[3] NEN, “NEN-EN 1995-1-1 Dutch NA 8.11 Ambachtelijke verbindingen.” Nederlands Normalisatie-Instituut, Delft, 2013.

[4] DIN, “DIN-EN-1995-1-1 German NA 12.1 Versätze.” DIN Deutsches Institut für Normung, Berlin, pp. 88–89, 2010.

[5] SIA, “Schweizer Norm SIA 265 - Holzbau.” SIA, Zürich, pp. 77–78, 2012.

[6] M. Poussa, P. Tukiainen, K. Mitsuhashi, and P. Anderisin, “Destructive Tension-, Shear- and Compression- (0 and 90) strength-tests for Finnish sawn timber,” Helsinki, 2007.

[7] P. Glos and J. Denzler, “Working Commission W18 - Timber Structures - Meeting 36, Colorado USA August 2003,” in *Characteristic shear strength values based on tests according to EN 1193*, 2003, no. August, pp. 91–101.

[8] R. Spengler, *Festigkeitsverhalten von Brettschichtholz unter zweiachsiger Beanspruchung*. 1982.

Technische Universiteit
Eindhoven
University of Technology

Where innovation starts

Part II - Numerical study

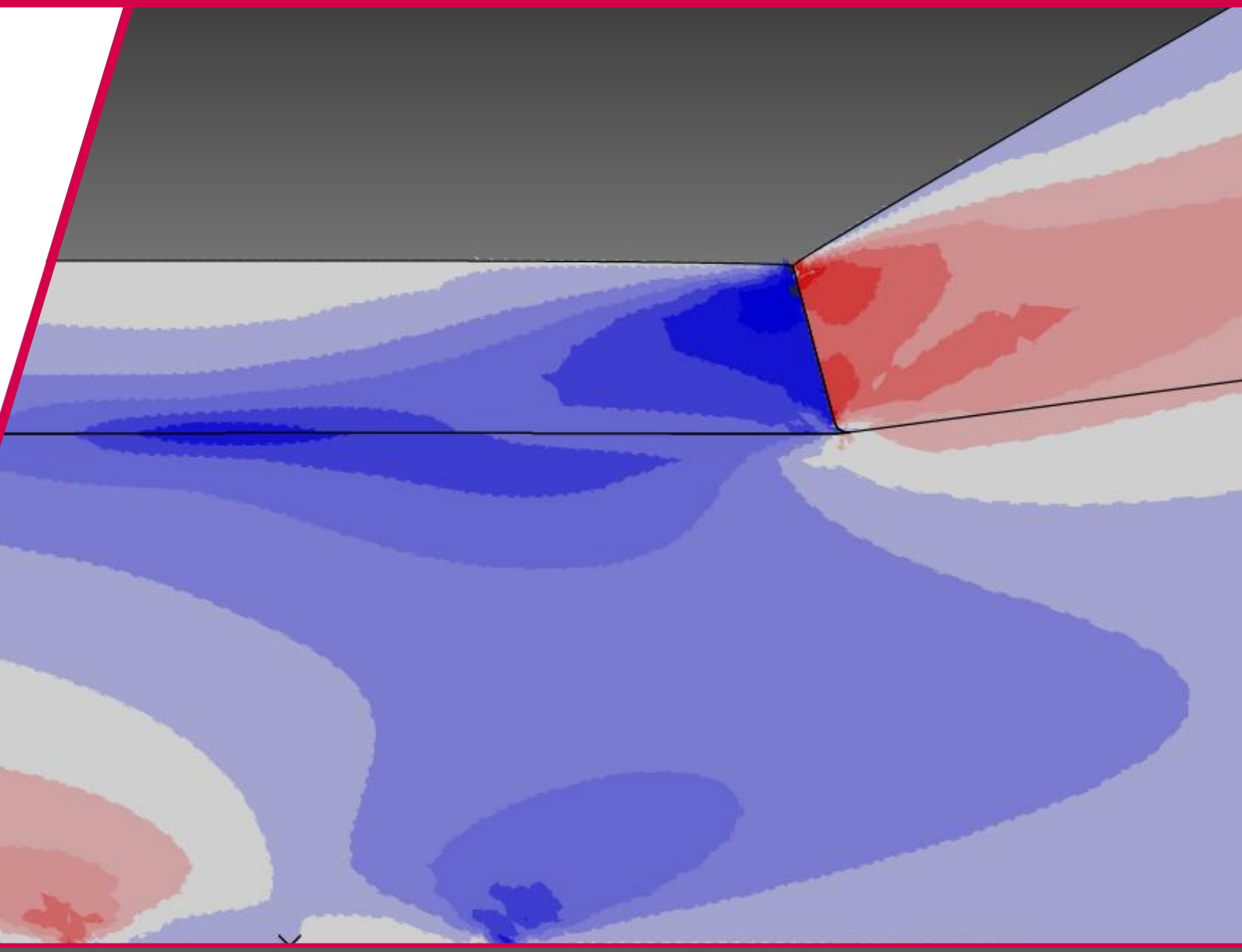

Stresses in a Single Step Joint

April 20, 2016 | Master thesis Structural Design | Richard de Rijk

Abstract

This numerical study contains all procedures which have been done to do a finite element (FE) simulation to find several interesting stress distributions in a Single Step joint. First, a geometric study has been done to determine which geometries and measurements are of interest for the numerical simulations. Second, the numerical parameters which suite the material behavior of wood are explained and determined. Third, the choices and assumptions which have been made to model a practical model which simulates the behavior of the connection as it would in reality. Fourth, the full model is explained and choices are justified, the results of the numerical simulations are presented. Fifth, results are compared with each other and to the 'Electronic Speckle Pattern Interferometry' (ESPI) results of the experimental study.

Table of Contents

1 Geometric study

1.1 Dimensional boundaries

Beam dimensions

The first step to find dimensions for the numerical model is to find a suitable beam dimension. Since the numerical model is verified using experiments, the beam dimensions in the numerical model are dependent on the practical situation. A cross-section of b_i = 70mm, h_i = 250mm is chosen. This is a practical dimension since a standard size of 75x250 (planed 70x245) is available. The height of about 250mm is chosen because this means a bigger notch depth is allowed. This enlarges the space for measuring instruments in the experiments. The width of 70mm has no (or very little) influence on the results of the stress distribution. This width is only important in the experimental tests to give the specimen out-of-plane stiffness and thereby stability.

Figure 1: Specimen for the experimental campaign

Inclination angle β

The inclination of the connection for this research is set at an angle β of 30°. The range of angles β that could appear varies from the lower limit of 0°, which is impossible to make and meaning the chord would be loaded parallel to the grain. The upper limit is 90°, where the chord would be loaded perpendicular to the grain, but this type of connection would not be classified as a carpentry connection. An angle of 45° is the middle of the range and is an angle which is most used when applying a Single Step Joint since it is most used in roof-supporting structures which often have an inclination of ± 45°. For this research, using the angle of 45° would result in equal horizontal and vertical force components. Since the vertical component would be mainly transmitted through the bottomnotch and act as a force on the weaker perpendicular to the fiber direction of the chord this would only result in large deformations of the chord under the bottomnotch. For this research the most interesting situations (Shear stresses and failure of the shearplane, and the angle of the frontnotch) are dependent of the horizontal force component. Using a slightly steeper angle β of 30° ensures the geometry is still practically relevant and gives a positive contribution to the stress situations in the investigated areas.

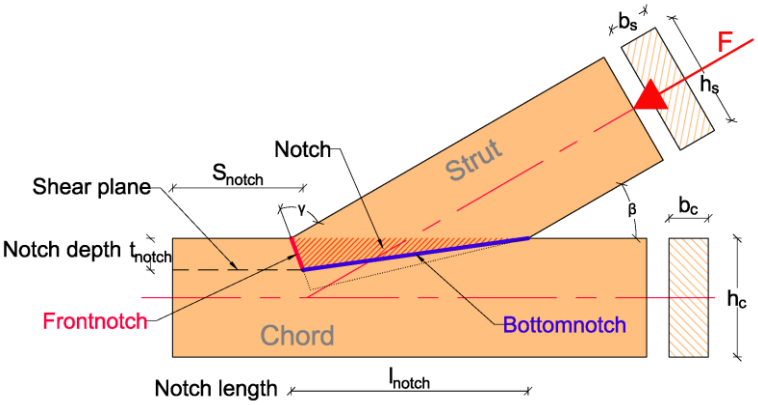

Figure 2: Geometry of a Single Step Joint

Frontnotch depth t_{notch}

The depth of the frontnotch is based on a maximum depth value of beam height $h_c/4$ following from several national annexes to Eurocode 1995-1-1.[1]–[3] Since this maximum depth also offers the maximum area of the frontnotch this offers the biggest benefit for the overall strength of the connection. It is logical that, if the practical situation allows it, the maximum depth is chosen.
For this research, using a beam height of 250mm, the notch depth is 250 / 4 = 62.5mm.

Shearplane length s_{notch}

The length of the chord (beam element) from the notched area to the end of the chord is used to transmit shear stresses resulting from the force transmitted through the frontnotch area. This length is therefore called the shearplane. This length varies in this research. The codes [2] give an upper limit for this length, over which it may be assumed that the shear stresses act, of 8 * t_{notch}. This length, of 8 * 62.5 = 500mm, is the reference variable length in this research. Also, a larger length of 750mm is chosen to measure the influence on the stress distribution of a larger length than 8 * t_{notch}, and a much shorter length of 300mm is chosen to investigate the stress distribution and possible failure mechanism of a length which is much smaller than the upper limit.

Frontnotch angle γ

The angle of the notched part of the connection is varied in this research. In most national codes the angle of the frontnotch is set at a fixed value of γ = 90° - β/2 as shown by the middle line in Figure 3. This value is based on the intermediate value of two limits for this angle:

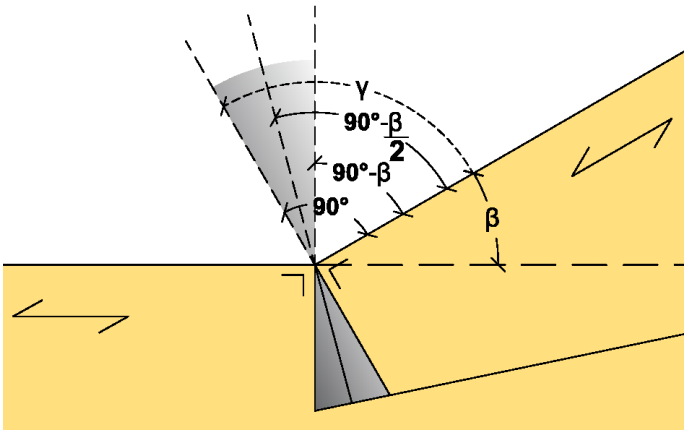

Figure 3: Range of angles of the frontnotch

- The smallest angle is γ = 90° - β. This angle means that the frontnotch is perpendicular to the length (and fiber direction) of the chord. If the angle is made any steeper, the strut could wedge out the top side of the chord along the shearplane length due to the load in the strut.
- The upper limit is an angle γ of 90°. This means that the front of the strut is right angled. If this angle is made any bigger, the possibility exists that the strut could “pop out” of the notched chord because of the load overcoming the friction between the surfaces.

The upper limit, lower limit, and the intermediate angle of γ are used in this research.

1.2 Numerical models

With all mentioned boundary conditions given in the codes to Single Step joints, a selection of numerical models is simulated. These geometries are also tested in the experimental campaign.

Table 1: Numerical simulations for different boundary conditions

Frontnotch angle → Shearplane length ↓	γ = 90° - β = 60°	γ = 90° - β/2 = 75°	γ = 90°
S_{notch} = 300mm		SHEARPLANE300	
S_{notch} = 500mm	FNANGLE90B	REFGEOM	FNANGLE90D
S_{notch} = 750mm		SHEARPLANE750	

REFGEOM

This geometry is most favorably to design, since the design rules allow the highest loads. This geometry is used as a reference for all other numerical simulations because each other simulation has only one different boundary, making it easy to see the influence of this boundary.

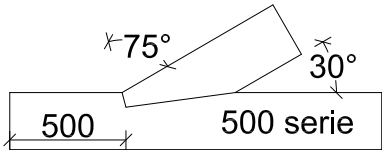

SHEARPLANE300

This geometry has a short shearplane length of only 300mm; 200mm shorter than the reference geometry. In this simulation, the distribution of the shear stresses over the shearplane length is most important.

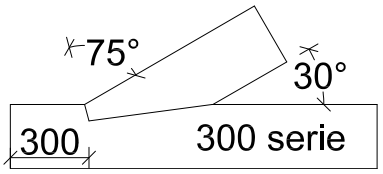

SHEARPLANE750

This geometry has a larger shearplane length than the reference geometry. This means that in this simulation, also the distribution of the shear stresses is most interesting.

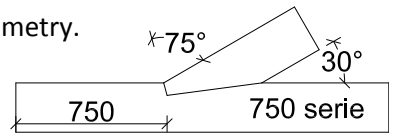

FNANGLE90D

The abbreviation for this simulation means that the angle of the frontnotch is perpendicular (90°) to the Diagonal element. In this model the shearplane length is 500mm, as used in the reference geometry. Only the angle of the frontnotch differs from the reference geometry, γ = 90° instead of 75°.

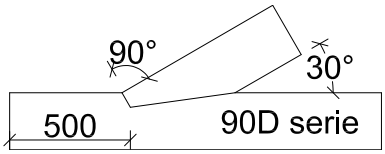

FNANGLE90B

In this geometry, the frontnotch angle is perpendicular to the Beam element. Meaning γ = 60°.

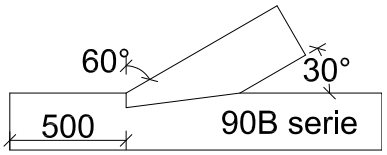

1.3 Boundary conditions

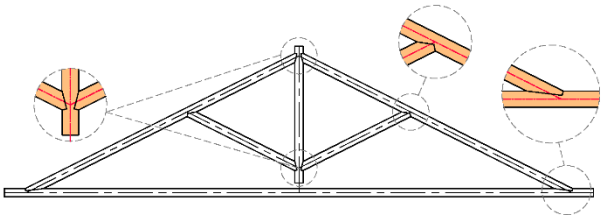

Figure 4: Single Step joints in a triangular roof-truss structure

Now that the geometries are determined, the boundary conditions which are given to the model can be determined. The connections occurs most often in a timber triangular roof-truss structure. This can be in all the connections in the truss which are loaded in compression. For larger trusses, this can be in secondary structural elements, but in almost all historical trusses, the connection occurs at the foot of the truss, near the vertical support of the structural walls. This research investigates that connection. Therefore the boundary conditions at the foot of a triangular truss must be satisfied in the simulations.

In reality, the mechanical scheme of the connection would look like this:

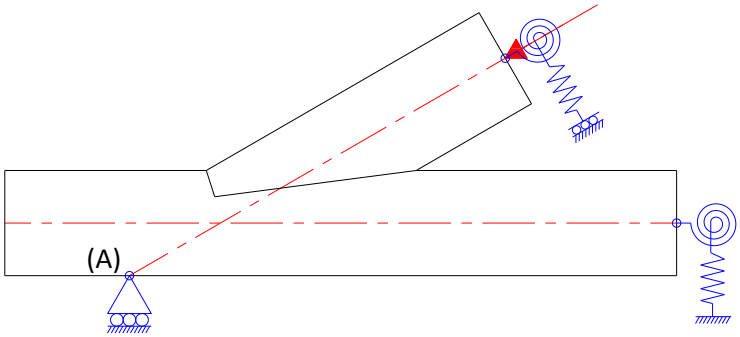

The vertical truss support (of the structural walls)(A) can be seen as a roller support, which is fixed in vertical direction, and can move freely in horizontal direction. Also, the beam is free to rotate in this point. The other two boundary conditions occur when the structure is cut to the geometry which is presented, but the internal forces must stay the same. The boundary conditions in the cut of the beam must have stiffness against rotating, and moving vertically. Therefore, two springs must be simulated in this cut. The diagonal has the same boundaries, but this boundary is also free to move in horizontal direction, to allow the force to apply deformation.

Although these boundaries can be applied in the numerical simulation very easily, to simulate them in the experimental campaign would be very difficult. Therefore, the boundary conditions which can be created in the experiments, closest to reality, are applied in both the experiments and the numerical simulation. These are:

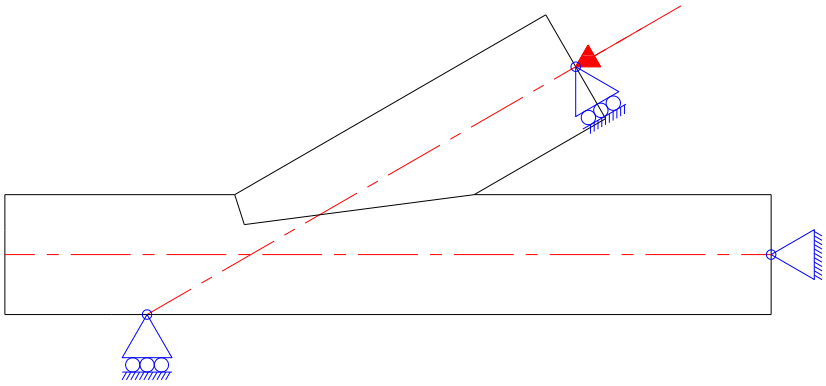

This means that the beam element is hinge supported at the back in both horizontal and vertical direction, representing the full length truss beam. And the beam is vertically supported at the front, which represents a structural wall. The diagonal is supported along the longitudinal direction, and free to deform in force direction. Although this diagonal element in practice is also loaded in bending (due to self-weight of the roof cladding, and live (snow) loads), this is neglected in this research. The effect of bending (rotation) in the diagonal on the strength of a Single Step joints has been often researched in other researches.
As the applied supports do not give accurate internal bending forces, these bending forces must be reduced as much as possible.

Location of the vertical roller support

For determining the ideal position of the support under the beam, a numerical study has been done, comparing the deformation shape and stiffness of the overall connection. Three different locations are investigated:

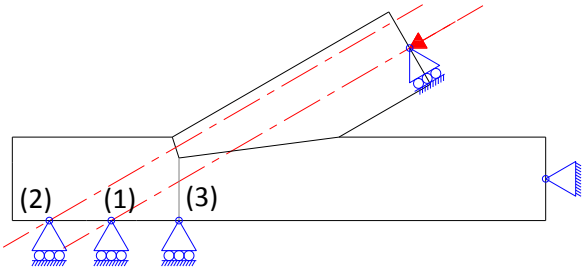

Figure 5: different support locations of the chord

1. The first location is in the line of the acting force. (middle support in Figure 5) This position was chosen to reduce a shear force in the beam to a minimum, meaning that the beam would be mainly loaded in tension. *[Reference geometry]*
2. The second option for the support was based on the force flow through the frontnotch. Since the frontnotch is loaded more parallel to the grain than the bottomnotch, this part has a much larger stiffness. The stresses resulting from the applied force would therefore concentrate at the frontnotch plane. If a force line would be drawn here, the support would be much closer to the frontend of the beam. (Left support in Figure 5) *[Frontsupport]*
3. A third options was investigated to get more insight in the behavior of the varying support location. In this variant the support is placed directly under the notch. *[Backsupport]*

The first step in the investigation is determining the stiffness for the three different support locations using linear elastic material behavior. The force-displacement behavior and reaction forces are compared.

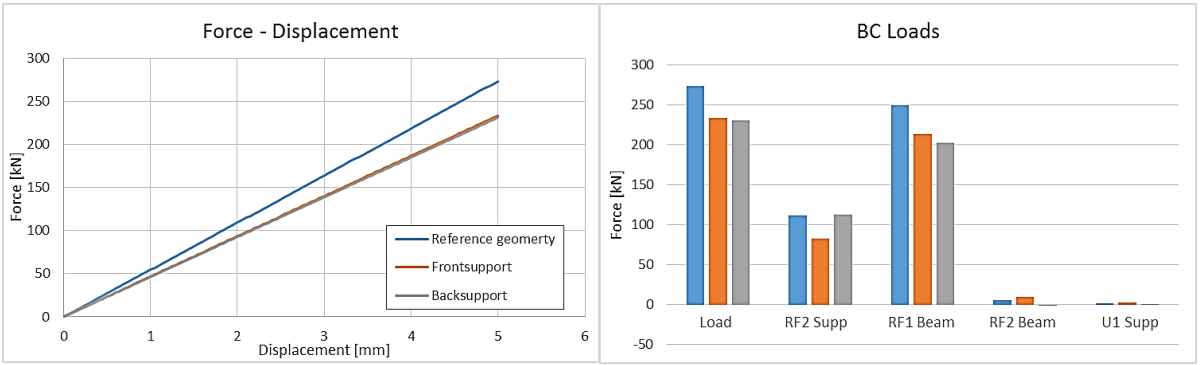

Figure 6: a) Force-Displacement of the top-center of the strut, b) Load and Reaction forces in the supports of the model. LE

From Figure 6 it can be concluded that geometry (1) has got the highest stiffness and leads to the highest reaction forces for an introduced displacement of 5mm. Since this is only linear elastic behavior, more numerical simulations have been done including; LE material behavior with the

possibility of shear failure along the shearplane, Plastic behavior without shear failure, and finally plastic material behavior with possible shear failure which is most comparable with reality.

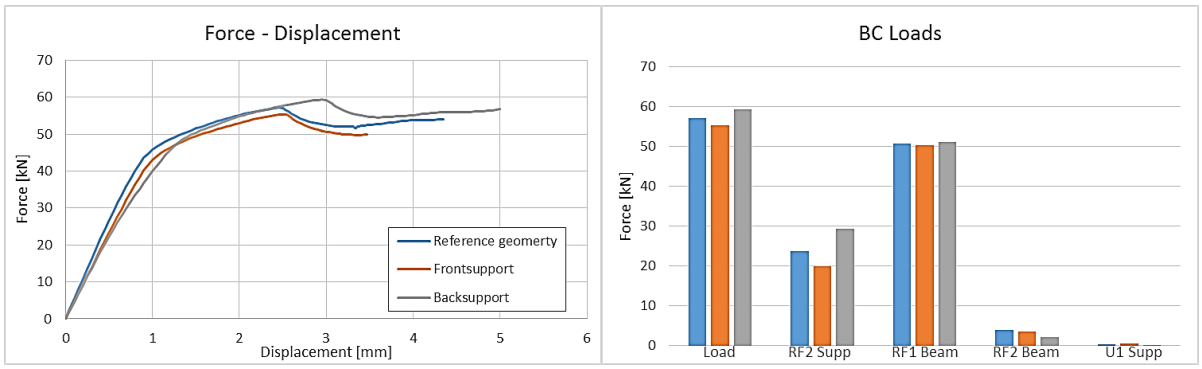

Figure 7: a) Force-Displacement of the top-center of the strut, b) Load and Reaction forces in the supports of the model.

The plastic behavior is presented in Figure 7. Again, the stiffness in the linear elastic part of geometry (1) is highest but it does not reach to the highest failure load. This can be explained by failure along the shearplane. As this geometry is the stiffest, it has the lowest deformation capacity due to which all stresses increase, resulting in early shear failure. From the previous comparison it can be concluded that the support placed in (1) has the highest stiffness, resulting in higher stresses and lower deformations. This is desirable in this research. The deformation of the plastic (with shear) cases is also visually compared:

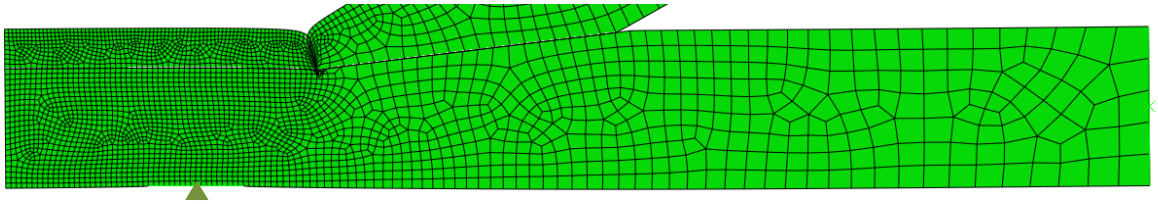

Figure 8: Deformations of geometry (1) [Reference geometry] (scale 10:1)

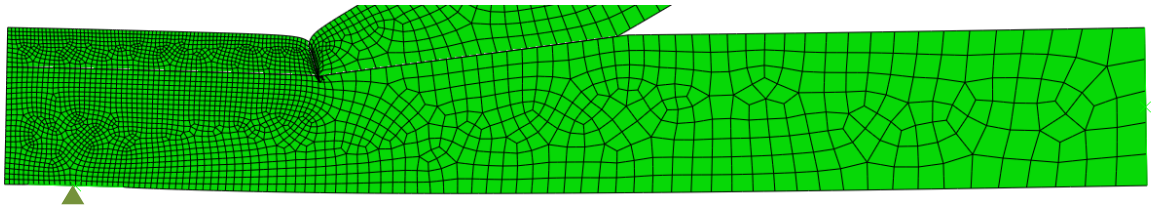

Figure 9: Deformations of geometry (2) [Frontsupport] (scale 10:1)

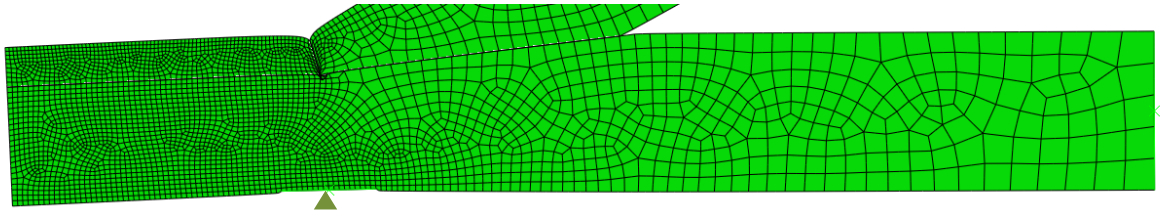

Figure 10: Deformations of geometry (3) [Backsupport] (scale 10:1)

From these figures it can be concluded that placing the support directly in the line of the applied load (1.) leads to minimal bending deformations of the beam element, resulting in the stiffest geometry.

2 Parametric study

During modelling of the geometries, several material properties of wood have to be defined. Parameters for these values can be obtained with literature or experimental tests. This chapter threats all used parameters; where they are obtained from, and why this was chosen.

2.1 General values for C24 timber

Density

Although the density of the material does not influence the behavior of the model in the numerical simulations, this value is defined in the model. It gives the option to take gravitational forces into account. This was not done during these simulations.
The density value is obtained from the characteristic value for C24, defined in EN 338. [4]

350 [kg/m^3] → 3.4335E^{-6} [N/mm^3]

Strength values

The axial strength and shear strength values of timber can be defined. These values do not alter the elastic and plastic behavior of the model in any way. Defining these values gives a (simple) graphical option to monitor when these values have been reached. Since, like the density, these values do not influence the material behavior in any way, also standard characteristic values from EN 338 [4] are used, and are statistically rewritten to mean values. (Process described in Experimental study.)

Table 2: Mean strength values of C24 timber [N/mm^2]

Tensile strength fiber direction	Compr. strength fiber direction	Tensile strength transv. direction	Compr. strength transv. direction	Shear strength
21	-31.5	0.75	-3.75	3.75

2.2 Elastic behavior

To describe elasticity, several parameters are needed:

- Modulus of elasticity: E1, E2, E3
- Poisson's ratio: v12, v13, v23
- Shear modulus: G12, G13, G23

These values can be found in several sources:
Since the model is in 2D, directions 2 and 3 equal. The following mean values can be found in EN 338: [4]

$E_{0;mean}$ = E1 = 11000 N/mm^2, $E_{90;mean}$ = E2 = E3 = 370 N/mm^2, G_{mean} = G12 = G13 = G23 = 690 N/mm^2.

During the experimental campaign, several secondary material tests were done one the specimens. These tests included tests on compression parallel-, and perpendicular to the grain direction. The results of these tests can be used to find the modulus of elasticity in these directions, giving:

E_0 = 12345 N/mm^2

E_{90} = 117 N/mm^2

The third source is the Wood Handbook. [5] This book contains tables of material properties of a large amount of wood species. Using tables in chapter 5 of the book, the following strength values can be found, using the average of all Pine species:

E_L = E1 = 11044 N/mm^2. This value may be increased with 10% to neglect the effect of shear deformation during stiffness tests, meaning that the final E1 value is: 12149 N/mm^2. Using this value, the modulus of elasticity in the other directions and the shear modulus in all directions can be determined in a table containing ratios between E_L and the other stiffnesses.

Table 3: Modulus of elasticity and shear modulus of Pine wood according to the Wood Handbook.[5] [N/mm^2]

E_L	E_T	E_R	G_{LR}	G_{LT}	G_{RT}
(E1)	(E2)	(E3)	(G12)	(G13)	(G23)
12149	728	1189	968	867	136

The Poisson's ratio is also given per species. Taking the average of all Pine species leads to:

Table 4: Average Poisson's ratios of Pine according to the Wood Handbook.[5]

μ_{LR}	μ_{LT}	μ_{RT}
(v12)	(v13)	(v23)
0.335	0.358	0.416

Several simulations have been done using each source, and also a combination of multiple sources was investigated. The results of these simulations are compared to the experimental tests. Measurements of force and displacements that were made at the actuator in the experiments is compared with the same force and displacements in the numerical simulations. Also the displacement results in the beam that were measured using ESPI is compared with the numerical simulation to determine which parameters should be used to describe the elastic behavior of the material. This comparison led to the conclusion that the shear modulus has a big influence on stiffness of the material. The numerical simulations showed a higher stiffness than in the experiments. The comparison of all simulations with the experimental tests led to the choice of the following parameters to describe the elastic behavior of the material:

Table 5: Used elastic parameters in the numerical simulations

	EN 338	Experiments	Wood Handbook	
E1	**11000**	~~12345~~	~~12149~~	N/mm^2
E2	~~370~~	**117**	~~728~~	N/mm^2
E3	~~370~~	**117**	~~1189~~	N/mm^2
v12	-	-	**0.335**	
v13	-	-	**0.358**	
v23	-	-	**0.416**	
G12	**690**	-	~~968~~	N/mm^2
G13	**690**	-	~~867~~	N/mm^2
G23	~~690~~	-	**136**	N/mm^2

During the comparison of all parameters, it became clear that G12 and all elastic moduli had an influence on the stiffness of the elastic behavior. G13 and G23 had no influence, which is not surprising since a 2D model is used. The Poisson's ratios did have a very slight influence on the stiffness, but this was negligible.

2.3 Plastic behavior

The plastic behavior is based entirely on the experimental compressive test that was performed on the specimen with the grain in load direction (parallel to the grain). This test is described in the Experimental study (Part III). The numerical model requires the plasticity to be defined from the stress at which plasticity starts to take place in the material. The plastic strain at this point is 0. In the test, the stress at which plasticity starts is at 21 N/mm^2. The data from this point on was taken as base for a second order trend line as shown in Figure 11. The function of this trend line is of high enough accuracy (R^2 = 0.9852) to assume that this function describes the plastic behavior of the wood. This function is used in the model:

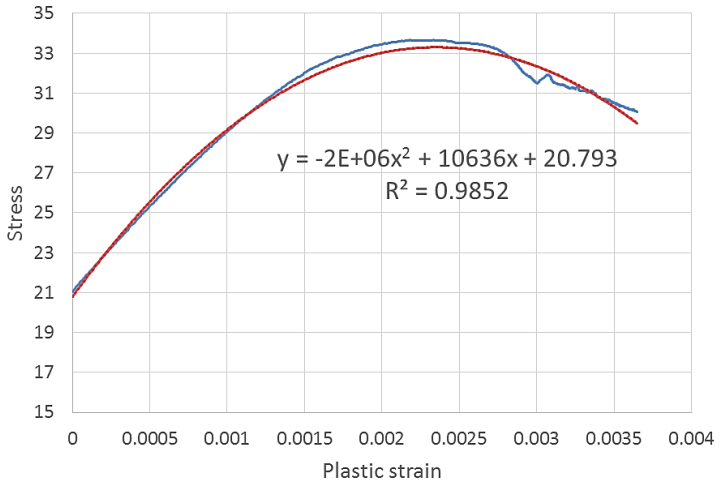

Figure 11: Plastic behavior for the experiments described by a second order polynomial function.

$$y = -2262000 * x^2 + 10636 * x + 20.793 \qquad (2.3\text{-}1)$$

Potential

The plastic behavior as described above only describes the plastic behavior in the '1' direction (parallel to the fiber). To apply plasticity to all other direction, Hill's yield criterion is used in the model. This is done using the following potential factors:

Table 6: Potential factors for all model directions using Hill's yield criterion

R_{11}	R_{22}	R_{33}	R_{12}	R_{13}	R_{23}
1	0.119	0.119	0.371	0.371	0.371

As the '1' direction is used to defined plasticity, this potential factor is 1. Stresses in the other directions are scaled down. Strain is not reduced.

Hill yield criterion (Anisotropic yield) [6]:

$$R_{11} = \frac{\bar{\sigma}_{11}}{\sigma^0},\ R_{22} = \frac{\bar{\sigma}_{22}}{\sigma^0},\ R_{33} = \frac{\bar{\sigma}_{33}}{\sigma^0}$$

$$R_{12} = \frac{\bar{\sigma}_{12}}{\tau^0},\ R_{13} = \frac{\bar{\sigma}_{13}}{\tau^0},\ R_{23} = \frac{\bar{\sigma}_{23}}{\tau^0},\ \tau^0 = \frac{\sigma^0}{\sqrt{3}}$$

Where:

$\bar{\sigma}_{ij}$ = the material strength in that direction;

σ^0 = the reference material strength ($\bar{\sigma}_{11}$).

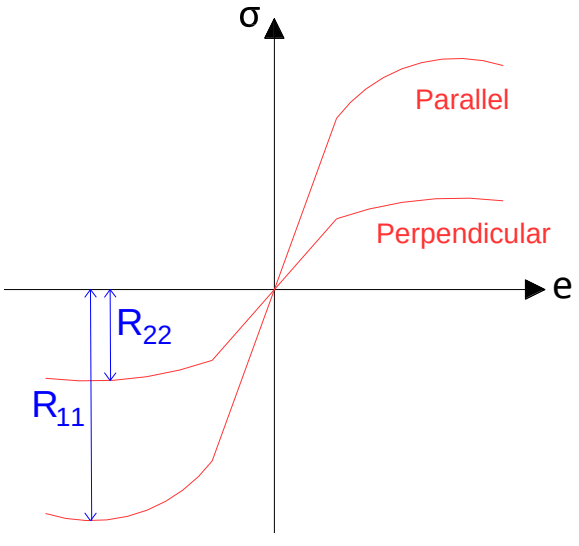

Figure 12: Scaling stresses with Hill's yield criterion

2.4 Friction

To describe the contact areas between the elements, friction must be defined. This can be done using a friction coefficient for contact between two wooden objects. For clean wood, this coefficient is in the range of 0.25 - 0.5. As the contact surfaces of the specimens in the experimental campaign are sawn using CNC cutting, these surfaces were very smooth. Therefore the lower range friction coefficient of 0.25 is used in the numerical simulations.

2.5 Cohesion

In order to model the possibility of shear failure in the timber, the simulation uses two parts which are connected using cohesion. This cohesion represents the internal bond of the growth-rings of the wood. The cohesion is defined using stiffnesses in all three directions. The cohesion is applied for a shear failure simulation. Therefore the stiffnesses that are being used are the shear moduli as given in chapter 2.2 :

Table 7: Stiffness parameters for cohesive behavior [N/mm^2]

K_{nn}	K_{ss}	K_{tt}
690	690	136

Damage

As this cohesion has to break when the ultimate stress is reached, this behavior can be simulated using damage of the cohesive behavior. For this damage, the limit stresses for tension and shear have to be defined:

Table 8: Damage parameters [N/mm^2]

Normal only	Shear-1 only	Shear-2 only
0.75	3.75	1

Failure of the cohesive interaction due to tension is defined using the tensile strength perpendicular to the fiber as defined in Table 2. Failure due to shear is also found in this table. The third parameter (Shear-2 only) is used to define the strength against shear in out-of-plane direction. As this does not occur in the 2D model, this parameter is set to a value of 1.

Once this stress occurs, the interaction does not fail instantly, but instead has a damage evolution in which still energy exists in the interaction. This is explained in chapter 3.4 and Figure 18. In literature, Sandhaas [7], this shear energy is of a value of 1.2 for Spruce (Picea Abies).

3 Numerical modelling in Abaqus CAE

Now that the numerical parameters are defined and explained, this chapter explains the implementations (behavior) of these values in the model. This chapter also explains how the model was built, and why certain choices are made. Modelling was done using FEM software "Simulia Abaqus CAE" [8].

3.1 Material properties

Elasticity

Wood is a highly anisotropic material which is very complicated to model accurately. For this research this fully anisotropic behavior is simplified using the 'engineering constants' elastic definition in Abaqus. This definition requires the modulus of elasticity in the three main directions of the material orientation. These '1', '2' and '3' directions are assigned separate elastic stiffnesses. Also the Poisson's ratios between these three directions ('12', '13', '23') can be defined separately, as well do the shear moduli in these directions. Values which are used to define elastic behavior are given in Table 5.

Fail stress

As mentioned in chapter 2.1, the ultimate stresses of the timber using mean strength values can be defined in Abaqus. These values do not influence the behavior of the simulation. The response of the simulation to the strength is shown in Figure 13, with the dashed line continuing unchanged after the stress limit is reached. The fail stress values are defined to be able to check weather and where this limit occurs in the model as a check. Using the 'fail stress' and the command: 'TSAIW' in the Field output request in Abaqus, the results can be graphically checked using a unity-check principal: values > 1 reached the fail stress.

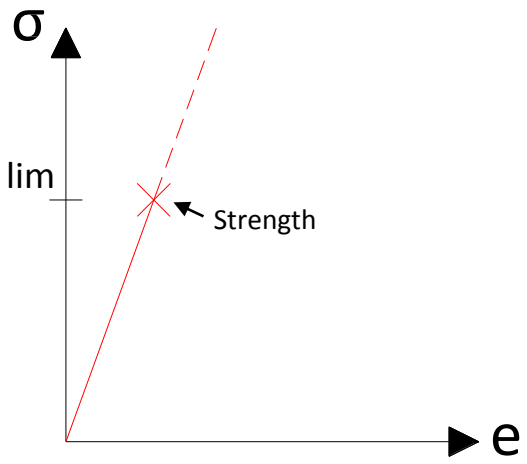

Figure 13: Sigma-Epsilon graph representing the simulation's behavior after reaching fail stress

Plasticity

Plasticity is defined using tabular data in Abaqus. This table consists of two columns for 'Yield stress' and 'Plastic strain' following equation (2.3-1). According to this equation, which is based on an experimental test, the ultimate stress is found at a strain of 2.4‰. After this strain is reached, the behavior is undefined and the calculation will therefor exit with an error. Peak stresses are likely to cause this ultimate strain very early in the calculation. Therefore, an additional last tabular value is given with a yield stress slightly higher than the previous, but with a strain of 10%. This ensures the calculation to carry on with very large strains (crushing) at points where peak stresses occur. This additional point does have a large influence on the model's behavior.

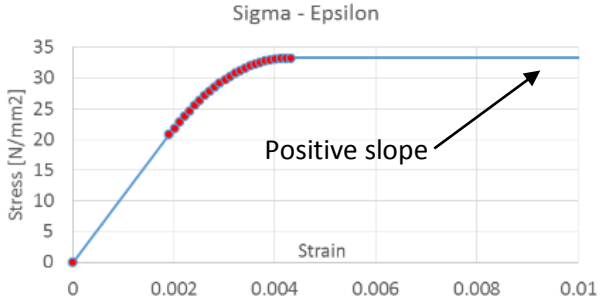

Figure 14: Graph of the full material behavior (elastic + plastic)

3.2 2D Section

To model the Single Step joint it is assumed that a 2D model will be sufficient to describe the stress distributions accurately. The model is build using 2D planar shell elements. Unlike to model itself, the modeling space is in 3D. The section has a width of 1 mm. This width has no influence on the value of the stresses in the results. Reaction-, and axial forces need to be multiplied with 70 as the width of the beam in reality is 70 mm.

3.3 Parts

Sketches

The full geometry of the joint is divided into 6 parts. The geometry of these paths is created using a dxf sketch made with Autodesk AutoCAD in order to increase accuracy of the contact surfaces. These parts are created individually, giving the possibility to use different material properties, sections, orientations, etc. in the same model.

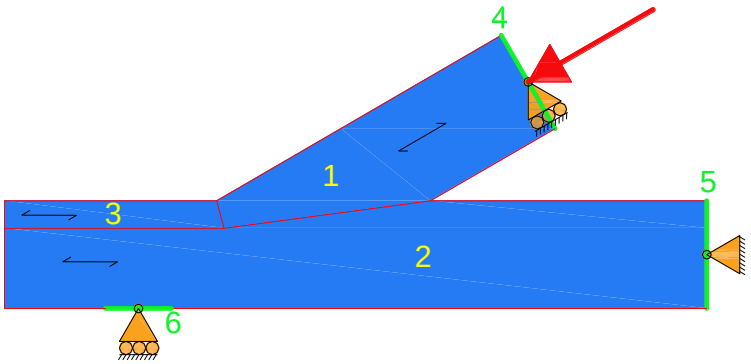

Figure 15: The full FE model consisting out of 6 parts

1 Diagonal

The diagonal is orientated under a 30° angle to the beam. The part is a deformable solid element with the wood material properties. The orientation of the material is also rotated 30° in compliance with the orientation of the part itself. To smooth out peak stresses in the diagonal, the edge in the tooth of the notch is rounded.

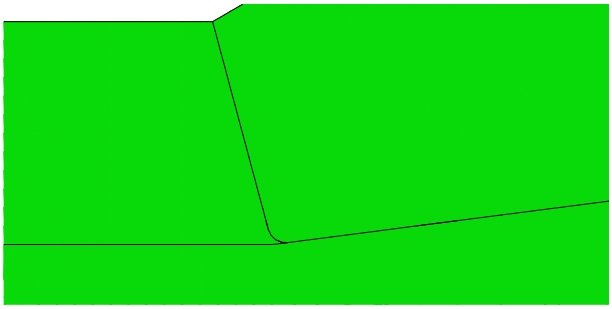

Figure 16: Rounded edge at the tooth of the notch

2 Beam

The beam is divided into two separate parts. The biggest part of the beam is considered the ‘Beam’ element. The small part is named ‘Shearplane’. This separation was made to create a contact area at which the cohesive interaction can be applied. The separation is made at the location where the beam would fail in shear under ideal homogeneous conditions. The orientation of the material is equal to the global model orientation, and is therefore not defined explicitly during modelling.

3 Shearplane

As mentioned, this beam part is separated from the rest of the beam. All other properties that are given to this part are equal to that of the ‘beam’ part. Due to the rounded edge of the diagonal part, this part contains a pointy edge at the tooth of the notch. This creates peak stresses in the corner element of the later applied mesh. This mesh element is disregarded in the results.

4, 5, 6 Rigid Bodies

Lastly, three undeformable ‘rigid bodies’ are applied at locations where the deformable parts are supported by boundary conditions. This is done to prevent peak stresses in the deformable parts, as

boundary conditions are applied to single points. Rigid bodies can be equipped with a reference point at which boundary conditions can be applied. As these parts are undeformable, this means that the boundary conditions are translated 1 to 1 to the edge of the deformable element, creating equally distributed boundary conditions without peak stresses.

Mesh

The deformable parts can be equipped with a mesh structure. A large range of element types for this mesh is available. The model consists entirely of quad shaped mesh elements, since triangular elements have a stiffer behavior. A plane stress family element is chosen to avoid stresses in the out-of-plane '3' direction of the model. Finally, a quadratic geometric order is chosen to give a single element more degrees of freedom to deform, which is beneficial for describing plasticity. To reduce the amount of calculation time, reduced integration is chosen. This reduces the amount of integration points from 9 to 4 for each mesh element.

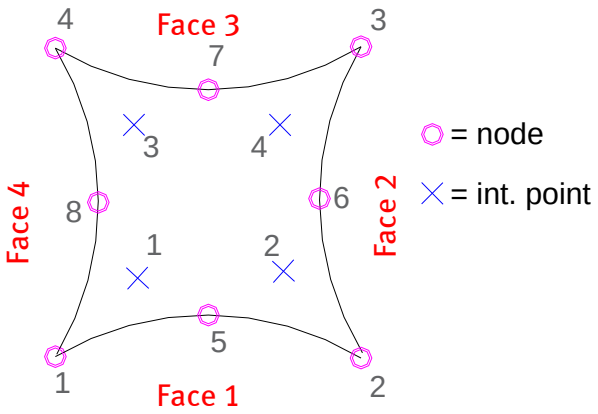

Figure 17: CPS8R mesh element; 8-node biquadratic plane stress quadrilateral, Reduced Integration

3.4 Interactions

Three types of interactions are used to connect the 6 parts shown in Figure 15. The rigid bodies are connected using fixed interaction properties. The beam and diagonal element are connected with friction. And the connection between the two beam parts use cohesion and damage.

Fixed

To connect the supported rigid bodies to the deformable parts, two properties are used to define the behavior of the connection:

- Normal behavior; '"Hard" contact' without the ability to separate after contact.
- Tangential behavior; 'Rough'.

This means that the both parts cannot merge into each other and that the friction between the two surfaces is infinite. Once the surfaces intersect, which is instantly when running the simulation, the parts are locked together, meaning that also tension can be transferred.

Friction

The two contact planes of the notch of the connection also have '"Hard" contact' as normal behavior, whit the difference that this interaction is allowed to separate, meaning no tension can be transferred. Instead of using infinite 'Rough' tangential behavior, now the option 'Penalty' in Abaqus is used. This gives the option to define a friction coefficient as defined in chapter 2.4.

Cohesion and damage

The third interaction property is applied at the contact surfaces of the beam and shearplane parts. This interaction comprises four behaviors: Normal-, and Tangential behavior as used in the notch surfaces. Additionally, cohesion and damage of this cohesion is defined. These last two properties are used to describe the failure mechanism due to shear stresses. To model cohesion, three stiffness parameters have to be defined. As the contact surfaces are loaded mainly by shear, the shear stiffness (shear modulus) is used here. A maximum stress for this cohesion is defined using 'damage' to give initiation to the failure of the cohesion. The cohesion can fail due to two stress situations: Shear and tension perpendicular. The ultimate material strength is used to define the initiation of failure. The damage evolution after the ultimate stress has been reached can be described using energy. It is chosen to use linear softening (Figure 18). The used parameters can be found in chapter 2.5.

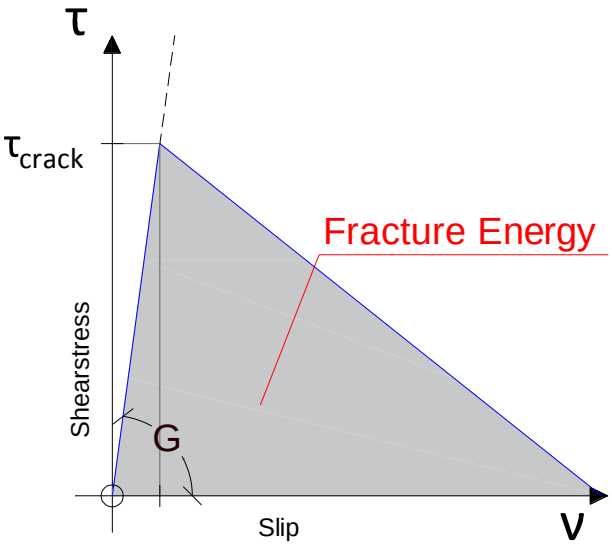

Figure 18: Behavior of the cohesive interaction property

3.5 Amplitudes

A force is applied to the model by using the boundary condition at the upper end of the diagonal which is deforming inwards along the axis of the diagonal. This deformation is applied using an amplitude. The standard speed of this amplitude is to apply 0.1 mm deformation per step. As this increment causes a fast growth in (reaction) force on the diagonal, this speed makes it very hard to compare the numerical results to the ESPI measurements done during the experimental tests. Therefore the amplitude speed is reduced twice to have an increment of approximately 1 kN in reaction force per amplitude point.

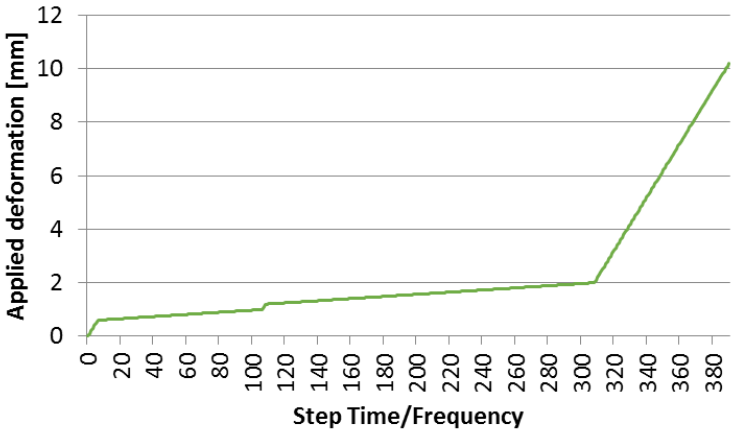

Figure 19: Evolution of the applied deformation over the calculation time

3.6 Jobs

A total of four calculations can be made using the model. This is with-, and without plasticity, meaning that two calculations are Linear Elastic (LE), and two are Plastic (PL). The second option is the shearplane interaction with cohesion (SHEAR), and the other using the fixed interaction as used at the rigid bodies (INFSHEAR). The different calculations are used to see the effect of each of the used conditions. In the end, the simulation using plasticity and cohesion is most representative for reality.

3.7 Script

Using Abaqus CAE to build the FE model gives an opportunity to reproduce the whole model with one-click and to apply adjustments (easily) without rebuilding the whole model. This is done using 'Python' scripting. [9]

The same can be done for the output database. In this way, small changes in the model lead to differences in the calculation. Using scripts, the new results can be one-click extracted from the database into MS Excel to process.

Copies of all used scripts are enclosed in appendix B.

These scripts were made using Abaqus CAE version 6.14. Caution must be used when running the scripts in newer and older version of Abaqus CAE, it must be verified that all commands are recognized correctly and the model is reproduced as intended.

4 Electronic Speckle Pattern Interferometry (ESPI) validation

The first results which are extracted from the output database of the numerical simulations are the displacements of the beam in the frontnotch area. These results can be compared with the ESPI results in order to verify the behavior of the simulation compared to the results of the experiments. *More information on the principle of ESPI and measurements which have been done are threated in the experimental study.*

4.1 ESPI data extraction

Seven sections are made in the measured surface (Figure 20a), with a center to center distance of 40 mm. These sections are plotted in a graph, displaying their horizontal (Y) displacement in Figure 20b.

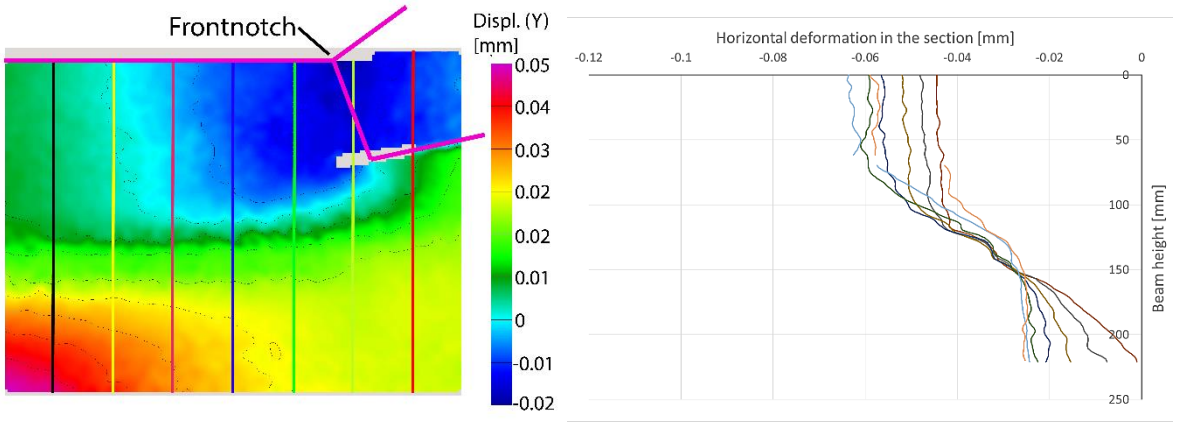

Figure 20: a) Sections made on the measured surface. (Specimen 500-3) **B)** Graph of the displacements for each section

The plotted displacement represents the incensement of deformation during the measurement, which was from 22.37 kN to 25.25 kN. In other words; for a ΔF, a ΔU is found. To extract the ΔU from the results, an arbitrary reference point in the surface is chosen of which the displacement is zero. In order to compare the ESPI results with the Abaqus results, the ESPI results are shifted along the displacement axis (Y axis in Figure 20b).

4.2 Abaqus data extraction

In Abaqus, six paths are taken, all 40 mm apart. The location of these paths match the sections made in ESPI with some margin. Deviations in the location of the sections are not of great influence on the accuracy. In Abaqus, the horizontal displacement of the paths are extracted (‘1’ direction in Abaqus). This is done by finding the displacements in the steps which give the closest reaction forces compared to the range of the ESPI measurements (22.37 kN – 25.25 kN). From these two displacements, again the ΔU can be found. These numerically obtained values are compared with the ESPI measurements.

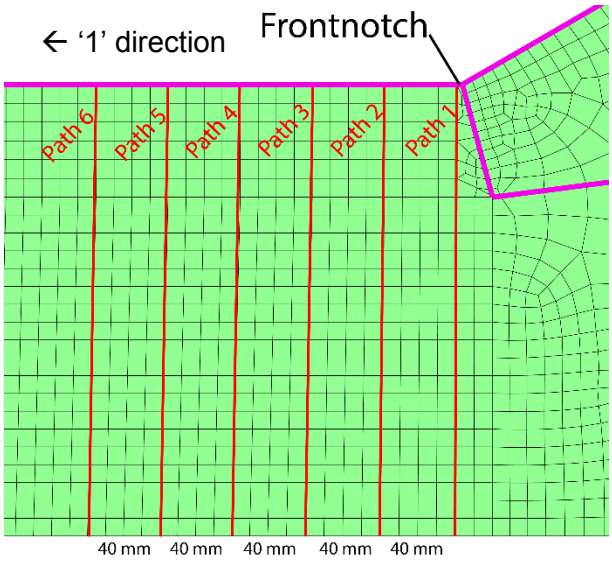

Figure 21: Paths in Abaqus

4.3 Comparison

When comparing the results of the ESPI experiments with the numerical model, it immediately stands out that there can be large differences between ESPI results per test specimen. As shown in Figure 22, the ESPI results of test specimen 500-3 shows very different behavior compared to the numerical simulation:

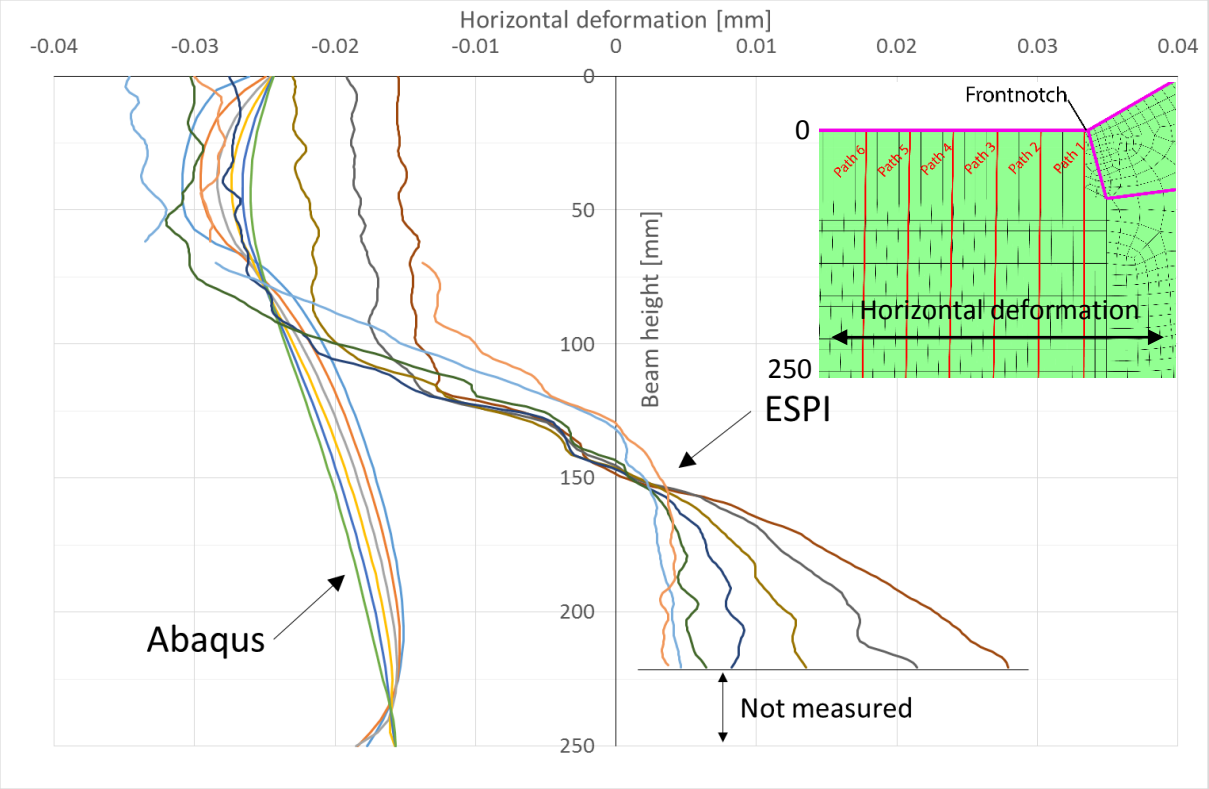

Figure 22: Comparison of 500-3 specimen ESPI results and the numerical simulation of REFGEOM

This different behavior can be explained by imperfections in the material. When analyzing the deformation of the surface (Figure 23) it can be seen that the largest deformation, which are caused by the shear stresses do not concentrate near the shearplane as it would be in an ideal homogeneous material (black line). Instead the large deformations are concentrated lower, near the heart of the wood (red line). From this it can be concluded that the difference in results from the numerical simulation and the experiments can be explained by the non-homogeneous experimental specimen. When comparing another specimen (500-2) with the same geometry to this specimen (500-3) it can be concluded that the 500-3 specimen was much weaker. The numerical

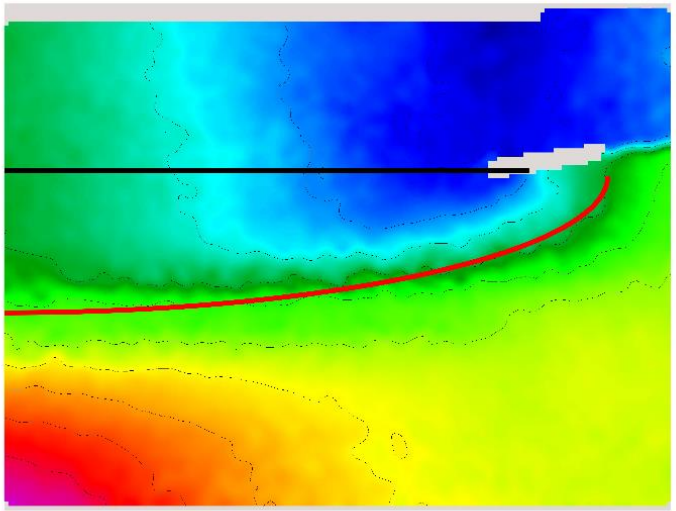

Figure 23: Assuming shear deformations in the shearplane (black line), versus concentration in reality (red line)

simulation and the results from ESPI on the 500-2 test specimen show a much higher match between ESPI and Abaqus results as shown in Figure 24:

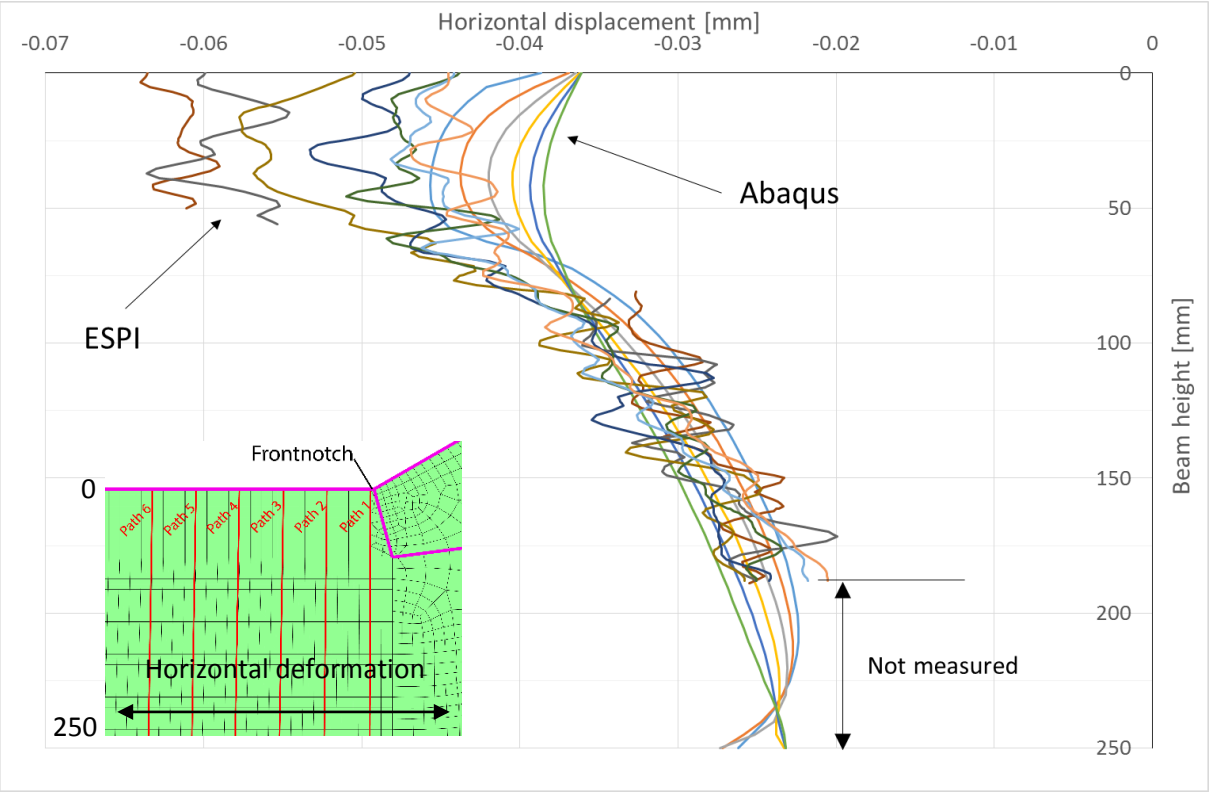

Figure 24: Comparison of 500-2 specimen ESPI results and the numerical simulation of REFGEOM

The biggest difference between both results can be found near the notched area. (The first 50 mm of the 'Beam Height' axis is Figure 24.) This difference can be related to the deviations in the location of the sections in the numerical simulations and ESPI results as explained in chapter 4.2.

Next to the good correlation of the 500-2 specimen results, what also stands out is the behavior of the first and last section that is made on the surface. In Figure 25, the dark black line is the ESPI result of the section nearest to the notch, the gray line represents the cut farthest from the notch. The deformation behavior is mirrored near the 50 mm beam height line. The same behavior can be seen in the numerical simulation, represented by the red colored lines.

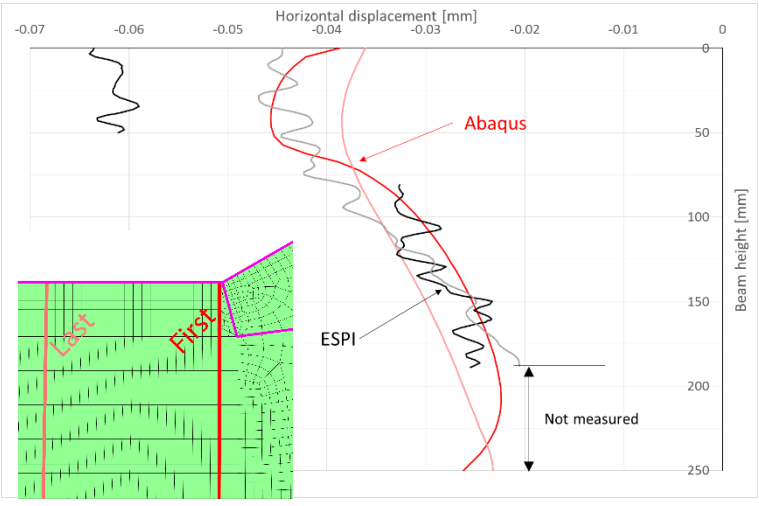

Figure 25: comparable behavior of the first and last section in both results

All other comparisons are enclosed in appendix C.

5 Results

5.1 Notch

To investigate the compressive stresses in the notch area, the parallel- (S11), perpendicular- (S22), and shear (S12) stresses in the model are extracted along the sections as shown in Figure 26:

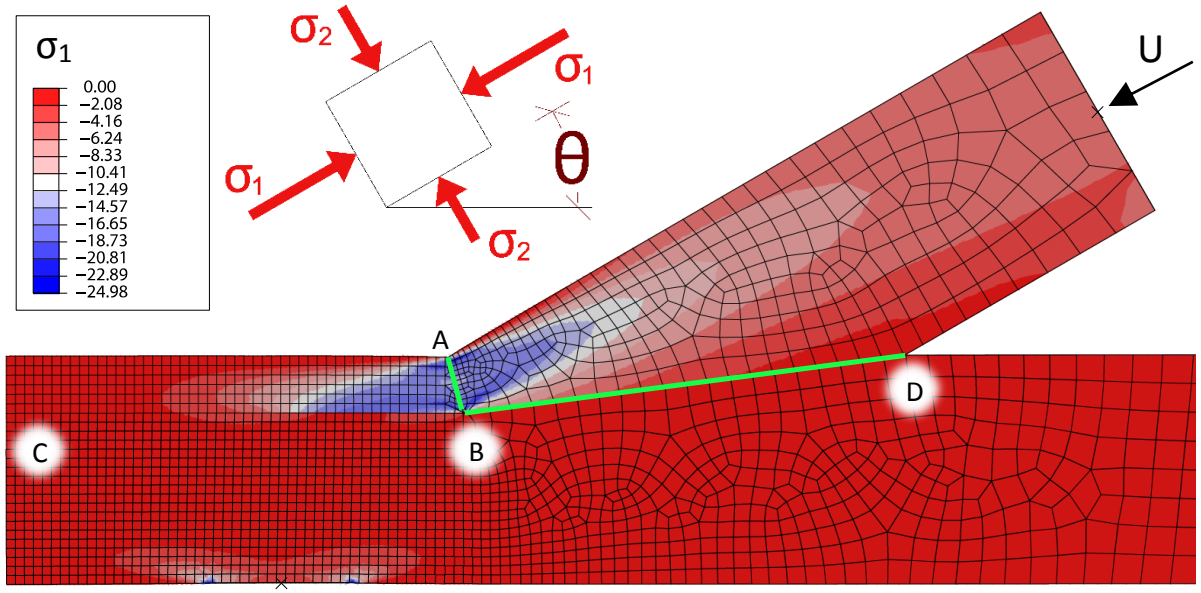

Figure 26: Locations of the sections in the model in which the principal stresses are found (AB) (BD)

The stresses that are particularly interesting are the principal stresses and their orientation. These principal stresses can be obtained from S11, S12, S22 using Mohr's circle as explained in [10]:

$$\sigma_{1/2} = \left(\frac{S11 + S22}{2}\right) \pm \sqrt{\left(\frac{S11 - S22}{2}\right)^2 + S12^2} \quad (5.1\text{-}1)$$

$$\theta = \tan^{-1}\left(\frac{2 * S12}{S11 - S22}\right)/2 \quad (5.1\text{-}2)$$

This results in three parameters:

- σ_1 : This is the principal stress in the main direction (highest stress);
- σ_2: This is the principal stress in the secondary direction (smallest stress);
- θ: This is the angle of the main direction compared to the defined normal direction in the model in degrees.

These parameters are found over the length of the sections as shown in Figure 26, and also during increasement of the load in the numerical simulation. The stresses can be plotted graphically using a 3D area plot.

The 3D area plots are made using-, and are online available, at plot.ly/~Richardderijk/folder/home [11].

REFGEOM

The stress distributions of interest are the principal stresses which are orientated closest to perpendicular to the contact surfaces of the front-, and bottomnotch. For the frontnotch, this principal stress is σ_1, as the biggest stresses act perpendicular to the surface. For the bottomnotch the highest stresses are caused by the tension force in the beam. The other direction gives the stress distribution due to contact of the diagonal. σ_2 is used. Also the angle of these stresses are of interest. This can be graphically shown with four 3D area plots.

Frontnotch:

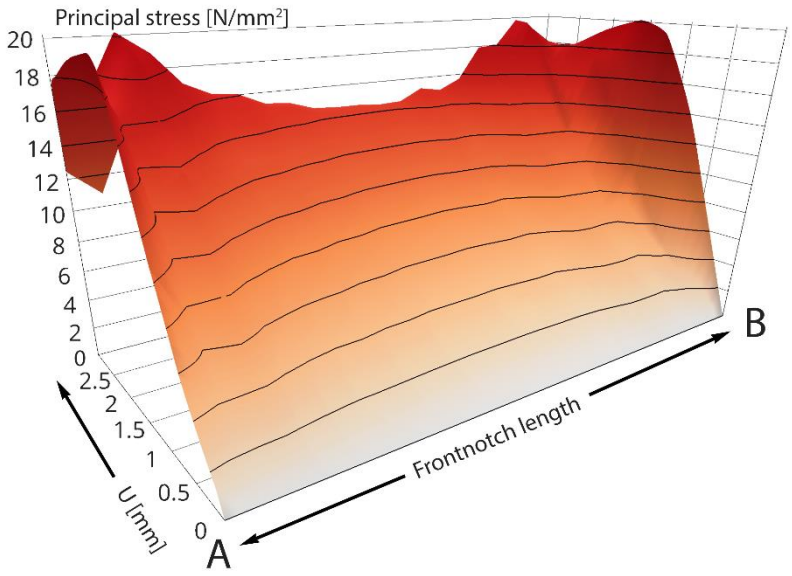

Figure 27: Stress distribution of principal stresses σ_1 perpendicular to the frontnotch surface (AB)

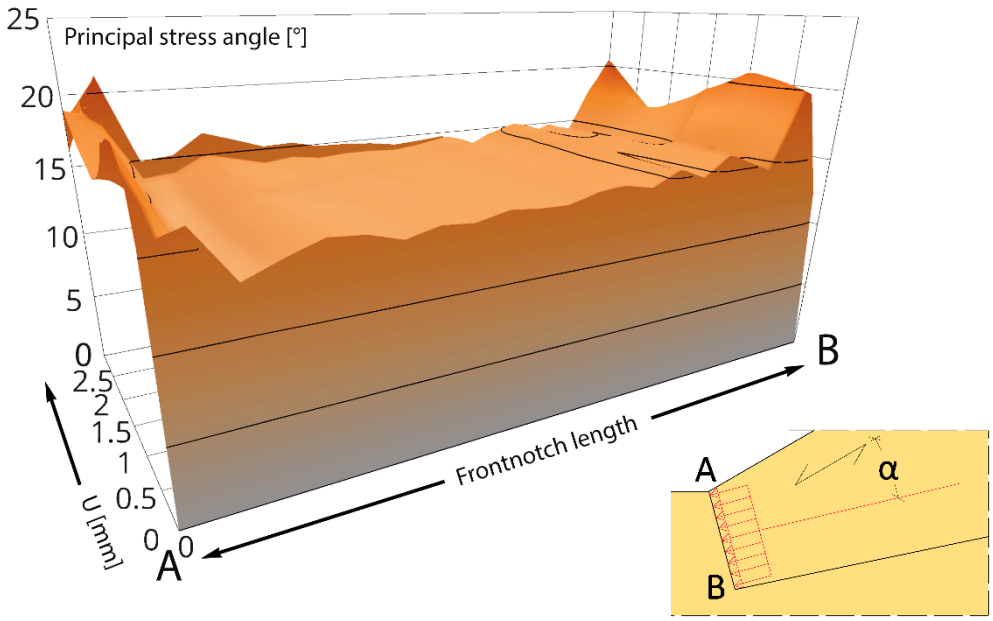

Figure 28: Orientation angle [°] of main principal stresses compared to the direction of the grain (α)

Figure 27 shows the stress distribution of the principal stresses in the frontnotch. A parabolic stress distribution is found in the frontnotch, showing peak stresses at the corners of the contact surface.

Figure 28 shows the corresponding angle of these principal stresses. The graph shows that the orientation of the stresses, compared to the normal (longitudinal) direction of the diagonal, stays steady around 15°, and shows values up to 20° near the corners of the contact surface. The value of 15° is expected since the orientation of the frontnotch is perpendicular to this angle.

In order to also compare the influence of the different geometries on the stress distribution, next to the 3D plots, also the stress distribution is extracted at the following loads:

- The characteristic ultimate load, according to [1]–[3];
- 50 kN;
- The ultimate load, found in the numerical simulation.

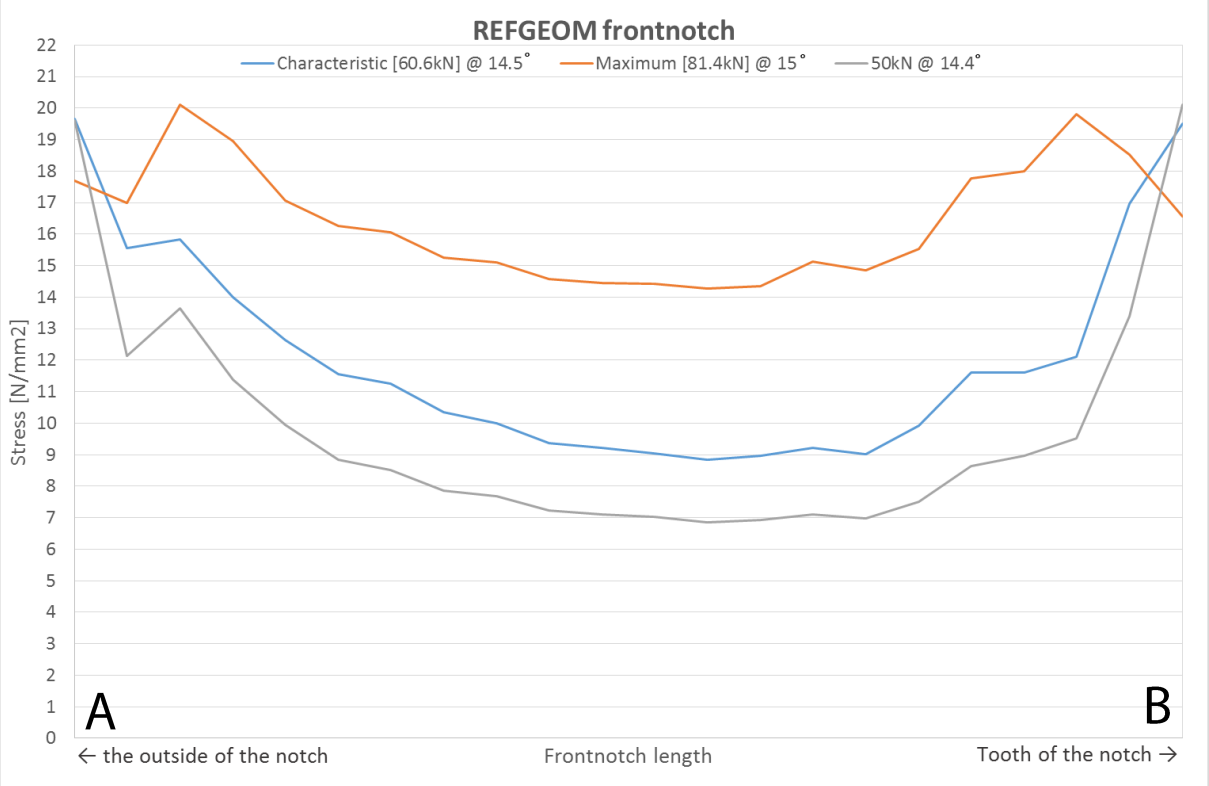

Figure 29: Principal stress distribution σ_1 in the frontnotch (AB) at important load conditions, @ is angle to the fiber direction α

Figure 29 shows the parabolic stress distribution at a load of 50kN, and the characteristic design load of 60.6kN with peak stresses at both sides of the contact surface. When the ultimate load in the model is reached, these peak stresses move inwards. The stress distribution itself behaves more evenly distributed. The stresses that are reached of around 20N/mm^2 are still in elastic territory, as plasticity is defined for stresses higher than 21N/mm^2. This leads to the conclusion that this model did not fail due to overloading of the frontnotch (butting).

The same results can be plotted for σ_2 in the bottomnotch:

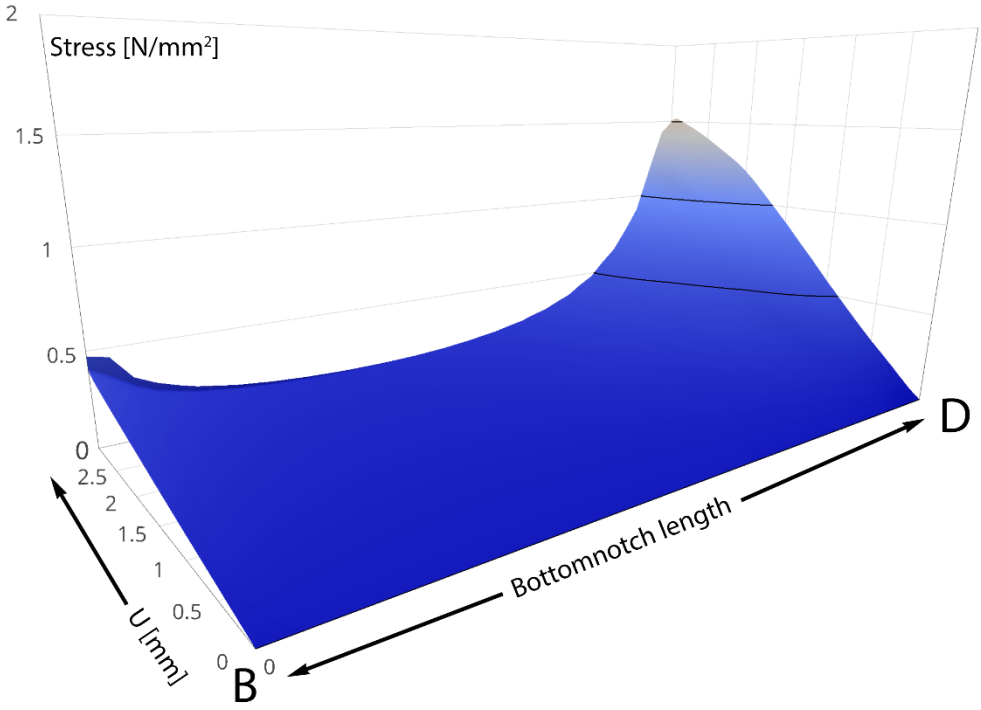

Figure 30: Stress distribution of principal stresses σ_2 perpendicular to the bottomnotch surface (BD)

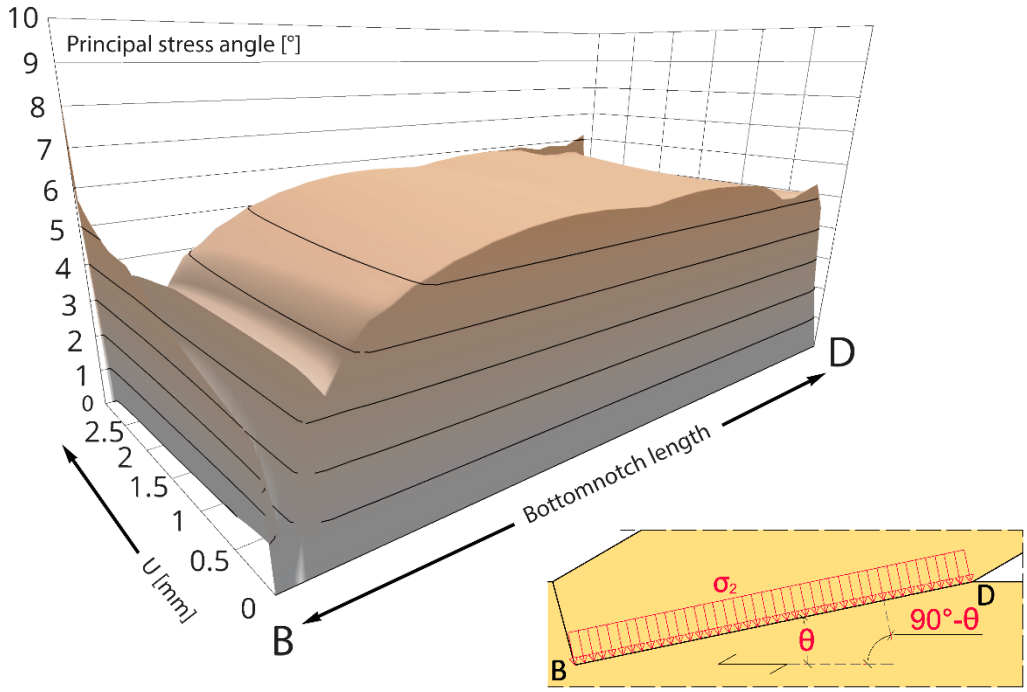

Figure 31: Orientation angle [°] of principal stresses σ_1 compared to the direction of the grain in the beam (θ)

The angles displayed in Figure 31 (θ) are related to the main principal stress σ_1, the orientation of σ_2 is rotated 90° (90°-θ). The plot shows the secondary principal stresses act under an angle of ± 85° to the normal (longitudinal) direction of the beam. This means that the stresses act perpendicular to the bottomnotch.

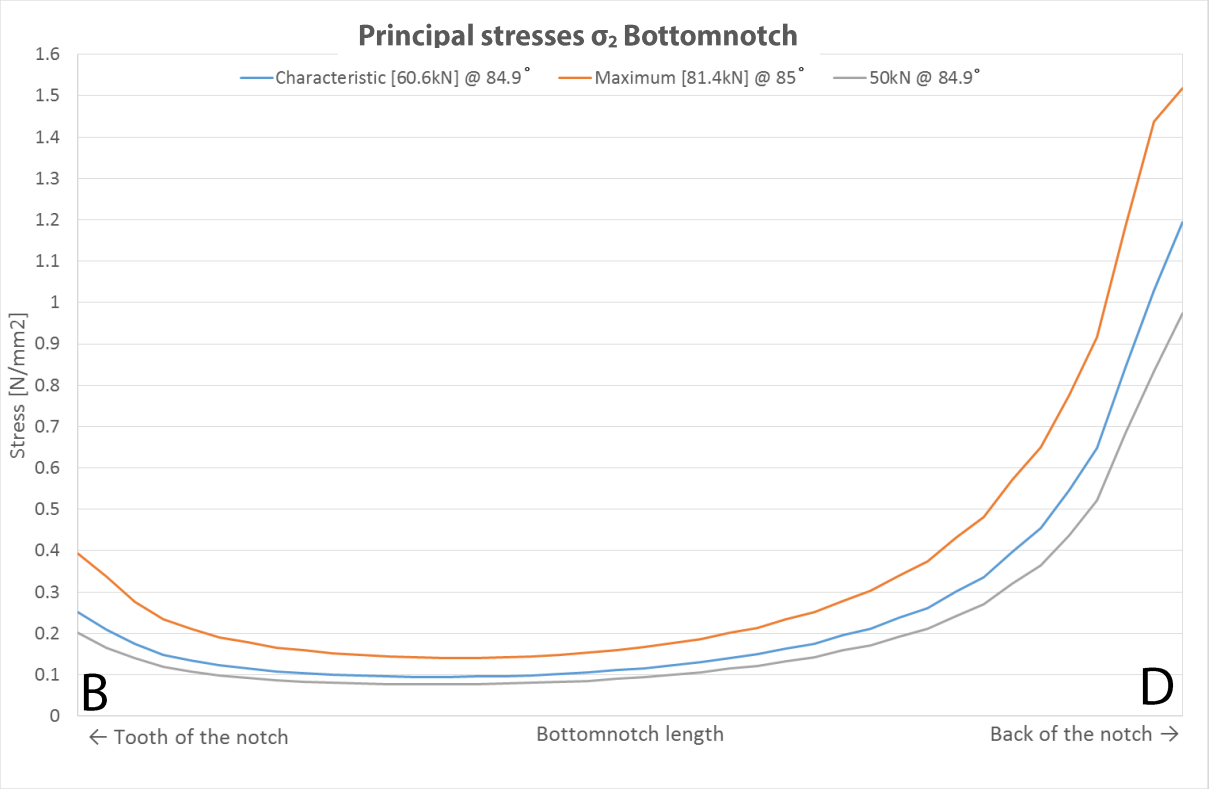

Figure 32: Principal stress (σ_2) distribution in the bottomnotch (BD) at important load conditions, @ is angle to the fiber direction α

Figure 30 and Figure 32 show the stress distribution of the principal stresses perpendicular to the bottomnotch surface. Peak stresses can be found near the back of the notch, and slightly elevated stresses can be found at the tooth of the notch. Since even the peak stresses are much lower than the timber's perpendicular compressive strength ($f_{c;90}$), this stress distribution is not of interest for this research. Therefore, in all other models, these stresses are not investigated.

Other models

The difference in geometry of the tested models proved to have little influence on the stress distribution in the frontnotch as is discussed in the comparison in the next chapter. The 3D area plots do not show any significant deviations, therefore they are not presented in this rapport.

Comparison

A comparison of the stress distribution is done for a load of 50kN. Also the angle in which the principal forces are acting in each model is compared.

50kN

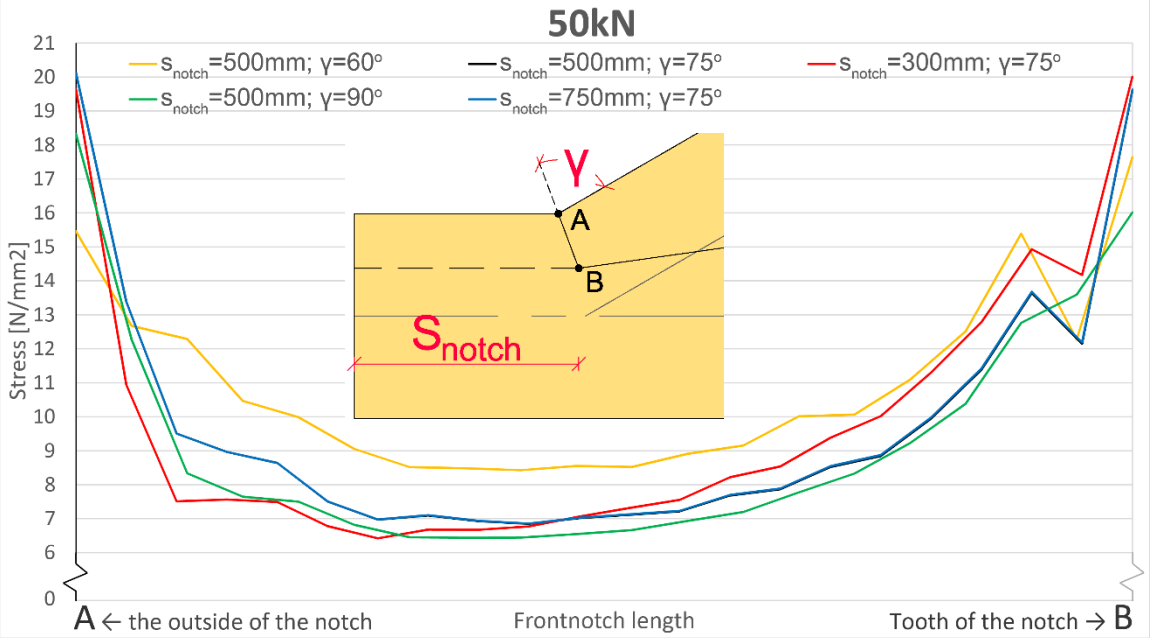

Figure 33: Comparison of the stress distribution of all tested models at 50kN load, @ is angle to the fiber direction

Figure 33 shows that the stress distribution in all simulations is very similar. The "*500mm75°*" and "*750mm75°*" show almost exact the same stress distribution, the "*300mm75°*" shows lower stresses at the outside of the notch, but higher stresses near the tooth of the notch. When the cumulative stresses of these three models are compared, as done in Table 9, it can be seen that the total stress in the surface is very similar.

The stress levels in the "*500mm90°*" simulation are much lower. This can be explained by the larger length of the frontnotch. As this model has the highest angle γ of all geometries, and the depth of the notch is kept constant in all geometries, the largest frontnotch length is available.
For the same reason that the "*500mm90°*" simulation has the lowest stresses, the "*500mm60°*" simulation has the highest stress distribution, as can be seen in Figure 33 and Table 9. This geometry has got the smallest frontnotch length due to the small angle γ.

Table 9: Accumulated principal stresses in the frontnotch at 50kN

Geometry	500mm75°	300mm75°	750mm75°	500mm90°	500mm60°
Accumulated stress at 50kN	216.9517	217.7590	217.2893	185.6612	219.4909

Average stress angle

In Figure 33, the legend shows the angle at which the principal stresses are acting in the frontnotch surface is varying a little between 13.6° and 15.2°. The direction of the principal stresses in the frontnotch in all geometries during the simulations is shown in Figure 34:

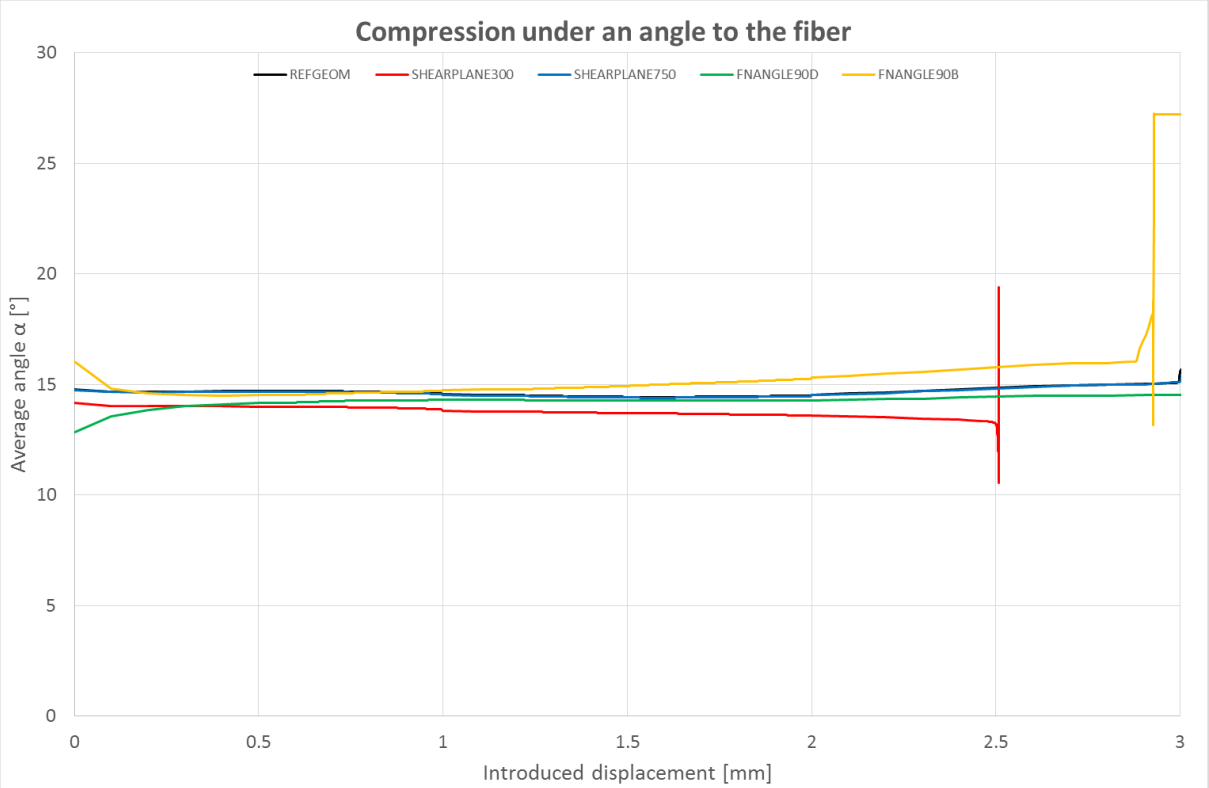

Figure 34: Comparison of the average stress angle of all tested models during loading

The angle of the principal stresses varies along the length of the frontnotch. From all the values in this length, an average angle is found. This average angle is shown in Figure 34 for the duration of the simulation (while displacement is introduced into the diagonal).

The plot shows that all simulations simulate the principal stresses under an angle of approximately 15° to the direction of the fiber. This is remarkable since the angle of the frontnotch (γ) varies in the simulations, as shown in Figure 35.

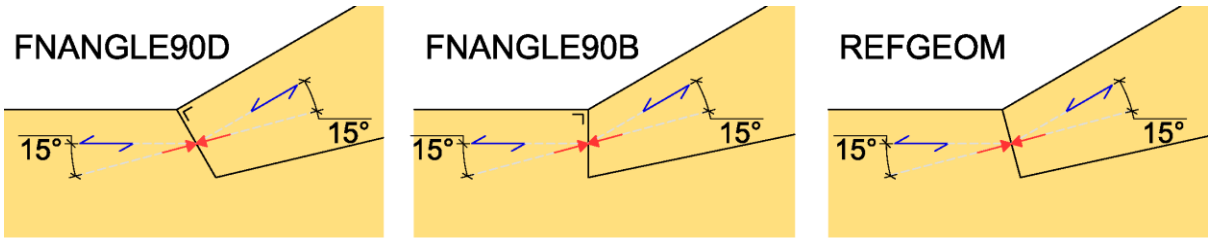

Figure 35: Orientation of the principal stresses in each simulations with differing frontnotch angles

The principal stresses do not act perpendicular to the frontnotch surface in the FNANGLE90D and FNANGLE90B simulations. This can be explained by the frictional behavior that has been defined in the simulations between the contact surfaces in the frontnotch. The influence of this friction is further investigated to determine what influence it has on the orientation of the principal stresses.

Friction

The influence of friction on the angle of the principal stresses can be calculated using the friction coefficient given to the contact surface. The friction coefficient used in this model, as mentioned in chapter 2.4, is 0.25. This means that for every kN of friction allowed to build up in the contact surface, 4kN of compression has to be applied perpendicular to this surface, as shown in Figure 36. This fixed ratio has got a fixed angle, defined as α'.

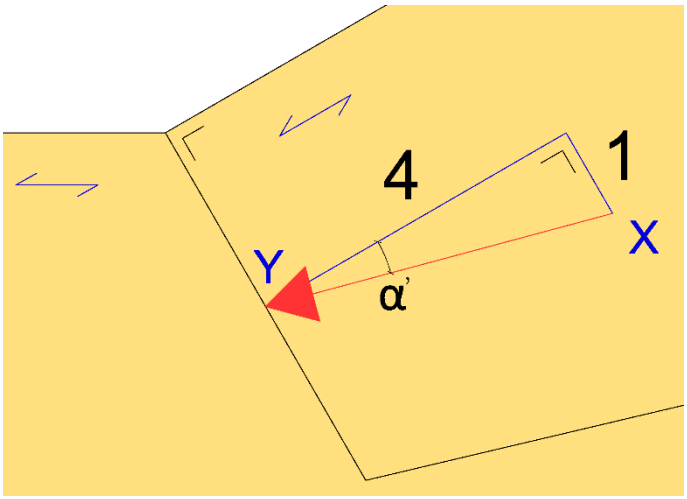

Figure 36: Influence of friction on the angle of principal stresses

This angle can be found using (5.1-3).

$$\alpha' = \tan^{-1}\left(\frac{Opposite}{Adjacent}\right) \approx 14° \qquad (5.1\text{-}3)$$

In which:

$Opposite$ is the length which is opposite to angle α' ('X' in Figure 36);

$Adjacent$ is the length adjacent with angle α' ('Y' in Figure 36).

For a friction coefficient of 0.25, angle α' is 14°. This means that the principal stresses can rotate up to 14° from the perpendicular to the frontnotch direction because of the presence of friction between the two timber elements in the frontnotch.

Depending on the present friction coefficient, this angle can increase further:

Table 10: Maximum stress angle per frontnotch friction coefficient

Friction coefficient	Maximum stress angle α'
0.25	14°
0.30	16.7°
0.35	19.3°
0.40	21.8°
0.45	24.2°
0.50	26.6°

5.2 Shearplane

To investigate the shear stresses which occur in the shearplane, the shear stresses (S12) in the model are extracted along the section as shown in Figure 37:

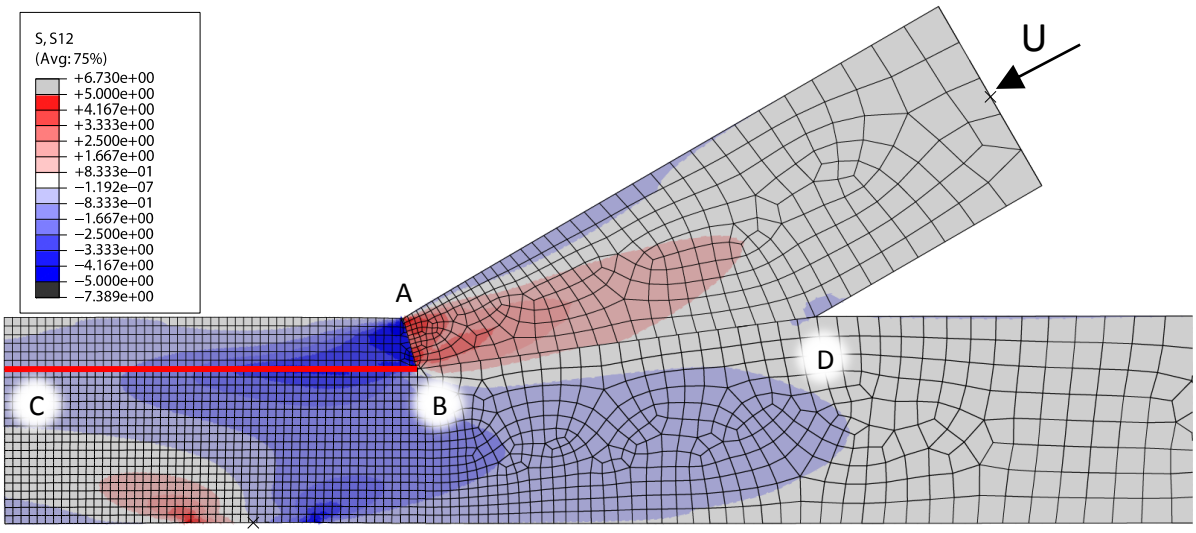

Figure 37: Location of the section in the model in which the shear stresses are found (CB)

In this section, the stress distribution of the shear stresses is found for the full calculation. This means that the evolution of the stress distribution for an increasing load can be found. This is shown graphically in a 3D area plot.

The 3D area plots are made using-, and are online available, at plot.ly/~Richardderijk/folder/home [11].

In order to also compare the influence of the different geometries on the stress distribution, next to the 3D plots, also the stress distribution is extracted at the following loads:

- The characteristic ultimate load, according to [1]–[3];
- 50 kN;
- The ultimate load, found in the numerical simulation.

REFGEOM

The results from the model REFGEOM (with a shearplane length s_{notch} of 500mm) along the shearplane length are extracted from the results and are graphically shown in Figure 38.

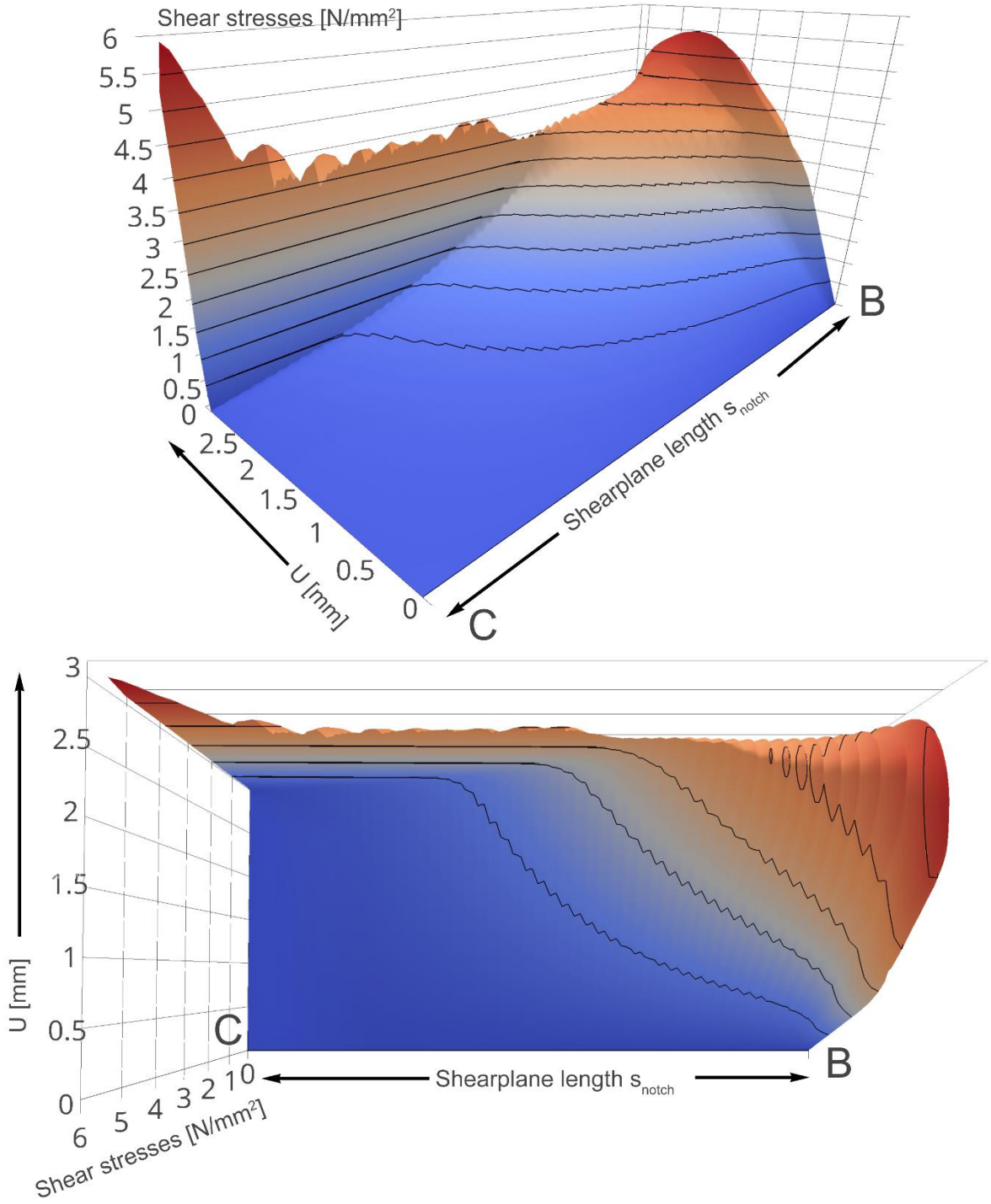

Figure 38: Shear stresses in the shearplane (CB) of the REFGEOM model, while the model is loaded

The left side of the 'shearplane length' axis is also the left side of the section as displayed in Figure 37. The right side of this axis shows the shear stresses near the tooth of the notch.

What can be concluded from the graphs in Figure 38 is that no significant shear stresses occur at the far left side of the shearplane. The shear stresses near the tooth of notch reach values of about 5.5 N/mm^2, whilst a damage value of 3.75 N/mm^2 is given. This overshoot can be explained by the stress conditions perpendicular to the shearplane. Near the notch, large compressive stresses occur perpendicular to the shearplane. These stresses allow a higher shear capacity of the material. This was modeled in the simulations by the presence of a friction coefficient. The last thing that stands out in the graph is the large peak stress that occurs at the left side of the shearplane, while the contact surface is failing. These stresses can be explained by the very small simulation increment that is needed in the calculation. In this increment, the found equilibrium results in these high stresses. As this stress occurs whilst the material is cracking, which is literally in a fraction of a second, this peak stress can be neglected.

Three sections in the 3D graph are shown in Figure 39. The stress distribution at several key load conditions are plotted. A 50kN load is chosen to later compare the stress distribution of all geometries. Next to this arbitrary load, also the maximum load in the simulation (81.4kN), and the load which is allowed in the codes (60.6kN) are used to find the stress distribution at these points.

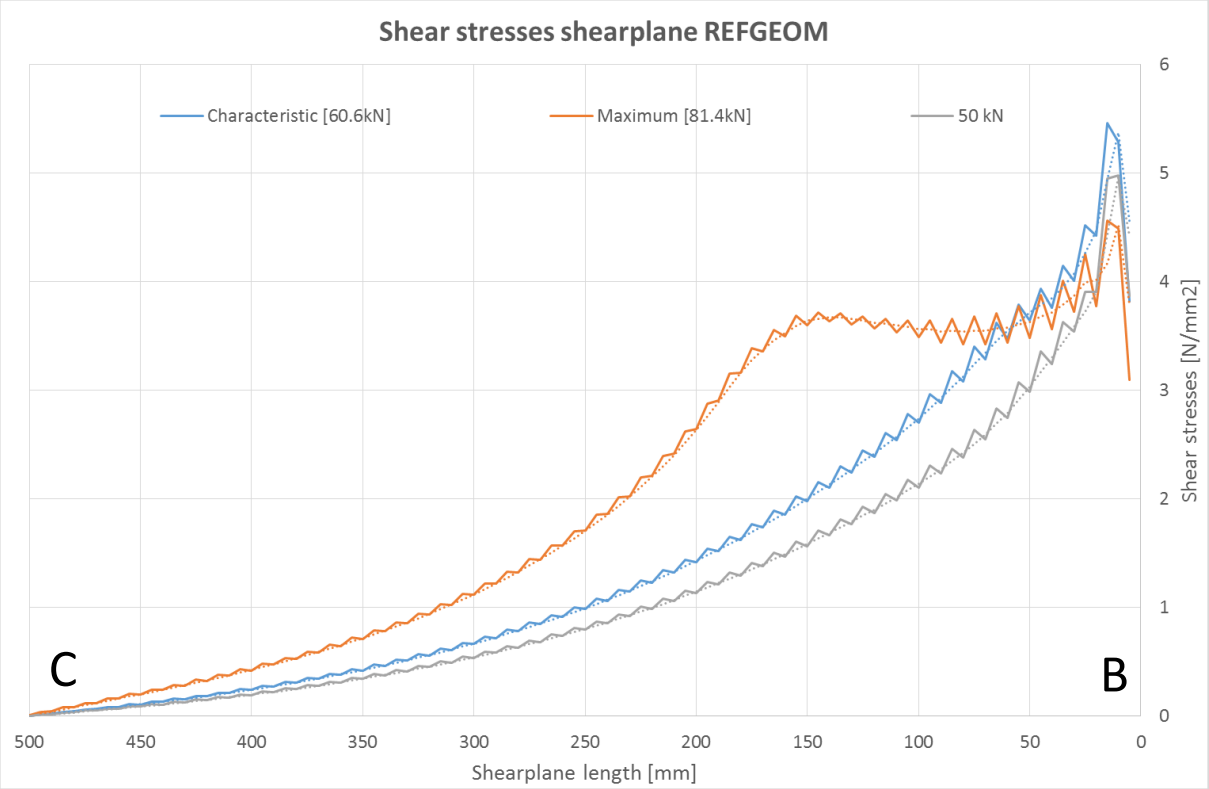

Figure 39: Stress distribution in the shearplane (CB) at important load conditions

50kN

At a load of 50 kN the shear stress distribution in the shearplane spreads over the full 500mm available length, although shear stresses are lower than 1 N/mm^2 after the first 225mm. The distribution reaches a peak stress of about 5 N/mm^2 near the tooth of the notch. The distribution shows an “exponential” behavior.

Characteristic [60.6kN]

The shear stress distribution in the shearplane at the characteristic design limit load shows behavior which is comparable to the 50kN load line, with slightly higher values, as also the load has increased. No signs of failure of the cohesion in the shearplane can be spotted, although, peak shear stresses have already passed the shear strength value. The absence of a failure in this stage can be related to the compressive stresses perpendicular to the shearplane, increasing the shear strength.

Maximum [81.4kN]

The maximum load which was reached in the simulation of 81.4kN, shows that already a big part of the shearplane cohesion has failed. The stress distribution shows a plateau in the first 150mm of the shearplane. The stresses in this plateau are around the shear strength value of 3.75 N/mm^2.

SHEARPLANE300

The results from the model SHEARPLANE300 (with a shearplane length s_{notch} of 300mm) along the shearplane length are extracted from the results and are graphically shown in Figure 40.

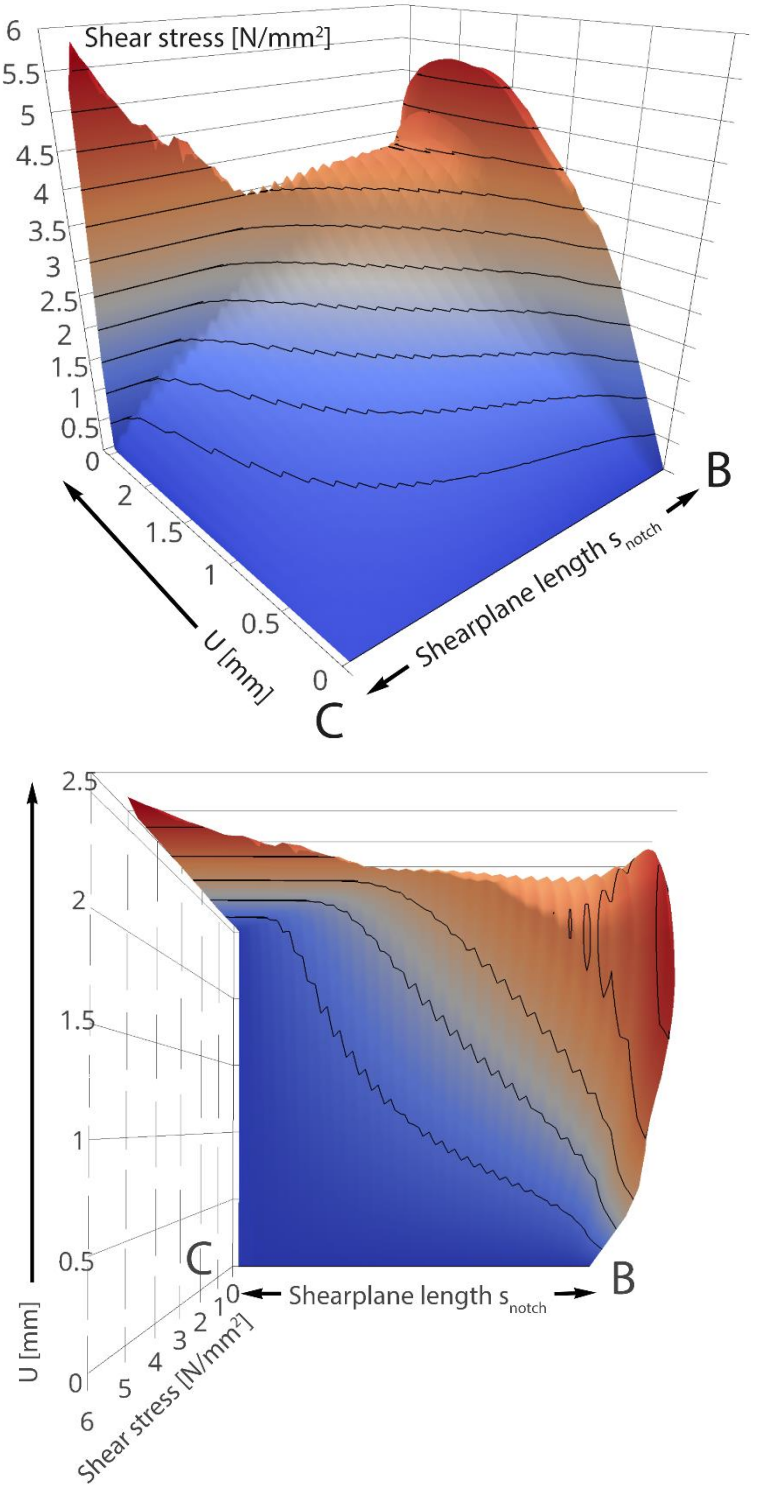

Figure 40: Shear stresses in the shearplane (CB) of the SHEARPLANE300 model, while the model is loaded

The 3D plots show similar behavior of the stress distribution as for the REFGEOM model, with the difference that, since less shearplane length is available, the decrease in the shear stresses from the tooth of the notch to the end of the beam is much more linear than in the REFGEOM model. Again,

peak stresses during failing of the cohesive shearplane can be neglected, as these stresses occur just a fraction of a second before failure.

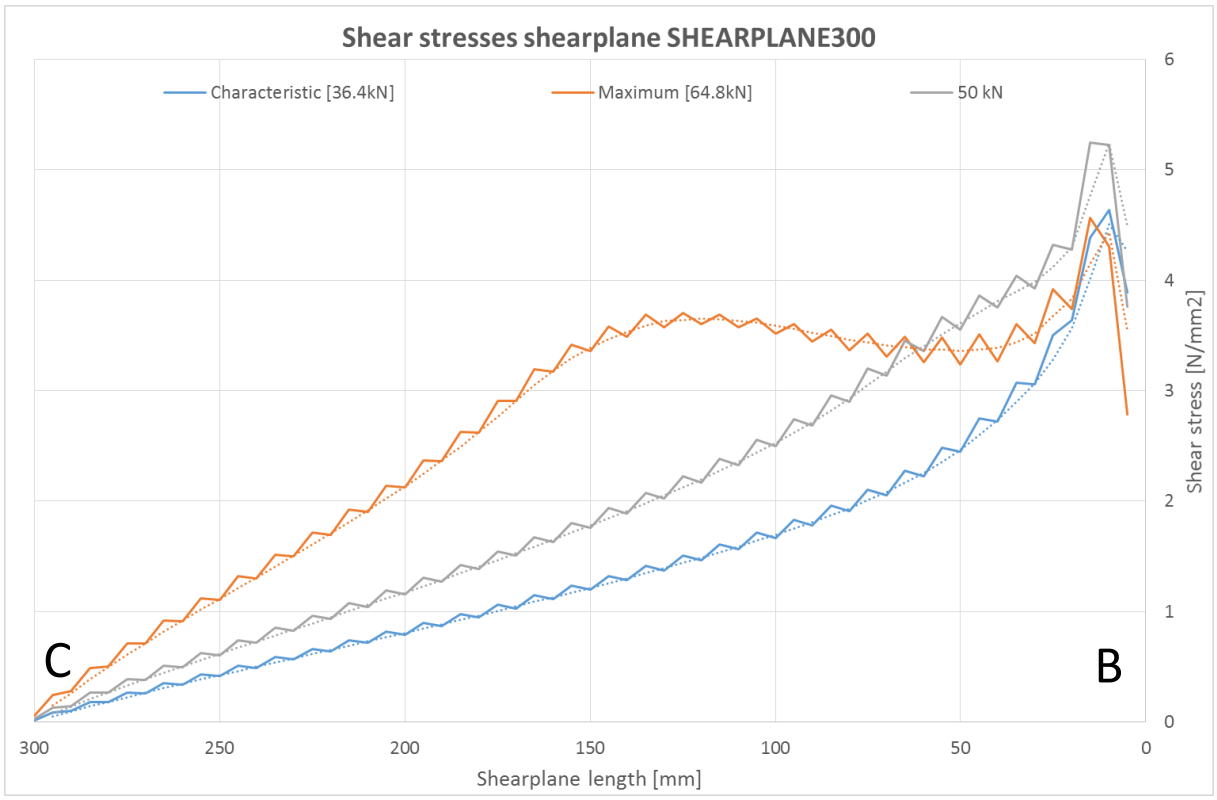

Figure 41: Stress distribution in the shearplane (CB) at important load conditions

Characteristic [36.4kN]

The stress distribution at the characteristic design load shows an "exponential" behavior, although the distribution in the left half of the shearplane length can be described as linear. From this, it can be concluded that the reduced shearplane length of just 300mm already has an influence on the stress distribution at a design load value. This justifies the codes reduction of ultimate limit load of almost 50% (60.6kN →36.4 kN) compared to the REFGEOM, as the reduced length indeed has got an impact on the stress distribution.

50kN

At a load of 50kN, the linear behavior in the stress distribution is even more notable.

Maximum [64.8kN]

The distribution of the shear stresses at the maximum simulation loads, again show a stress plateau of around 3.75N/mm^2. This behavior is very similar to the behavior of the REFGEOM at the maximum load.

SHEARPLANE750

The results from the model SHEARPLANE750 (with a shearplane length s_{notch} of 750mm) along the shearplane length are extracted from the results and are graphically shown in Figure 42.

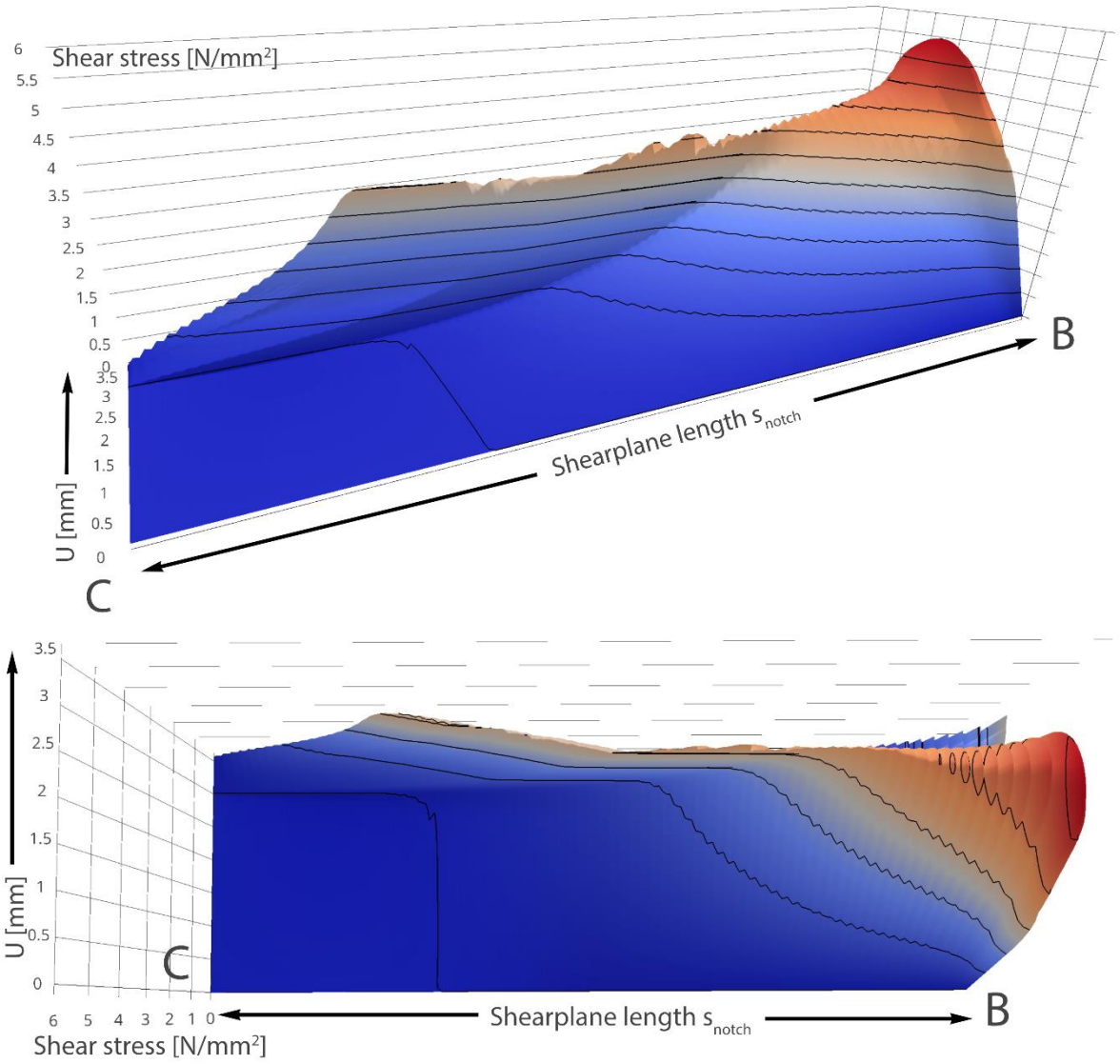

Figure 42: Shear stresses in the shearplane (CB) of the SHEARPLANE750 model, while the model is loaded

In the 3D plot it can be seen that the stress distribution is very similar to the REFGEOM simulation. The extra shearplane length in this geometry of 250mm is not loaded in (positive) shear until failure of the cohesion. According to the simulation, this geometry does not fail in shear completely, as the other geometries did. In the plot it can be seen that the first ± 300mm fails instantly while the crack starts growing. After this, the sudden rupture stops, and only cracks further after additional displacement is applied on the diagonal during the simulation. This behavior continues as the introduced displacement is enhanced. The simulation cannot complete until the crack has grown to the other end of the shearplane.

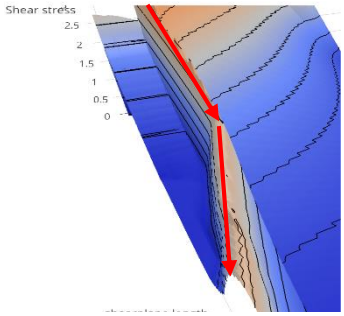

Figure 43: crack growth

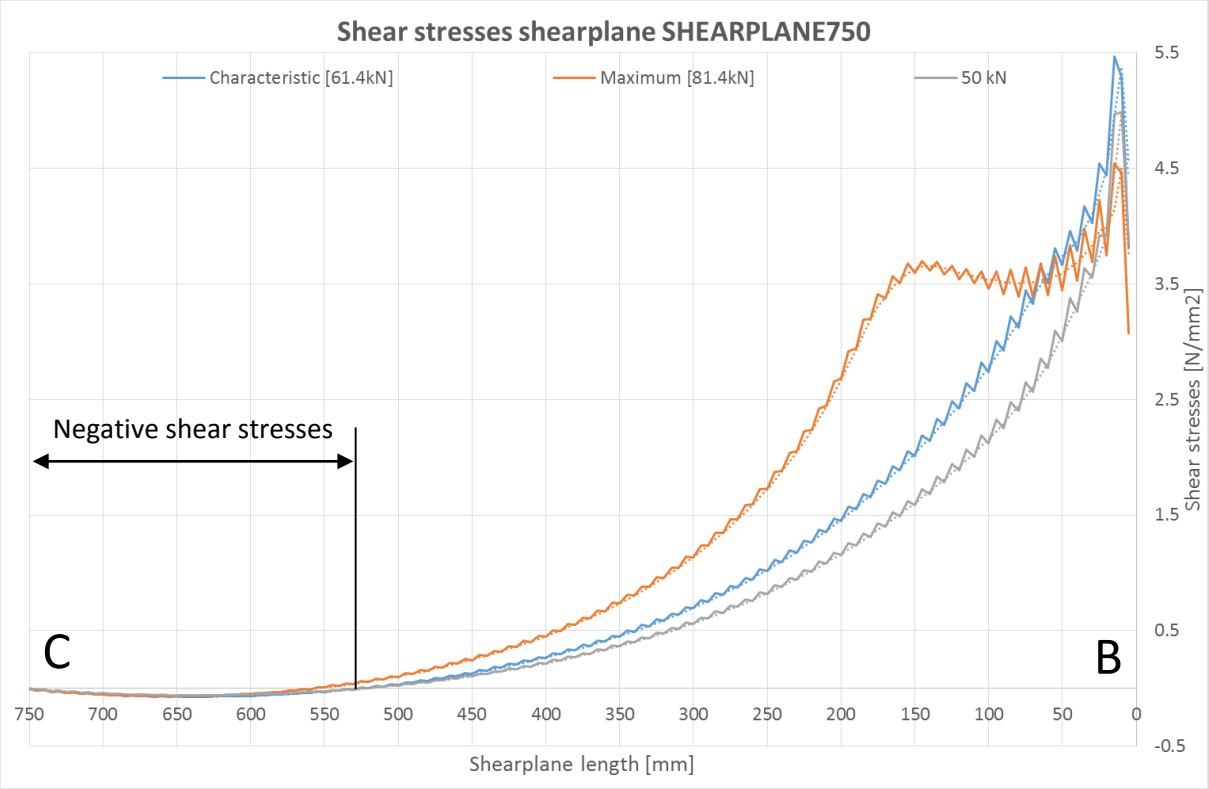

Figure 44: Stress distribution in the shearplane (CB) at important load conditions

50kN

At a load of 50kN, The shear stress distribution is “exponential”. The line crosses the ‘Shearplane length’ axis ± 525mm from the tooth of the notch. After this point, the shear stresses are negative, meaning that they act in the other direction. As these stresses are very low, it can be assumed that the shearplane is not loaded in shear after the first 500 to 525mm.

Characteristic [61.4kN]

At the characteristic design load of 61.4kN, the shear stress distribution is behaving similar to the 50kN distribution, with the difference that stresses are slightly higher. The line already shows a small dip near the peak stress at the tooth of the notch. The shear influenced length of 500 to 525mm does not change.

Maximum [81.4kN]

The highest load in the simulation is 81.4kN. The stress distribution again shows a plateau in the first 150mm. Shear stresses are around 3.75N/mm^2, as defined as shear strength. The influenced length has increased slightly to ± 575 mm.

FNANGLE90D

The results from the model FNANGLE90D (with a frontnotch angle γ of 90°) along the shearplane length s_{notch} (500mm) are extracted from the results and are graphically shown in Figure 45.

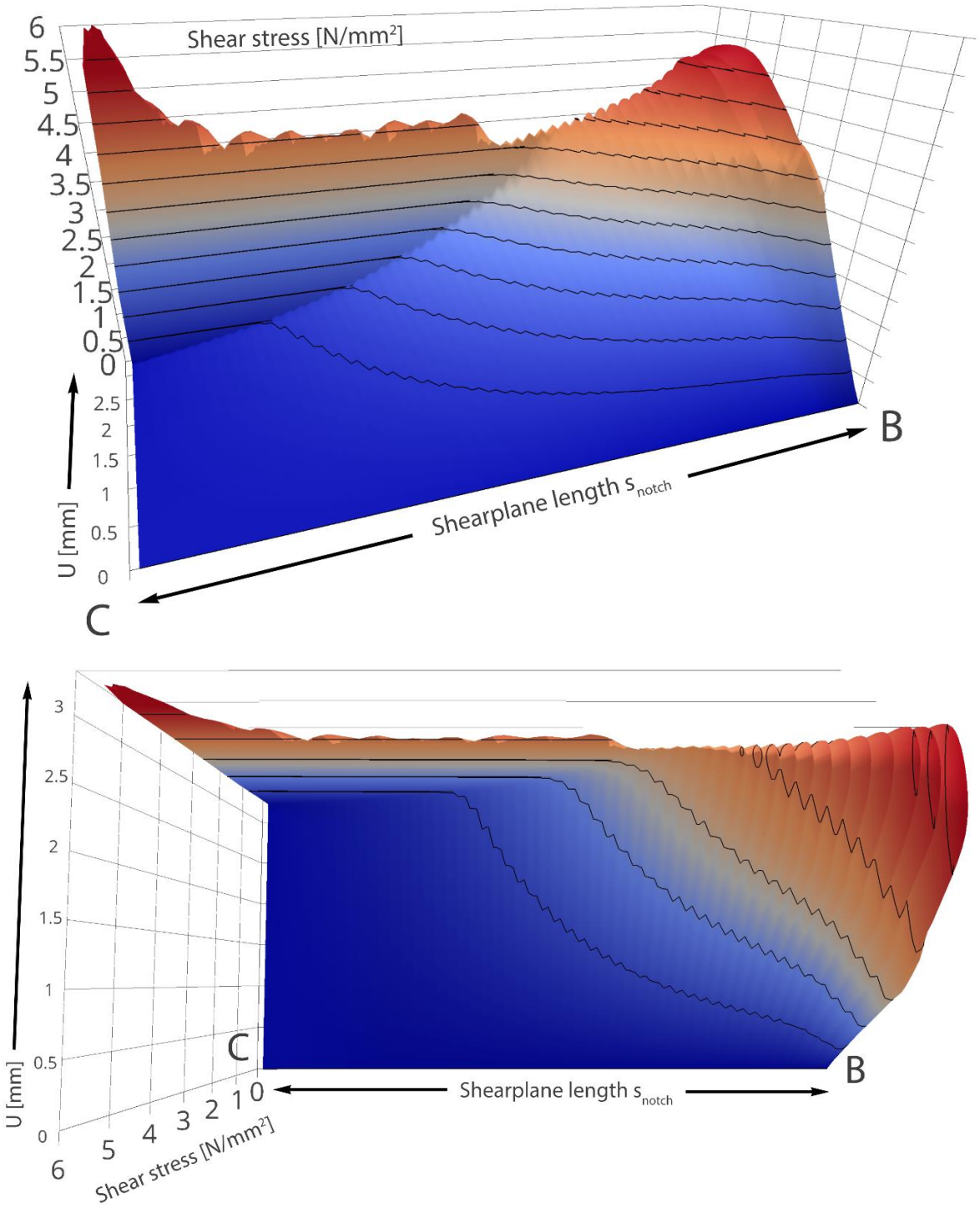

Figure 45: Shear stresses in the shearplane (CB) of the FNANGLE90D model, while the model is loaded

The 3D plot of the FNANGLE90D simulation shows similar behavior to the REFGEOM model. A slight incensement in shear stress capacity can be seen. This is verified by the higher maximum load of 87.6kN compared to 81.4kN in the REFGEOM.

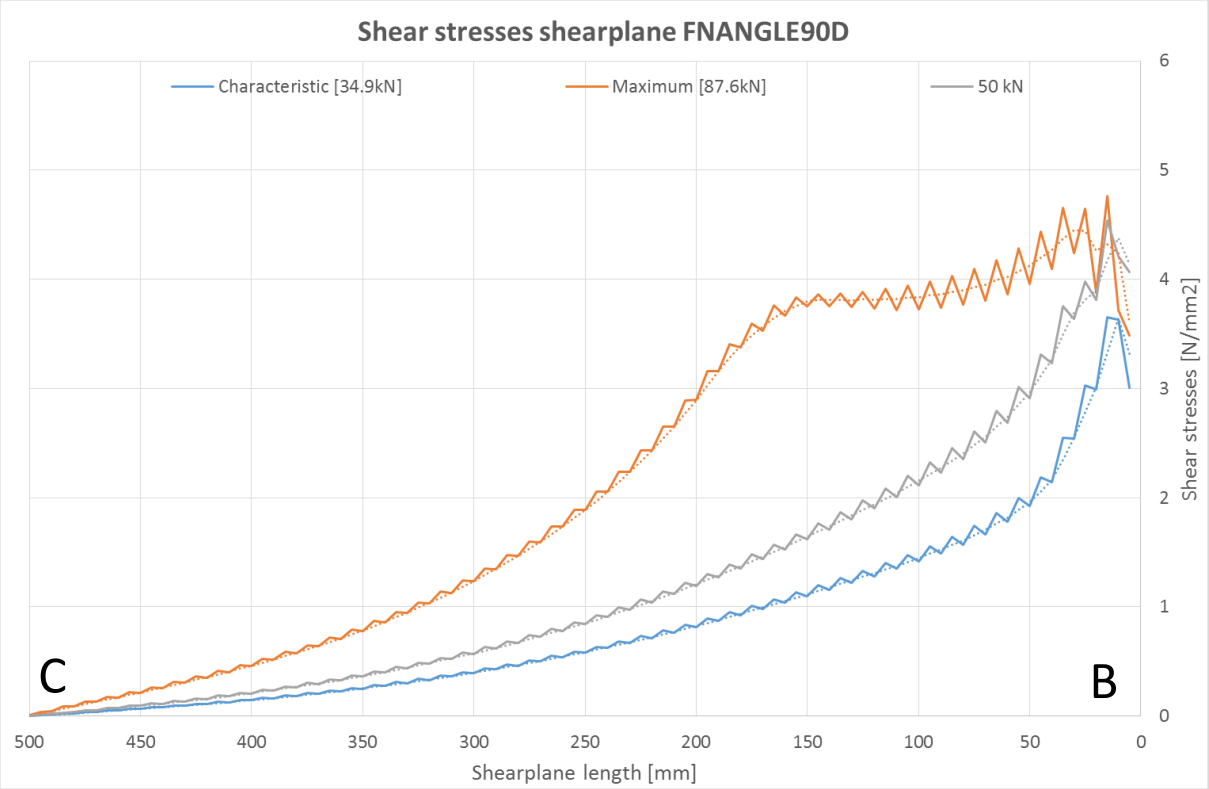

Figure 46: Stress distribution in the shearplane (CB) at important load conditions

Characteristic [34.9kN]

The stress distribution of the characteristic design load of 34.9kN differs a little from the REFGEOM simulation, as it shows more linear behavior. This although, can be explained by the very conservative design load that codes give because of the alternate frontnotch angle.

50kN

What stands out in the stress distribution at 50kN is that no high peak stresses appear at the tooth of the notch. The highest stresses appear to be in line with the “exponential” behavior of the distribution.

Maximum [87.6kN]

As previously mentioned, the maximum (failure) load on this geometry is higher compared to the other simulations. The stress distribution still shows a plateau in the first 150mm with stresses a little higher than 3.75N/mm^2.

FNANGLE90B

The results from the model FNANGLE90B (with a frontnotch angle γ of 60°) along the shearplane length s_{notch} (500mm) are extracted from the results and are graphically shown in Figure 47.

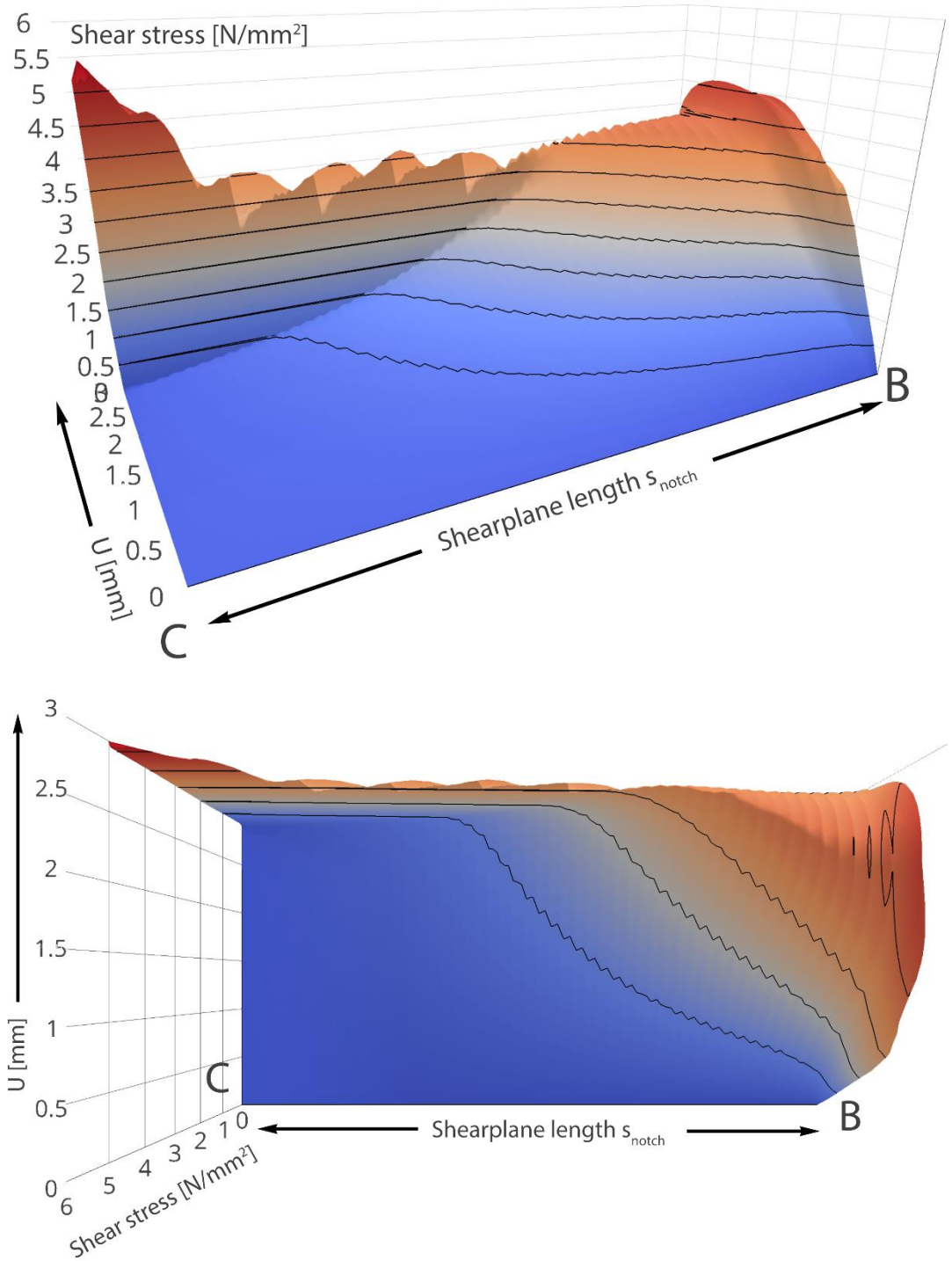

Figure 47: Shear stresses in the shearplane (CB) of the FNANGLE90B model, while the model is loaded

The 3D plot of the FNANGLE90B simulation shows a more flattened behavior of the stresses near the tooth of the notch over time (introduced displacement). Peak stresses near this tooth appear to be much lower compared to the reference REFGEOM simulation.

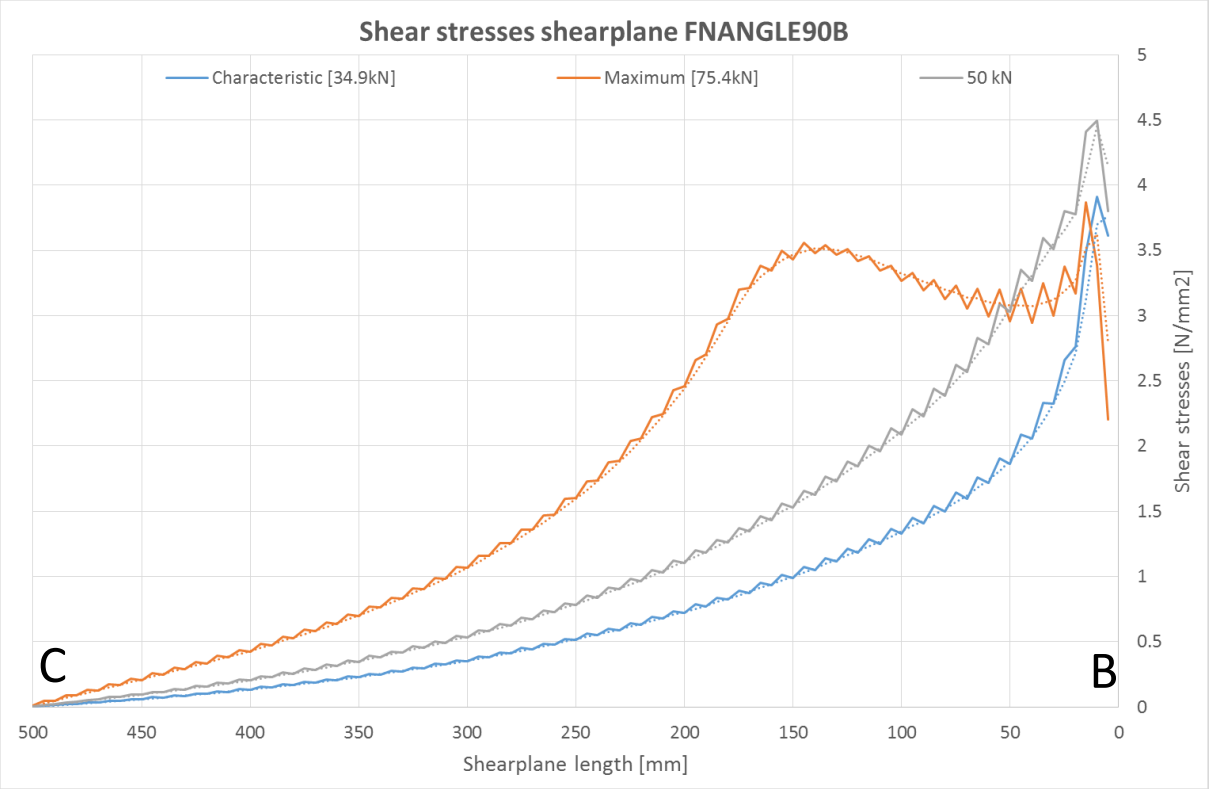

Figure 48: Stress distribution in the shearplane (CB) at important load conditions

Characteristic [34.9kN]

The stress distribution at the conservative characteristic design load again shows more linear behavior at the back (left) side of the shearplane compared to the REFGEOM. A peak stress appears near the tooth of the notch, although this seems to be in line with the “exponential” behavior.

Maximum [75.4kN]

The plateau in the stress distribution, which is present at the maximum load in all simulations shows differ behavior in the FNANGLE90B simulation. First, the stress level is much lower, under 3.5N/mm^2 instead of an average of 3.75N/mm^2. Secondly, a big drop in shear stresses can be spotted after the plateau starts.

Comparison

To compare all geometries, all five simulations are plotted for two load levels. First, the stress distribution of all models at a load of 50kN is compared. After this, the stress distribution at different maximum (failure) loads is compared.

50kN

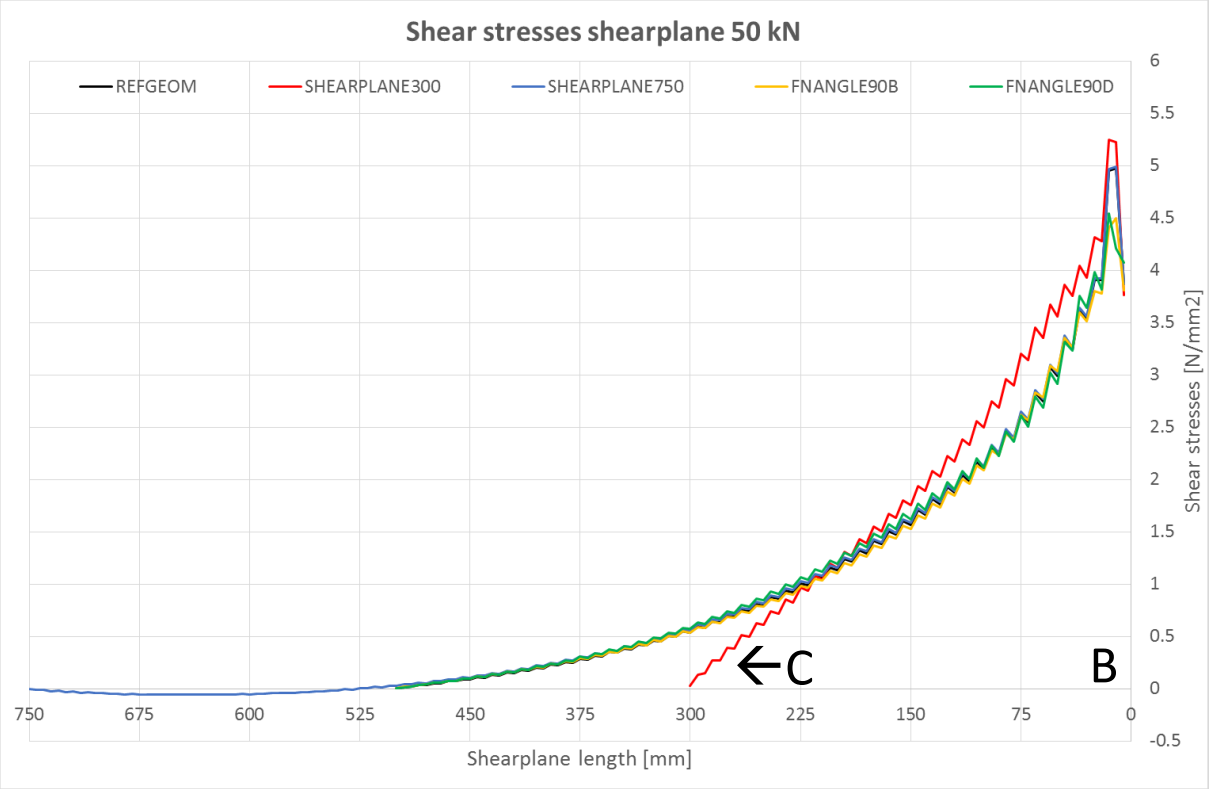

Figure 49: Comparison of distribution of shear stresses in the shearplane (CB) for each simulation, loaded with 50kN

The stress distribution of the shortest SHEARPLANE300 geometry differs from the rest of the simulations. With this, it can be concluded that the short shearplane length does not give the shear stresses enough length to distribute the stresses naturally. Instead, the stresses are forced to distribute over an insufficient length, leading to a higher stress concentration resulting in early shear failure.

Although it is not very clear from Figure 49, the REFGEOM and SHEARPLANE750 lines are almost identical. From this it can be concluded that the 250mm extra shearplane length does not change the stress distribution at loads up to 50kN.

The three models with alternating shearplane lengths and standard frontnotch angle, (REFGEOM, SHEARPLANE300, SHEARPLANE750), all show relatively high peak stresses near the tooth of the notch, compared to the two models with different frontnotch angles (FNANGLE90D, FNANGLE90B). The rest of the stress distribution of these last two models is very similar to the stress distributions of the other sufficient shearplane length models.

Maximum load

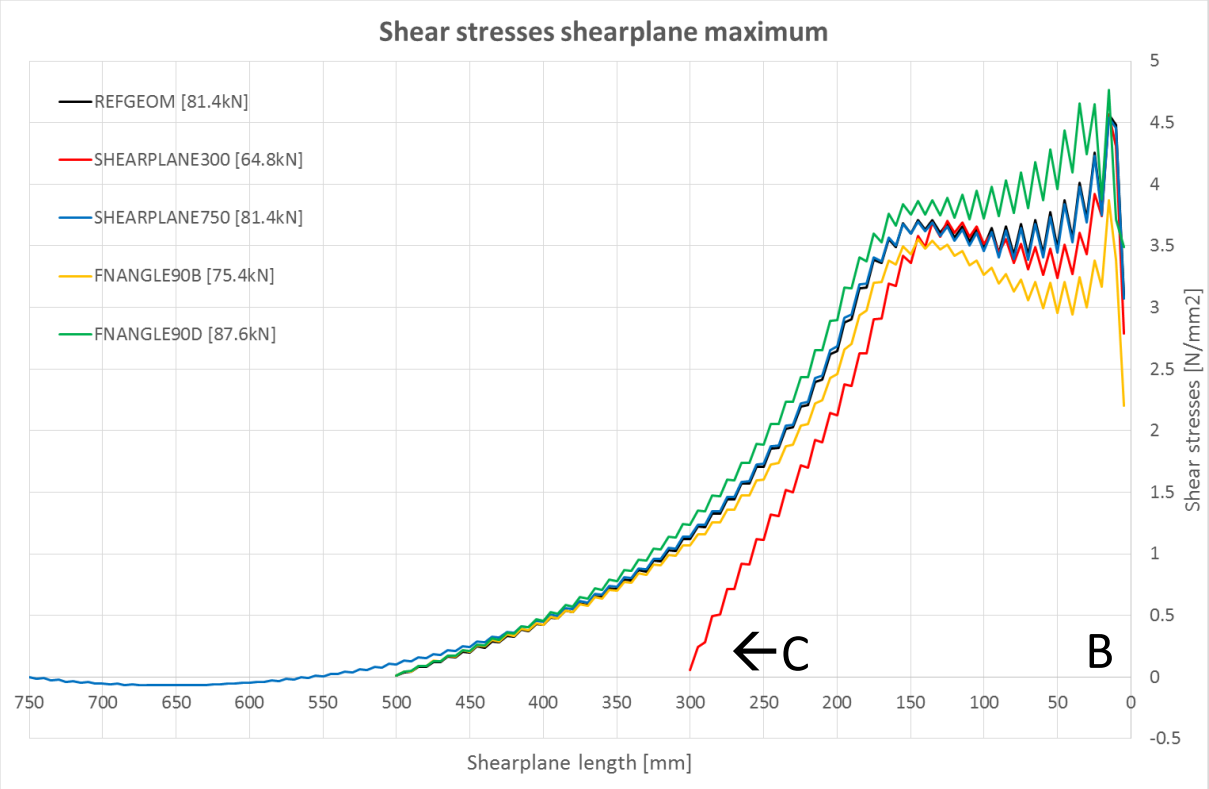

Figure 50: Comparison of distribution of shear stresses in the shearplane (CB) for each simulation, at maximum load

Also the stress distribution at the maximum load is compared. As these failure loads are different for all models, the full stress distribution cannot be compared. Instead, only the stress plateaus which are mentioned at each model are compared.

The graph in Figure 50 shows that all plateaus have about the same length of ± 150mm. This leads to the conclusion that the different geometries do not influence this crack length.

The stress distribution in the plateaus differs per geometry. Again, the REFGEOM and SHEARPLANE750 show almost identical behavior. The SHEARPLANE300 geometry's plateau is a fraction shorter than the other geometries, and stresses are reduced a bit more, compared to REFGEOM and SHEARPLANE750. The stresses in the plateau of the FNANGLE90D simulation are highest. This can be explained by the beneficial compression perpendicular to the shearplane, allowing a higher shear resistance of the material. This higher stress capacity, ultimately leads to the highest load of all models. The lack of compression perpendicular to the shearplane in the FNANGEL90B simulation leads to the lowest stresses in the plateau.

6 Bibliography

[1] NEN, “NEN-EN 1995-1-1 Dutch NA 8.11 Ambachtelijke verbindingen.” Nederlands Normalisatie-Instituut, Delft, 2013.

[2] DIN, “DIN-EN-1995-1-1 German NA 12.1 Versätze.” DIN Deutsches Institut für Normung, Berlin, pp. 88–89, 2010.

[3] SIA, “Schweizer Norm SIA 265 - Holzbau.” SIA, Zürich, pp. 77–78, 2012.

[4] “NEN-EN 338:2009,” no. December. NEN; BrisWarenhuis, Delft, pp. 1–10, 2009.

[5] Forest Products Laboratory, “Wood Handbook: Wood as an Engineering Material,” 2010.

[6] Simulia, “23.2.6 Anisotropic Yield/Creep,” *Abaqus Analysis User’s Guide*. [Online]. Available: http://50.16.225.63/v6.14/books/usb/default.htm?startat=pt05ch23s02abm22.html#usb-mat-canisoyield.

[7] C. Sandhaas and J. W. G. van de Kuilen, “Material Model for wood,” vol. 58, no. HERON. pp. 179–200, 2013.

[8] Systèmes Dassault, “Simulia Abaqus/CAE.” .

[9] Python software foundation, “Python scripting.” [Online]. Available: https://www.python.org/. [Accessed: 22-Mar-2016].

[10] H. J. M. Janssen, “Dictaat Constructief gedrag van elementen,” no. Mechanica 4, 2012.

[11] R. de Rijk, “Plotly,” 2016. [Online]. Available: https://plot.ly/~Richardderijk/folder/home.

Technische Universiteit
Eindhoven
University of Technology

Where innovation starts

Part III - Experimental study

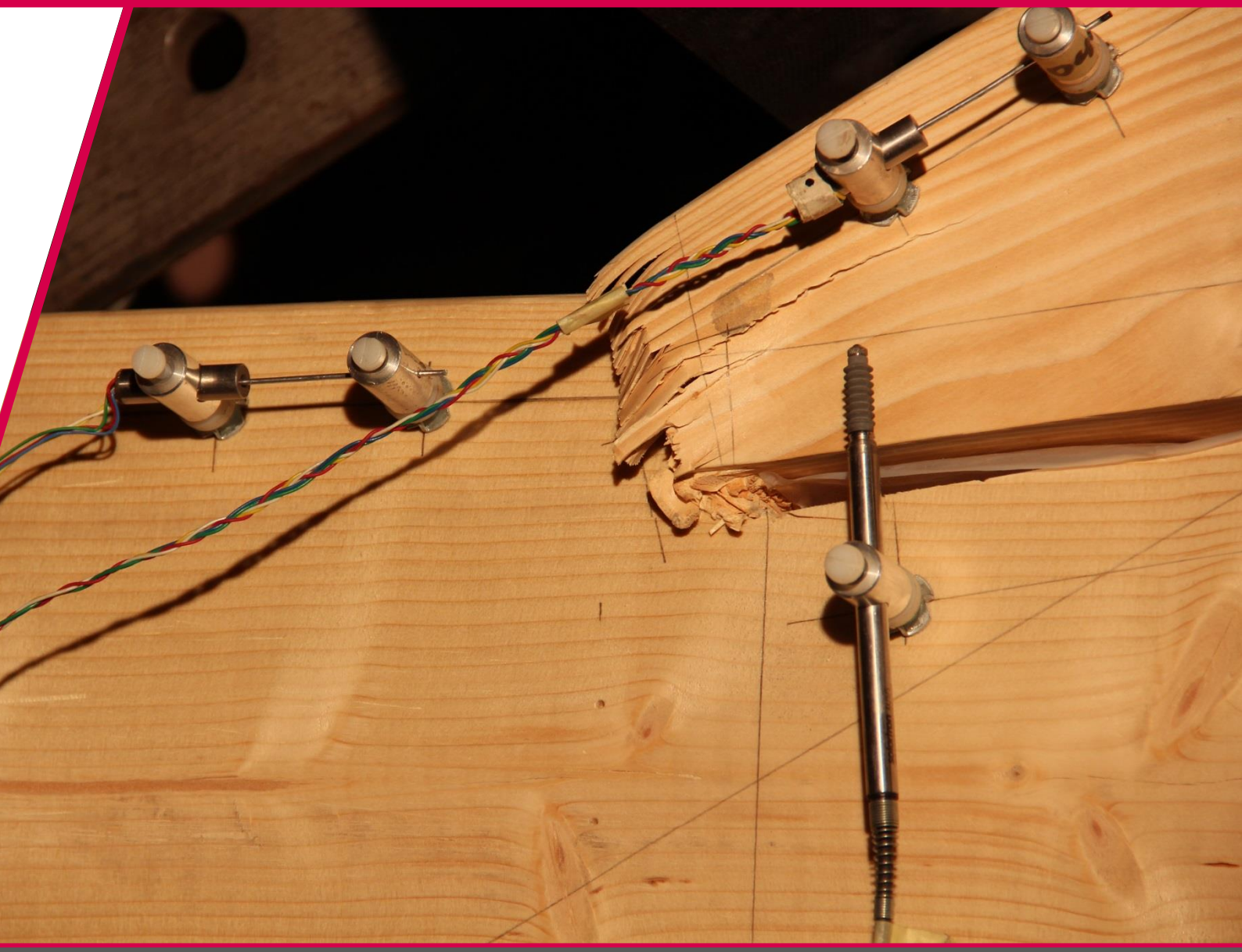

Stresses in a Single Step Joint

April 20, 2016 | Master thesis Structural Design | Richard de Rijk

Abstract

In this part, experiments conducted in the “Pieter van Musschenbroek” laboratory at Eindhoven University of Technology on the timber ‘Single Step Joint’ connection are described and analyzed. First, details about the used test setup are described. Explaining the chosen boundary conditions and realization of creating these in the test setup. Also the used measuring instruments and measurements are presented. Second, the test specimens are threated, explaining the chosen geometries and population. Also the material properties of the specimens are investigated. The hypothesis of the load bearing capacity of each test specimen series is given. The hypothesis is done using several national standards on Single Step Joints (Germany, Switzerland, the Netherlands), giving a good insight in the correctness of these standards in reality. The results of the test are compared to this hypothesis and any abnormalities in the test are mentioned. Conclusions are drawn related to failure loads and failure mechanisms which occurred during the tests. Also the under-, or overestimation of the codes on several topics are discussed.

Table of Contents

1 Test setup

The experimental study was carried out at the Pieter van Musschenbroek laboratory at the Eindhoven University of Technology. For this study a custom made test-setup is designed and built using steel HEB300 beams.

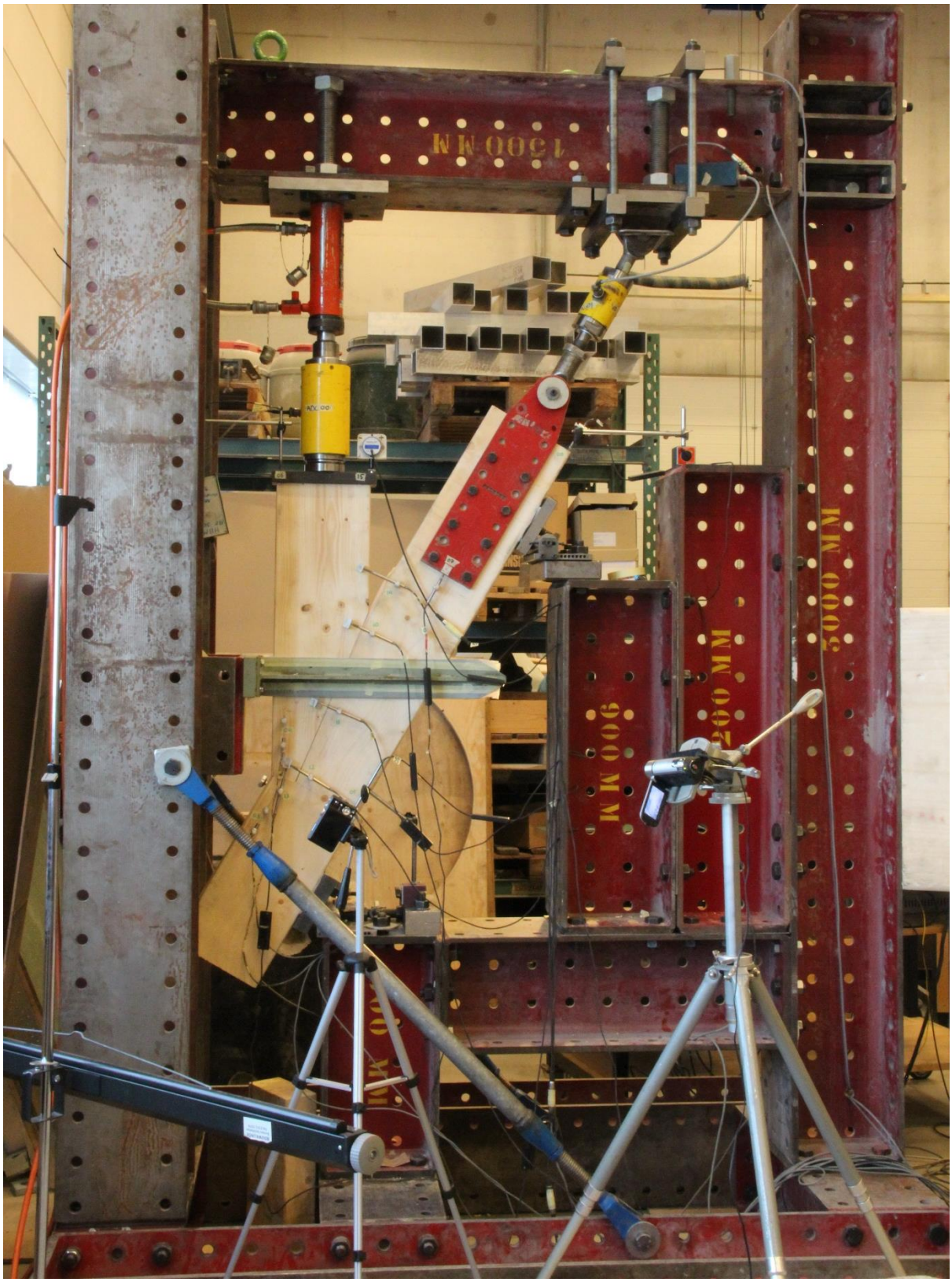

1.1 Boundary Conditions

Loading under a 30° angle

Single Step Joints are made of two timber elements intersecting under a certain angle. It was convienient to design a test frame where the diagonal (strut) is in the upright position, as shown in Figure 1.

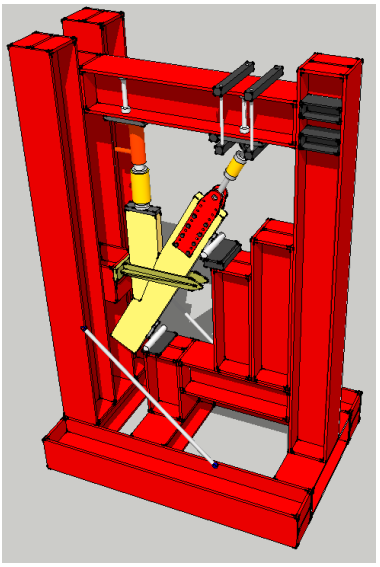

Figure 1: The specimen in placed in the test-setup under a 60° angle.

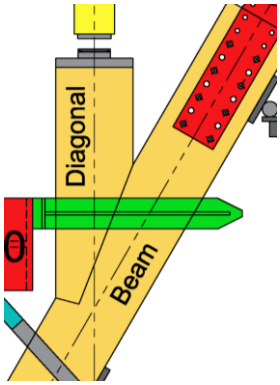

Figure 2: Terminology

* Remark: Because the test specimen is placed diagonally in the test frame this can lead to misunderstandings with the terminology for the test specimens. To clarify:
The diagonal (strut) element in the specimens is placed in upright position. The Beam (chord) is placed diagonally. When the report refers to the diagonal, the diagonal (strut) as shown in Figure 2 is meant.

Vertical support

For this test series the boundary conditions are based on the practical situation where a triangular roof truss is placed on the structural walls of a building. This means that the specimen has a vertical support, roughly near the intersection of the system lines of the diagonal and the horizontal beam element, representing a structural wall. In order to prevent stresses and deformations due to shear force (eccentricity), the front vertical support underneath the beam is placed in the system line of the force introduced by the actuator in the diagonal. The specimen is free to deform in horizontal direction and to rotate on the support.
In order to achieve this boundary condition, steel roller supports are used to provide the vertical support of the specimen. Due to the support's ability to rotate, no forces in other directions than perpendicular to the beam (Vertical direction) can be transferred, ensuring a pure vertical reaction force. An extra vertical support is placed at the back of the specimen's beam to prevent vertical displacement. These displacements will only occur due to (small) misalignment and (small) shear forces in the beam. This vertical support also ensures that the pendulum rod at the back of the specimen stays aligned with the length axis of the beam.

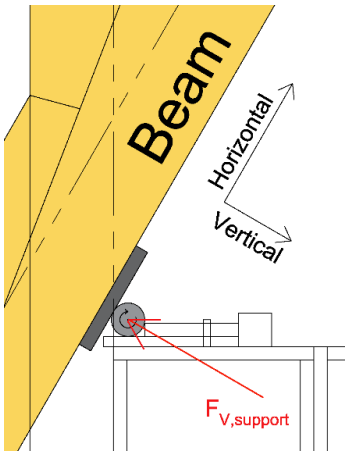

Figure 3: Support force $F_{V,support}$

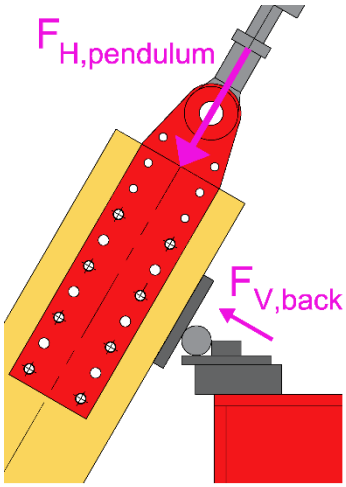

Figure 4: Vertical support at the back of the beam

Horizontal support

The specimen must also be supported in the horizontal direction. This support is placed at the back end of the beam, representing a

continuous beam. In the test setup it was chosen to ensure horizontal support via a pendulum rod because:

- A pendulum rod can transfer only a pure tension or compression force in the axial direction of the rod, ensuring a pure horizontal support;
- Since only one axial force can be transferred, this forced can be measured with a load cell without any distortion in the measurements due to eccentric forces. (vertical components)
- With the use of rod ends the length of the rod can be adjusted to align the test specimen with the supports and actuator.

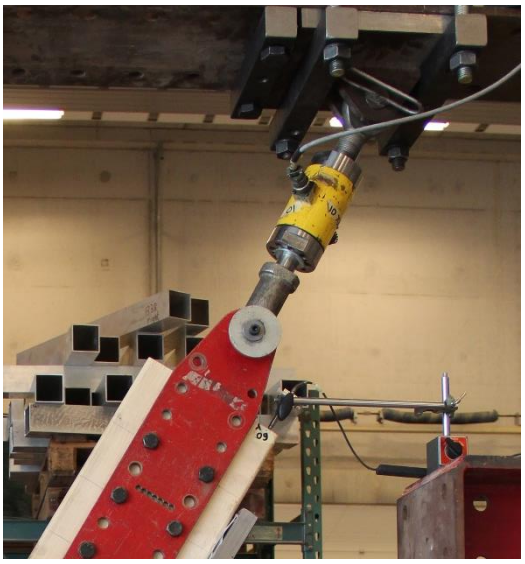

Figure 5: Pendulum rod horizontal support

To connect the pendulum rod to the specimen's beam, steel plates are mounted at both sides of the beam with bolts. This connection is designed using EN 1995-1-1 (8.2.3),(8.5.1),(appendix A) [1] and EN-1993-1-1 (6.2.3),(6.2.6),(3.5) [2]. These calculations can be found in appendix D. This resulted in a connection with 10mm thick steel plates with 2 rows of 4 M16 bolts at 100mm spacing. To reduce deformations (slip) between the steel plates and timber beam during the test, after mounting the specimen in the test setup, the specimen is loaded to a 20kN force before the bolts are tightened. During tightening of the bolts eventual flaws between the contact area of the steel plates and the timber beam due to shrinkage of the timber are resolved. The bolts are prestressed using a hand-torque-wrench to ensure the connection transfers the applied force using friction between the steel and timber as well as shear in the bolts.

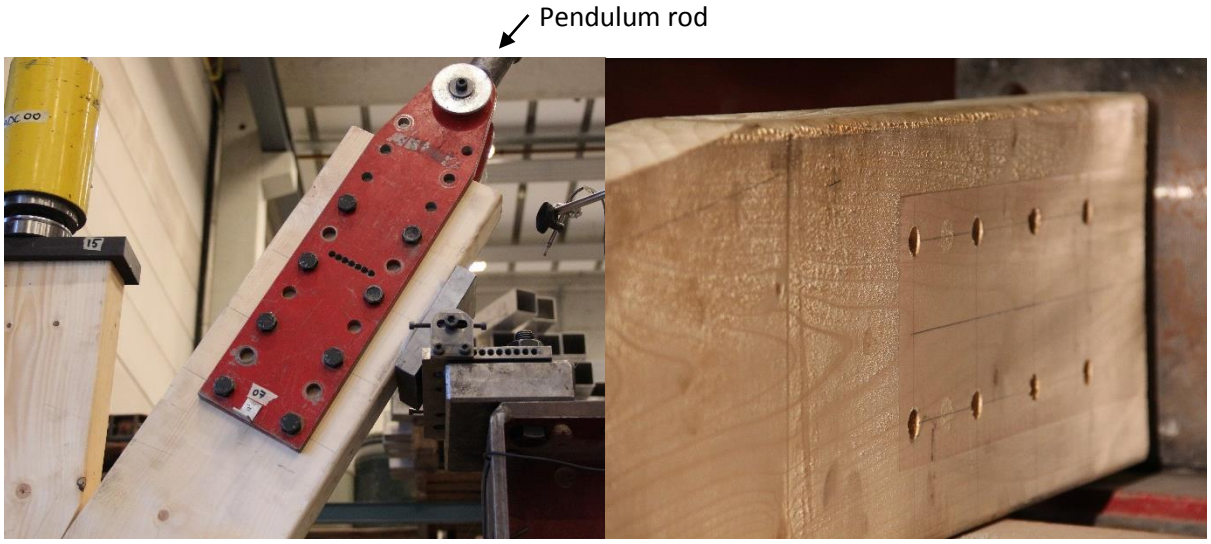

Figure 6: a) Bolted steel to timber connection with 4x2 M16 bolts b) Result of tightening of the bolts

Out-of-plane support

Because the connection consists of two slender beam elements in compression, which could be unstable in out-of-plane direction, the specimen must be supported to prevent this out-of-plane motion. For this, a steel fork is placed near the intersection of the elements, providing out-of-plane support to both elements. The fork is clamped to both sides of the specimen. To prevent load bearing of the fork due to friction between the fork and the specimen, Teflon layers are applied to both the specimen and the fork.

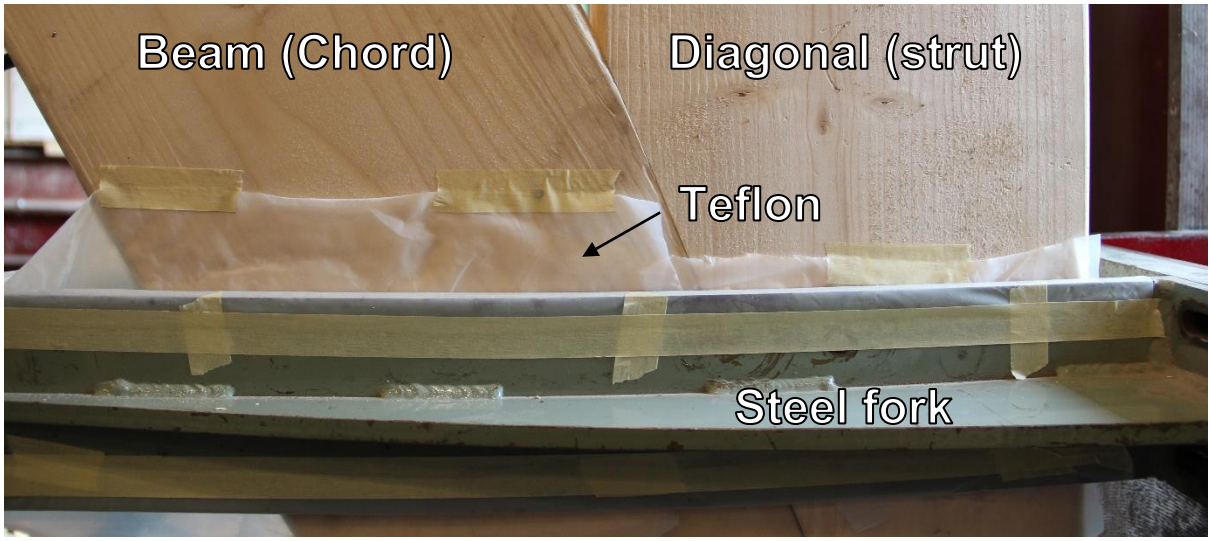

Figure 7: Steel fork, with Teflon applied between the contact areas, providing out-of-plane stability to the specimen

Test frame stiffening

Because measurements on the specimen are done using Electronic Speckle Pattern Interferometry (ESPI), the test setup needs to be very stiff to reduce displacement of the specimen due to deformations in the test setup. Therefore, several components are added to the test setup to enhance the stiffness. Were the specimen is supported or loaded, extra adjustable rods are placed between the flanges of the beams of the setup frame to prevent local buckling. These rods are also placed between flanges under the columns of the setup frame. To prevent the frame from swaying, the corners of the frame are stiffened by adding tensioned diagonals. Were this is not possible, extra steel stiffeners are placed.

Figure 8: a) Adjustable rod near actuator b) Steel stiffeners c) Steel diagonal prestressed in tension

Flexibility / Adjustability

5 different test series are carried out with different specimen geometries. The test setup must be adjustable to these different geometries, meaning that enough space has to be available to allow for shearplane lengths of the beam varying from 300mm to 750mm. Also, since the angle of the frontnotch is varying, the whole specimen must be able to shift along the beam's axis. This is accomplished by using rod ends with long internal thread in the pendulum rod, allowing to elongate the pendulum rod, and thereby shifting the specimen into place. Finally, the test setup is able to compensate small deviations in each specimen's geometry by adjusting the positions of the roller supports slightly and adjusting the position of the fork slightly to align the specimen in both in-plane and out-of-plane directions.

1.2 Measurement instruments

Two different types of measurements are done during the test. The first, most conventional group of measuring instruments, translate analog movements to digital measurable movements. The second measuring instrument, ESPI, uses laser light frequency to translate small movements in a surface to a speckle pattern which can be translated to displacements and strains.

LVDT, Inclinometer, Load cell measuring devices

To measure deformations of the specimen and the test setup, several measurement devices are used. Table 1 and Figure 9 show the locations and type of measurement devices.

Table 1: List of used ADC measuring instruments and their measurements

NUMBER	DEVICE	MEASUREMENT
ADC-00	Load Cell (350kN)	Load applied in diagonal by actuator
ADC-01	Load Cell (150kN)	Horizontal force in beam
ADC-02	LVDT (250mm)	Deformation of the test setup (diagonally)
ADC-03	LVDT (4mm)	Deformation beam over 60mm length, 90mm from notch surface
ADC-04	LVDT (4mm)	Deformation diagonal over 60mm length, 90mm from notch surface
ADC-05	LVDT (20mm)	Displacement top of the diagonal (elongation of the actuator)
ADC-06	LVDT (20mm)	Displacement of the beam directly below the notch tooth
ADC-07	LVDT (5mm)	Slip in connection with bolted steel plates
ADC-08	LVDT (5mm)	Slip between diagonal and beam parallel to bottomnotch
ADC-09	LVDT (5mm)	Displacement of the back of the beam (elongation pendulum rod)
ADC-10	LVDT (10mm)	Butting bottomnotch (back)
ADC-11	LVDT (10mm)	Butting bottomnotch (middle)
ADC-12	LVDT (10mm)	Butting bottomnotch (front)
ADC-13	LVDT (10mm)	Butting frontnotch
ADC-14	LVDT (10mm)	Gape/closure skew angle between diagonal and beam
ADC-15	Inclinometer (±15°)	Rotation of the top of the diagonal (in plane)

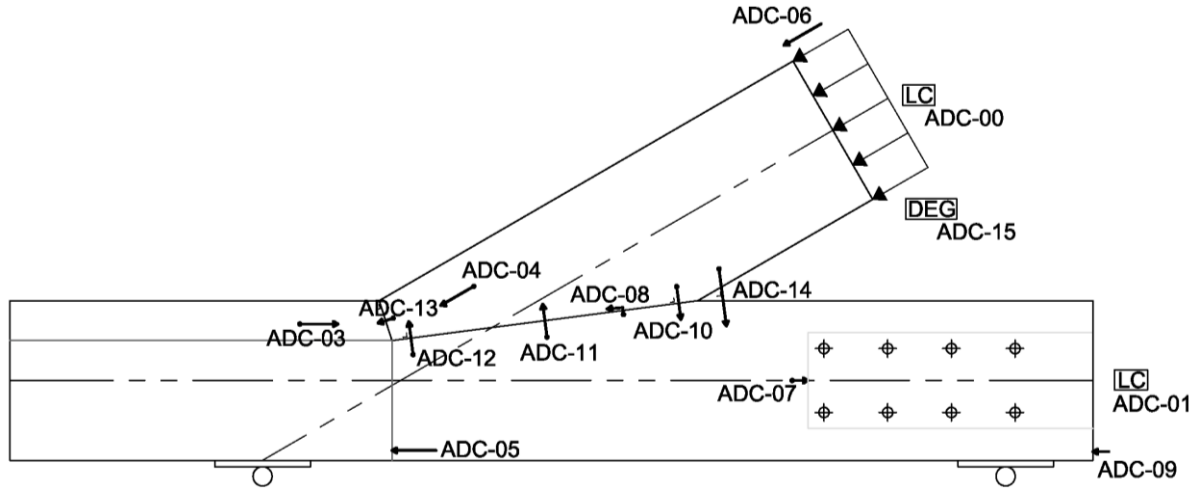

Figure 9: Locations of measurement devices on the specimen

ADC-00 350kN Load Cell

This Load Cell is mounted directly under the actuator. A capacity of 350kN is chosen because this exceeds the expected failure load. The concentrated force coming from the actuator travels through the Load Cell into an axial spherical plain bearing, ensuring a one-directional force in the diagonal of the specimen, and preventing bending moments from being introduced into the actuator. An extra steel bearing plate is placed on the total cross-sectional area of the specimen to help spread the concentrated force over the full cross-section of the specimen.

Figure 10: ADC-00 Load Cell

ADC-01 150kN Load Cell

To measure the tensile force in the beam element, a Load Cell is placed in the pendulum rod supporting the specimen. This Load Cell measures the force traveling through the pendulum rod which is supposed to be the same as the force travelling through the frontnotch area of the carpentry connection. A capacity of 150kN is chosen as about 80kN is expected as ultimate load and the bolted connection is designed to withstand 100kN (characteristic).

Figure 11: ADC-01 Load Cell

ADC-02 250mm LVDT

In order to monitor the deformation of the test setup during the tests, an LVDT-based measurement device was used. This device measures the length over which a string is pulled out of the device. This string is connected to a wire which is placed diagonally through the frame of the test setup, and back to the meter. The range of this instrument of 250mm is very big compared to the measured deformation and proved to be quite inaccurate. Since this instrument posed a quick and simple way to measure the deformations, and the measured deformations were only meant for monitoring the test, this device was used.

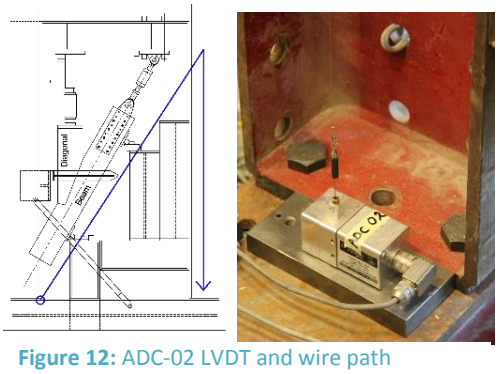

Figure 12: ADC-02 LVDT and wire path

ADC-03, ADC-04 4mm LVDT

LVDT ADC-03 and ADC-04 are placed on the specimen's beam and diagonal, in parallel to the grain direction, to measure the elastic and plastic behavior of the wood. The displacements are measured over a length of 60mm. With this info the strain of the material can be determined. Therefore, a LVDT measurement range of 4mm was chosen, allowing precise measurements for small deformations. The LVDTs are placed with an offset of 90mm from the frontnotch surface of the connection. This is done to prevent to influence peak-stresses, and early crushing of the wood due to geometric imperfections in the connected surfaces, as much as possible.

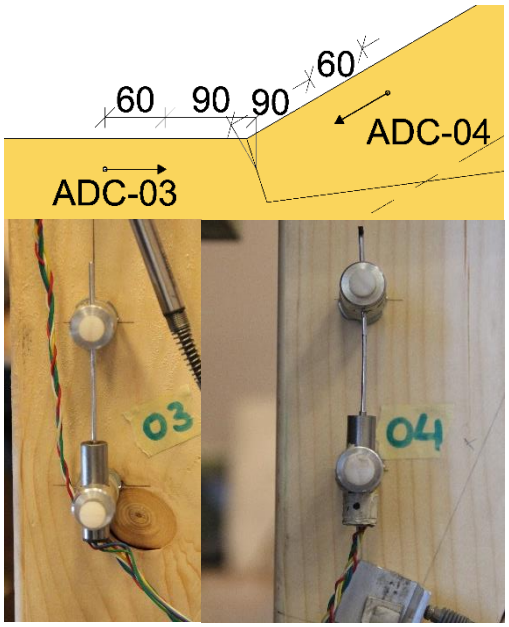

Figure 13: ADC-03 and ADC-04 LVDTs

ADC-05 20mm LVDT

ADC-05 measures the displacement of the beam in axial direction, and can therefore be linked to the force measured with ADC-01 to create a force-displacement diagram of the beam. ADC-05 is located directly beneath the tooth of the notch. This location is chosen so the results from ESPI can be linked to displacements obtained from the finite element model. The LVDT is mounted directly to the loaded test setup near the vertical roller support. Extra displacements in the measurement of the LVDT due to deformations of the test setup are assumed very small and are therefore neglected.

Figure 14: ADC-05 LVDT

ADC-06 20mm LVDT

LVDT-06 measures the elongation of the actuator via the sagging of the steel bearing plate on top of the diagonal element. The measured displacement is coupled to the force in ADC-00 to form a force-displacement diagram of the specimen. Again, this LVDT is mounted to the loaded test setup, since the deformations of the test setup are assumed to be very small, these deformations are neglected.

Figure 15: ADC-06 LVDT

ADC-07 5mm LVDT

This LVDT is placed between the timber en steel elements of the bolted support connection on the back-end of the beam. This is done to monitor the slip in the connection. If any sudden slip would occur during ESPI measurements, this LVDT could help stabilizing ESPI images.

Figure 16: ADC-07 LVDT

ADC-08 5mm LVDT

This LVDT measures the slip of the diagonal compared to the beam parallel to the bottomnotch surface. This was also done to monitor slip, and potentially help stabilizing ESPI images.

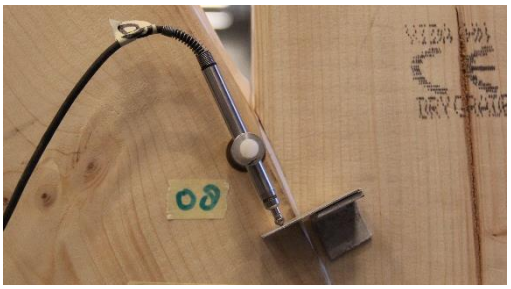

Figure 17: ADC-08 LVDT

ADC-09 5mm LVDT

ADC-09 measures the sagging of the beam in its axial direction which is caused by elongation of the pendulum rod. This rod is equipped with rod ends beared with PTFE fabric. This PTFE fabric, together with the elastic elongation of the steel, allows relatively large deformations to occur in the pendulum rod. These deformations are subtracted from ADC-05 and ADC-06 measurements to give actual deformation of the timber beam and diagonal element.

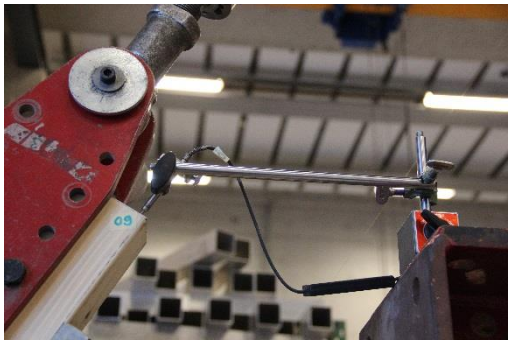

Figure 18: ADC-09 LVDT

ADC-10, ADC-11, ADC-12, ADC-14 10mm LVDTs

In the direction perpendicular to the bottomnotch, three LVDTs are placed over the length of the bottomnotch to measure deformations perpendicular over the bottomnotch length. These deformations could give an indication on stress distribution over the length of the bottomnotch and location of stress peaks.
ADC-14 is placed aligned with the three bottomnotch LVDTs but is placed higher so timber deformations do not affect this measurement. This leads to a measured displacement due to rotation of the diagonal only.

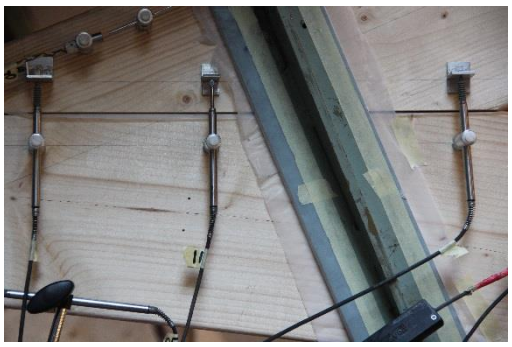

Figure 19: (f.l.t.r.) ADC-12, ADC-11, ADC-10 LVDTs

ADC-13 10mm LVDT

ADC-13 is placed perpendicular to the frontnotch surface. This device is placed to identify first signs of crushing the timber fibers. Since the small range of 10mm, small displacements can be measured accurately.

Figure 20: ADC-13 LVDT

ADC-15 ±15° Inclinometer

The last ADC device used in the test is an inclinometer which is mounted to the steel bearing plate on top of the diagonal. This device measures the rotation in-plane of the diagonal (in degrees) due to the applied load. Since this rotation is very low, the inclinometer with the smallest degree range available is used. This still gives a very rough measurement, so the data is only used to monitor the test.

Figure 21: ADC-15 Inclinometer

Electronic Speckle Pattern Interferometry (ESPI)

An ESPI measurement is used to obtain information about the deformations in the front of the frontnotch (shown in Figure 25). Here, shear stresses are acting on the shearplane from the tooth of the notch to the front of the beam. These can never be measured by LVDT's or strain gauges since also bending and compression deformation is acting in this area. The horizontal displacements in front of the connection, which is related to the shear force, are measured using ESPI. This measuring device is able to record displacements at the surface of the investigated area. It uses two expanded laser beams (two for direction x and y) which are calibrated to be aimed at the same surface of the specimen. The reflection of the laser beams off of the surface is measured using a camera. Because the specimen has a rough surface, small deformations of the surface cause a difference in the reflection of the laser light. The first image is a reference for all following images. The differences in reflection is translated to a certain grey scale of a pixel of the image creating a speckle pattern. For these experiments ESPI was used when specimens are loaded from 20kN to 25kN and from 40kN to 45kN. After the measurement has taken images every 5 seconds, the computer analyses the speckle images to create fringe images. On these images the behavior of the deformations is clearly shown using lines of equal deformation. These fringe images are used to calculate deformations and strains in the measured surface and show them graphically in a color plot of the deformations/strains.

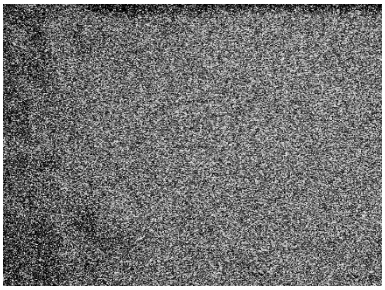

Figure 22: Speckle pattern image

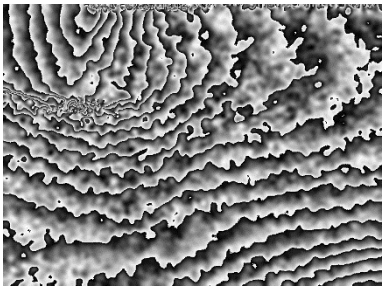

Figure 23: Fringe image of deformations in x-direction

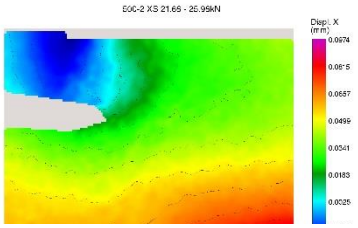

Figure 24: Color plot of deformations in x-direction of the measured surface

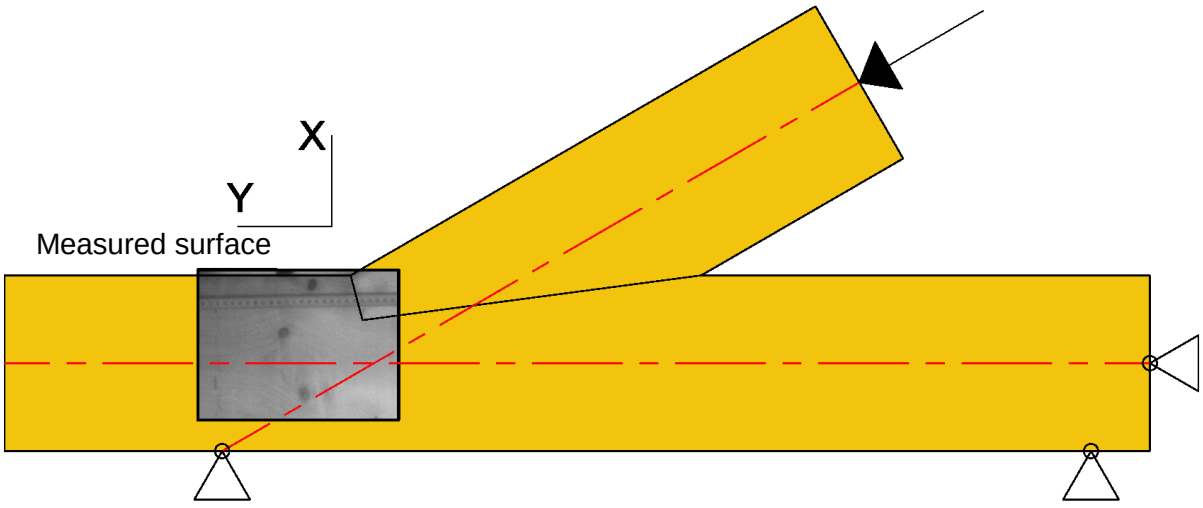

Figure 25: Location of the measured surface in front of the connection (surface roughly 280x210mm)

2 Test specimens

2.1 Geometry

5 different geometries are tested. These 5 series have different lengths of shearplane and differences in the angle of the frontnotch as shown in Table 2.

Shearplane length: The length of the shearplane is varied to see if there is any in- or decrease of the load carrying capacity of the connection. Also, using ESPI, changes in shear stresses can be seen. 500mm length was used as reference since this length is used in the German code [3] as the allowable maximum length to use in calculations ($8 \cdot t_{notch}$). 300mm was the shortest possible length to be supported, since the vertical support is placed in line with the actuator. To investigate whether a length longer than allowed to use according to the German code, 750mm ($12 \cdot t_{notch}$) is used as the longest length.

Frontnotch angle: The angle of the frontnotch is also varied to investigate what the effect of this angle is on the load carrying capacity of the connection. The angle is varied as shown in Figure 26. The angle of 15° results from half of the angle between the beam and diagonal element (30° in this test series). This angle for the frontnotch is set to be used by the German and Swiss [4] codes. The Dutch [5] code allows the angle to vary between (in this case) 15° and 30°. Also, a 0° angle of the frontnotch was tested to see a trend in the different behavior of the frontnotch.

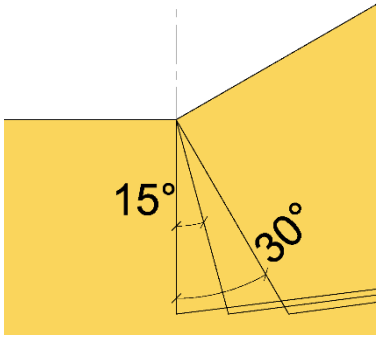

Figure 26: Different frontnotch angles

Table 2: Matrix of the tested specimen series

Shearplane → angle ↓	300mm	500mm	750mm
0°		90B series	
15°	300 series	500 series	750 series
30°		90D series	

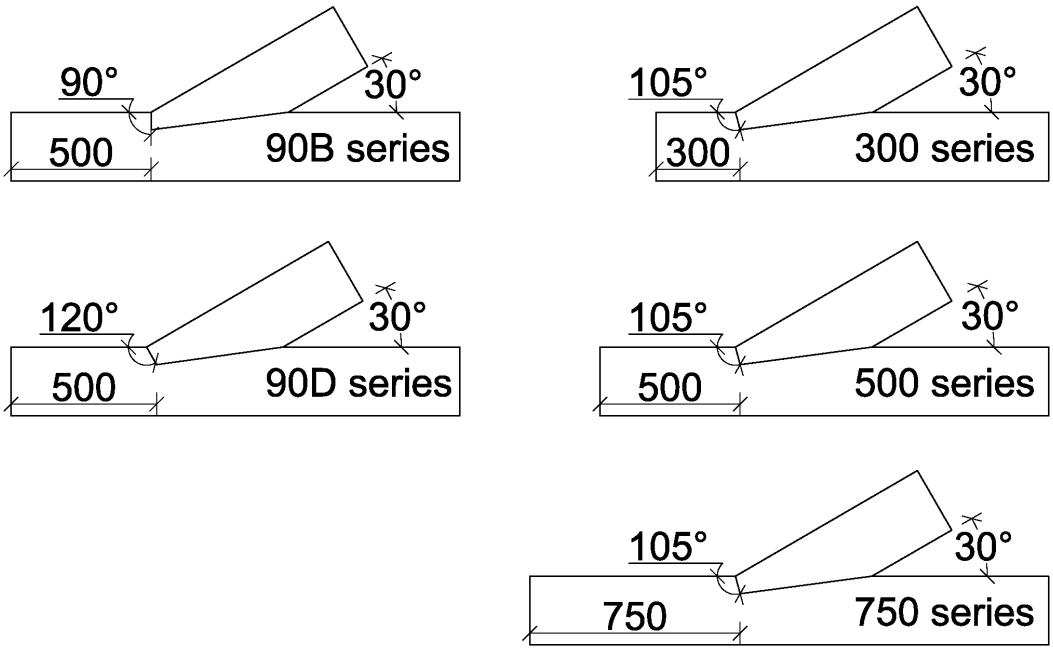

Figure 27: Geometries of the different test series

2.2 Population

Per test series, 3 specimens are made, giving a total of 15 specimens. The specimens are numbered by i.e.: 01-500, where the first number represents the test-number and the second number represents the specimen's series as mentioned in Table 2.
ESPI was used in 2 out of 3 specimens for each series. During each test, two measurements are done, resulting in 4 ESPI measurements for each test series.

2.3 Material properties

The tests are performed using spruce timber beams of strength class C24. A total of 20 beams are ordered to make the 15 specimens. Using a Timber Grader MTG the Young's modulus of each beam was measured, ensuring the best beams being used to manufacture the specimens.

Figure 28: a) Moisture content FME meter, b) Timber Grader MTG

Also the moisture content and specific gravity of the beams are measured at the following moments during the experimental research: After delivery (before manufacturing), after manufacturing and, after testing. The results of these test are enclosed in appendix E.

2.4 Manufacturing

The specimens are manufactured at the company 'Heko Spanten' in Ede using CNC cutting.

Figure 29: Specimens being fabricated with CNC cutting equipment at HEKO spanten

2.5 Test protocol

All steps made during placing of the test specimens ahead of the test are presented in the test protocol. This protocol can be found in appendix F.

3 Loading procedure

The load on the specimen is applied using a computer controlled actuator for all tests, except the first specimen (500-1). During the first test, the load was applied using a hand-controlled pump.

The specimen is loaded according to ISO 6891. [6] This standard prescribes to load the specimen to a load of 40% of the estimated ultimate load. This 40% force must be kept constant for 30 seconds. Hereafter the load is decreased to 10% of the estimated ultimate load and must also be kept constant for 30 seconds. This procedure is shown in Figure 30.

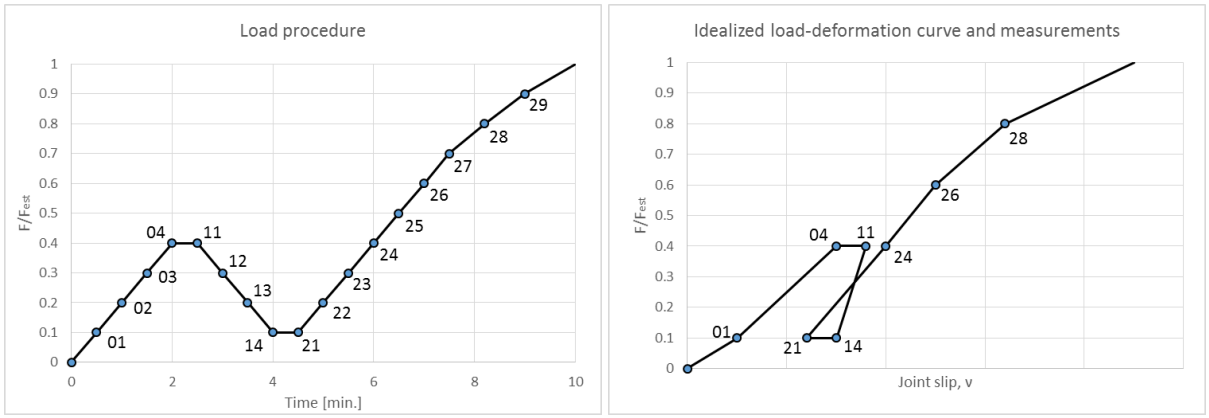

Figure 30: Loading procedure and idealized load-deformation curve according to ISO 6891

The estimated ultimate load is set to 100kN for al tests. In order to roughly follow the time schedule for the load procedure the test speed of the actuator is set to 5mm/min. As this speed is too high to perform an ESPI measurement the speed during these measurements at 20-25kN and 40-45kN are decreased to 0.25mm/min. This results in a load procedure as shown in Figure 31.

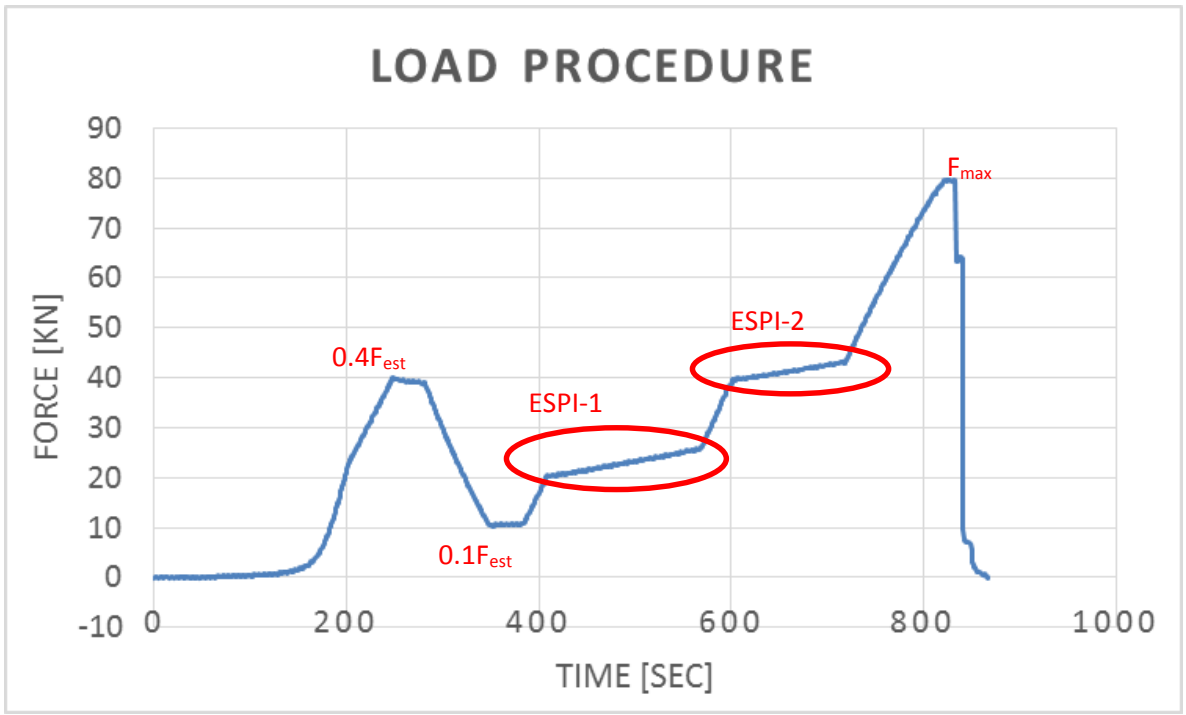

Figure 31: Load procedure (in test 90B-13, load cell ADC-00)

4 Secondary material tests

Figure 32: Compression test for perpendicular to grain loading

Compression tests have been done for several angles to the grain. These tests allow to determine the compressive strength and the elastic behavior of the material. The tests for compression parallel (0°) and perpendicular (90°) to the grain are done according to EN 408. [7] Also specimens with grain angles of 15° and 30°, which are actual loading situations in the Single Step Joint specimens, have been tested to determine the material characteristics. For these two tests, depending on the behavior of the measured data-set, the analysis procedure for 0° or 90° is chosen.

The tests are performed in a 2.5mN test setup at the Pieter van Musschenbroek Laboratory in Eindhoven. Deformation measurements have been done with two methods:

- 4 Mitutoyo measurement devices on each corner of the steel bearing plates of the test apparatus, providing an average displacement in the center of the bearing plates and test specimen.
- 2 ADC LVDTs on the side surfaces of the specimens, placed according to EN 408.

Both displacement measurements are worked out in the data. The measurement which is deemed most accurate is used to conclude on strength and stiffness of the material.

The specimens are taken from the same batch of beams used for the joint specimens. A beam with few knots is chosen, and for the sawing of the specimens, knots are avoided as much as possible.

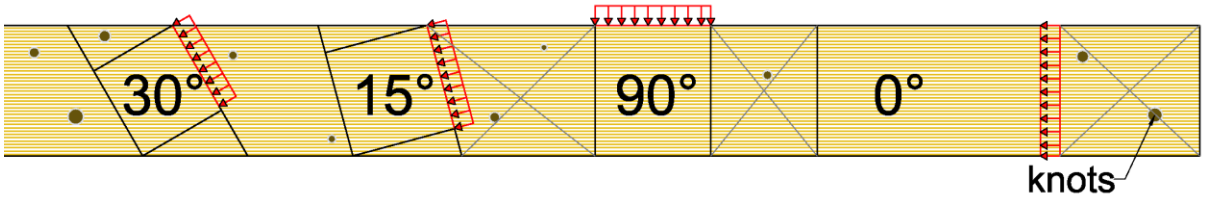

Figure 33: Sawing plan of the specimens in the C24 timber beam.

The results of the tests are presented in appendix G. A summary of the obtained stress resistance and stiffness are shown in Table 3 together with the mean values of C24 timber.

Table 3: Strength parameters for tested C24 specimens for several angles to the grain

Angle α to the grain	$f_{c;\alpha;\mu}$** [N/mm²]	$f_{c;\alpha}$ [N/mm²]	Obtained results vs. mean values	$E_{c;\alpha}$ [N/mm²]
0°	31.5	33.67	+7%	12345
15°	21*	27.05	+29%	4458.2
30°	11.1*	17.15	+55%	2572.3
90°	3.75	1.61	**-57%**	127

* Based on Hankinson equation

** Mean values for C24 are obtained as presented hereafter

5 Hypothesis

A hypothesis of the maximum load that can be applied to each of the specimen series is made using the German [3], Swiss [4], and Dutch [5] standards on Single Step Joints. This is been done using the geometric dimensions of each variant, the characteristic strength values, and mean strength values derived from the characteristic values.

5.1 Geometric parameters

The following geometric parameters are used by the national standards in the hypothesis:

Nr.	Name	α [°]	β [°]	h [mm]	b [mm]	t_{notch} [mm]	l_{notch} [mm]	s_{notch} [mm]
500 series	Reference geometry	15	30	245	70	62.5	490	500
300 series	Small shearplane	15	30	245	70	62.5	490	300
750 series	Large shearplane	15	30	245	70	62.5	490	750
90D series	Strut (diagonal) perp.	30	30	245	70	62.5	490	500
90B series	Chord (beam) perp.	30	30	245	70	62.5	490	500

With:

α is the largest angle of the force to the grain of the element in the frontnotch surface;

β is the angle of the connection between the beam and diagonal;

h is the height of the element;

b is the thickness of the element;

t_{notch} is the depth of the notch in the beam element;

l_{notch} is the length of the notched area in the beam element;

s_{notch} is the length of the shearplane.

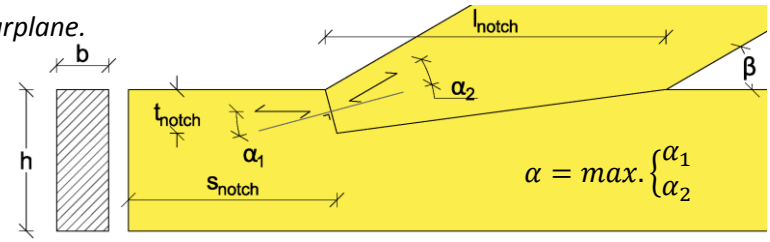

5.2 Characteristic strength values

The characteristic strength values are used to find the lower limit of the expected ultimate load in the connection, as the connection-strength is assumed sufficient with this characteristic values according to the standards. The strength values that are relevant to these standards are; parallel to the grain ($f_{c;0}$), perpendicular to the grain ($f_{c;90}$) and shear (f_v). These values from EN 338:2009 [8] are:

Table 4: Characteristic strength values for C24 according to EN 338:2009

$f_{c;0;k}$ [N/mm²]	$f_{c;90;k}$ [N/mm²]	$f_{v;k}$ [N/mm²]
21	2.5	2.5

5.3 Mean strength values

For compression parallel and perpendicular to the grain the mean value can be calculated by the statistical formula used in strength grading of timber:

$$\boldsymbol{f_{c;\alpha;k} = \mu - K_s * \sigma}$$

Where:

$\boldsymbol{\mu}$ = The mean strength value found by a population test. This value corresponds to $f_{c;\alpha;mean}$ which is to be obtained.

$\boldsymbol{\sigma}$ = The standard deviation obtained from the population test.

$\boldsymbol{K_s}$ = Amplification factor related to wood properties → 1,64 (for $n = \infty$)

The standard deviation in wood typically is around 20% of the mean value. This means that the mean value for C24 can be found as follows:

$\boldsymbol{f_{c;\alpha;k} = \mu - K_s * \sigma}$ with $\boldsymbol{K_s = 1.64}$, $\boldsymbol{f_{c;0;k} = 21\ N/mm^2}$ and $\boldsymbol{\sigma \approx 0.2\mu}$

$$\boldsymbol{21 = \mu - 1.64 * 0.2\mu}$$

$$\boldsymbol{21 = 1\mu - 0.328\mu = 0.672\mu}$$

$$\boldsymbol{\mu \approx 31,5\ N/mm^2}$$

It is assumed that the same holds for the strength value of compression perpendicular to the grain resulting in a mean value of 3.75 N/mm^2.

Translating the characteristic shear strength to a mean value is not so straight forward. Since much uncertainty over the shear strength value still exists, research that has been done on this subject is used to find a mean value for the shear strength.
In research done by M. Poussa et al. [9] and P. Glos et al. [10] several statements are made on shear strength of timber:

- The shear strength of the material has no correlation to the density, meaning that the shear strength of a species is constant in all strength classes.
- The orientation of the growth rings in the test specimens has an influence on the shear strength. Since glulam mostly consists of relatively weak tangential laminations, the shear strength of glulam should not be significantly higher than for sawn timber.

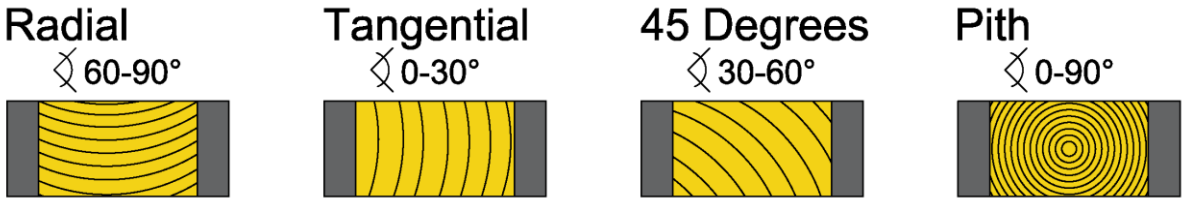

Figure 34: Growth ring orientation of the tested specimens in [10]

- The moisture content of the wood has no influence on the shear strength. [11]

Results obtained in [10] show mean and 0.05 characteristic values for spruce of:

Table 5: Results of spruce shear strength tests [10] for different growth ring orientations. 30 tests per orientation.

Growth ring orient.	Mean shear strength	5^{th} percentile shear strength	Stand. Dev.
Radial	6.5 N/mm^2	4.4 N/mm^2	1.36
Tangential	5.4 N/mm^2	4.0 N/mm^2	0.83
45 Degrees	5.4 N/mm^2	4.0 N/mm^2	0.76
Pith	5.6 N/mm^2	3.4 N/mm^2	1.15

The growth ring orientation which is related to the Single Step Joint specimens is 45 degrees and a small amount has a tangential orientation. The test results show a mean shear strength value of 5.4 N/mm^2. Since the test where performed on glulam spruce specimens, a 5 N/mm^2 strength is used in the hypothesis for the sawn timber Single Step Joints.

Table 6: Mean strength values for C24

$f_{c;0;\mu}$ [N/mm^2]	$f_{c;90;\mu}$ [N/mm^2]	$f_{v;\mu}$ [N/mm^2]
31.5	3.75	5

5.4 Hypothesis

Using the three mentioned codes, a hypothesis for characteristic values, resulting in a lower limit ultimate load, and mean values, resulting in an expected ultimate load, is made. This calculation is enclosed in appendix H. The equations used are presented in chapter 2.1 to 2.3 of Part I.

Dutch standard

The dutch code checks:

1. Horizontal axial component with strength parallel to grain;
2. Vertical axial component with strength perpendicular to grain;
3. Shear force with shear strength;
4. Strength under an angle to the grain in the frontnotch.

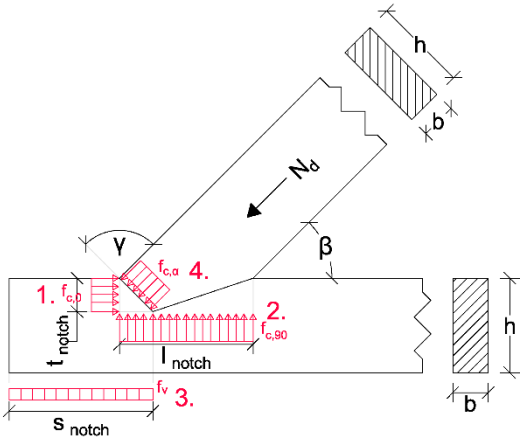

Figure 35: Checks of the Dutch NA to EC5

Using the described geometric parameters and characteristic/mean strength values, the force N_d as shown in Figure 35 is calculated, where the lowest value is governing. This results in the following expected ultimate loads:

Table 7: Expected loads on the specimen according to NEN-EN 1995-1-1 NA 8.11 using characteristic and mean values

Geometry	Fulfills geom. BCs?	Lower limit (Characteristic)	Governing value obtained from	Expected (Mean)	Governing value obtained from
500 series	Yes	63.59 kN	4.	95.39 kN	4.
300 series	Yes	48.50 kN	3.	95.39 kN	4.
750 series	Yes	63.60 kN	4.	95.39 kN	4.
90B series	No	37.22 kN	4.	55.84 kN	4.
90D series	Yes	37.22 kN	4.	55.84 kN	4.

Following the Dutch standard, the failure mechanism should be crushing due to governing stresses under and angle to the grain for all but one test series. The 300 series characteristic calculation is governed by shear failure of the shearplane.

German standard

The German standard only checks the stresses under an angle to the grain in the NA part on Step Joints. Using the German formulas for stresses under an angle to the grain, the following strengths are acquired:

Table 8: Expected loads on the specimen according to DIN-EN 1995-1-1 NA 12.1 using characteristic and mean values

Geometry	Fulfills geom. BCs?	Lower limit (Characteristic)	Governing value obtained from	Expected (Mean)	Governing value obtained from
500 series	Yes	66.40 kN	4.	113.87 kN	4.
300 series	Yes	66.40 kN	4.	113.87 kN	4.
750 series	Yes	66.40 kN	4.	113.87 kN	4.
90B series	No	47.58 kN	4.	84.75 kN	4.
90D series	No	41.20 kN	4.	73.40 kN	4.

Swiss standard

The Swiss standard checks three different stress cases. The stresses in the frontnotch, which act under angle α, are checked by giving a minimum depth of the notch (4.). Also the shear stresses are checked by giving a minimum shearplane length (3.). The last check is on the stress that is present in the diagonal due to the axial load. Although these stresses act parallel to the grain, stresses under the full angle between beam and diagonal (β) are used in the check.

Table 9: Expected loads on the specimen according to SIA 265 using characteristic and mean values

Geometry	Fulfills geom. BCs?	Lower limit (Characteristic)	Governing value obtained from	Expected (Mean)	Governing value obtained from
500 series	Yes	60.62 kN	3.	106.39 kN	4.
300 series	Yes	36.37 kN	3.	106.39 kN	4.
750 series	Yes	61.36 kN	4.	106.39 kN	4.
90B series	No	34.93 kN	4.	55.84 kN	4.
90D series	No	34.93 kN	4.	55.84 kN	4.

Combination

The results provided by the three standards are combined to give a range in which the connections could fail. The characteristic values give a load which is considered a lower limit for the ultimate load range. The mean values give a window in which the connection is expected to fail.

Table 10: Minimum and maximum loads of according to the combined standards

	MINIMUM		MAXIMUM	
	Characteristic	Mean	Characteristic	Mean
500 series	60.6 kN	95.4 kN	66.4 kN	113.9 kN
300 series	36.4 kN	95.4 kN	66.4 kN	113.9 kN
750 series	61.4 kN	95.4 kN	66.4 kN	113.9 kN
90B series	34.9 kN	55.8 kN	47.6 kN	84.8 kN
90D series	34.9 kN	55.8 kN	41.2 kN	73.4 kN

6 Test data & Analysis

6.1 Data processing

To analyze the test results, first, the relevant part of the data measurements has to be selected.

Initial deformations

The load procedure as described earlier is done to eliminate initial deformations caused be settling of the specimen and test setup. The loop that is created due to the loading procedure has to be deleted from the results. The resulting line, which starts at a 10% load, has to be extended towards the Y=0 axis. As this line is extended parallel with the linear part of the data, this extended line does not cross the origin of the graph, but instead with an 'x offset'. This offset represents the initial deformation of the test. This value than is extracted from all other data-points resulting in true deformations of the test specimen.

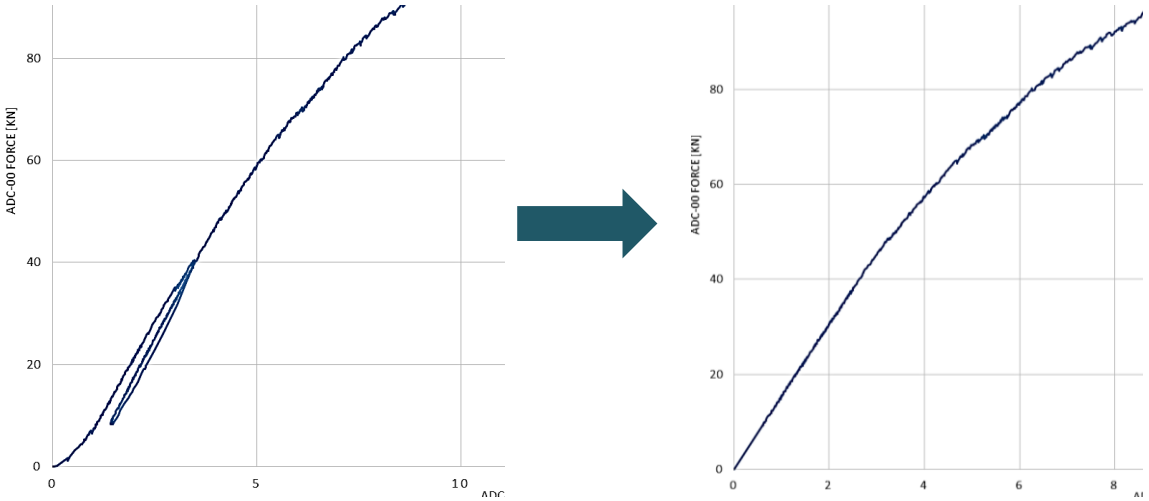

Figure 36: From original data graph to processed data graph

For processing this initial deformation data, an Excel-file is written to automatically give the x-offset value and equation of the linear part of the graph. This 'zero reset' Excel-file is enclosed in appendix I. The Excel-file is made, assuming the graph (which represents a behavior of the deformation of the specimen) is linear. This is the case for all specimens when loaded for the second time from 20kN to 25kN (which is also the range of the low-speed ESPI measurements). Around 20kN, a data-line is copied from the test results into the 'zero reset' file. This data-line contains the points y_1 and x_1. The data-line around 25kN contains y_2 and x_2. Using these points, and assuming a $\boldsymbol{y = ax + b}$ shape of the equation, the values for $\boldsymbol{a}$ and $\boldsymbol{b}$ are obtained. The 'x offset' value can be found by stating $\boldsymbol{y = 0}$.

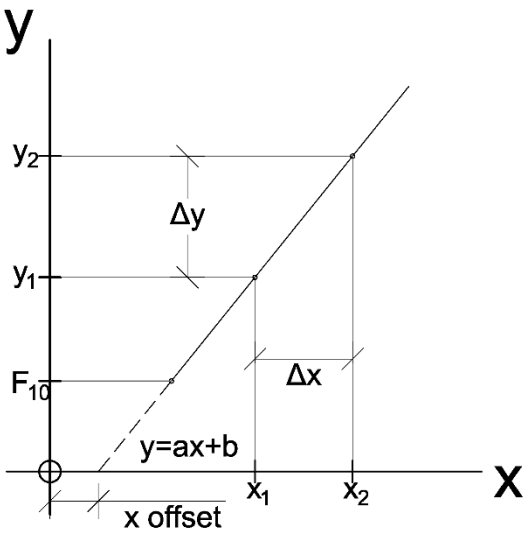

Figure 37: Determination of equation

The point to where the data is cut away is determined visually by linear behavior of the force-displacement diagram. Although this diagram is already linear, other measurements still have some curvature resulting from commencing loading. To remove this curvature from the data set, the equation of the line obtained from the 'zero reset' Excel-file is implemented instead of the measured data points for the first few points in the measurements. The result is shown in Figure 38.

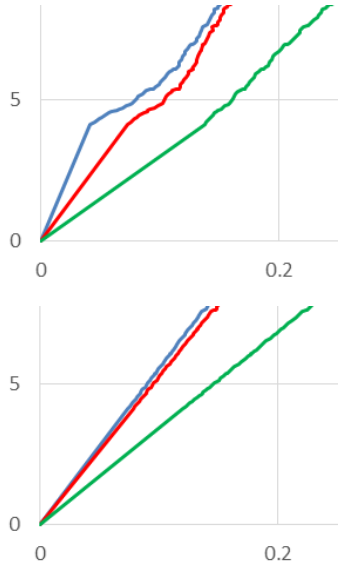

Figure 38: a) Curvature in start dataset, b) Implemented equation

Failure and device maximum

Also the last part of the data set requires attention. Here, all data after failure of the connection has to be deleted as all ADC devices are falling from the specimen and give a maximum or minimum of their measurement range.
If a device reaches a maximum/minimum during the test, all data after this point is deleted.

Combination of ADC devices

As explained earlier, the deformation of the beam was measured using ADC-05. However, deformations measured by this device include elongation of the pendulum rod. This was measured by ADC-09. By subtracting the ADC-09 measurements from the ADC-05 displacements, the real deformation of the beam element is obtained. Multiplying ADC-09 with *COS(30°)* gives the vertical deformation of the pendulum rod. This deformation is subtracted from ADC-06 measurements.

Processing to other unities

Strain

For ADC-03 and ADC-04, located in fiber direction near the frontnotch surface on both beam and diagonal, the measured displacements can be divided by the measured length to obtain the strain of the material.

Sigma

The force measured in the diagonal (ADC-00) is divided by the area of the frontnotch, in perpendicular to the fiber direction as shown in Figure 39. For i.e. the 500 series, this means that the force measured by ADC-00 is divided over an area of 62.5 x 70 mm^2 to obtain the stresses in the diagonal near the frontnotch.
The same is done for the measured force in the diagonal (ADC-01) to determine the stresses in the beam near the frontnotch.

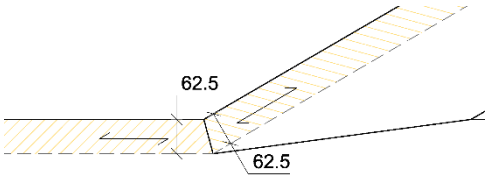

Figure 39: Determination of the stress area (500 series)

Global stiffness (E-modulus)

Both the stresses and strains parallel to the fiber in both elements are now obtained. These can be plotted in a sigma-epsilon diagram. Also, the stiffness behavior of the timber can be found in terms of a Young's modulus. The behavior of the stiffness during the test is described by plotting the applied force together with the calculated E-modulus (stiffness) in a graph. In this way, plastic behavior of the connection, can be very well spotted. (Figure 40)

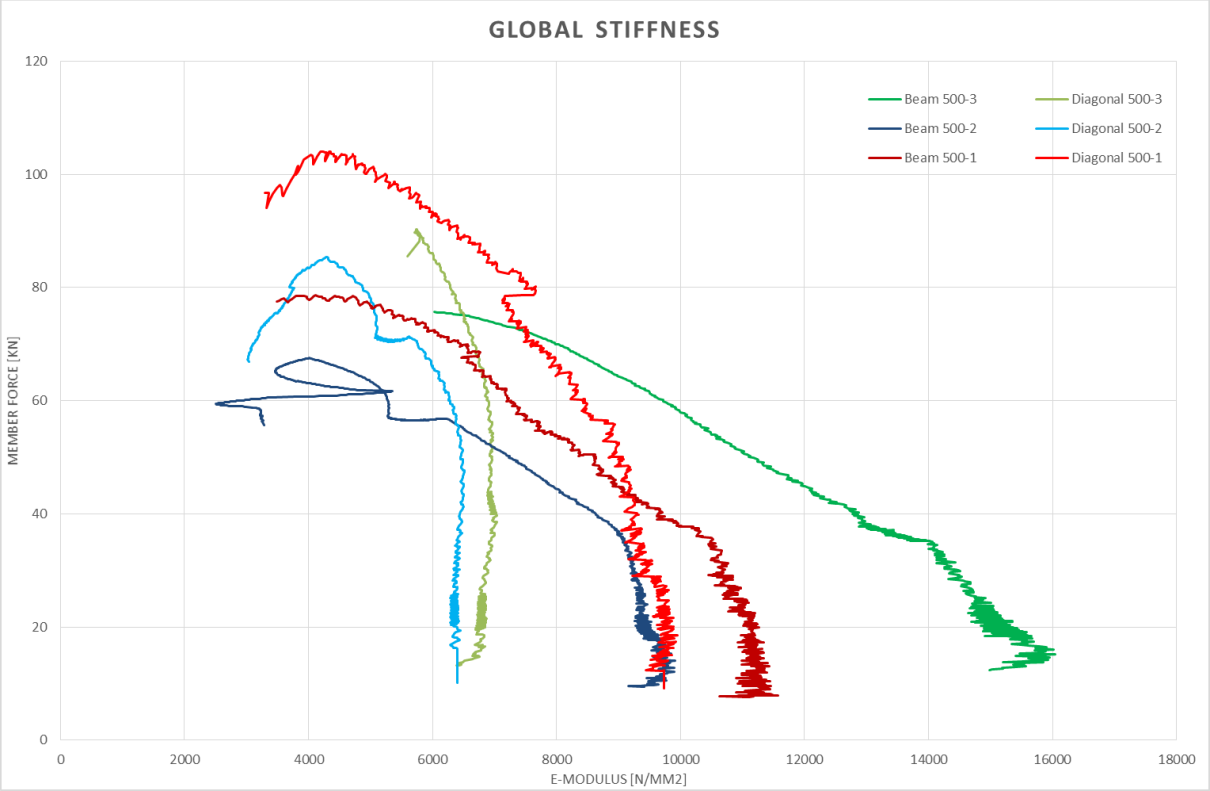

Figure 40: Stiffness behavior of the tested 500 series specimens compared to the height of the load.

Contact surface forces

As explained in the measurement devices section, several instruments are placed; perpendicular to the front- and bottomnotch surfaces to measure deformations; and parallel to the bottomnotch surface to measure slip between diagonal and beam element. These measurements are plotted together with the relevant force component. These components are determined as follows:

The force which is related to the slip between the elements is F_{BN0} (force parallel to bottomnotch). This force is determined by multiplying the force in the diagonal (ADC-00) with the cosine of the angle between the forces. The same is done for the force perpendicular to the bottomnotch F_{BN90}, and for the force component perpendicular to the frontnotch.

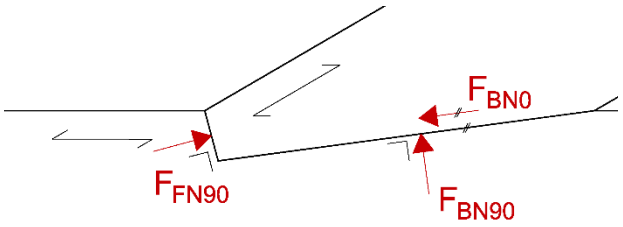

Figure 41: Determination of force components

The forces presented in Figure 41 are described in the y-axes of the plots as follows:

F_{BN0} : Parallel Bottomnotch Force

F_{BN90} : Perpendicular Bottomnotch Force

F_{FN90} : Perpendicular Frontnotch Force

7 Results

The results of the tests are presented per test series. For all tests, the force-displacement diagram of the specimen, measured in the diagonal is shown together with a comparison between the hypothesis and the test. When other diagrams show any point of interest this is also threated. All diagrams of the test can be found in appendix J.

7.1 500 series

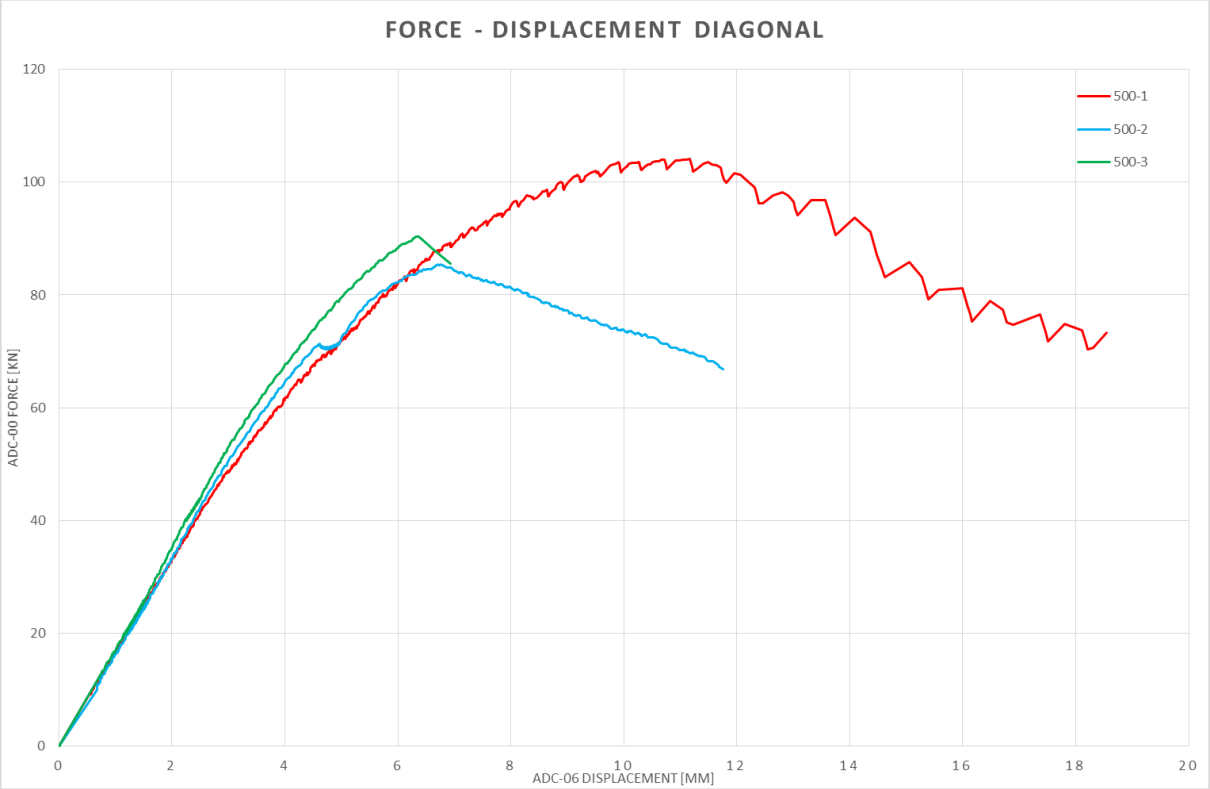

Figure 42: Force-displacement diagrams of specimens in the 500 series

Table 11: Failure -loads and -mechanisms of the hypothesis and experiments

	Hypothesis		Experiment	
Specimen	Failure load	Failure mechanism	Failure load	Failure mechanism
500-1	95.4 – 113.9 kN	Butting	104.05 kN	Butting
500-2	95.4 – 113.9 kN	Butting	85.38 kN	Butting (+ Shear)
500-3	95.4 – 113.9 kN	Butting	90.34 kN	Shear
Average	95.4 – 113.9 kN	Butting	93.3 kN	Butting

The 500 series is used as a benchmark for all other tested geometries. The tests show similar elastic behavior during loading. Specimen 500-2 (blue line) shows a drop in strength at a load of 70 kN. This is due to the lower testing speed that was required by the second ESPI measurement. This low loading speed clearly has an influence on the behavior of the specimen. Because the ESPI measurement showed no results because deformations are too large, together with the influence on the specimen's behavior, it was decided to run the second ESPI measurement at a lower 40 kN load for the remainder of the tests. When comparing the 500-2 specimen's (blue) and the 500-3 (green) specimen's behavior to the behavior of specimen 500-1 (red), which had no ESPI measurements, no

noticeable differences in behavior can be seen. Therefor it can be concluded that ESPI measurements at 20kN and 40kN do not influence the behavior of the specimen during the tests.

The irregularity in the line of the 500-1 (red) specimen at high loadings and deformations is due to the usage of a hand pump to control the actuator. To prevent this irregularity, and to make ESPI measurements possible, it was decided to use a computer controlled actuator for the remainder of the tests.

Only one of the specimens reached the expected failure load window. This results in an average failure load which is slightly lower than expected. The failure mechanism 'butting' was expected and occurred twice out of three tests. An interesting phenomenon is observed at the 500-2 specimen. Here, the specimen starts to fail because of butting. Because of this, cracks are formed at the growth rings of the wood. This than leads to a shear failure, starting from these butting cracks.

Figure 43: Shear failure after butting of the frontnotch

7.2 300 series

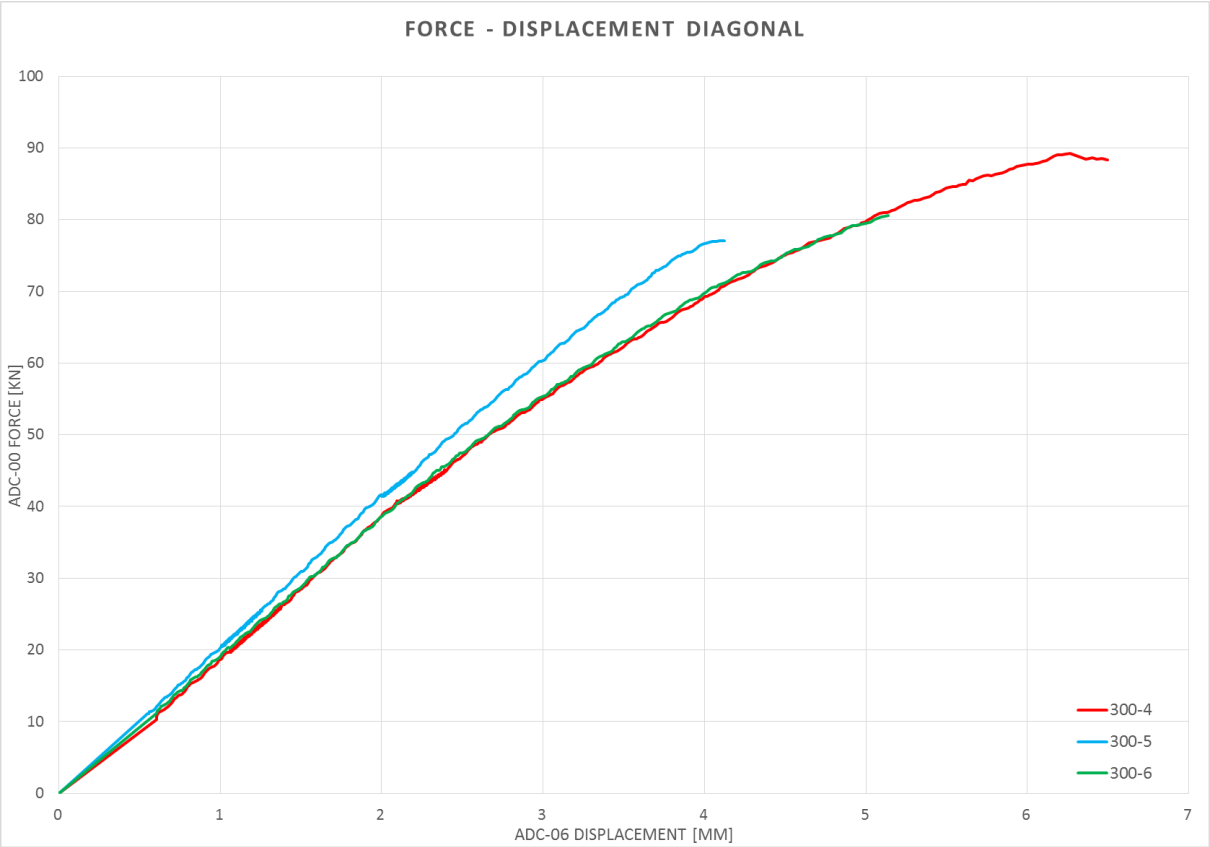

Figure 44: Force-displacement diagrams of specimens in the 300 series

Table 12: Failure -loads and -mechanisms of the hypothesis and experiments

	Hypothesis		Experiment	
Specimen	Failure load	Failure mechanism	Failure load	Failure mechanism
300-4	95.4 – 113.9 kN	Butting	89.18 kN	Shear
300-5	95.4 – 113.9 kN	Butting	77.06 kN	Shear
300-6	95.4 – 113.9 kN	Butting	80.57 kN	Shear
Average	95.4 – 113.9 kN	Butting	82.27 kN	Shear

As the hypothesis of the 500 series is based on butting behavior of the wood, differences in shear length does not have any influence on the strength of the specimens calculated in the hypothesis. Therefore, the expected failure loads of the 500, 300 and 750 series are the same. However, the experiments showed shear failure in all 300 series specimens, all at much lower ultimate loads than expected, average of 82 kN. The codes predict shear failure at ultimate loads close to 120 kN, this is a big overestimation in the codes.

The average failure load of 82.27 kN is slightly lower than the average of the reference 500 series. This series reached an average ultimate load of 93.3 kN. Together with the differences in failure mechanism, it can be concluded that a very small shearplane length does have a minor negative effect on the overall strength of the connection.

7.3 750 series

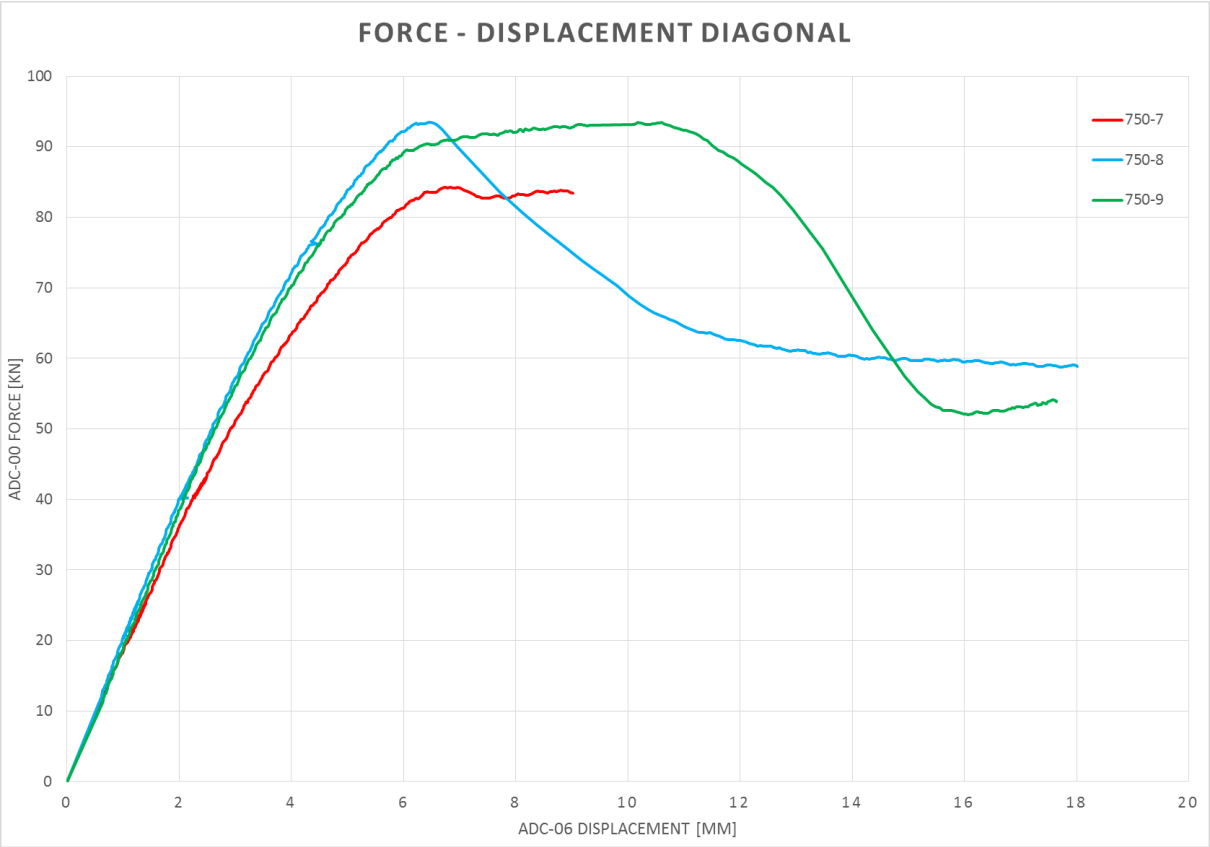

Figure 45: Force-displacement diagrams of specimens in the 750 series

Table 13: Failure -loads and -mechanisms of the hypothesis and experiments

	Hypothesis		Experiment	
Specimen	Failure load	Failure mechanism	Failure load	Failure mechanism
750-7	95.4 – 113.9 kN	Butting	84.26 kN	Shear
750-8	95.4 – 113.9 kN	Butting	93.45 kN	Butting
750-9	95.4 – 113.9 kN	Butting	93.4 kN	Butting
Average	95.4 – 113.9 kN	Butting	90.37 kN	Butting

Although a shearplane length of 750 mm is much larger than required, and even larger than the allowed calculation length, this test series still showed shear failure in 1 out of 3 cases. The two specimens which showed butting failure reached an ultimate load which was very close to the expected failure load in the hypothesis. The average failure load of 90.37 kN is not significantly different from the average failure load of the reference 500 test series. Therefor it is concluded that an increase of the shearplane length from 500mm to 750mm does not add any strength to the connection.

7.4 90D series

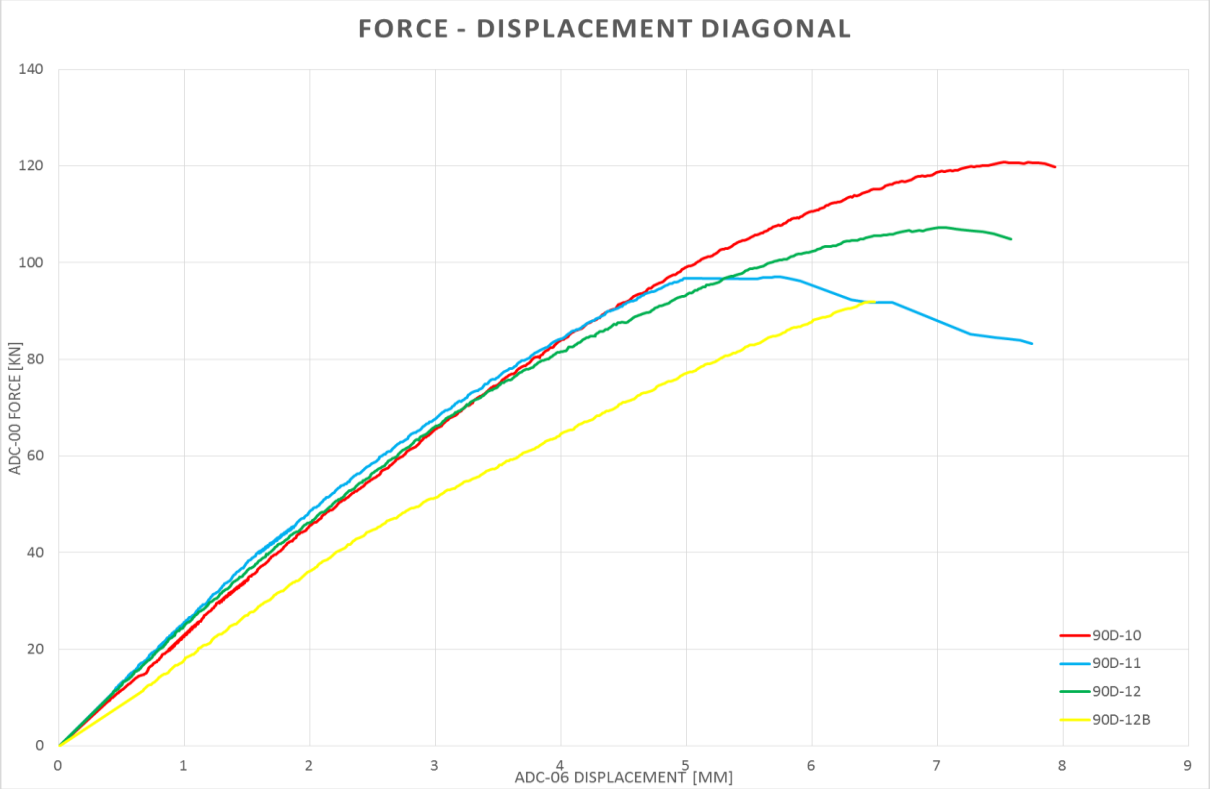

Figure 46: Force-displacement diagrams of specimens in the 90D series

Table 14: Failure -loads and -mechanisms of the hypothesis and experiments

	Hypothesis		Experiment	
Specimen	Failure load	Failure mechanism	Failure load	Failure mechanism
90D-10	55.8 – 84.8 kN	Butting	120.79 kN	Shear
90D-11	55.8 – 84.8 kN	Butting	97.11 kN	Shear
90D-12	55.8 – 84.8 kN	Butting	107.21 kN	Butting (imperfection)
Average	55.8 – 84.8 kN	Butting	108.37 kN	Shear

The 90D series also comprised 3 specimens. During the last test in this series (90D-12), the diagonal element, which is loaded parallel to the grain, failed by butting in an area where the orientation of the fibers was compromised due to an imperfection. Since this failure was related to the imperfection instead of the geometry of the specimen, this specimen was tested for a second time using an already used diagonal from another specimen. This second test is shown in Figure 46 by the yellow line (90D-12B). It can be seen by comparing the yellow and green line in the graph, that the specimen never regained full stiffness, and eventually failed on shear before it reached its original strength. (During the preparation of the retest, shear

Figure 47: Butting failure of the diagonal element due to an imperfection causing a different growth-ring orientation.

cracks were noticed already in the beam. Meaning that the cross-section was already compromised due to this crack. This crack is shown in Figure 48.) Therefore, results of this re-test are ignored.

Figure 48: Visible shear cracks before the retest

The average ultimate load of the test of 108.37 kN is significantly higher than was expected in the hypothesis. Since the orientation of the frontnotch surface was unbeneficial for the strength of the wood, and butting would occur earlier, the hypothesis of this series is much lower than for the previous experiments. The average ultimate load of 108.37 kN was also much larger than the other test series. This can be explained by the failure mechanism; 'shear' instead of 'butting'. The applied angle is unbeneficial for the strength of the wood against butting, but it is beneficial for resistance against shear failure. The way the force in the diagonal is decomposed is presented in Figure 49. The first circle represents the frontnotch orientation as used in the 500, 300 and 750 test series. Decomposing force F_{15} leads to a relatively large horizontal force H_{15} and a small vertical force V_{15}. A large horizontal force H_{15} leads to high shear stresses. Shear resistance is increased if a compressive force acts perpendicular to the shearplane, in this case a relatively small vertical force V_{15} is present here. When the angle of the frontnotch is changed as has been done in the 90D test series, decomposing the diagonal force is done as presented in the second circle in Figure 49.
Here, horizontal force component H_{30} is lower compared to H_{15}, and force V_{30} is larger than V_{15}. Both force components now contribute to a much more beneficial situation for the shear resistance.

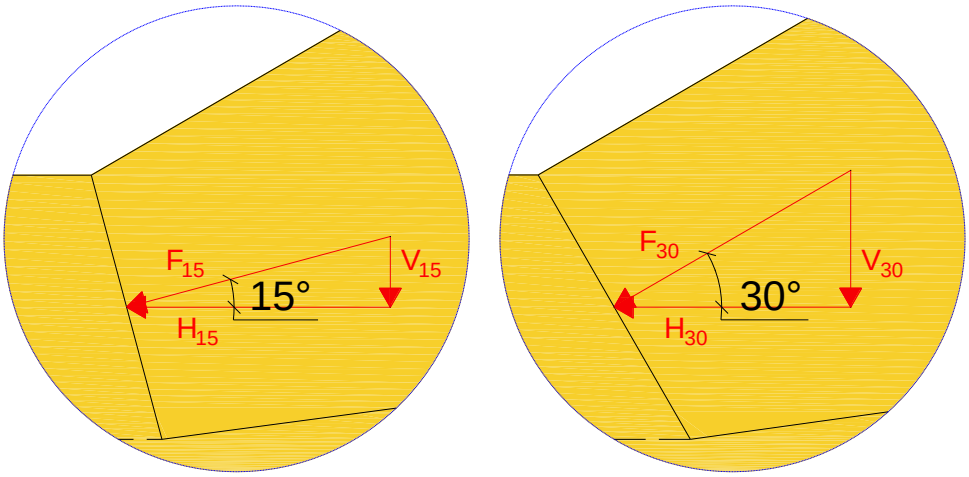

Figure 49: Decomposing the force in the diagonal to a horizontal and vertical force component.

Since two test specimens failed in shear earlier than butting, orientating the angle of the frontnotch perpendicular to the diagonal leads to a higher load resistance of the connection.

7.5 90B series

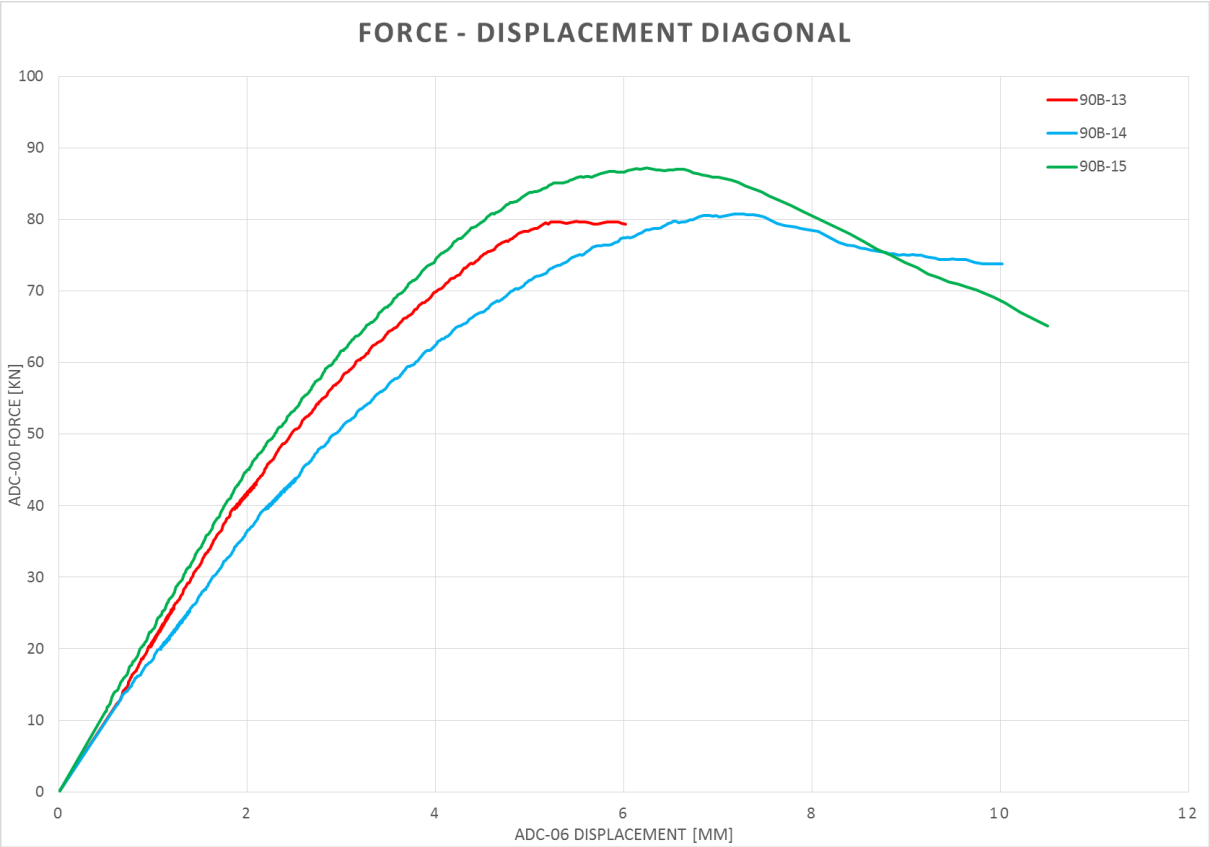

Figure 50: Force-displacement diagrams of specimens in the 90B series

Table 15: Failure -loads and -mechanisms of the hypothesis and experiments

	Hypothesis		Experiment	
Specimen	Failure load	Failure mechanism	Failure load	Failure mechanism
90B-13	55.8 – 73.4 kN	Butting	79.70 kN	Shear
90B-14	55.8 – 73.4 kN	Butting	80.75 kN	Shear
90B-15	55.8 – 73.4 kN	Butting	87.14 kN	Butting
Average	55.8 – 73.4 kN	Butting	82.53 kN	Shear

The three specimens of the 90B series show a much lower average failure load than the 90B series. This can be explained by the absence of a vertical force component in the shearplane. This decreases the resistance against shear failure of the geometry. As two out of three specimens failed in shear, this explains the lower average failure load. Again, the failure mechanism according to the hypothesis was butting, shear failure was the dominant failure mechanism.
The average failure load is lower than that of the reference geometry, meaning that, the frontnotch orientated perpendicular to the beam, has weakened the strength of the test specimens. The average failure load is comparable to the shortened shearplane length 300 series.

7.6 Comparison

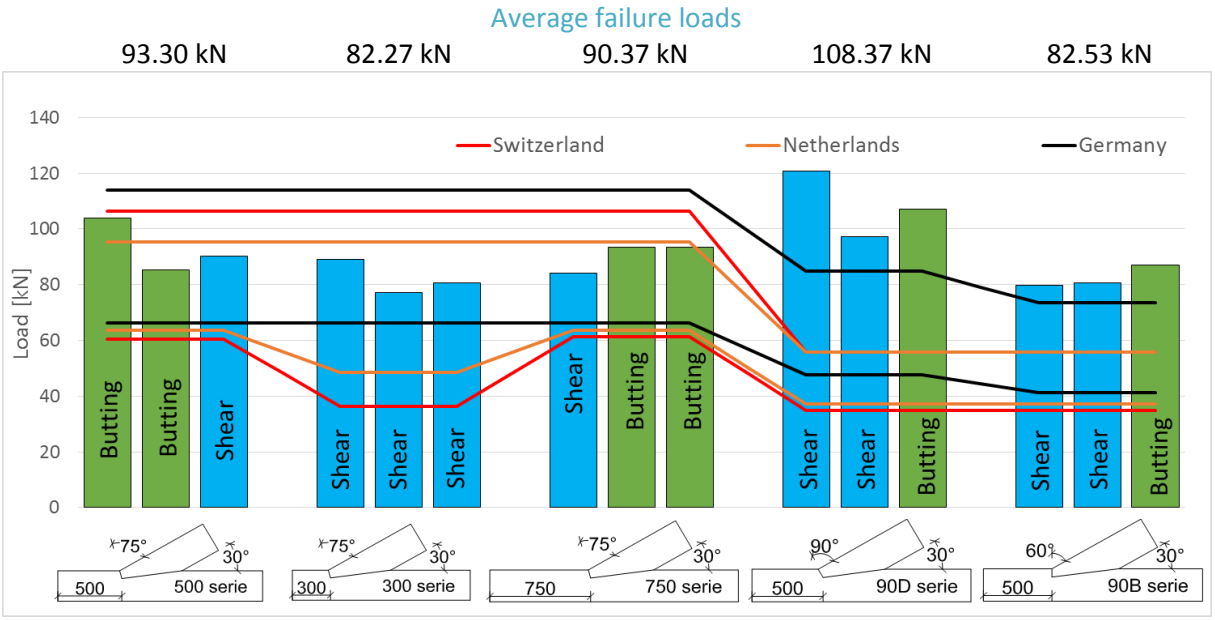

Figure 51: Comparison of all failure loads and mechanisms during the test, together with hypothesis (mean and characteristic)

The results from all test series are bundled in a histogram shown in Figure 51. The lines show the failure load predicted by the three used codes. The upper lines give the failure loads of the hypothesis, in which the mean strength values are used. The lower lines give the failure loads found by using characteristic strength values. It is important to notice that all specimens failed after this characteristic failure loads are exceeded.

The mean value lines, used in the hypothesis, show an overestimation of the strength for the different shear lengths, and underestimate the strength when the angle of the frontnotch γ is not equal to 75°.

The average failure loads of the test series can be compared with the reference 500 series geometry. The 300 series gives an average failure load 10 kN lower than the 500 series, while the 750 series shows no significant in- or decrease of the failure load compared to the 500 series. When the angle of the frontnotch is orientated perpendicular to the diagonal's axis (γ = 90°) in the 90D series, the average failure load is 15 kN higher than for the reference 500 series. Meaning a big increase in strength. When the angle of the frontnotch is orientated perpendicular to the beam axis (γ = 60°) in the 90B series, the average failure load is, like the 300 series, 10 kN lower than the 500 series.

7.7 Shear stresses resistance

In order to analyze the shear stresses at the moment of a shear failure, several assumptions have to be made in order to determine the shear stresses. To determine the shear stresses, two parameters are needed for:

$$\tau = \frac{V}{A}$$

Where V is the shear force which, in this case, is equal to the horizontal force in the beam. From the test, this force can be determined in two ways. Using the force which was measured in the pendulum rod at the back of the beam. This measurement directly gives the shear force in the shearplane. Also, the shear force can be determined using the actuator force multiplied with the COS (30°) to give the shear force component. As the force measured at the pendulum rod directly gives the shear force, and the actuator force is decomposed without taking rotations due to loading into account, this directly measured force gives the most accurate shear force value.

The second parameter is A, which is the surface in which the shear force V is acting. Parameter A, in its turn consists out of “b”, which is the width of the beam, and “l” which is the length of the plane over which the shear stresses act. This “l” parameter is much harder to determine, as the tests have shown that the area over which the shear stresses spread is not equal to the available shearplane length. Several possibilities for shear-loaded lengths are investigated:

a. Full available shearplane length, assuming equally distributed load;

b. Using the tangential crack pattern length following from the shear-failed test specimens, assuming equally distributed load. (threated on page 108);

c. Average tangential crack pattern of all tests, assuming equally distributed load.

As b. possibly gives the best estimation of the height of the present shear stresses in the specimen, an underestimation of the shear stresses occurs when the whole shearplane length fails tangentially. Which was the case in several tests. This underestimation effects the average failure shear stress. To smoothen out this phenomenon, in c., the average tangential loading length of all the specimens is taken as shear affected length for all specimens. Average shear stresses for all cases are:

Table 16: Average shear stresses at moment of failure, compared with characteristic shear strength for C24.

Case	a.	b.	c.	Characteristic
Average stress	2.30 N/mm^2	5.47 N/mm^2	3.30 N/mm^2	2.50 N/mm^2

Data sheet with calculation of these values and individual values, together with calculations using decomposed actuator force, is enclosed in appendix K.

Due to too much assumptions, a single representative failure shear stress cannot be given.

7.8 Conclusions

Expected failure mechanisms

The hypothesis predicted butting failure before shear failure for every specimen. The tests however, showed 9 shear failures and only 6 butting failures. Since a failure due to shear is very brittle, this type of failure is undesirable for a Single Step Joint and timber connections in general. The codes seem to overestimate the shear strength of the connection. Also, the 90D and 90B series should have butting failure much earlier than the 500, 300 and 750 series. This was not the case. So the resistance against butting seems to be underestimated by the codes when the orientation of the frontnotch is perpendicular to one of the two system axes.
From the test results of the shearplane lengths of 500mm or bigger, it can be concluded that shear-, and butting failure are very close together in this geometry.

Expected failure loads

In the series with varying shearplane length (500, 300, 750 series), the hypotheses overestimated the failure loads of the specimens by a relatively small margin. It cannot be concluded that the codes overestimate the failure loads, since this small margin can also be linked to the specimens having a lower strength than the mean strengths.
The underestimation of failure loads in the specimens with varying frontnotch angle (90D, 90B series) is much larger. All specimens are stronger than the highest expected failure load.
At least a small part of this underestimation by the codes can be linked to the presence of friction between the two surfaces in the frontnotch. This is illustrated in Figure 52. When no friction is present in the contact surfaces, only a force purely perpendicular to the contact surface can be transmitted. When friction is present, a friction component parallel to the contact surface appears. This changes the loading angle of the force which is transmitted in a positive direction; the angle of loading to the grain is reduced. This allows higher compressive strength values, increasing the capacity of the connection.

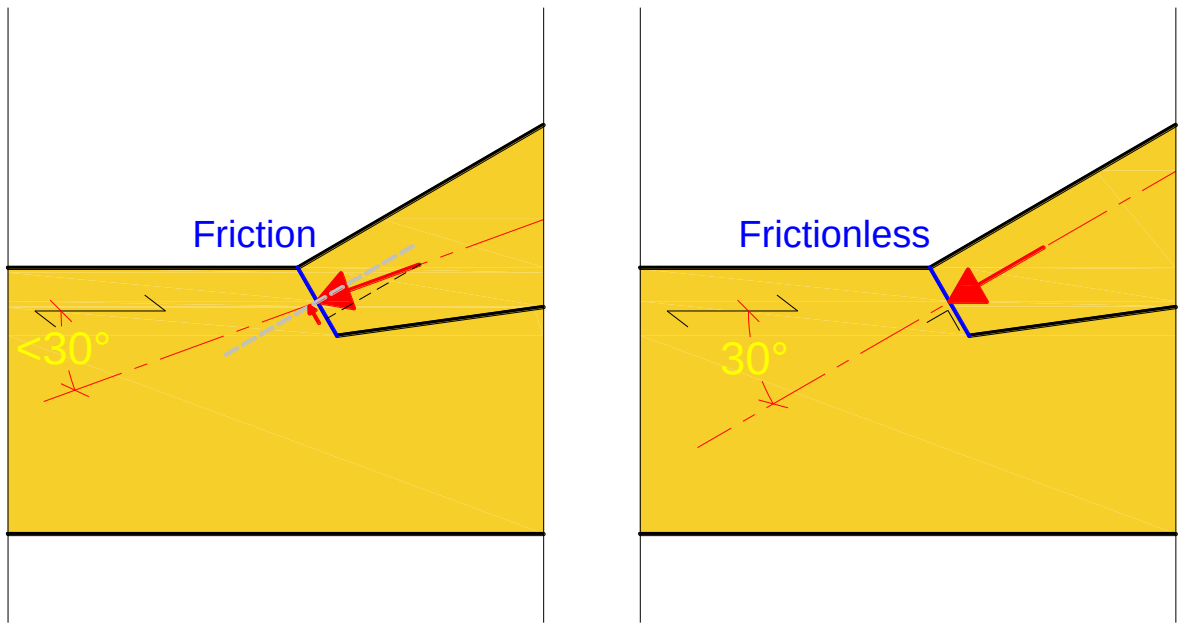

Figure 52: Difference in loading angle due to friction between the frontnotch surfaces

Shearplane length

From the test results it can be concluded that increasing the shearplane length larger than the German code's limit of 8 * t_{notch} (500 mm) does not lead to higher shear failure loads. This supports the assumption that the shear stresses do not spread over the full available shearplane length, and that in the calculations in the codes, the shearplane length needs to be limited by a maximum length.

Although the average failure load of the 300 series is about 10 kN lower than the reference 500 series, this is mainly due to the higher butting failure loads. When comparing the shear failures of the three altering shearplane length series, no big in- or decrease in failure loads can be seen (Figure 51). An explanation for this could be the small length in the shearplane that is actually loaded in shear. Although it was not measured during the tests, the crack pattern of the shear failures show a resemblance in most specimens.

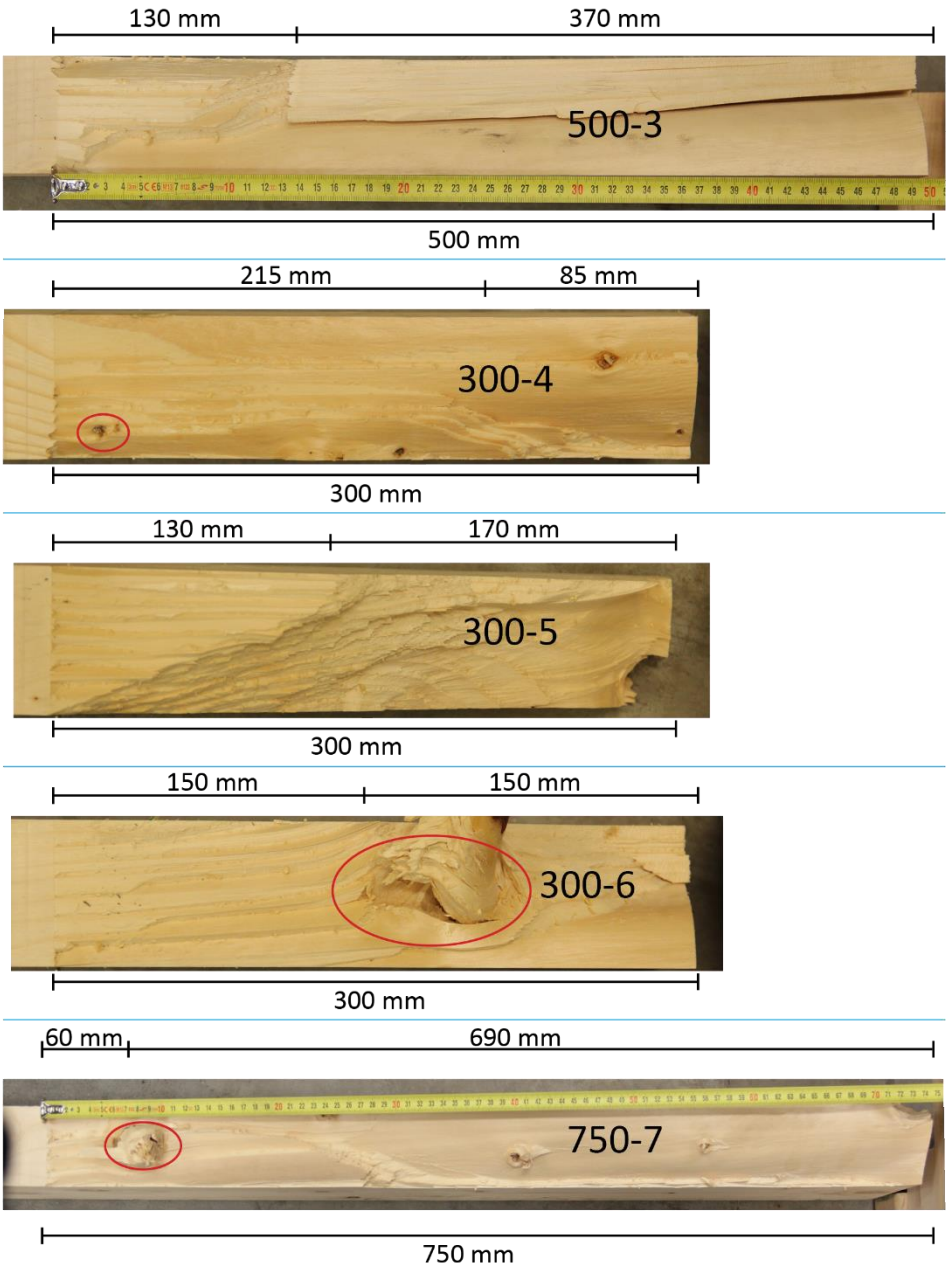

Figure 53: Tangential and radial crack pattern of the shearplane. Knots highlighted in red

As shown in Figure 53, the crack pattern near the notched (left) part of the image, is in tangential direction. The length of this tangential part varies a lot, and is very depending on the appearance of imperfections (knots) in the shearplane surface. When the shearplane surface has no imperfections, the length of the tangential cracks is about 130mm. After this tangential direction of the cracks, the crack continues in radial direction, and follows the growth rings of the wood. From this crack analysis it appears that the shear stresses concentrate in the shearplane line for the first 130mm. After this first part of the plane fails, the resuming length does not matter anymore, as the crack presumably has built up momentum, the rest of the timber fails along the path of least resistance. (Figure 54)

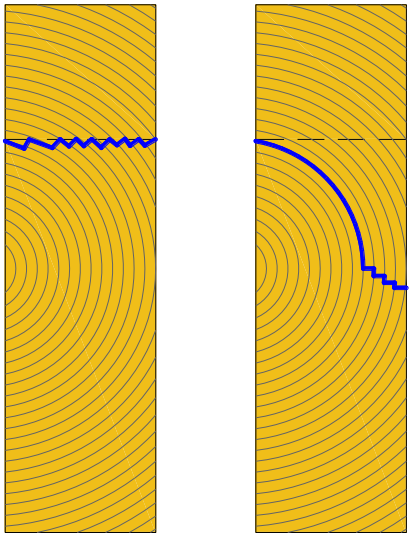

Figure 54: Tangential and radial crack direction

Frontnotch angle

The higher failure load of the 90D series can be explained by the force components as explained in chapter 7.4. The negative effect of the frontnotch angle on the butting strength is canceled at least a little because of the presence of friction between the contact surfaces as explained on page 107.

Population of all test series

The initial intention of the experimental tests was to verify a numerical simulation using FEM. During the tests, as mentioned in this report, several phenomena are spotted concerning stress distribution and failure mechanisms which are explained using several theories. In order to confirm these phenomena and theories, the used statistical test population of three specimens per series is very low as material properties of individual specimens have a too large influence. Therefore, the theories and conclusions in this report need further research with larger populations.

7.9 Recommendations for further experimental research

During the tests, several topics came to light of which it is recommended to perform further research on. These recommendations concern a bigger test population and measuring specific material properties and behavior.

Shear failure

The first recommendation is to investigate shear failure of the connection. Here, the length which is influenced by shear stresses needs more investigation. Also the resistance against shear of the material is important. The influence of imperfections in the shearplane, and the orientation of the growth rings in the shearplane, on this shear resistance needs to be investigated. If growth ring orientation has an influence on the strength, a study must be conducted to find the most common orientations in this connection, related to the beam dimensions, concluding whether differences in orientations need to be taken into account when assuming a shear resistance of the material. Also, since shear failure is very brittle and related to a specimens unique material properties, a large population of tests is recommended.

Codes' underestimation of the resistance against butting when $\gamma \neq 90 - \beta / 2$

To investigate the underestimation of the codes of the resistance against butting, two things can be checked:

a. Does the orientation of the stresses under an angle to the grain differ from what is assumed in the codes' calculations? This can be checked by testing a notched geometry with-, and without friction between the contact surfaces and compare the differences.

b. Do Hankinson's and Norris' formulas, which are used in the codes, underestimate the fiber strength in a notched geometry?

Failure mechanism probability in relation with connection angle β

Diagonal force F is loading the fibers in the beam in horizontal and vertical direction, as shown in Figure 55. Shear failure of the connection is caused by the horizontal force component H. Butting can be caused by both force components. Angle β determines the ratio between component H and V. As this angle increases, the horizontal force component H decreases, meaning that shear failure is becoming less likely. Because shear failure is brittle, and therefore undesired, it is important that design rules take angle β into account when setting boundary conditions or reduction factors. To do this, the tipping point between shear-, and butting failure must be found using an analytic and experimental study.

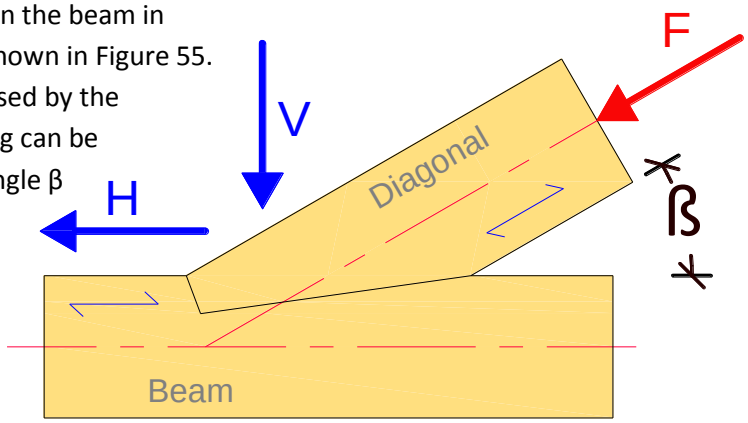

Figure 55: Axial force components

8 Bibliography

[1] NEN, “NEN-EN 1995-1-1.” 2005.

[2] NEN, “NEN-EN 1993-1-2 + C2,” vol. 2005, no. december 2011. 2011.

[3] DIN, “DIN-EN-1995-1-1 German NA 12.1 Versätze.” DIN Deutsches Institut für Normung, Berlin, pp. 88–89, 2010.

[4] SIA, “Schweizer Norm SIA 265 - Holzbau.” SIA, Zürich, pp. 77–78, 2012.

[5] NEN, “NEN-EN 1995-1-1 Dutch NA 8.11 Ambachtelijke verbindingen.” BRISwarenhuis, Delft, 2013.

[6] “ISO 6891-1983 (E).” International Organisation for Standardization, 1983.

[7] CEN, “EN 408 - Timber structures - Structural timber and glued laminated timber - Determination of some physical and mechanical properties.” CEN, Brussels, 2010.

[8] “NEN-EN 338:2009,” no. December. NEN; BrisWarenhuis, Delft, pp. 1–10, 2009.

[9] M. Poussa, P. Tukiainen, K. Mitsuhashi, and P. Anderisin, “Destructive Tension-, Shear- and Compression- (0 and 90) strength-tests for Finnish sawn timber,” Helsinki, 2007.

[10] P. Glos and J. Denzler, “Working Commission W18 - Timber Structures - Meeting 36, Colorado USA August 2003,” in *Characteristic shear strength values based on tests according to EN 1193*, 2003, no. August, pp. 91–101.

[11] R. Spengler, *Festigkeitsverhalten von Brettschichtholz unter zweiachsiger Beanspruchung*. 1982.

Appendices

		Hardcopy	Digital
A.	Literature study on stresses in a Single Step joint	●	●
B.	Abaqus CAE scripts	◌	●
C.	Numerical & ESPI comparison	◌	●
D.	Calculation bolted connection	●	●
E.	Determination material properties	◌	●
F.	Test protocol	●	●
G.	Secondary material test results	◌	●
H.	Hypothesis calculation	◌	●
I.	Zero reset	◌	●
J.	Full test results	◌	●
K.	Shear stress determination	◌	●

Technische Universiteit
Eindhoven
University of Technology

Where innovation starts

Literature Study

Research thesis on Single Step Joints in Traditional Timber Structures

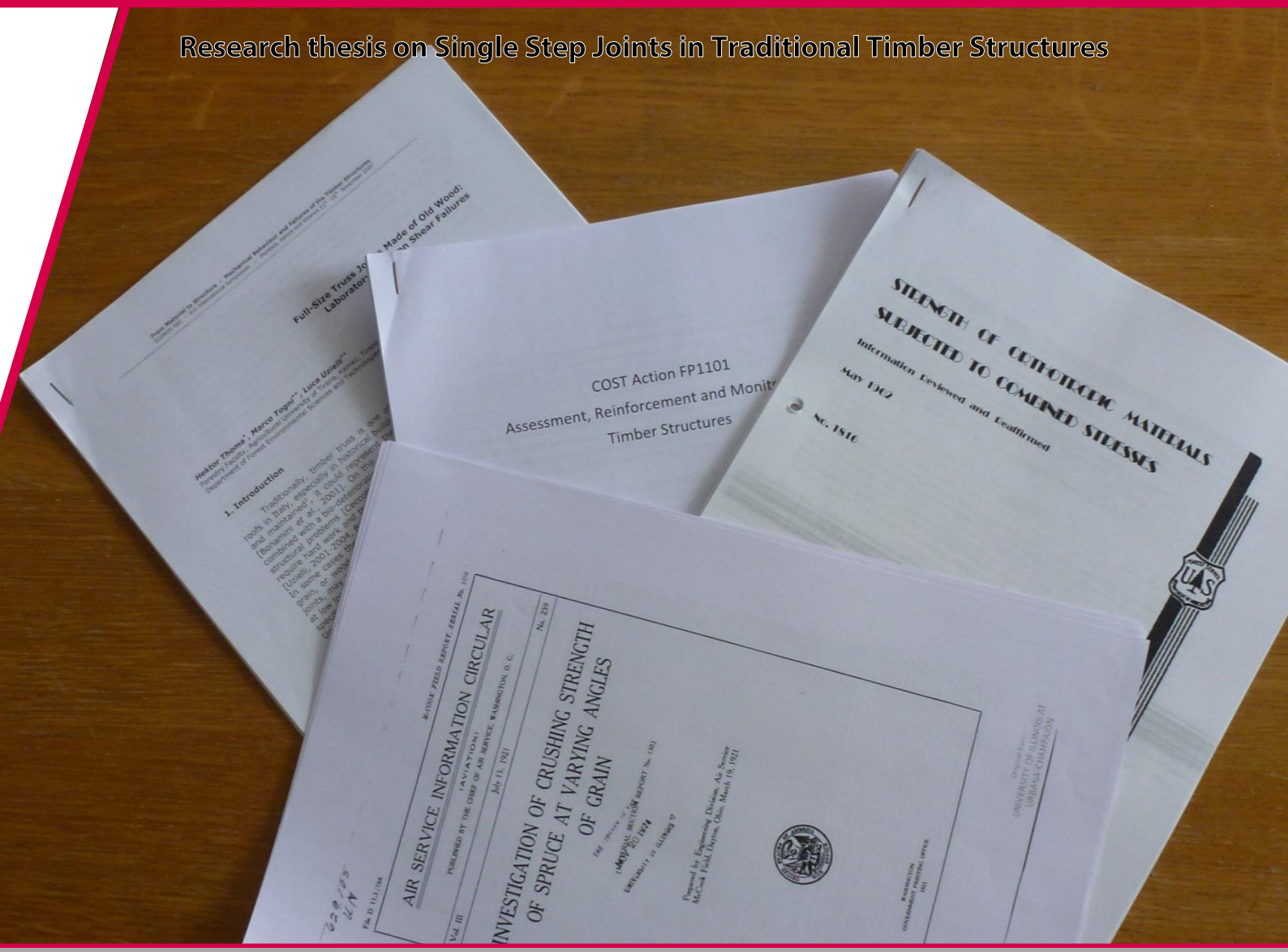

Student
Richard de Rijk
Bladvlinder 12
5345EX, Oss
06 - 31 06 08 56
0823656

Supervisors
Prof. dr. ir. A.J.M. Jorissen
Dr. ir. A.J.M. Leijten
Prof. ir. H.H. Snijder
L. van den Bosch

April 5, 2016

Version 4

Abstract

In this literature study all available literature that was studied during the research is evaluated. All literature is divided into three sections. In the first section literature concerning assessment of traditional timber structures is presented. The second section contains an evaluation of several international standards on carpentry joints and contains literature being the background of these standards. The third section presents literature that was published after research on carpentry connections.

Terminology

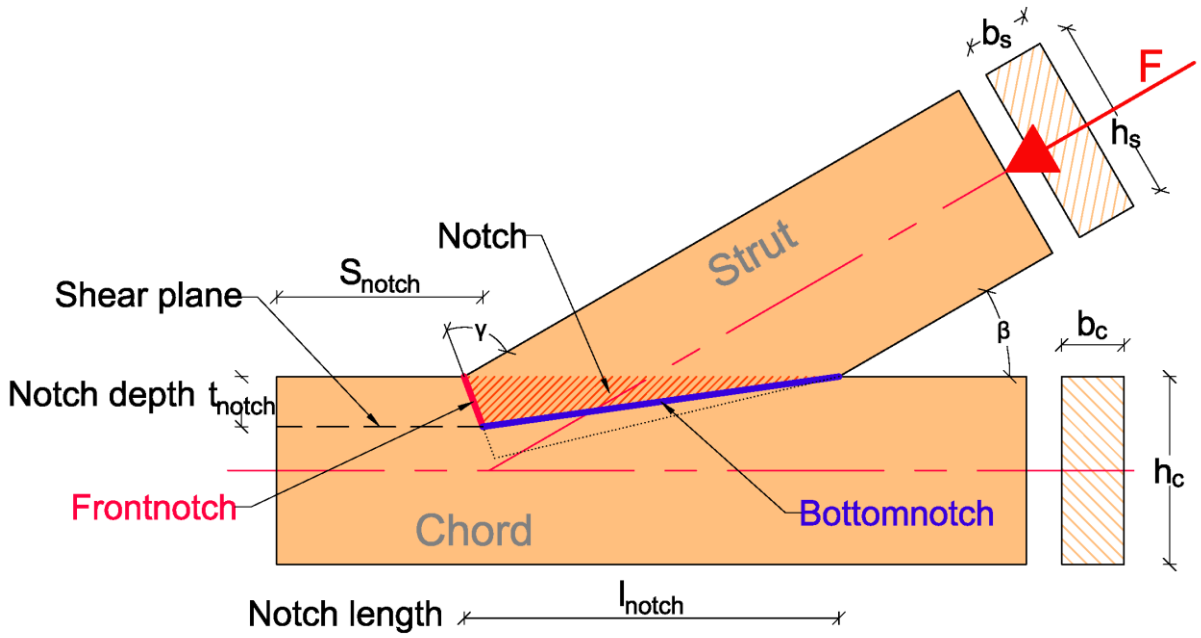

Strut	Diagonal element loaded in compression
Chord	Notched element, generally column or beam
Frontnotch	Front surface of the notched joint (marked in red)
Bottomnotch	Bottom surface of the notched joint (marked in blue)
Notch depth	The depth of the notch from the upper side of the chord [t_{notch}]
Notch length	The length over which the chord is notched [l_{notch}]
Shearplane	Line from the tooth of the notch to the side of the chord on which the shear stresses act [s_{notch}]

Table of contents

1. Research motivation

This master thesis project on Single Step Joints in timber is based on a subject of a working group within the European COST FP1101 framework. In this chapter a short summary of the importance and goals of COST and the working group are presented and the Single Step Joint is introduced.

1.1. COST FP1101

COST[1] (European Cooperation in Science and Technology) is a framework that is funded by European Union members. It allows researchers to cooperate on a European level. This project was to reduce the large fragmentation in research investments that has been done in different European member states. Because the framework consists of many European researchers there is a lot of knowledge in COST. This opens the possibility to cooperate with researchers worldwide.
COST is divided in several domains. One of them is the domain on “Forests, their Products and Services (FPS)”. COST FP1101 is an action within this domain. The objective is to increase acceptance of using timber in newly designed buildings, and also to repair and restore existing timber structures. The goal is to reach this objective by developing methods to assess-, (if necessary) reinforce- and monitor existing timber structures.

1.2. Workgroup on carpentry joints

Within the action group FP1101 a workgroup focusses solely on carpentry connections. The goal of this workgroup is to create uniform design rules on carpentry joints as they are not included in the European standard on timber structures (Eurocode 5 [2]) yet.
The workgroup uses literature on carpentry joints and (old) national standards as bases of the research. [3] These codes are analyzed from the point of their different approaches and their (mostly empirical) background. These topics will be discussed in the next chapter.
Carpentry joints are common in historical structures as technology was not advanced enough at the time of construction to make complex geometries or large amounts of mechanical fasteners. This resulted in wood-to-wood connection, meaning that the force is translated mainly by wood contact (compression and shear). A selection of carpentry joints is given in Figure 1

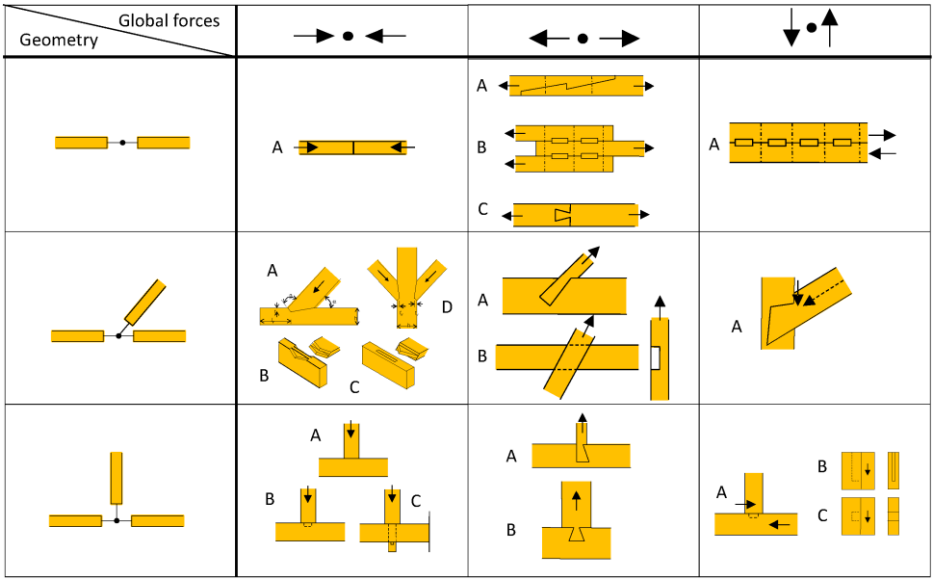

Figure 1: Most common carpentry joints in plane structures [3]

1.3. Carpentry connections – Step joints

Within the framework of carpentry joints as shown in Figure 1, the Step joint is often used for a connection between a strut (diagonal) and a chord, with the diagonal loaded in compression. Figure 2 shows multiple variants of the Step joint:

a) is the geometry that is called the Single Step joint. This geometry is the main topic of this literature study.
b) is the Heal joint and c) is the Heal Step joint
d) is the Double Step joint.
e) and f) are variants of the Single Step joint in which the front-contact area is closer to the cross-sections neutral line, which reduces eccentric forces in the strut.

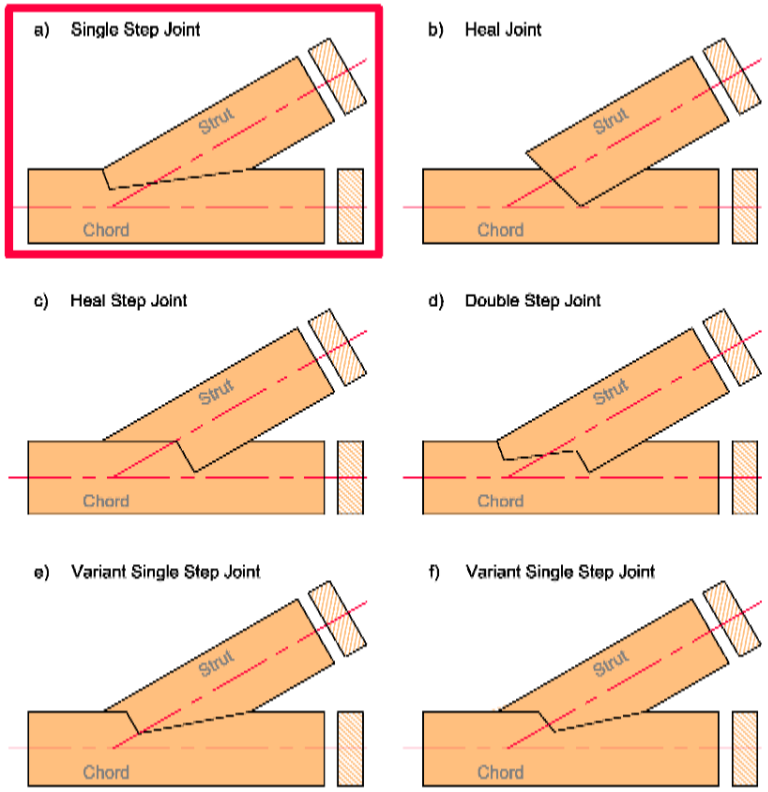

Figure 2: Different geometries of the Step joint

The connection is classified as a wood-to-wood connection with a diagonal element loaded in compression which connects to a horizontal or vertical element under an angle β. This connection is often seen in truss structures at the connection between the horizontal (beam) element and the diagonal (rafter) element, but also in trusses with multiple diagonals and vertical elements this connection is used to connect the diagonals if loaded in compression. The connection also appears at connections between beam and column in portal frames. (Figure 3)

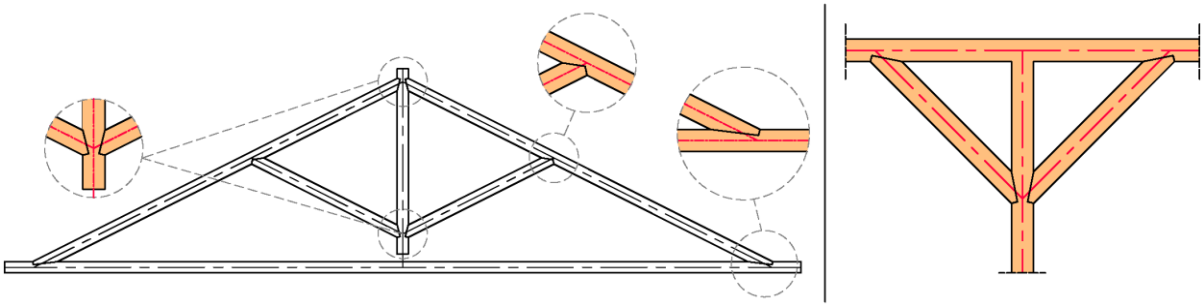

Figure 3: Often seen locations for a Step joint

2. (Inter)National Standards

Although there are no design rules on carpentry joints in the international part of EC5[2], several countries use their NCCI document (mostly incorporated in the national annex) for design rules from their previous national standards. Such as the Netherlands[4] and Germany [5].

2.1. Geometry

2.1.1. Dutch national annex to NEN-EN-1995-1-1 [4]

The last paragraph of chapter 8 in the international part of the Eurocode 5, dealing with connections, stops at paragraph 10. The Dutch national annex adds a paragraph 11 named ''Carpenters connections''. This text sets conditions to several maximum and minimum values in the geometry of the Single Step connection. If these conditions are satisfied, assumptions can be made to calculate the stress level in the joint, and formulas described in the next paragraph are allowed to be used. Several geometric boundary conditions need to be fulfilled:

8.11.2.1 Notch depth

$$t_{notch} \leq \frac{1}{5} * h \qquad for\ \beta > 50° \qquad (2.1.1.)$$

$$t_{notch} \leq \frac{1}{4} * h \qquad for\ \beta \leq 50° \qquad (2.1.2.)$$

Where h is the height of the chord (mm), and α is the angle between the center lines of the strut and chord (°).

8.11.2.2 Notched area at the front

$$90° - \frac{1}{2} * \beta \leq \gamma \leq 90° \qquad (2.1.3.)$$

Where β is the angle between the center lines of the strut and chord (°), and γ is the angle of the frontal area of the front notch and the center line of the components (°).

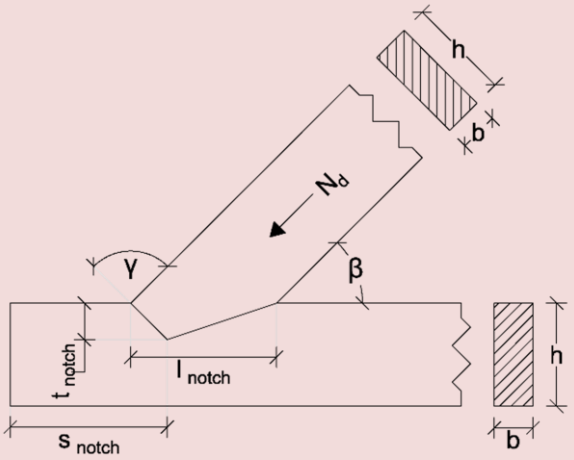

Figure 4: Example of a Single Step Joint

Quote 1: Geometric boundary conditions in the Dutch National Annex to Eurocode 5, chapter 8.11: 'Carpenters connections'

Notch depth

The first geometric condition gives a maximum boundary for the depth of the notch compared to the full height of the chord. For angles larger than 50° the maximum notch depth is 1/5th of the full height (Quote 1, equation 2.1.1.). The notch depth for angles smaller than 50° are allowed to have a slightly bigger depth of 1/4th of the full height of the chord (Quote 1, equation 2.1.2.). The notch depth is most important for small angles α since these angles give a relatively large horizontal component which acts on the frontnotch of the connection. Deeper notch depths give a larger frontnotch area through which the horizontal component has to be transferred. As the angle α increases, the horizontal component gets smaller and less area is needed in the frontnotch area. Meaning that a large depth will have the biggest effect in a reduced cross-section of the chord. If the connections require a great depth than allowed, the following solution can be applied:

- Using Double Step Joints;
- Enhance area by adding width to the cross-section;
- Bigger dimensions for the diagonal;
- Adding dowels through the bottomnotch;
- Using stirrups;
- Using full-height steel plates. (or steel shoes)

Angle of the frontnotch

The angle of the frontnotch influences the capacity and the stability of the connection. The capacity is influenced by the angle because it determines under which angle to the grain the stresses are transferred. Also the stability of the loaded connection is depending on angle γ. This angle has two extreme (maximum and minimum) values as also graphically shown in Figure 5:

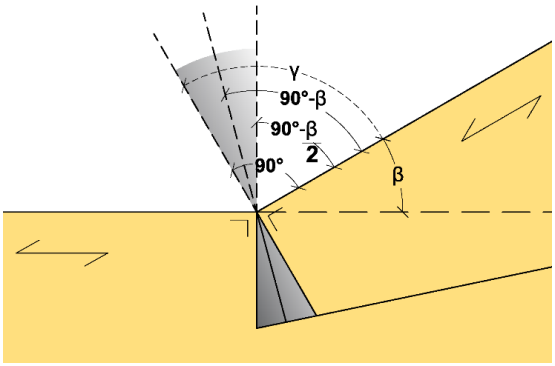

Figure 5: Extreme values and average value for angle γ of the frontnotch

- If the frontnotch is perpendicular to the neutral axis of the strut (γ=90°) the biggest threat is the possibility of the strut 'popping out' of the chord because of the shallow angle.
- Making the frontnotch perpendicular to the chord's axis (γ=90°-α) is the absolute limit to prevent wedging of the front part of the chord. An angle smaller than (γ=90°-α) will cause tension stresses perpendicular to the grain, which gives a weak resistance for wood. Tension stresses perpendicular to the grain also decrease the shear resistance of the shearplane.

As can be seen in Quote 1, equation (2.1.3.), the Dutch NA to Eurocode 5 gives a range of allowable angles γ between 90°-β/2 and 90°. This range is shown in Figure 6.

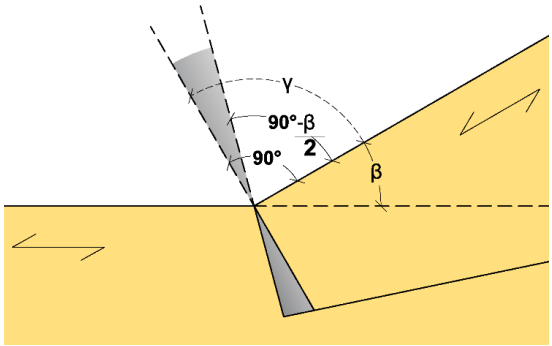

Figure 6: Boundaries for angle γ of the frontnotch in the Dutch national annex to Eurocode 5

2.1.2. German national annex to DIN-EN-1995-1-1 [5]

The German national annex gives similar boundary conditions for the notch depth in a Single Step joint, allowing a shallower depth for large angles and using linear interpolation for angles between 50° and 60°. Unlike the Dutch national annex, the angle of the frontnotch is set to one single boundary, being always 90°-β/2.

NCI NA.12.1 Versätze

$$t_v \leq \begin{cases} \frac{h}{4} & for \quad \beta \leq 50° \\ \frac{h}{6} & for \quad \beta > 60° \end{cases} \qquad (2.1.4.)$$

Where h is the height of the notched chord (mm),
and β is the angle of the connection (°)

Values between 50° and 60° may be interpolated.

The notch depth t_{notch} of a two-sided Single Step Joint may not be larger than $h/6$ also for $\beta \leq 50°$.

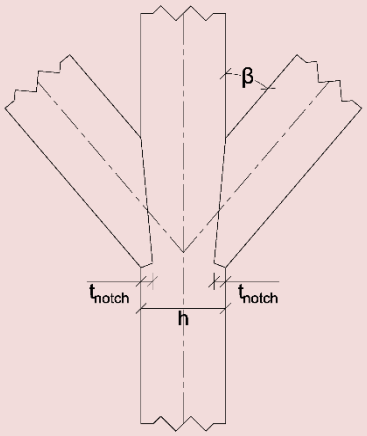

Figure 7: Two-sided Single Step Joint

Quote 2: Geometric boundary conditions in the German national annex to Eurocode 5, chapter 12.1: 'Versätze'

2.1.3. Swiss national standard SIA 256 Holzbau [6]

The Swiss national standard gives the same geometrical boundaries for a Single Step Joint as the German NA to EC5 [5] as can be seen in Table 1 and Figure 8 within Quote 3:

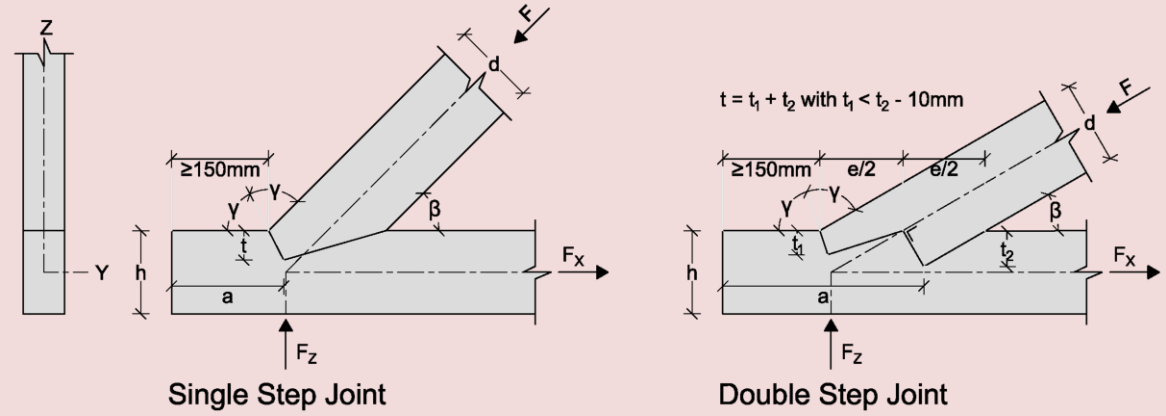

Figure 8: Example of a Single Step Joint and a Double Step Joint

6.9.2.2 The boundaries for t are set in Table 1

Table 1: Notch depth *t* in carpentry connections

Single Step Joint	Double Step Joint
$t \leq \frac{h}{4} \quad for \quad \beta \leq 50°$	$t_1 \leq \frac{h}{6}$
$t \leq \frac{h}{6} \quad for \quad \beta \geq 60°$	$t_2 \leq \frac{h}{4}$
Angles between 50° and 60° can be interpolated linearly	$t_1 < t_2 - 10mm$

Quote 3: Geometric boundary conditions in the Swiss SIA 256 Holzbau, chapter 6.9: 'Holzverbindungen'

Shearplane length

The length needed for the shearplane is determined in several ways. The Dutch national annex to EC5 takes the length of the shearplane into account in the calculations of the shear-stresses. A larger shearplane length results in lower shear stresses in the area.
The Swiss code indicates a minimum shearplane length of 150mm as shown in the figures in Quote 3 independent of the rest of the dimensions of the geometry. Using several geometric and resistance parameters, an exact minimum length for the shearplane length, indicated by 'a', can be calculated. This is further explained in paragraph 2.2.

The German national annex to EC5 sets a maximum length for the shearplane that is allowed to use. The shear-stresses are assumed to be distributed linearly over the length of the shearplane, where in reality these stresses are very high near the tooth of the notch and gradually decrease non-linear further towards the end of the chord, as shown in Figure 9.
For very long shearplanes, the ends are not influenced by shear-stress anymore. Since the stresses get distributed evenly over the length, for very large lengths, the assumed shear-stresses are much lower than in reality. That is why a maximum length of 8 * t_{notch} for distributing the calculated shear-stresses uniformly is set.

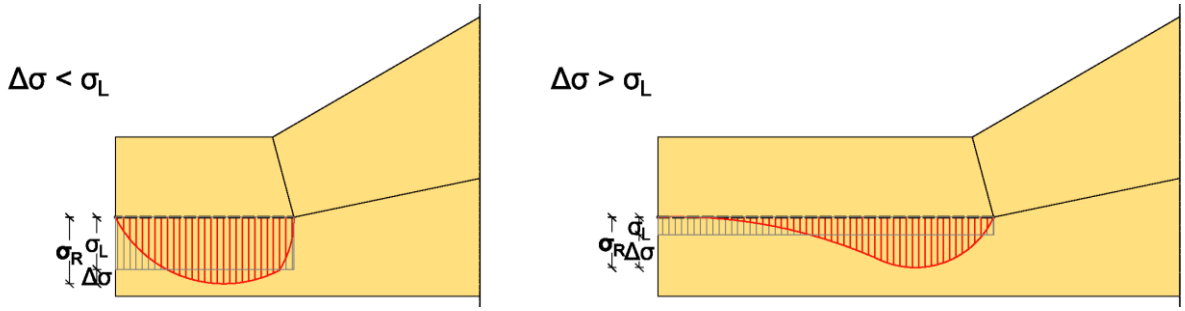

Figure 9: Difference (Δσ) in real stress distribution (σ_R) and linear distributed stresses (σ_L) for different shearplane lengths

2.2. Stresses

2.2.1. Dutch national annex to NEN-EN-1995-1-1 [4]

The formulas in section 8.11.3 of the Dutch national annex to EC5 may be used if a connection fulfills all geometrical conditions stated in paragraph 8.11.2 in the national annex to Eurocode 5, and the cross-sections comply with sections 6.1.4, 6.1.5, 6.1.7, 6.2.2, being unity checks for:

- 6.1.4: Compression parallel to fiber direction;
- 6.1.5: Compression perpendicular to fiber direction;
- 6.1.7: Shear;
- 6.2.2: Compression under an angle to fiber direction.

Unity checks according to chapter 6 of EC5

The above sections of chapter 6 in EC5 are mainly straight-forward checks for making sure the stresses in the members are lower than the resistance strength of the material ($\sigma \leq f$). From these sections, two things have to be described in more detail:

(1) $K_{c,90}$

The $K_{c,90}$ factor can contibute in increasing the characteristic material resistance for compression perpendicular to the grain ($f_{c,90,d}$) under certain conditions:
In situations where maximum compression perpendicular to the grain can cause failure of a total structure the calculation is assumed to be ULS and $K_{c,90}$ is 1.0. For situations where compression perpendicular to the grain leads to high deformations but does not cause a failure of the element or structure itself, for instance near point loads or near a support, a value for $K_{c,90}$ of up to 1.75 depending on the situation (Table 2) may be used.

Table 2: Values for $K_{c,90}$ according to EC5 section 6.1.5

$K_{c,90}$	$l_1 \geq 2h$		$l_1 < 2h$
	Continuous support	Discrete support	
Coniferous sawn timber	**1.25**	**1.5**	**1.0**
Coniferous Glulam	**1.5**	**1.75** ($l \leq 400\text{mm}$)	**1.0**

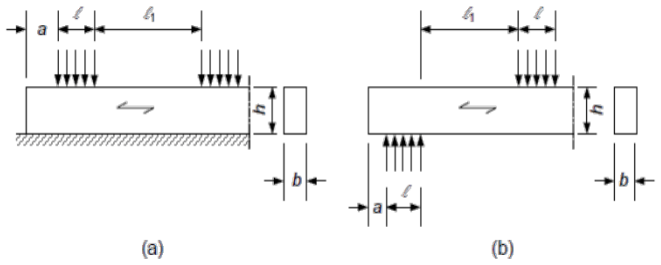

Figure 10: Element on continuous (a) and discrete (b) support. [7]

(2) Compression under an angle to fiber direction

In section 6.2.2 of Eurocode 5, a unity check for compression under an angle α to the grain is presented. This check uses the parameters for compression parallel-, and perpendicular to the grain in a formula which is based on Hankinson's [8] theory.

$$\sigma_{C,\alpha,d} \leq \frac{f_{c,0,d}}{\frac{f_{c,0,d}}{K_{c,90} * f_{c,90,d}} * \sin\alpha^2 + \cos\alpha^2} \qquad (2.2.1.)$$

The Dutch national annex allows the action force in a Single Step joint from the strut to be decomposed into two components which act parallel and perpendicular to the grain direction of the chord. This force then may be translated to a uniformly distributed stress.

8.11.3 Compressive and shear stresses

$\sigma_{c;0;d} \leq f_{c;0;d}$ *where* $\sigma_{c;0;d} = \frac{N_{c;d} * \cos\beta}{t_{notch} * b}$ (2.2.2.)

$\sigma_{c;90;d} \leq f_{c;90;d}$ *where* $\sigma_{c;90;d} = \frac{N_{c;d} * \sin\beta}{l_{notch} * b}$ (2.2.3.)

$\sigma_{v;d} \leq f_{v;d}$ *where* $\sigma_{v;d} = \frac{N_{c;d} * \cos\beta}{0.8 * s_{notch} * b}$ (2.2.4.)

Where

$N_{c;d}$ is the design value of the normal compressive force to be transmitted (N);

b is the width of the contact elements (mm);

s_{notch} is the shear-loaded end distance (shearplane) (mm);

t_{notch} is the front notch depth (mm);

l_{notch} is the length of the notch (mm);

β is the angle between axial compressive force $N_{c;d}$ and the center line of the adjoining member (°)

Quote 4: design stress resistance check in the Dutch National Annex to Eurocode 5, chapter 8.11: 'Carpenters connections'

All text in the Dutch national annex to Eurocode 5 section 8.11 is a copy of old NEN standards [9]. Since these rules also refer to section 6.2.2 of Eurocode 5, two different checks for stresses under an angle α to the grain are given:

(1) Equations 2.2.2., 2.2.3. and 2.2.4. from the Dutch NA to EC5 8.11.3 as presented in Quote 4 express the load in the strut ($N_{c;d}$) in stresses parallel to grain ($\sigma_{c;0;d}$), stresses perpendicular to grain ($\sigma_{c;90;d}$) and shear stresses ($\sigma_{v;d}$). When equating them to the characteristic compressive material properties of timber (e.g.: $\sigma_{c;0;d} = f_{c;0;d}$) these stresses can be rewritten to give the compressive strength when loaded under an angle α (f_α):

$$f_\alpha = \frac{f_{c;0;d}}{\cos^2\alpha} \quad (2.2.5.)$$

$$f_\alpha = \frac{f_{c;90;d}}{\sin^2\alpha} \quad (2.2.6.)$$

$$f_\alpha = \frac{0.8 * f_{v;d}}{\sin\alpha \cdot \cos\alpha} \quad \text{(0.8 is added since this relates to the reduction factor in (2.2.4.)} \quad (2.2.7.)$$

These three formulas create an envelope where always the minimum of the three values is governing. When plotting this line it explains the behavior of the Dutch NA (Quote 4).

(2) Equation (2.2.1.) from section 6.2.2 in Eurocode 5 is also expressed in the compressive strength when loaded under an angle:

$$f_\alpha = \frac{f_{c,0,d}}{\frac{f_{c,0,d}}{K_{c,90} * f_{c,90,d}} * \sin\alpha^2 + \cos\alpha^2} \qquad (2.2.8.)$$

These expressions of f_α can be used to graphically show the material strength resistance that is given following the Eurocode 5 checks for varying loading angles α. These checks are plotted for α = 0° to 90° for characteristic values of timber in strength class C24 and $K_{c,90}$ = 1.0 in Figure 11:

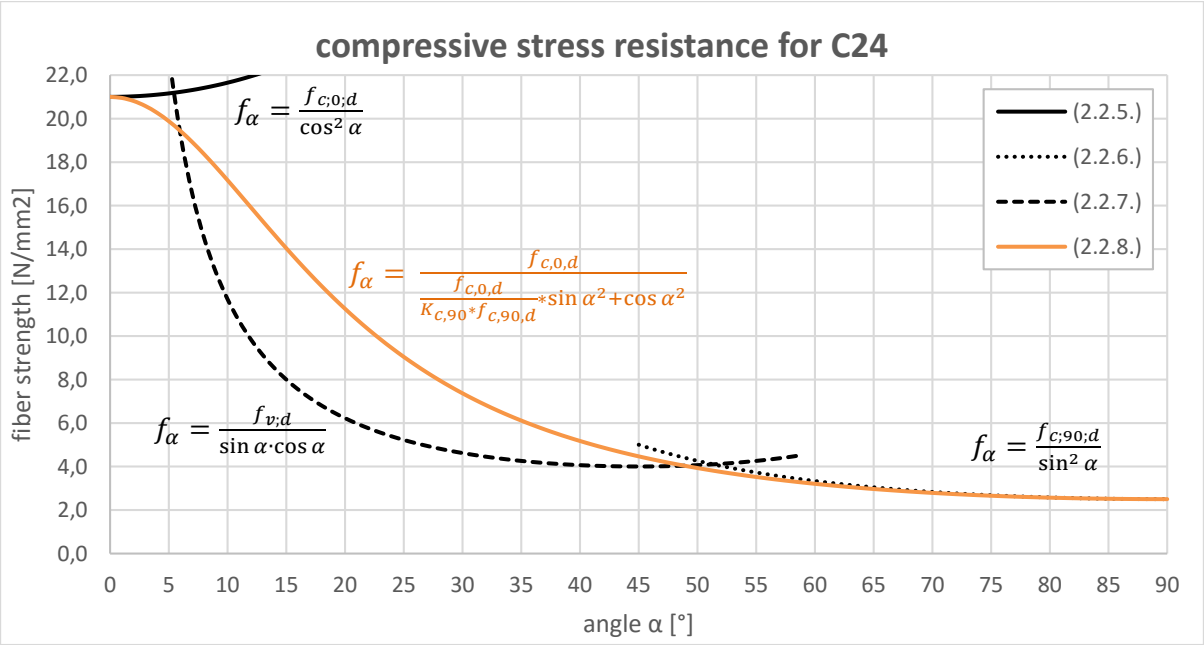

Figure 11: Stress resistance under an angle to the grain for Section 6.2.2 of EC5 and section 8.11 of the Dutch NA to EC5

2.2.2. German national annex to DIN-EN-1995-1-1 [5]

The German national annex has a different approach to the determination of the resistance of the material compared to the Dutch. It describes the stress which is acting on the surface of the frontnotch, and uses an equation which is based on the equation developed by Norris [10] to define the strength of the material under an angle (α) to the grain:

> Deviating from section 6.2.2 the compressive stresses in the connection can be found in the following manner:
>
> $$\frac{\sigma_{c,\alpha,d}}{f_{c,\alpha,d}} \leq 1 \qquad (2.2.9.)$$
>
> Where
>
> $$\sigma_{c,\alpha,d} = \frac{F_{c,\alpha,d}}{A} \qquad (2.2.10.)$$
>
> $$f_{c,\alpha,d} = \frac{f_{c,0,d}}{\sqrt{\left(\frac{f_{c,0,d}}{2*f_{c,90,d}}*sin^2\alpha\right)^2+\left(\frac{f_{c,0,d}}{2*f_{v,d}}\sin\alpha*\cos\alpha\right)^2+cos^4\alpha}} \qquad (2.2.11.)$$
>
> and
>
> A is the front notch surface area;
>
> α is the angle between the direction of the force and the direction of the grain.
>
> 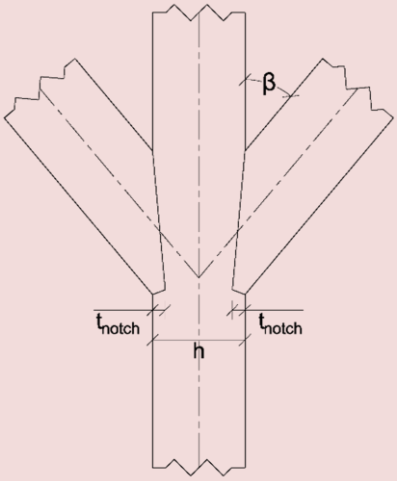
>
>
> The shear stresses in the connection can be assumed uniformly distributed along the length of the shear-plane. If this is assumed, a shear-plane length may not be longer then $8 * t_{notch}$
> For the calculation of the shear stress in this section an effective width according to 6.1.7 of Eurocode 5 must be taken into account.

Quote 5: Design stress resistance check in the German national annex to Eurocode 5, chapter 12.1: 'Versätze'

Angle α is further explained in Figure 12 on the next page.

Although it is not stated explicitly in the German NA to EC5 how the shearplane is calculated, an explanatory book for the DIN [11] gives a method to calculate as shown on the next page.

In the national annex the variable $F_{c,\alpha,d}$ is not clearly defined. From literature [11] it can be concluded that this is a component of the force in the strut which is acting perpendicular onto the frontnotch surface as indicated in Figure 12.

A factor 2 is added to the strength perpendicular to the grain ($f_{c,90,d}$) which can be related to the $K_{c,90}$ factor defined in Eurocode 5. and also to the shear strength $f_{v,d}$.

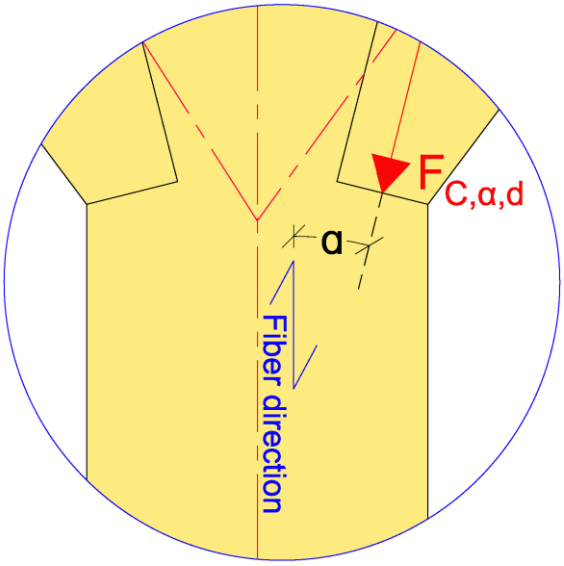

Figure 12: definition of angle α as used in German national annex to Eurocode 5 formula (NA.152)

Calculation of the shearplane

Although several statements are made in the German NA to EC5 (Quote 5) for calculation for the shearplane length, the actual method to calculate the shearplane is not defined. Using [11] a method for calculating stresses in the shearplane is given as follows:

$$F_{H,d} = F_{strut} * \cos\beta \qquad (2.2.12.)$$

$$\tau_{v,d} = \frac{F_{H,d}}{s_{notch} * b_{ef}} \qquad (2.2.13.)$$

$$\frac{\tau_{v,d}}{f_{v,d}} \leq 1.0 \qquad (2.2.14.)$$

Where F_{strut} is the load on strut and $F_{H,d}$ is the horizontal component of this force. This horizontal component is then distributed linearly over the area of the shearplane to give the shear stresses acting in the shearplane. A minimum shearplane length of 200mm is given.
It can be concluded from the German NA to EC5 that s_{notch} may not be considered larger than $8 * t_{notch}$ in the calculation and the width of the shearplane must be reduced according to section 6.1.7. in EC5 to an effective width as defined next.

Effective width

The German NA to Eurocode 5 (Quote 5) refers to section 6.1.7 in the general part of EC5 on shear stresses. This section gives an effective width which reduces the cross-sections in order to take the influence of longitudinal cracks into account. This effective width is determined by:

$$b_{ef} = k_{cr} * b \qquad (2.2.15.)$$

Where b is the width of the relevant cross-section of the member. Recommended values for k_{cr} are given as:

- $k_{cr} = 0.67$ for solid timber
- $k_{cr} = 0.67$ for glued laminated timber
- $k_{cr} = 1.0$ for other wood-based products in accordance with EN 13986 and EN 14374

Note: 6.1.7 is also reffered to in the Dutch NA, but since k_{cr} is 1.0 for all prismatic cross-sections according to the Dutch NA, this section was not further eleborated.

Also the German version to determine the stress resistance under an angle can be plotted for α = 0° to 90° for characteristic values of timber in strength class C24:

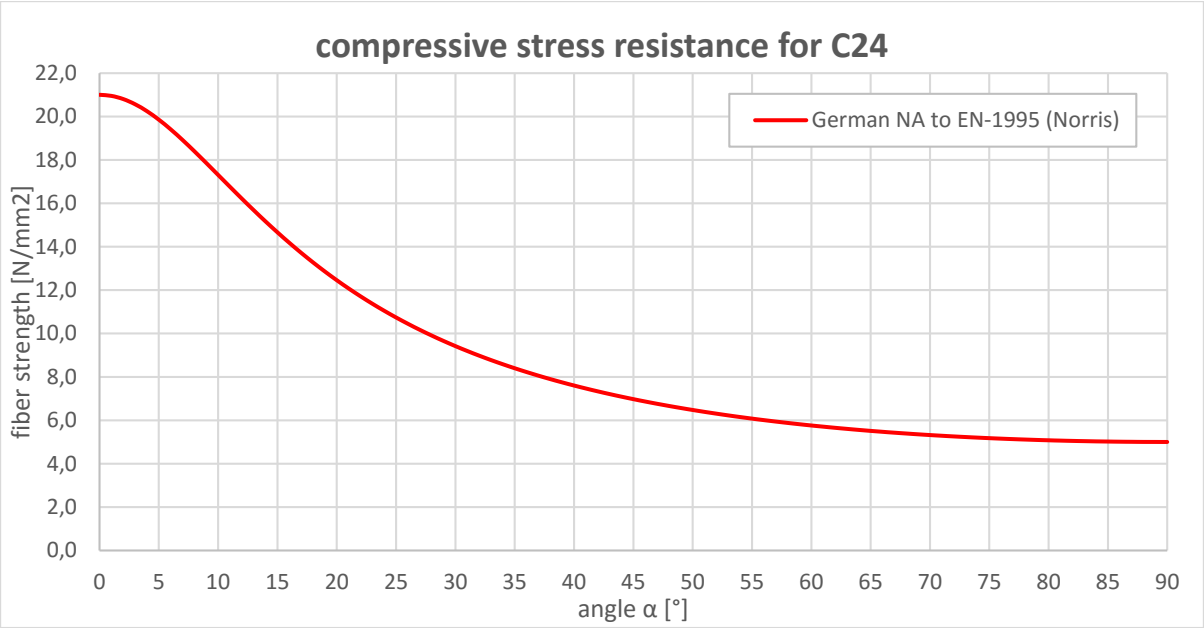

Figure 13: Stress resistance under an angle to the grain according to the German national annex to EC5

2.2.3. Swiss national standard SIA 256 Holzbau [6]

The Swiss standards relates the equation to find the stresses in the connection to the geometry of the connection. Equations to determine a minimum notch depth t (2.2.17.), strut width d (2.2.18.) and the shearplane a (2.2.16.) are given in terms of the acting force F_{Ed}, angle β and the characteristic material strengths.

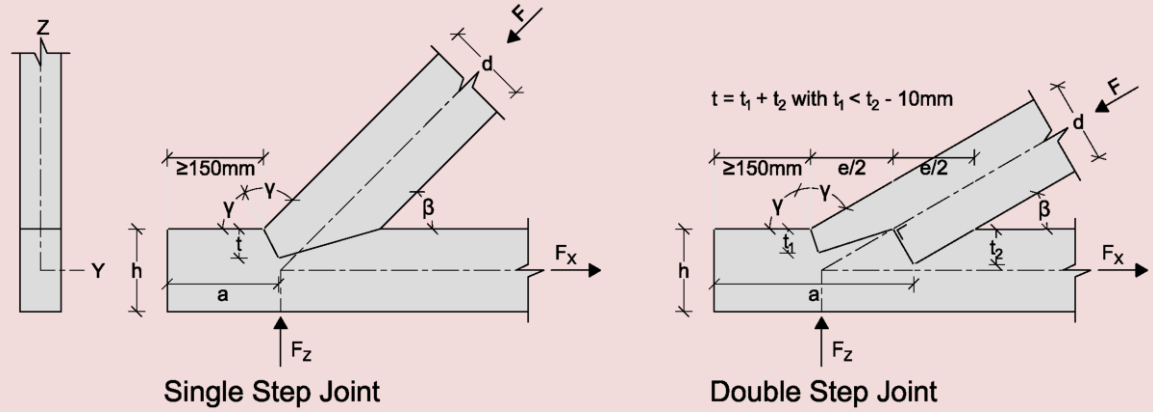

6.9.2 Versatz

For the transference of compressive force F_{Ed} the following equations may be used:

Shear-plane length: $a \geq \frac{F_{Ed} * \cos\beta}{b * k_{red} * f_{v,d}}$ (2.2.16.)
- k_{red}=0,6 *for sawn timber*
- k_{red}=0,8 *for glulam timber*

Notch depth: $t \geq \frac{F_{Ed} * \cos\beta}{b * f_{c,\alpha,d}}$ (2.2.17.)
- $\alpha=\frac{1}{2}\beta$ *for Single Step Joints*
- $\alpha=\frac{3}{4}\beta$ *for Double Step Joints*

Strut height: $d \geq \frac{F_{Ed}}{b * f_{c,\alpha,d}}$ (2.2.18.)
- $\alpha=\beta$

Where

b is the width of the strut;

β is the angle between force F_{Ed} and the fiber direction.

$f_{c,\alpha,d}$ is calculated as follows:

$$f_{c,\alpha,d} = \frac{0{,}8 * f_{c,0,d} * f_{c,90,d}}{0{,}8 * f_{c,0,d} * sin^2\alpha + f_{c,90,d} * cos^2\alpha} \quad (2.2.19.)$$

Quote 6: Design stress resistance check in the Swiss SIA 256 Holzbau, chapter 6.9: 'Holzverbindungen'

Although the geometric part of the standard is the same as the German standard, the stress-part is completely different. As the German NA to EC5 bases the stress on Norris' equation, the Swiss standard uses an equation derived by Hankinson [8](2.2.19.). This equation is used to find the resistance of the material when loaded under an angle to the grain. The strength parallel-, and perpendicular to the grain are used to determine the resistance. The strength parallel to the grain is reduced by a factor 0.8. The shear strength is not used to determine the strength under an angle, instead a separate shear-check is done in (2.2.16.). This formula also contains a reduction factor k_{red} which takes into account the difference in resistance against shear for sawn and laminated timber.

This Hankinson based expression for stress resistance under an angle to the fiber can again be plotted for angle α = 0° to 90° and strength class C24:

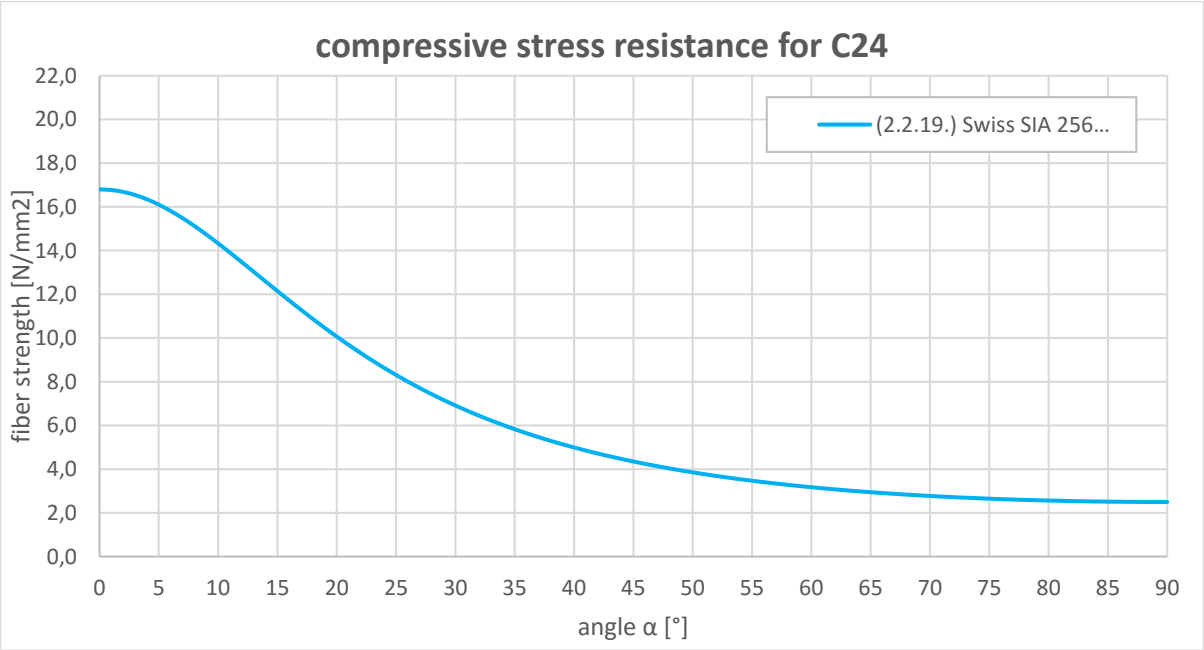

Figure 14: Stress resistance under an angle to the grain according to the Swiss SIA 256 code

2.2.4. Comparison of codes

All previous plots for the design strength under an angle to the grain for characteristic values of C24 and $K_{c,90}$ = 1.0 can be combined to see the divergence in assumed resistances:

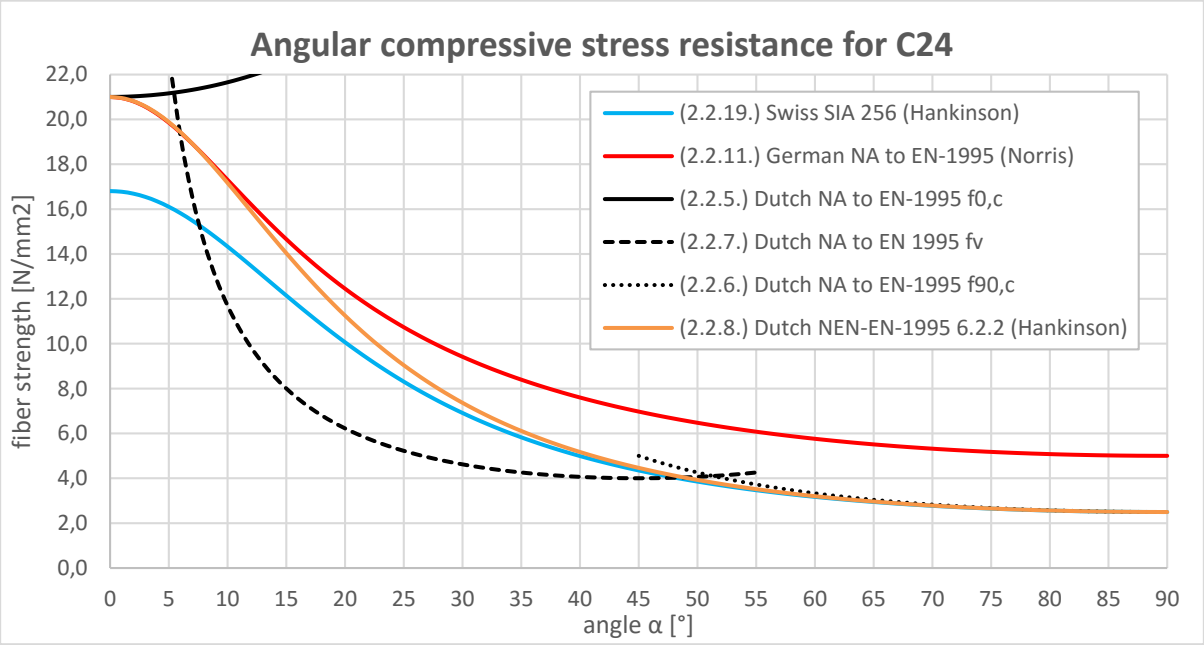

Figure 15: Material resistance to loading under an angle to the fiber according to different codes

For angle α = 0° it can be seen that for the Dutch and German NA to EC5 the fiber strength is equal to $f_{c,0,d}$ which is logical since the material is loaded parallel to the grain. The effect of the factor 0.8 on parameter $f_{c,0,d}$ in the Swiss code can be seen since the maximum fiber strength is reduced.

The dashed black line representing (Dutch NA to EC5 8.11.3) shear resistance 'f_v' gives by far the lowest resistance for angles between 8° and 45°. This can be explained by the very conservative nature of the characteristic value for shear resistance that is used. When implementing real (empirical) values this line is much closer to the German NA and Swiss code.

For all values for α, the German NA to EC5 allows the highest fiber resistance strength. This is due to the factor 2 on $f_{v,d}$ compensating the conservative characteristic shear strength, and the factor 2 on $f_{c,90,d}$ which can be related to a $K_{c,90}$ of 2.0 that are used in the Norris-based formula.

2.3. Bases of stress equations in (inter)national standards

As mentioned in the previous chapter several approaches with respect to the strength of the material are used.

2.3.1. Decomposing force to axial components

(As used in the Dutch National Annex to Eurocode 5)

The Dutch National annex uses a very rough method to check the resistance of the connection. It lets the user decompose the force F in the strut into two components which comply with the fiber direction of the chord. In the case of a geometry like Figure 16 this means two decomposed components N_{90} and N_0 in X, and Y direction. Component N_{90} may be distributed over notch length l_{notch} and component N_0 may be evenly distributed over notch depth t_{notch}. This gives the stresses in the chord in parallel and perpendicular grain direction. These stresses then may not exceed the resistance stresses of the material. In addition to the normal stress check, the shear stress must also be checked. This is done by evenly distributing component N_0 over the length s_{notch}. Because this shear stress in reality is not evenly distributed over the length of the shearplane, a reduction of 0,8 must be taken into account over this length s_{notch}.

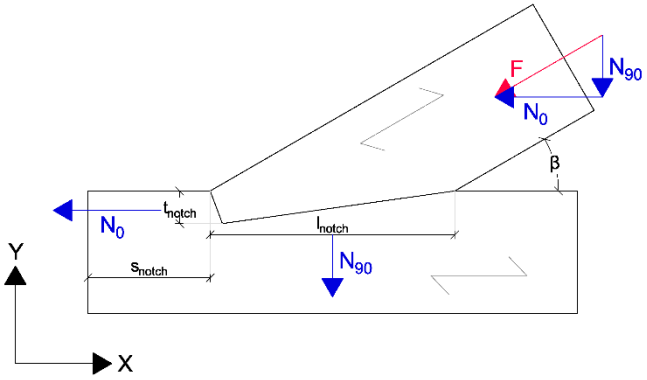

Figure 16: Decomposing force F into two components N_0 and N_{90}.

2.3.2. Hankinson's equation [8]

(As used as bases by the Swiss standard SIA 265)

In 1921 R. L. Hankinson (U.S. Air Service) derived an curve fitting formula from a series of conducted tests (Figure 17). When he started his research his aim was to come up with an equation which was closer to test results then existing formula's derived by prof. H.S. Jacoby:

$$(n = p * sin^2\theta + q * cos^2\theta) \qquad (2.3.1.)$$

and prof. M.A. Howe:

$$(n = q + (p - q)\frac{(\theta°)}{(90°)}5/2). \qquad (2.3.2.)$$

These formula's varied from test results up to 60% (Jacoby). Hankinson's research focused on Spruce and Pine but the formula proved to be applicable to more wood species.

$$n = \frac{p * q}{p * sin^2\theta + q * cos^2\theta} \qquad (2.3.3.)$$

Where:

n is the material resistance at angle θ [N/mm^2] ($f_{c,\alpha}$)
p is the material resistance at $\theta = 0°$ (parallel to the grain) [N/mm^2] ($f_{c,0}$)
q is the material resistance at $\theta = 90°$ (perpendicular to the grain) [N/mm^2] ($f_{c,90}$)

θ is the angle between the direction of the applied force and the direction of the grain [°]

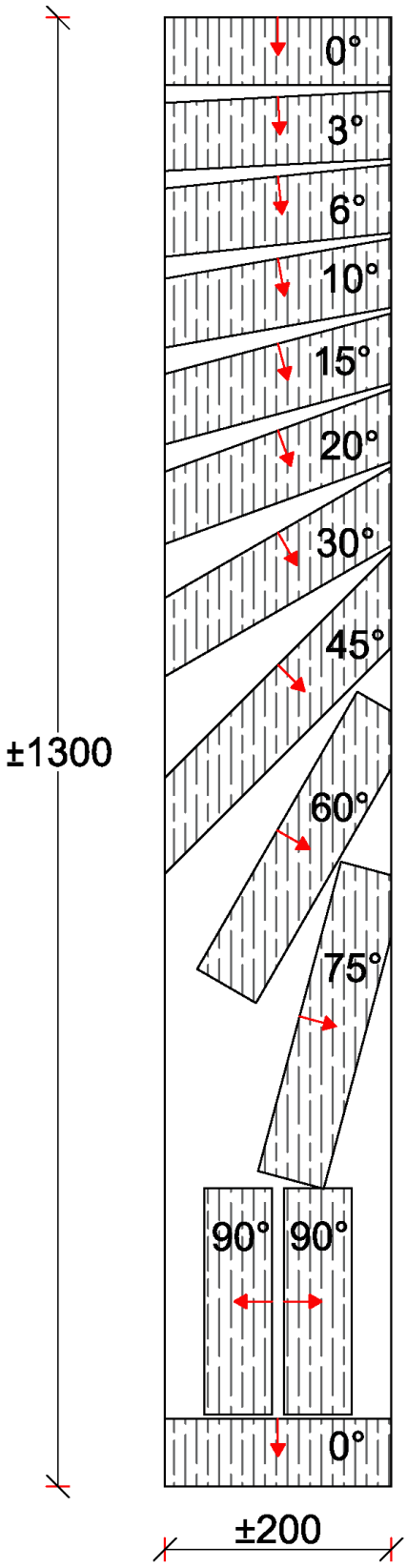

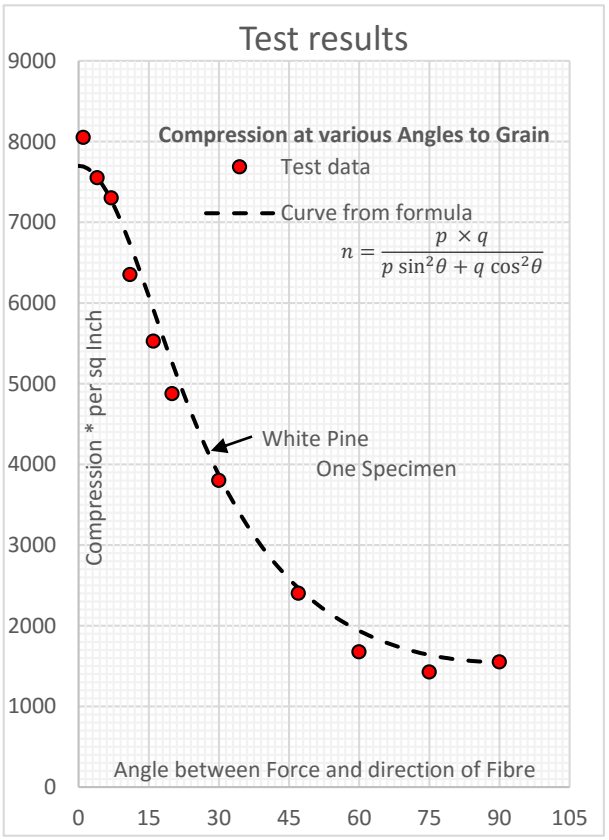

Figure 18: Test results from Hankinson's experimental campaign [8]

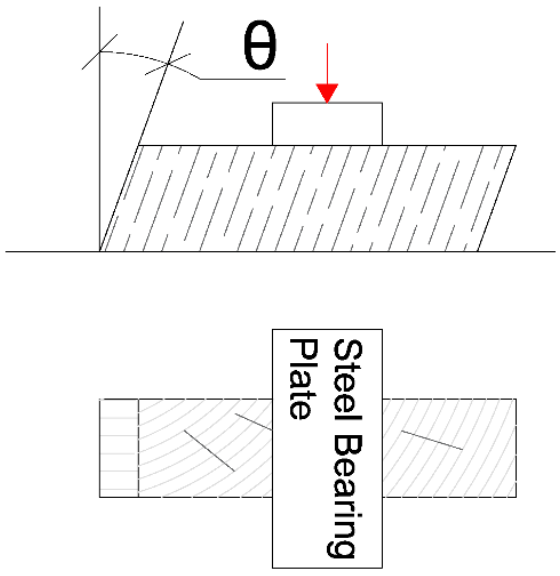

Figure 17: Specimens for compression test at various angles θ of Grain, Method of test [8]

2.3.3. Norris' theory [10]

(As used as bases by the German National Annex to Eurocode 5)

In 1962 Charles B. Norris (Forest Products Laboratory, Madison, Wisconsin) derived an equation which describes the strength of orthotropic materials subjected to combined stresses. The theory behind the equation is based on the Hencky-vonMises theory, which is based on work (energy) due to changes in the shape of an object. The strength of orthotropic materials with a single stress at an angle to the grain (natural axis) can be deduced from the Norris equation. A series of tests was done on several orthotropic materials to validate the equation and the results of these test were in conformation with the theory.

$$1 = \frac{{f_1}^2}{{F_1}^2} + \frac{{f_2}^2}{{F_2}^2} + \frac{{f_{12}}^2}{{F_{12}}^2} \qquad (2.3.4.a)$$

Where

f_i is the stress acting on the connection. Subscript 1 for stress parallel to the grain, 2 for stress perpendicular to the grain, 12 for shearstress.

F_i is the design resistance stress of the material. Subscript 1 for stress parallel to the grain, 2 for stress perpendicular to the grain, 12 for shearstress.

Unlike Hankinson's equation, which was a curve fitting equation, Norris' equation was mathematically derived. Norris' equation gives the failure criteria for the material for each parameter. With the strength parallel and perpendicular to the grain and shear this gives the failure criteria as seen in Figure 19:

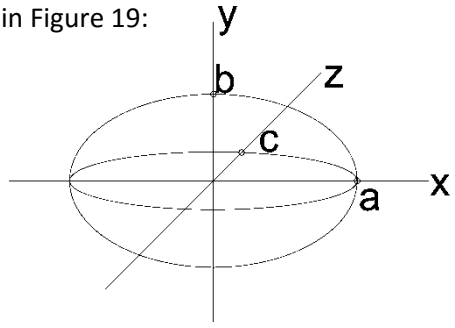

Figure 19: Strength envelop as ellipsoid, Norris (1962)

$$\left(\frac{x}{a}\right)^2 + \left(\frac{y}{b}\right)^2 + \left(\frac{z}{c}\right)^2 = 1 \qquad (2.3.4.b)$$

In common engineering symbols:

$$\left(\frac{\sigma_0}{f_0}\right)^2 + \left(\frac{\sigma_v}{f_v}\right)^2 + \left(\frac{\sigma_{90}}{f_{90}}\right)^2 \leq 1 \qquad (2.3.4.c)$$

By using equilibrium equations for an element loaded under an angle to the fiber, the following derivations can be made: (as illustrated in Figure 20 a)

$$\Sigma_{0-direction} = 0 \qquad -\sigma_0 * 1 \cdot \tan(\alpha) + \tau * 1 = 0 \;\rightarrow\; \boldsymbol{\tau = \sigma_0 \tan(\alpha)} \qquad (2.3.5.)$$

$$\Sigma_{90-direction} = 0 \qquad \sigma_{90} * 1 - \tau * 1 \cdot \tan(\alpha) = 0 \;\rightarrow\; \boldsymbol{\sigma_{90} = \tau \tan(\alpha)} \qquad (2.3.6.)$$

Using (2.3.5.) in (2.3.6.) gives:

$$\sigma_{90} = \sigma_0 \cdot \tan(\alpha)^2 \qquad (2.3.7.)$$

Using (2.3.5.) and (2.3.7.) in (2.3.4.c) gives: $(\tau = \sigma_v)$

$$\left(\frac{\sigma_0}{f_0}\right)^2 + \left(\frac{\sigma_0 \cdot \tan(\alpha)}{f_v}\right)^2 + \left(\frac{\sigma_0 \cdot \tan(\alpha)^2}{f_{90}}\right)^2 \leq 1 \qquad (2.3.8.)$$

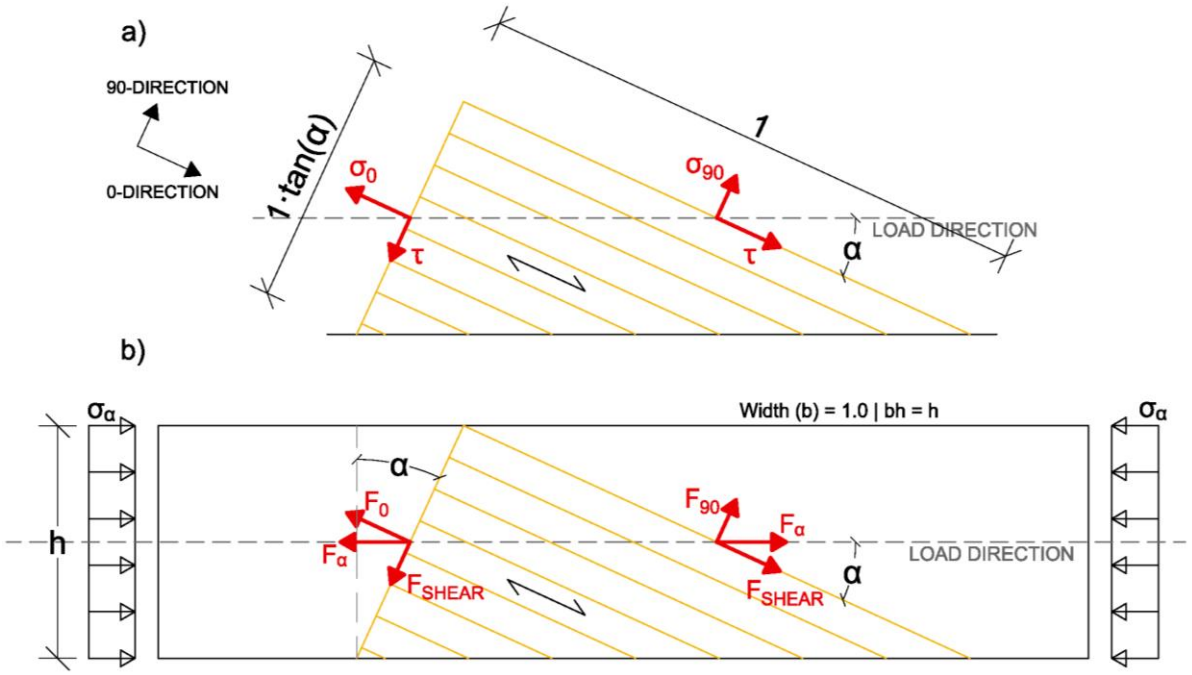

Figure 20: a) Equilibrium in a piece of wood loaded under an angle; b) Equilibrium in a timber element. [12]

Equation (2.3.8.) is still expressed in terms of σ_0. In order to find resistance under an angle to the grain an expression for σ_α relating to σ_0 must be found. This can be done by considering equilibrium of a timber element as shown in Figure 20 b:

$$F_\alpha = h \cdot \sigma_\alpha \tag{2.3.9.}$$

$$F_0 = \frac{h}{\cos(\alpha)} \cdot \sigma_0 \tag{2.3.10.}$$

$$F_0 = F_\alpha \cdot \cos(\alpha) \tag{2.3.11.}$$

Using (2.3.9.), (2.3.10.) and (2.3.11.) gives:

$$\frac{h}{\cos(\alpha)} \cdot \sigma_0 = h \cdot \sigma_\alpha \cdot \cos(\alpha) \;\rightarrow\; \sigma_0 = \sigma_\alpha \cdot \cos(\alpha)^2 \tag{2.3.12.}$$

Equation (2.3.8.) can be solved in terms of $\sigma_0 (= f_0)$ and equated with (2.3.12.) to form:

$$\sigma_\alpha = \frac{f_0}{\cos(\alpha)^2 \cdot \sqrt{1 + (\frac{f_0}{f_v})^2 \cdot \tan(\alpha)^2 + (\frac{f_0}{f_{90}})^2 \cdot \tan(\alpha)^4}} \tag{2.3.13.}$$

This equation is very similar to equation (2.2.11.) in the German national annex to Eurocode 5.

Norris does not make a difference between compression and tension force as material parameter. This is a limiting factor in Norris' equation as many materials like wood have different tensile and compression strength in the same direction. This is shown in Figure 21 for the strength parallel to grain and perpendicular to grain.

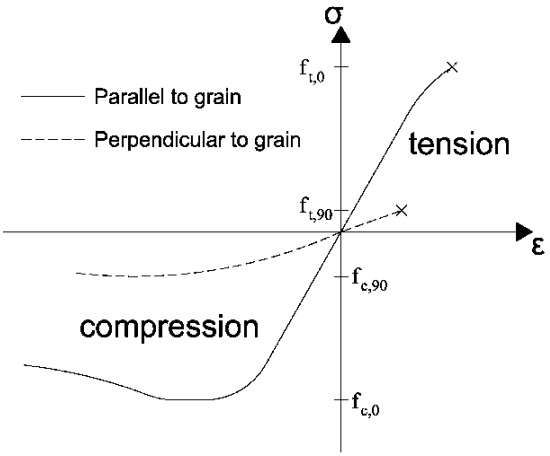

Figure 21: Stress-strain relation of wood

Also the effect of tension or compression perpendicular to the grain together with shear stresses is not taken into account. If an area loaded in shear is also loaded in compression perpendicular to the grain the shear strength is larger compared to a situation without- or tension stresses perpendicular to the grain. This leads to a variable behavior of the shear capacity.

During the years after Norris presented his equation in 1962 several researchers have tried to take the previously mentioned phenomena into account by altering the formula, adding strength parameters. Several of these altered equations were compared with experimental failures of specimens that were tested by Eberhardsteiner (2002). Table 3 shows the comparison of the failures in the test (red dots) with the envelope line representing the failure criterion formula's as given under the graph in terms of σ_{xx} and σ_{yy} (blue).

In the table it can be seen that from the tested failure criterions only "van der Put" uses different parameters for compression and tension.

Table 3: Several Norris-based failure criterion plotted together with test failures performed by Eberhardsteiner [13]

Linear	Norris (Quadratic)
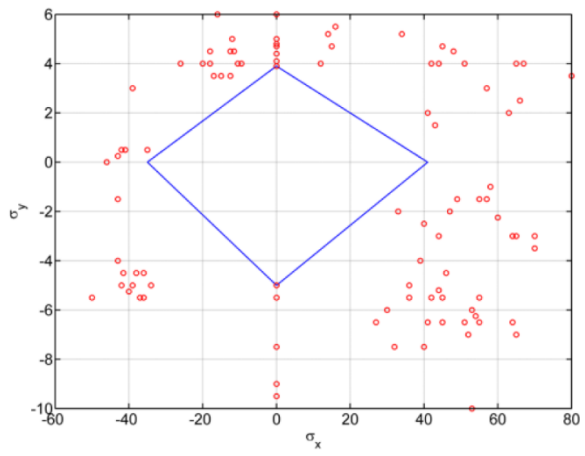	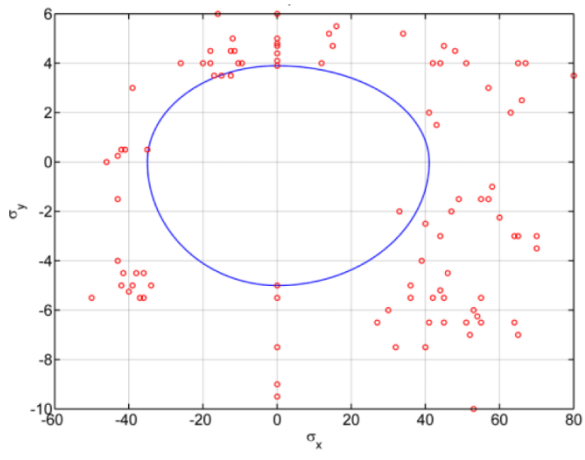
$\frac{\sigma_{xx}}{f_{xx}} + \frac{\sigma_{yy}}{f_{yy}} + \frac{\tau_{xy}}{f_{xy}} = 1$	$\left(\frac{\sigma_{xx}}{f_{xx}}\right)^2 + \left(\frac{\sigma_{yy}}{f_{yy}}\right)^2 + \left(\frac{\tau_{xy}}{f_{xy}}\right)^2 = 1$

(Table continued on the next page)

Tsai-Hill

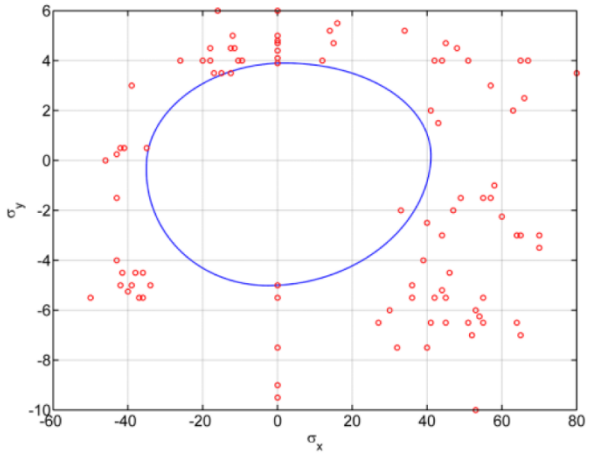

$$\left(\frac{\sigma_{xx}}{f_{xx}}\right)^2 - \frac{\sigma_{xx}\sigma_{yy}}{{f_{yy}}^2} + \left(\frac{\sigma_{yy}}{f_{yy}}\right)^2 + \left(\frac{\tau_{xy}}{f_{xy}}\right)^2 = 1$$

Norris II

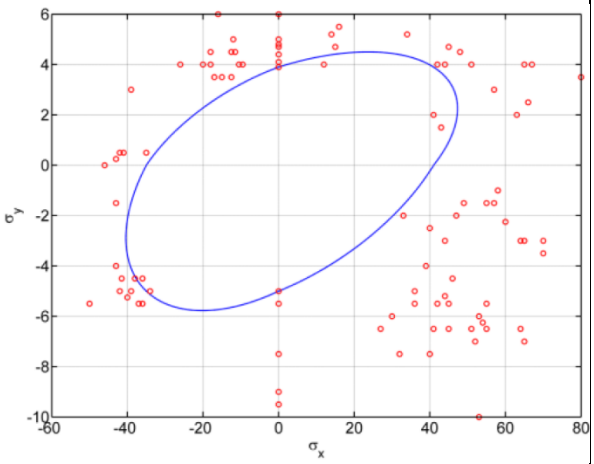

$$\left(\frac{\sigma_{xx}}{f_{xx}}\right)^2 - \frac{\sigma_{xx}\sigma_{yy}}{{f_{xx}}^2} + \left(\frac{\sigma_{yy}}{f_{yy}}\right)^2 + \left(\frac{\tau_{xy}}{f_{xy}}\right)^2 = 1$$

Von Mises

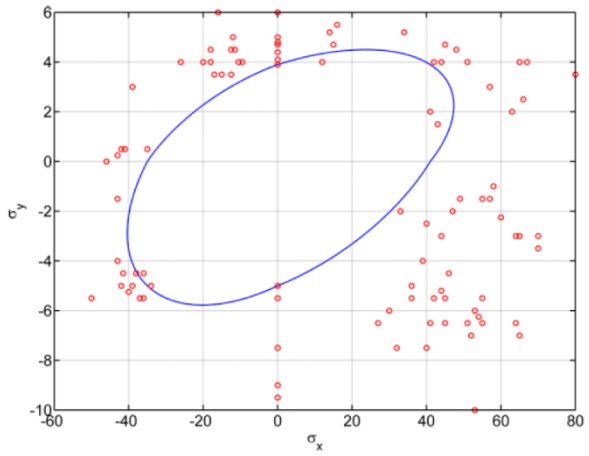

$$\left(\frac{\sigma_{xx}}{f_{xx}}\right)^2 - \frac{\sigma_{xx}\sigma_{yy}}{f_{xx}f_{yy}} + \left(\frac{\sigma_{yy}}{f_{yy}}\right)^2 + 3\left(\frac{\tau_{xy}}{f_{xy}}\right)^2 = 1$$

Van der Put

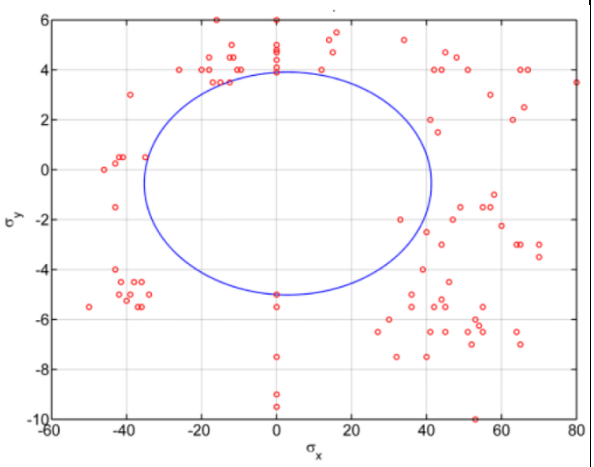

$$\left(\frac{1}{f_{xx}} - \frac{1}{f_{xx'}}\right)\sigma_{xx} + \left(\frac{1}{f_{yy}} - \frac{1}{f_{yy'}}\right)\sigma_{yy} + \frac{1}{f_{xx}f_{xx'}}{\sigma_{xx}}^2 + \frac{1}{f_{yy}f_{yy'}}{\sigma_{yy}}^2 \frac{1}{{f_{xy}}^2}{\tau_{xy}}^2 = 1$$

With:

f_{xx} = the material tensile resistance parallel to grain ($f_{t,0}$)
f_{xx}' = the material compression resistance parallel to grain ($f_{c,0}$)
f_{yy} = the material tensile resistance perpendicular to grain ($f_{t,90}$)
f_{yy}' = the material compression resistance perpendicular to grain ($f_{c,90}$)
f_{xy} = the material shear resistance (f_v)

2.3.4. Comparison of theories

A similar plotted comparison for the different theories can be made as for the national codes. Again using characteristic compressive strength values for C24:

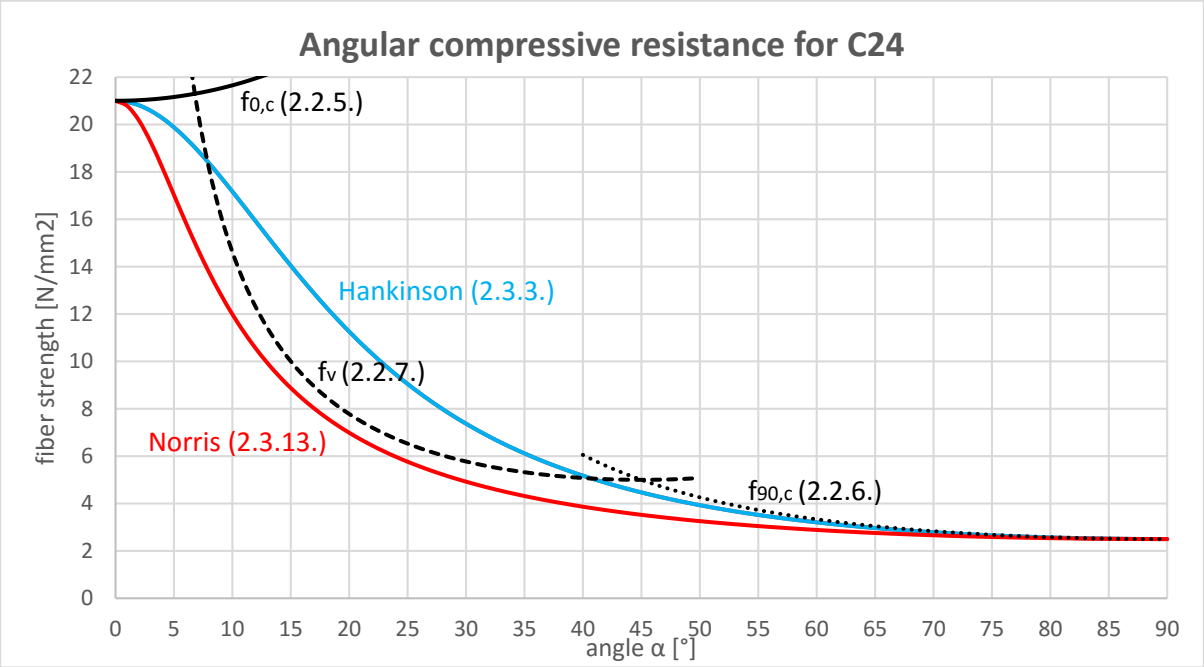

Figure 22: Comparison between several theories on timber loaded under an angle α to the fiber-direction.

Although the theories (graph lines) show large scattering in strength values, especially between $\alpha = 0° \rightarrow 45°$, this can be related back to the characteristic shear resistance value. Because this characteristic value is very conservative (safe) the decomposed (black) graph and Norris' (red) graph are effected, and as Hankinson (blue) does not take shear resistance into account, this line is not affected. To demonstrate the effect of the shear resistance on the course of the graphs, in Figure 23 the characteristic shear strength is doubled, which is realistic due to compression perpendicular to grain.

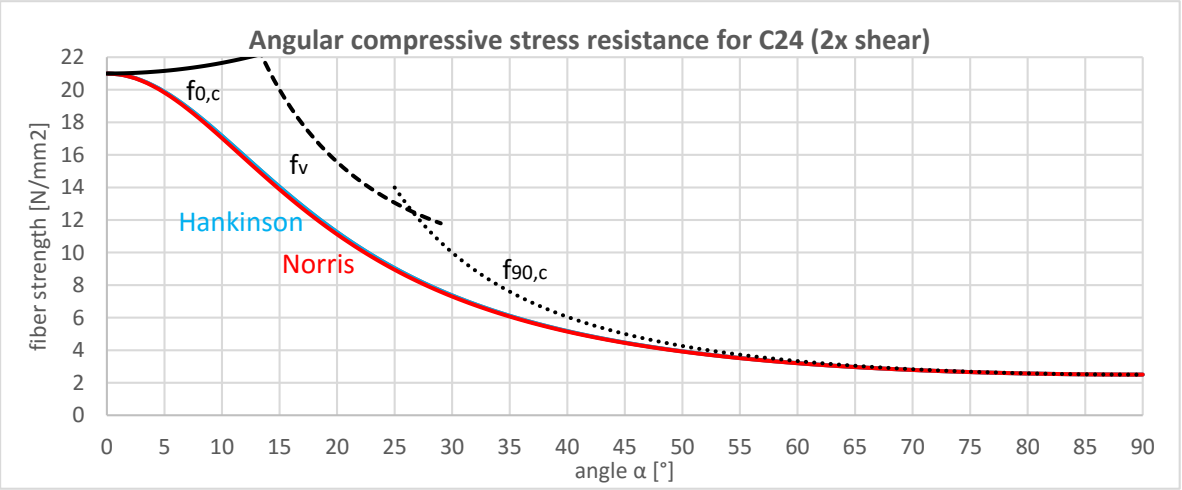

Figure 23: Comparison between theories on timber loaded under an angle α with doubled characteristic shear strength.

The (black) graph showing decomposing forces now overestimates the behavior greatly. The graphs of Norris (red) and Hankinson (blue) behave very similar.

2.3.5. Other (inter)national standard background information

The German standardization body DIN has published the book "Erläuterungen zu DIN 1052: 2004-08" [11] in 2005 which contains explanations of the background of the 2004 German DIN timber codes. This book refers to the book "Grundzüge des neuzeitlichen Holzbaues" (German for principles of modern timber construction) [14] published in 1981 , which explains the geometric boundaries and stress-distribution very well. Another book, "Træ og Staal konstructioner" (Danish for wood and steel structures) [15], already published in 1949, gives roughly the same content.

Frontnotch angle γ

As mentioned in section 2.1.1. the angle of the frontnotch is limited to prevent wedging on one hand, and popping out on the other hand. Where the Dutch NA to EC5 gives an upper and lower limit for the frontnotch angle γ, the German NA to EC5 and the Swiss SIA 256 standard present a fixed value of 90°-β/2. Choosing this angle gives the highest possible strength of the connection: Both the diagonal and the beam are loaded under an angle α of β/2 to the grain. Choosing one of both 90° angles means that one element is loaded parallel to the grain, but the other element is loaded under the full angle β to the grain. Since the resistance of the grains is less for α=β then for α=β/2, as proven in the previous chapters by Hankinson and Norris. This means the total strength of the connection is lower.

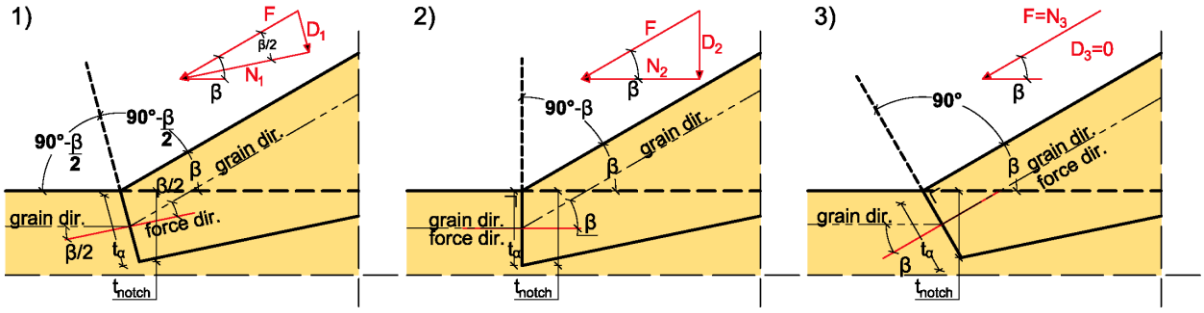

Figure 24: Difference in angles of the frontnotch surface resulting in different force components

The minimum notch depth for each situation can be calculated de decomposing force F into components which act parallel and perpendicular to the frontnotch area, as shown in Figure 24. This then can be translated to the minimum required notch depth t_{notch} using the material strength parameters:

$$1) \quad t_\alpha = \frac{N_1}{b \cdot \sigma_{\beta/2}} = \frac{F \cdot \cos \beta/2}{b \cdot \sigma_{\beta/2}} \qquad t_{notch} = t_\alpha \cdot \cos \beta/2 \qquad = \frac{F \cdot \cos^2 \beta/2}{b \cdot \sigma_{\beta/2}} \qquad (2.3.14.)$$

$$2) \quad t_\alpha = \frac{N_2}{b \cdot \sigma_\beta} = \frac{F \cdot \cos \beta}{b \cdot \sigma_\beta} \qquad t_{notch} = t_\alpha \qquad = \frac{F \cdot \cos \beta}{b \cdot \sigma_\beta} \qquad (2.3.15.)$$

$$3) \quad t_\alpha = \frac{N_3}{b \cdot \sigma_\beta} = \frac{F}{b \cdot \sigma_\beta} \qquad t_{notch} = t_\alpha \cdot \cos \beta \qquad = \frac{F \cdot \cos \beta}{b \cdot \sigma_\beta} \qquad (2.3.16.)$$

With σ_β and $\sigma_{\beta/2}$ determined by Norris' equation.

(2.3.14.) proves to require the smallest notch depth for loading angles to the grain α smaller than 66° as shown in Figure 25. (In situations 1), 2) and 3); α=β) Angles α of loading to the grain bigger than 66° are very uncommon. Therefore, for a step connection, it may be assumed that situation 1) is always the best geometry.

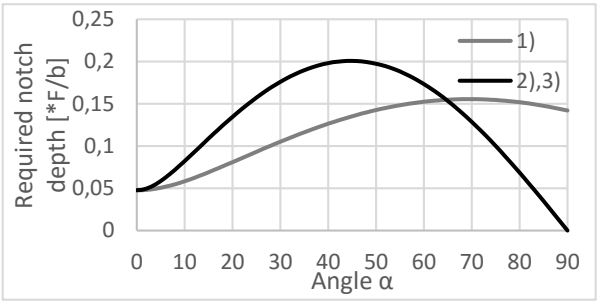

Figure 25: Behavior of formula's (2.3.14.),(2.3.15.) and (2.3.16) for different angles of loading to the grain α

Vertical component D in the bottomnotch surface

Equations 2.3.14. to 2.3.16. decompose force F to a component N_i which is acting on the frontnotch. Decomposing however, also results in a second component. This component D_i that also acts on the frontnotch via friction is disregarded. For a wood-to-wood connection a friction coefficient of $\mu = \tan \rho \approx 0.5$ may be taken into account which is big enough to not disregard component D as an acting force on the frontnotch. However, often it is chosen not take this friction into account in carpentry connections but instead state that the bottomnotch can take the D_i component.

Because of deformations due to the loading of the connection it can be expected that only a small length of the bottomnotch will be loaded. This makes it interesting to assume that the component D will act only on this surface. This means that the total axial force F will be transmitted through the connection as shown by the bold lines in Figure 26. The materials resistance against component D is much lower due to loading almost perpendicular to the grain. It may be assumed that this fact is compensated as component D is very small. Stresses from component N may assumed to be governing. Component N and D are perpendicular to both notch surfaces, so friction is not to be considered anymore. The size of the components N and D are dependent on the angle of the frontnotch γ.

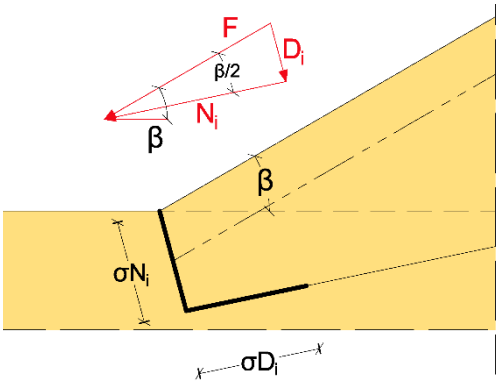

Figure 26: Distribution of force-components

Precision

It is of great importance that the connection between both elements is made with a high geometric precision in order to distribute the stresses, as intended in calculations, evenly over the length of the contact areas. Because of this, it is not recommended to make Double-, or even Triple Step joints in practice. They are very favorable in terms of eccentricity but it is also much harder to fit the two elements perfectly together since the geometry is much more complex (Figure 27). When the contact area of such a connection is reduced due to imperfections there is a high risk of overloading the element. This problem can be prevented by constructing a

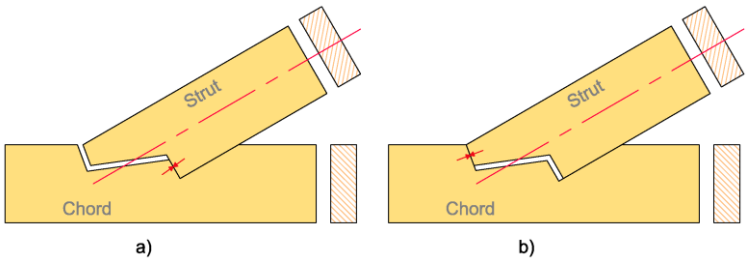

Figure 27: Geometric imperfections in Double Step joints

Double Step joint in two steps: First start with a Heal joint, partly load the connection, and then later make a fitting part for the front section of the connection using a wooden wedge.

Shrinkage

Even a perfect fitting connection can lose accuracy over time due to shrinkage of the wood. Since the fiber direction of both elements is different, the direction in which both element shrink is also different. Since wood is an anisotropic material, the shrinkage perpendicular to the fiber is big and the shrinkage parallel to the fiber is almost zero. This results in openings in the connection, creating peak stresses at the points which are still connected.

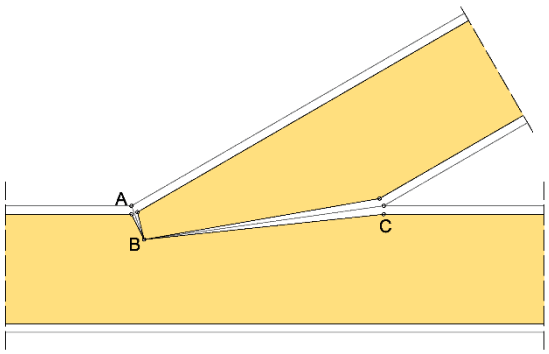

Figure 28: Shrinkage in a Single Step joint

In Figure 28, point A illustrates a big deformation due to shrinkage inwards, but also a very small disconection of both elements. This has an effect on length AB which is almost intirely disconnected due to this small opening. Stresses are now concentrated near point B. Due to deformations, the lower part of length AB will now transform all the forces. Length BC is also disconnected for a large part with very small deformations in this direction, this length will remain disconnected for a very large ammount. Because of safety and shrinkage, it is advised to disregard length BC for adding any resistance to the connection in the design of the connections. This means that the axial force S is transmitted intirely in plain AB.

Eccentricity

As shown in Figure 26 the diagonal force F is working eccentric to the neutral axis of the geometry. The eccentricity needs to be taken into account when designing the diagonal. Two types of eccentricities are occurring for step joints given in Figure 29. In geometry a) the eccentricity is constant along the length of the diagonal, meaning that the maximum buckling force must be reduced. In geometry b) the eccentricity varies linearly along the length of the element giving no eccentricity in the middle of the diagonal. In this case, no reductions are needed. The influence of eccentricity in the joint itself is very small, and therefore can be neglected.

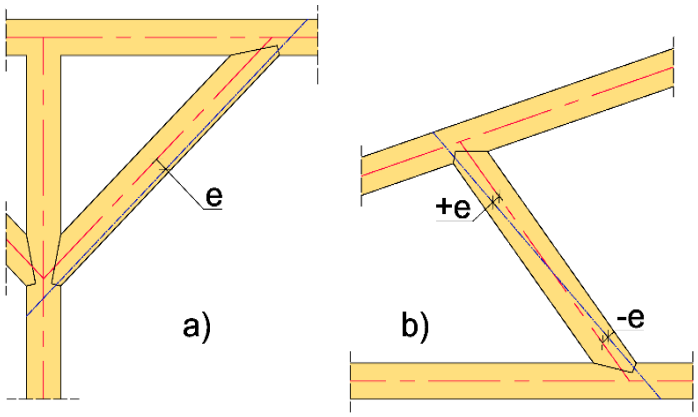

Figure 29: Eccentricity in the geometry

In the notched part of the connection, the forces of the diagonal are distributed over t_{notch} which causes an eccentric loading of the element. This can cause wedging of the notched element.

Wedging and splitting

To eliminate eccentric loadings in the connecting, the heal geometry can be used. Except lower-, or no eccentricities there is another advantage of a Heal joint. Because the forces are transmitted in the back of the connection, a larger shearplane length is available. A drawback for this connection can be splitting of the diagonal as can be seen in Figure 30. This is the result of tension stresses perpendicular to the grain that occur when the connection does not have a perfect fit, there are small rotations during usage, or due to shrinkage of the elements. This can be prevented by having a small space between the front of the diagonal and the notched element (Figure 30b), or by leaving the front part of diagonal out (Figure 30c). This is also beneficial for the timber beam length needed to construct the diagonal. To further prevent splitting in the diagonal, the contact area has a direction wich is perpendicular to the axes of the diagonal, leaving only compression stresses parallel to the grain in the diagonal.

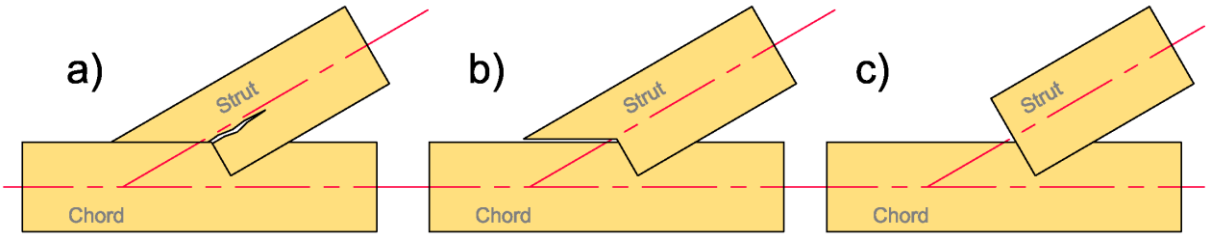

Figure 30: Splitting in Heal joints and solutions

Double Step joints

When applying a Double Step joint, both frontnotches may not have the same angular orientation. The angles of the front notch surfaces and the depth of both notches must be different. As can be seen in Figure 31, horizontal component H_1 is sheared along plane I and component H_2 is sheared along plane II. The length of both planes s_{notch}I and s_{notch}II must be checked according to their force component. The notch depth of the back notch t_{notch}II must be 10mm deeper, according to the Swiss code, than the first notch in order to not have interfering shearplanes. The axial force of the diagonal F is divided into equal components F_1=F_2=F/2. This simplification is made since making a detailed calculation of the distribution of F into F_1 and F_2 will give values close to this generalization. Due to safety reasons it is also recommended not to do so. (Imperfections in the higher loaded contact area will soon cause a much larger force than calculated in the other contact area.)

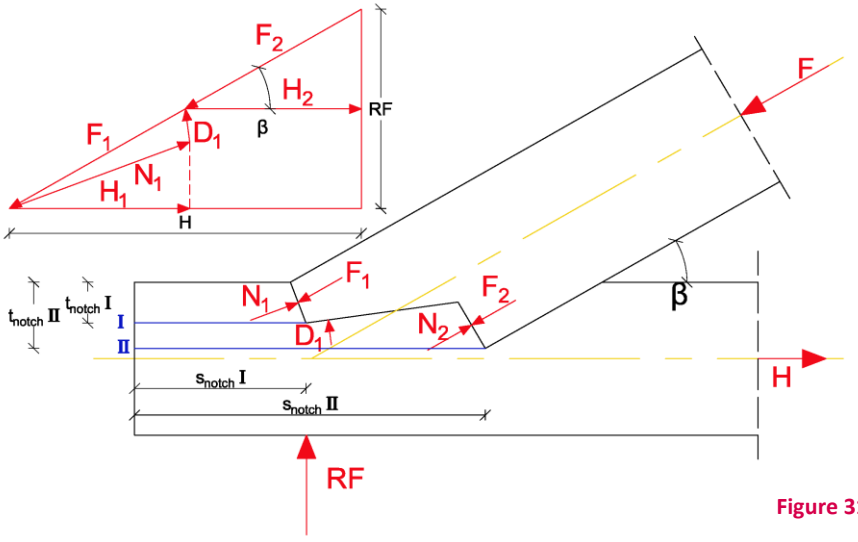

Figure 31: Double Step Joint

3. Research

Many experimental research projects were done on the Single Step Joint. Many of them are orientated in the strengthening of the connection in existing structures. As many “old” buildings in the Mediterranean region consist of these joints this research is done mostly by universities in Portugal, Spain and Italy. But there are also reports found coming from the USA, UK, Netherlands, Germany and Belgium.

3.1. Strengthening techniques

Most of the research projects were aimed at improving the strength of the connection. [16][17][18][19][20][21] The reason for this is damage that occurs to the connection as it decays over time. Also research was found that tested the influence of dynamic earthquake loadings on the stability of the connection.[22]

3.1.1. Mechanical fasteners

The focus of the investigations to strengthening the connection was mainly laid on a using steel parts to reinforce the connection. Three techniques stood out, as they have been the subject in a lot of investigations done by researchers at the Portuguese National Laboratory for Civil Engineering.[16], [17], [23]. They looked at improving the strength and the stiffness of the connection and used these three techniques:

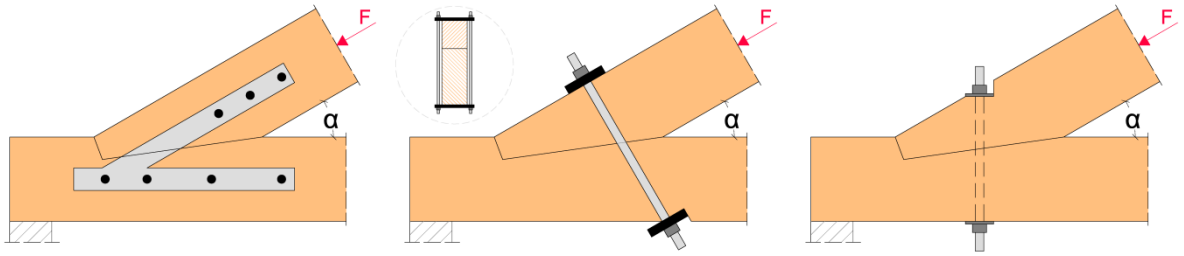

Figure 32: Different mechanical strengthening techniques on a Single Step Joint.

a) Bolted steel plates
b) External clamp
c) Internal clamp

Bolted steel plates

After taking action on flaws in the timber contact surfaces of the connection, on both sides of the connection steel plates are applied using bolts through the wooden beams to bind them together. The steel plates on each side are welded under an angle and connected with multiple bolts in each wooden part to prevent rotation in the connection. This prevents the contact surfaces of the notch from detaching under the influence of earthquake-loading, shrinkage and deflection (rotation of beam-ends). This has a positive influence on the stiffness of the connection. Due to the added steel cross-sections the compressive strength of the connection also gets enlarged. According to the research the connection increases in strength and stiffness with about 40% compared to the original untouched connection.

Internal and external clamps

The clamps in this research are applied near the front of the notch in the connection. Using clamps can be very beneficial to the stiffness of the connection but depends on a positive or negative change in angle α (closing or opening skew-angle). When closing the angle brittle failure does occur when the angle α becomes too small.

Conclusion: It can be concluded by the research that has been done on mechanical fasteners that the connection can be strengthened by making sure the notch surfaces are, and stay a tight-fit far more than using the strength-properties of steel to enhance the load bearing capacity.
This means that the importance of an as large as possible wood-to-wood surface to bear the wood-stresses in the notch is critical in a Single Step Joint.

3.1.2. Repairs

As mentioned in the previous paragraph the wood-to-wood surface is vital for any carpentry connection in compression. Over time these surfaces get damaged due to decay, shrinkage or temporary extreme loads. Local failure of the horizontal girder above the shear-plane of the front notch can occur. Often, this is fixed by removing the damaged area at the front notch and replace it by screwing a new section of timber on it.
Another problem is opening of the front notch due to different shrinkages of the element (due to different fiber directions). The same researchers that looked at mechanical fasteners also tested whether filling this opening with a wooden wedge restored the connection's strength. This wedge was made from hardwood to make sure its strength does not affect the test results. It was screwed in place just to make sure that it did not come out during the tests.

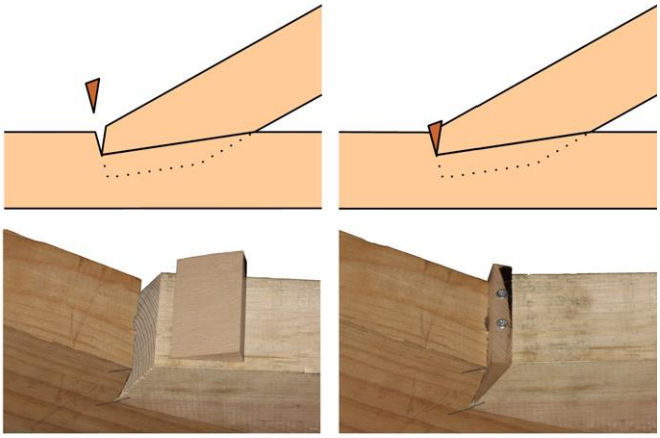

Figure 33: Hardwood wedge in front notch opening. [16]

Bibliography

[1] COST-FP1101, "FP1101 - Assessment , Reinforcement and Monitoring of Timber Structures," *http://www.costfp1101.eu/*, 2014. [Online]. Available: http://www.costfp1101.eu/.

[2] NEN, "NEN-EN 1995-1-1+C1+A1:2011." BRISwarenhuis, Delft, 2011.

[3] J. Siem and A. Jorissen, "COST Action FP1101 Assessment , Reinforcement and Monitoring of Timber Structures," Eindhoven, 2014.

[4] NEN, "NEN-EN 1995-1-1 Dutch NA 8.11 Ambachtelijke verbindingen." BRISwarenhuis, Delft, 2013.

[5] DIN, "DIN-EN-1995-1-1 German NA 12.1 Versätze." DIN Deutsches Institut für Normung, Berlin, pp. 88–89, 2010.

[6] SIA, "Schweizer Norm SIA 265 - Holzbau." SIA, Zürich, pp. 77–78, 2012.

[7] NEN, "NEN-EN 1995-1-1/A1." NEN, Delft, 2011.

[8] R. L. Hankinson, "Investigation of crushing strength of spruce at varying angles to the grain," *Air Serv. Inf. Circ.*, vol. 3, no. 259 (material section paper No. 130), 1921.

[9] NEN, "Nen 6760:2005." NEN, 2005.

[10] C. B. Norris, "Strength of orthotropic materials subjected to combined stresses," Madison (Wisconsin) USA, 1962.

[11] H. Blaß, H. Ehlbeck, H. Kreuzinger, and G. Steck, "Erläuterungen zu DIN 1052: 2004-08," in *Deutsche Gesellschaft für Holzforschung …*, vol. 08, no. 4, 2005.

[12] A. Jorissen, "Timber Structures 3 - Failure Criterion." Undated lecture notes TU/e, Eindhoven.

[13] J. Eberhardsteiner, *Mechanisches Verhalten von Fichtenholz: Experimentelle Bestimmung der biaxialen Festigkeitseigenschaften*. Springer, 2002.

[14] G. Dröge and K.-H. Stoy, "Versätze," in *Grundzüge des neuzeitlichen Holzbaues*, Berlin: Ernst & Sohn, 1981, pp. 73–97.

[15] G. J. Rasmussen, "Træ og Staal Konstruktioner," in *Træ og Staal Konstruktioner*, 1949, pp. 192–219.

[16] P. Palma, H. Garcia, J. Ferreira, J. Appleton, and H. Cruz, "Behaviour and repair of carpentry connections - Rotational behaviour of the rafter and tie beam connection in timber roof structures," *J. Cult. Herit.*, vol. 13, no. 3 SUPPL., pp. S64–S73, Sep. 2012.

[17] P. Palma, J. Ferreira, and H. Cruz, "MONOTONIC TESTS OF STRUCTURAL CARPENTRY JOINTS," *ewpa.com*.

[18] J. M. Branco, "Analysis and strengthening of carpentry joints," Guimarães, Portugal.

[19] M. Parisi and M. Piazza, "Mechanics of plain and retrofitted traditional timber connections," *J. Struct. Eng.*, no. December, pp. 1395–1403, 2000.

[20] J. Branco, P. Cruz, M. Piazza, and H. Varum, "Experimental analysis of original and strengthened traditional timber connections," 2006.

[21] J. Branco, M. Piazza, and P. Cruz, "Experimental evaluation of different strengthening techniques of traditional timber connections," *Eng. Struct.*, 2011.

[22] M. Parisi and M. Piazza, "Seismic strengthening of traditional carpentry joints," *Proceedings, 14th Conf. Earthq. …*, 2008.

[23] P. Palma and H. Cruz, "Mechanical behaviour of traditional timber carpentry joints in service conditions-results of monotonic tests," *From Mater. to Struct. Behav. …*, no. November, 2007.

NEN-EN 1995-1-1 Bolted steel-timber connection

Data Timber

Thickness	t_2	=	70	mm
Tensile strength ∥	$f_{t,0,k}$	=	14.00	N/mm^2
Shear strength	$f_{v,k}$	=	2.50	N/mm^2
Load duration	K_{mod}	=	1.0	
Safety factor	γ_m	=	1.3	
Density	ρ_k	=	350	kg/m^3
Embedment str.	$f_{h,2,k}$	=	24.11	N/mm^2

Gegevens bout

Diameter	d	=	16	mm
Amount	n	=	8	
Effective amount	n_{ef}	=	2.90	per bolt row
Tensile strength	$f_{u,k}$	=	800	N/mm^2 (8.8 bolt)
Pull-out strength	$F_{ax,r,k}$	=	0	(0, if unknown)
Yield strength	$M_{y,r,k}$	=	324282.3	Nmm

Load connection

Force Horizontal	F_{Ed}	=	100	kN
Force Vertical	F_{Ed}	=	10	kN

Gegevens geometrie boutverbinding

total connection length	l_{tot}	=	400	mm
Height beam	h	=	250	mm
number of bolt rows		=	2	
Pitch horizontal	$l_{v,i}$	=	100	mm
Pitch vertical	$l_{t,i}$	=	100	mm
horizontal end distance	$l_{v,end}$	=	112	mm
vertical end distance	$l_{t,end}$	=	75	mm

8.2.3 Steel-to-timber connections

For thin steel plates as the outer members of a double shear connection:

Strength

$$F_{v;r;k} = \min \begin{cases} 0.5 * f_{h,2,k} * t_2 * d = 13500 \text{ N} \\ 2.3 * \sqrt{(M_{y,r,k} * f_{h,2,k} * d)} + F_{ax,r,k} / 4 = 25723 \text{ N} \end{cases}$$

$F_{v;r;k}$ = 13.50 kN

Resistance of the connection

F_{Rd} = 157

Reduced cross section

$A_{red;h}$ = 250 mm

$F_{Rd;A;h}$ = 245 kN > 157 kN **Sufficient**

Unity check

F_{Ed} / F_{Rd} 0.639 ≤ 1

Sufficient

8.5.1 Laterally loaded bolts Parallel to the grain

(2) For bolts up to 30mm diameter, the following characteristic embedment strength values in timber and LVL should be used, at an angle α to the grain:

Embedment str. $f_{h,0,k} = 0.082 * (1 - 0.01\ d) * \rho_k$

$= 24.108 \quad N/mm^2$

$\alpha = 7.81$ °

$k_{90} = 1.59$ for softwoods

$$f_{h,\alpha,k} = \frac{f_{h,0,k}}{k_{90} * \sin^2\alpha + \cos_2\alpha}$$

$f_{h,\alpha,k} = 23.63$

(3) Minimum spanings and edge an end distance

Parallel to grain	a_1	= 4 * d	=	64	mm
Perpend. to grain	a_2	= 4 * d	=	64	mm
Loaded end	$a_{3,t}$	= 7 * d > 80	=	112	mm
Loaded edge	$a_{4,t}$	= (2 + 2 sinα)d > 3d=		48	mm

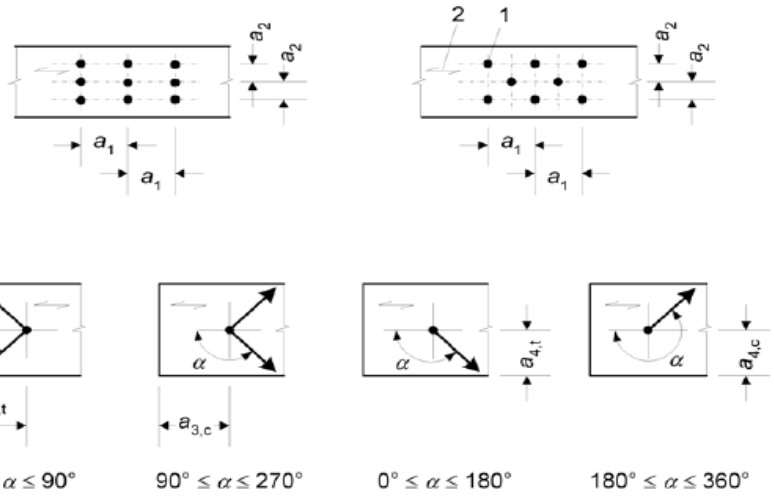

-90° ≤ α ≤ 90° 90° ≤ α ≤ 270° 0° ≤ α ≤ 180° 180° ≤ α ≤ 360°

Unity check

$a_1 / l_{v,i}$ 0.64 ≤ 1

Sufficient

$a_2 / l_{t,i}$ 0.64 ≤ 1

Sufficient

$a_{3,t} / l_{v,end}$ 1 ≤ 1

Sufficient

$a_{4,t} / l_{t,end}$ 0.64 ≤ 1

Sufficient

Bijl. A Block shear and plug shear failure at multiple dowel-type steel-to-timber connections

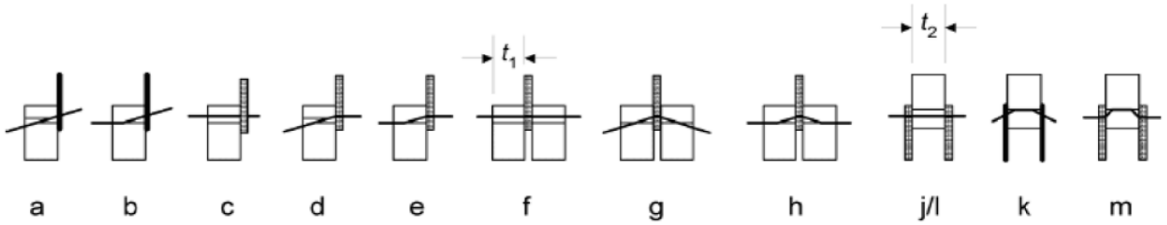

Failure mode = j/l

For thin steel plates (for failure modes given in brackets)

NVT t_{ef} = max

$0.4 * t_2$	(a)	28.0	mm
$1.4 * \sqrt{(M_{y,r,k}/f_{h,2,k} * d)}$	(b)	40.6	mm

$L_{net,v} = \Sigma l_{v,l} - n * d$ = 824 mm

$L_{net,t} = \Sigma l_{t,l} - n * d$ = 100 mm

$A_{net,t} = L_{net,t} * t_2$ = 7000 mm^2

$A_{net,v}$ = min

$L_{net,v} * t_2$	=	57680 mm^2	(c,f,j/l,k,m)
$L_{net,v} / 2 * (L_{net,t} + 2 * t_{ef})$	=	64272 mm^2	(other)

$A_{net,v}$ = 57680 mm^2

$F_{bs,Rk}$ = max

$1.5 * A_{net,t} * f_{t,0,k}$	147000 N
$0.7 * A_{net,v} * f_{v,k}$	100940 N

$F_{bs,Rk}$ = 147.0 kN

Unity check

$F_{Ed} / F_{bs,Rk}$ 0.68 ≤ 1

Sufficient

NEN-EN 1993-1-1 Bolted steel-timber connection

Bolt pattern

Boltrows		=	2	
	$l_{v,i}$	=	100.00	mm
	$l_{t,i}$	=	100	mm

Bolt data

Diameter	d_0	=	16	mm
Amount	n	=	8	
Tensile strength	$f_{u,k}$	=	800	N/mm^2

Steelplate data

Thickness	t_s	=	10	mm
Height	h_s	=	150	mm
Length	l_s	=	450	mm
	l_s	**>**	**419.2**	**mm**
Yieldpoint	$f_{y,k}$	=	235	N/mm^2
Amount of steelplates		=	2	

Connection load

Force	F_{Ed}	=	100	kN

6.2.3 Tension

A_{net} according to 6.2.2.2

$A_{net,t} = h_s * t_s - n * d_0 * t_s = 1180$ mm^2

$N_{t,Rd} = A_{net} * f_{y,k} = 554600$ N

Unity check

$F_{Ed} / N_{t,Rd}$ 0.18 ≤ 1 **sufficient**

6.2.6 Shear

A_{net} according to 6.2.2.2

$A_{net,v} = l_s * t_s - n * d_0 * t_s = 3500$ mm^2

$N_{v,Rd} = A_{net} * (f_{y,k} / \sqrt{3}) = 949741$ N

Unity check

$F_{Ed} / N_{t,Rd}$ 0.105 ≤ 1 **sufficient**

3.5 Bolt pattern distances

					Minimaal			Praktisch		Check
End distance	e_1	=	50	mm	$1.2 * d_0 =$	19.2	mm	35	mm	**Sufficient**
Side distance	e_2	=	17	mm	$1.2 * d_0 =$	19.2	mm	30	mm	**Unpractical**
Pitch	p_1	=	100	mm	$2.2 * d_0 =$	35.2	mm	55	mm	**Sufficient**
Pitch	p_2	=	100	mm	$2.4 * d_0 =$	38.4	mm	55	mm	**Sufficient**

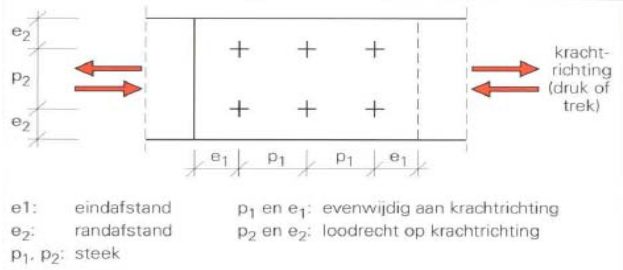

e1: eindafstand
e2: randafstand
p1, p2: steek

p1 en e1: evenwijdig aan krachtrichting
p2 en e2: loodrecht op krachtrichting

Protocol setup specimen

1. Fetch timber beam and matching diagonal from climate chamber.
2. Marking specimen:
    a. Force axis (from top of the diagonal to the support);
    b. Holes for the steel plate connection. 122mm from the backend of the beam. With a pitch of 100mm;
    c. Location of the ADC's.
3. Drilling holes for the steel plated connection. Ø16mm.
4. Adjusting pendulum rod to the correct length (M32, 3mm per full revolution).
5. Mounting beam element to the steel plates in the test setup. (non-tightened bolts).
6. Adjusting beam to 30° angle by slightly adjusting vertical support and adjusting the thickness of the steel support bearing plates.
7. Placing Teflon on the bottomnotch surface.
8. Placing the diagonal element on the beam.
9. Applying Teflon on both sides of the specimen near the out-of-plane support fork.
10. Align the specimen out of plane by shifting the supports and rotating the fork.
11. Clamping the specimen in the fork and secure the fork.
12. Checking alignment of the actuator.
13. Placing load bearing plate and spherical bearing plate.
14. Placing measurement devices.
15. Placing measurement devices in measuring reach.
16. Applying 20kN load.
17. Tighten bolts of the steel plate connection.
18. Unloading specimen.

Test protocol

1. Dropping window blinds
2. Placing light screens.
3. Placing and aim video cameras.
4. Set ESPI.
5. Start test.